

**FOSSIL
FUELS
RESEARCH**

**DOE/FE/61114-2
(DE90000241)**

**DEVELOPMENT OF EFFECTIVE GAS SOLVENTS INCLUDING CARBON
DIOXIDE FOR THE IMPROVED RECOVERY OF WEST SAK OIL**

Final Report

**By
G.D. Sharma**

June 1990

Performed Under Contract No. FG01-86FE61114

**University of Alaska Fairbanks
Fairbanks, Alaska**



**National Petroleum Technology Office
U. S. DEPARTMENT OF ENERGY
Tulsa, Oklahoma**

DISCLAIMER

This report was prepared as an account of work sponsored by an agency of the United States Government. Neither the United States Government nor any agency thereof, nor any of their employees, makes any warranty, expressed or implied, or assumes any legal liability or responsibility for the accuracy, completeness, or usefulness of any information, apparatus, product, or process disclosed, or represents that its use would not infringe privately owned rights. Reference herein to any specific commercial product, process, or service by trade name, trademark, manufacturer, or otherwise does not necessarily constitute or imply its endorsement, recommendation, or favoring by the United States Government or any agency thereof. The views and opinions of authors expressed herein do not necessarily state or reflect those of the United States Government.

This report has been reproduced directly from the best available copy.

DEVELOPMENT OF EFFECTIVE GAS SOLVENTS INCLUDING
CARBON DIOXIDE FOR THE IMPROVED RECOVERY OF WEST SAK OIL

Final Report

By
G. D. Sharma

June 1990

Work Performed Under Contract No. FG01-86FE61114

Prepared for
U.S. Department of Energy
Assistant Secretary for Fossil Energy

Royal J. Watts, Project Manager
Morgantown Energy Technology Center
P.O. Box 880
Morgantown, WV 26505

Prepared by
University of Alaska Fairbanks
Petroleum Development Laboratory
Fairbanks, AK 99775-1260

ABSTRACT

The West Sak reservoir located on the North Slope of Alaska is estimated to contain up to 25 billion barrels of heavy oil in place and represents the largest known heavy oil accumulation in the United States. The absence of natural drive mechanism in this reservoir makes it a target for enhanced oil recovery processes. High degree of variation in the oil gravity (14 to 22.5 °API) and fluid properties in these highly heterogeneous unconsolidated fine-grained sands; presence of clay minerals; low permeability; highly faulted structure; and close proximity of this reservoir to the overlying permafrost, makes it a unique, special heavy oil reservoir. The possibility of sharing the existing Kuparuk River Unit facilities makes the development and production of West Sak reservoir, a near-term target.

The research undertaken in this project pertains to study of thermal and miscible processes for the recovery of West Sak crude. This report provides a description of the West Sak reservoir along with the petrophysical properties of various sand members based on the analysis of well log data; experimentally measured fluid properties (PVT) of West Sak crude and phase behavior of CO₂-West Sak crude mixtures; slim tube experiments, asphaltene precipitation tests and equation of state predictions (in presence and absence of aqueous phase) conducted to study applicability of miscible flooding with enriched hydrocarbon gas solvents and carbon dioxide.

The studies pertaining to thermal recovery processes described in this report include: prediction of steamflood performance with a simplified steamflood model, experimental one dimensional corefloods conducted to study effect of addition of gases such as carbon dioxide, nitrogen and methane to steam on the recovery of West Sak crude and development of analytical heat transfer model to simulate injection of steam/hot water in a one dimensional linear reservoir.

ACKNOWLEDGEMENT

This report was prepared for the U.S. Department of Energy under the Cooperative Agreement No. DE-FG01-86FE61114. The financial support of the U.S. Department of Energy, Morgantown Energy Technology Center is gratefully acknowledged. The matching support was provided by the Petroleum Development Laboratory, University of Alaska Fairbanks. The research work described herein was made possible by the cooperation and assistance of, North Slope Operators who provided Prudhoe Bay natural gas, natural gas liquids and West Sak crude samples; and Alaska Oil and Gas Conservation Commission who provided well log data. This report is a result of the work performed by following co-investigators: Dr. Vidyadhar A. Kamath, Dr. Kaveh Dehghani, Dr. Russell D. Ostermann and Dr. David O. Ogbe, and following graduate students: Arun K. Sharma, Marc Hornbrook, Max Roper, Michael T. Lu, Manmath N. Panda, Menggui Zhang, Jinchun Jiang, Raj P.S. Bhandari, Nadem Siddiqui, and Gui-yun Zhang. In addition, Mr. Shirish L. Patil, Research Associate contributed in these efforts towards experimental data gathering and data analysis. This report was prepared by Dr. Vidyadhar A. Kamath and Mr. Shirish L. Patil and typed by Ms. Judy Ward.



Dr. G.D. Sharma, Director
Petroleum Development Laboratory

TABLE OF CONTENTS

	<u>Page</u>
ABSTRACT	iii
ACKNOWLEDGEMENT	iv
LIST OF FIGURES	xi
LIST OF TABLES	xxiv
EXECUTIVE SUMMARY	xviii
CHAPTER ONE: WEST SAK RESERVOIR DESCRIPTION	1
A. Introduction	1
B. Geology of Alaskan North Slope	2
C. Classification and Spatial Distribution of West Sak Sands and Petrophysical Properties	7
D. Depositional Environment	18
E. References	19
CHAPTER TWO: PHASE BEHAVIOR AND FLUID PROPERTIES MEASUREMENTS	21
A. Abstract	21
B. Experimental PVT Apparatus	21
C. Experimental Procedure	28
D. Constant Composition Expansion Data	30
E. Differential Expansion Data	32
F. Single Contact Tests With CO ₂ -West Sak Crude Mixtures	32
F1. 60 Mol% CO ₂ - 40 Mol% West Sak Crude Mixture	32
F2. 80 Mol% CO ₂ - 20 Mol% West Sak Crude Mixture	41
G. Effect of Gas Solubility on West Sak Crude Viscosity	47
H. Conclusions	49
I. References	50

TABLE OF CONTENTS (CONT'D)

	<u>Page</u>
CHAPTER THREE: MISCIBLE DISPLACEMENT STUDIES	51
PART I: Determination of Minimum Miscibility Pressures and Mechanism of Miscibility Development For Enriched Gases	51
A. Abstract	51
B. Introduction	52
C. Slim Tube Miscibility Set-Up	55
D. Experimental Procedures	60
E. Experimental Results	63
E1. Carbon Dioxide as Solvent	63
E2. N-Butane as Solvent	63
E3. NGL/PBG Mixtures as Solvent	67
F. EOS Predictions	70
F1. Limitations of Pseudo-Ternary Diagram Method	70
F2. Solvent-Crude Oil Pressure Composition Diagram	74
F3. Determination of Thermodynamic Compositional Path	76
G. Conclusions	81
H. References	82
PART II: Effect of Presence of Aqueous Phase on Phase Behavior and Miscibility Conditions For Solvent - West Sak Crude Mixtures	84
A. Abstract	84
B. Introduction	85
C. Model Predictions and Discussion	85
D. Conclusions	97
E. References	97

TABLE OF CONTENTS (CONT'D)

	<u>Page</u>
PART III: Study of Asphaltene Precipitation During Addition of Solvents to West Sak Crude	98
A. Abstract	98
B. Introduction	99
C. Asphaltene Precipitation From Tank Oils Upon Addition of Solvents	103
D. Tests with (Live) Recombined Oils Asphaltene Precipitation	108
E. Conclusions	110
F. References	114
CHAPTER FOUR: FEASIBILITY OF STEAMFLOODING FOR WEST SAK	117
A. Abstract	117
B. Introduction	117
C. Model Description	118
C1. Steamflood Performance Prediction Model	120
C1.1 Prediction of Heat and Pressure Losses	120
C1.1.1 Surface Heat Losses	122
C1.1.2 Wellbore Heat and Pressure Losses	123
C1.1.3 Underburden and Overburden Heat Losses ..	126
C1.2 Steam Zone Shape Factor	129
C1.3 Areal Sweep Efficiency	131
C1.4 Critical Time	131
C1.5 Steam Zone Growth	133
C1.6 Hot Condensate Zone	134
C1.7 Pressure Drop in the Reservoir	141

TABLE OF CONTENTS (CONT'D)

	<u>Page</u>
C1.8 Calculations of Fluids Displaced	142
C1.9 Model Validation	142
C1.9.1 Wellbore Heat Losses	143
C1.9.2 Prediction of Oil and Water Produced	145
C2. Steamflood Economic Model Description	149
C2.1 Gross Revenue and Operating Costs	149
C2.2 Depreciation Schedules and Depletion	152
C2.3 Royalties, Severances, and Tax Scheduling	154
D. Application of Model to West Sak Reservoir	159
D1. Reservoir Data Used	160
D2. Sensitivity Analysis	162
D2.1 Sensitivity of Steam Injection Parameters	163
D2.2 Sensitivity of Windfall Profit Tax and ELF	187
D2.3 Sensitivity of Drilling and Well Completion Cost	193
D2.4 Sensitivity of Surface Equipment and Steam Generator Costs	194
D2.5 Sensitivity of Water and Fuel Costs	201
D2.6 Sensitivity of Inflation	203
D2.7 Sensitivity of Residual Oil Saturation	207
D2.8 Average Best and Worst Case Scenarios for West Sak	213
D2.9 Summary of Sensitivity Analysis	215
E. Conclusions	217

TABLE OF CONTENTS (CONT'D)

	<u>Page</u>
F. References	218
G. APPENDIX: FLOW CHART OF THE MODEL	224
CHAPTER FIVE: STEAM-SOLVENT DISPLACEMENT STUDIES	230
A. Abstract	230
B. Introduction	230
C. Steam - Solvent Displacement Apparatus	232
D. Steam Distillation Apparatus	235
E. Density Measurement Apparatus	235
F. Experimental Procedures	237
G. Results and Discussion	241
G1. Steam Injection Only Runs	241
G2. Carbon Dioxide - Steam, Nitrogen-Steam, Methane-Steam, Injection Runs	241
G2.1 Reduction of Steam Injection Temperature	243
G2.2 Effect of CO ₂ on Steam Distillation	245
G2.3 Compositional Analysis of Produced Oil	248
G2.4 Effect of CO ₂ on Oil Density	252
G2.5 Nitrogen-Steam Injection Runs	252
G2.6 Methane-Steam Injection Runs	254
G2.7 Analysis of Pressure Drop and Temperature Profiles ..	254
H. Conclusions	260
I. References	264

TABLE OF CONTENTS (CONT'D)

	<u>Page</u>
CHAPTER SIX: DEVELOPMENT OF ONE DIMENSIONAL (LINEAR) HEAT TRANSFER MODEL FOR STEAM-SOLVENT INJECTION STUDY	265
A. Introduction	265
B. Heat Transfer Model Development	265
C. Model Validation	278
D. West Sak Rock and Fluid Properties	278
E. Summary	283
F. Nomenclature	285
G. References	287

LIST OF FIGURES

	<u>Page</u>
<u>CHAPTER ONE</u>	
1. Location Map of Major Oil Fields in Alaskan North Slope	3
2. A Schematic Showing the Hierarchy of the Major Reservoir Units of the Alaskan North Slope	3
3. A Generalized Stratigraphic Column for Kuparuk River Area Depicting Heavy Oil Bearing Sands	6
4. Contour Map Showing Depths to the Top of West Sak Upper Sand 1 (AA': SW-NE Cross-Section, BB': NW-SE Cross-Section)	11
5. West Sak Sands Depicted on the SW-NE Stratigraphic Cross-Section AA'	12
6. West Sak Sands Depicted on the SW-NE Stratigraphic Cross-Section BB'	13
7. West Sak Upper Sand 1 Gross Pay Zone Thickness Contour Map	14
8. West Sak Upper Sand 2 Gross Pay Zone Thickness Contour Map	14
9. West Sak Lower Sand 1 Gross Pay Zone Thickness Contour Map	14
10. West Sak Lower Sand 2 Gross Pay Zone Thickness Contour Map	15
11. West Sak Lower Sand 3 Gross Pay Zone Thickness Contour Map	15
12. West Sak Lower Sand 4 Gross Pay Zone Thickness Contour Map	16
13A. Iso-Porosity Contour Map of West Sak Sands	16
13B. 3-D Plot Illustrating Porosity Distribution in West Sak Sands	17
14A. Iso-Water Saturation Map of West Sak Sands	17
14B. 3-D Plot Illustrating Water Saturation Distribution	17
<u>CHAPTER TWO</u>	
1. Experimental Apparatus for PVT and Phase Behavior Studies	23
2. PVT Cell Volume Calibration Chart	25

LIST OF FIGURES (CONT'D)

	<u>Page</u>
3. Viscometer Constant at Low Pressures	25
4. Shifting of Viscometer Constant with Pressures	25
5. Heating Element Calibration	25
6. Relative Total Volume Versus Pressure (Constant Composition Expansion of West Sak Crude at 80°F)	31
7. Volume Fraction Liquid Versus Pressure (Constant Composition Expansion of West Sak Crude at 80°F)	31
8. Solution GOR Versus Pressure (Differential Liberation of West Sak Crude at 80°F)	36
9. Oil FVF Versus Pressure (Differential Liberation of West Sak Crude at 80°F)	36
10. Relative Total FVF Versus Pressure (Differential Liberation of West Sak Crude at 80°F)	36
11. Incremental Gas Gravity Versus Pressure (Differential Liberation of West Sak Crude at 80°F)	37
12. Gas Deviation Factor Versus Pressure (Differential Liberation of West Sak Crude at 80°F)	37
13. Gas FVF Versus Pressure (Differential Expansion of West Sak Crude at 80°F)	37
14. Oil Density Versus Pressure (80°F)	37
15. Oil Viscosity Versus Pressure (80°F)	37
16. Analysis of Oil Viscosity Data (80°F)	38
17. Viscosity of Incremental Gas at 80°F (Calculated)	38

LIST OF FIGURES (CONT'D)

	<u>Page</u>
18. Relative Total Volume Versus Pressure (Constant Composition Expansion at 80°F for 60 Mol% CO ₂ - 40 Mol% West Sak Crude)	40
19. Volume Fraction Oil-Rich Liquid Versus Pressure (Constant Composition Expansion at 80°F for 60 Mol% CO ₂ - 40 Mol% West Sak Crude)	40
20. Oil Swelling Index Versus Pressure (60 Mol% CO ₂ - 40 Mol% West Sak Crude at 80°F)	40
21. Oil Viscosity Reduction By CO ₂ at 80°F	42
22. Oil Density Increase By CO ₂ at 80°F	42
23. Relative Total Volume Versus Pressure (Constant Composition Expansion at 80°F For 80 Mol% CO ₂ - 20 Mol% West Sak Crude)	43
24. Volume Fraction Oil-Rich Liquid Versus Pressure (Constant Composition Expansion at 80°F For 80 Mol% CO ₂ - 20 Mol% West Sak Crude)	43
25. Oil Swelling Index Versus Pressure (80 Mol% CO ₂ - 20 Mol% West Sak Crude)	44
26. Three Phase Region at 80°F (Constant Composition Expansion For 80 Mol% CO ₂ - 20 Mol% West Sak Crude)	44

CHAPTER THREE

PART I

1. Slim Tube Miscibility Apparatus	56
2. Slim Tube Oil Recovery Versus PV of CO ₂ Injected (1750 psi, 100°F) ...	66
3. Slim Tube Oil Recovery Versus PV of N-Butane Injected (2375 psia, 80°F)	66

LIST OF FIGURES (CONT'D)

		<u>Page</u>
4.	Slim Tube Oil Recovery Versus PV of NGL/PBG Injected	69
5.	EOS Predicted P-T Envelope for West Sak Crude	69
6.	P-T Envelopes for Various Mixtures of Prudhoe Bay Gas (PBG) and Natural Gas Liquids (NGL)	71
7.	Ternary Diagram Developed Using Three Pseudo-Component Flashing Technique	71
8.	Pressure-Enrichment Correlation For West Sak Crude (Pseudo-Ternary Tie Line Method)	73
9.	P-X Diagram For West Sak Crude/N-Butane Mixtures at 80°F	73
10.	P-X Diagram For West Sak Crude/(NGL/PBG) Solvent Mixtures at 80°F	75
11.	Compositional Path of West Sak Crude/(NGL/PBG) Solvent Mixtures at 80°F Using 23-Component Model	77
12.	Pressure-Enrichment Correlation For West Sak Crude (23-Component Model)	79
 <u>PART II</u>		
1.	Phase Behavior of CO ₂ - West Sak Crude Mixture at 80°F	88
2.	Phase Behavior of CO ₂ - West Sak Crude Mixture at 250°F	88
3.	Phase Behavior of CO ₂ - West Sak Crude Mixture at 700°F	89
4.	Phase Behavior of West Sak Crude in the Presence of Water at 80°F	89
5.	Effect of Water on Phase Behavior of 20% CO ₂ - 80% West Sak Crude Mixture at 80°F (Water Included)	90

LIST OF FIGURES (CONT'D)

		<u>Page</u>
6.	Effect of Water on Phase Behavior of 40% CO ₂ - 60% West Sak Crude Mixture at 80°F (Water Included)	90
7.	Effect of Water on Phase Behavior of 60% CO ₂ - 40% West Sak Crude Mixture at 80°F (Water Included)	92
8.	Effect of Water on Phase Behavior of 20% CO ₂ - 80% West Sak Crude Mixture at 80°F (Water Excluded)	92
9.	Effect of Water on Phase Behavior of 40% CO ₂ - 60% West Sak Crude Mixture at 80°F (Water Excluded)	93
10.	Effect of Water on Phase Behavior of 60% CO ₂ - 40% West Sak Crude Mixture at 80°F (Water Excluded)	93
11.	Effect of Water on the Phase Behavior of N-Butane - Crude Mixture at 80°F (Water Excluded)	94
12.	Effect of Water on the Phase Behavior of (80% Mol% PBG/20 Mol% NGL) - West Sak Crude Mixture at 80°F (Water Included)	94
13.	Effect of 20% Water on Minimum Miscibility Pressures for PBG/NGL Mixtures	96
14.	Effect of 80% Water on Minimum Miscibility Pressures for PBG/NGL Mixtures	96
 <u>PART III</u>		
1.	Schematic of Experimental Apparatus for Asphaltene Precipitation Studies	109
2.	Effect of CO ₂ Addition to West Sak Crude Oil A on Asphaltene Deposition at (1705 psia and 80°F)	111

LIST OF FIGURES (CONT'D)

		<u>Page</u>
3.	Effect of Pressure on Asphaltene Precipitation (30 Mol% CO ₂ : 70 Mol% Oil A)	112
4.	Effect of Pressure on Asphaltene Precipitation (50 Mol% CO ₂ : 50 Mol% Oil A)	113
<u>CHAPTER FOUR</u>		
1.	Comparison of Predicted Wellbore Heat Losses	144
2.	Comprison of Predicted Kern River Simulated Steamflood	144
3.	Cumulative Fluids Produced for Injection Rates with Steam Quality = 0.60	165
4.	Cumulative Oil Produced for Injection Rates with Steam Quality = 0.60	165
5.	Cumulative Water Produced for Injection Rates with Steam Quality = 0.60	166
6.	Fractional Oil Produced for Injection Rates with Steam Quality = 0.60	166
7.	Cumulative Fluids Produced for Injection Rates with Steam Quality = 0.70	167
8.	Cumulative Oil Produced for Injection Rates with Steam Quality = 0.70	167
9.	Cumulative Water Produced for Injection Rates with Steam Quality = 0.70	168
10.	Fractional Oil Produced for Injection Rates with Steam Quality = 0.70	168

LIST OF FIGURES (CONT'D)

	<u>Page</u>
11. Cumulative Fluids Produced for Injection Rates with Steam	
Quality = 0.80	169
12. Cumulative Oil Produced for Injection Rates with Steam	
Quality = 0.80	169
13. Cumulative Water Produced for Injection Rates with Steam	
Quality = 0.80	170
14. Fractional Oil Produced for Injection Rates with Steam	
Quality = 0.80	170
15. Cumulative Fluids Produced for Injection Rates with Steam	
Quality = 0.90	171
16. Cumulative Oil Produced for Injection Rates with Steam	
Quality = 0.90	171
17. Cumulative Water Produced for Injection Rates with Steam	
Quality = 0.90	172
18. Fractional Oil Produced for Injection Rates with Steam	
Quality = 0.90	172
19. Average Oil Production Rate for Injection Rates with Steam	
Quality = 0.60	173
20. Average Oil Production Rate for Injection Rates with Steam	
Quality = 0.70	173
21. Average Oil Production Rate for Injection Rates with Steam	
Quality = 0.80	174
22. Average Oil Production Rate for Injection Rates with Steam	
Quality = 0.90	174

LIST OF FIGURES (CONT'D)

	<u>Page</u>
23. Cumulative Oil Steam Ratios for Injection Rates with Steam Quality = 0.60	175
24. Cumulative Oil Steam Ratios for Injection Rates with Steam Quality = 0.70	175
25. Cumulative Oil Steam Ratios for Injection Rates with Steam Quality = 0.80	176
26. Cumulative Oil Steam Ratios for Injection Rates with Steam Quality = 0.90	176
27. Fractional Wellbore Heat Losses for Injection Rates with Steam Quality = 0.60	177
28. Fractional Wellbore Heat Losses for Injection Rates with Steam Quality = 0.70	177
29. Fractional Wellbore Heat Losses for Injection Rates with Steam Quality = 0.80	178
30. Fractional Wellbore Heat Losses for Injection Rates with Steam Quality = 0.90	178
31. Cumulative Heat Losses to the Reservoir for Injection Rates with Steam Quality = 0.60	179
32. Cumulative Heat Losses to the Reservoir for Injection Rates with Steam Quality - 0.70	179
33. Cumulative Heat Losses to the Reservoir for Injection Rates with Steam Quality = 0.80	180
34. Cumulative Heat Losses to the Reservoir for Injection Rates with Steam Quality = 0.90	180

LIST OF FIGURES (CONT'D)

		<u>Page</u>
35.	Preliminary Results of Price of Oil vs. Rate of Return with Steam Quality = 0.60	185
36.	Preliminary Results of Price of Oil vs. Rate of Return with Steam Quality = 0.70	185
37.	Preliminary Results of Price of Oil vs. Rate of Return with Steam Quality = 0.80	186
38.	Preliminary Results of Price of Oil vs. Rate of Return with Steam Quality = 0.90	186
39.	Sensitivity Analysis with Windfall Tax Repealed, ELF = 0.25	189
40.	Sensitivity Analysis with Windfall Tax and Elf = 0	189
41.	Sensitivity Analysis with Windfall Tax Repealed, ELF = 0.0	190
42.	Sensitivity Analysis with Windfall Tax Repealed, ELF = 0.10	190
43.	Sensitivity Analysis with Windfall Tax Repealed, ELF = 0.20	191
44.	Sensitivity Analysis with Windfall Tax Repealed, ELF = 0.30	191
45.	Sensitivity Analysis with Windfall Tax Repealed, ELF = 0.50	192
46.	Sensitivity Analysis with Drilling and Well Completion Cost = \$2,000,000	192
47.	Sensitivity Analysis with Drilling and Well Completion Cost = \$2,200,000	195
48.	Sensitivity Analysis with Drilling and Well Completion Cost = \$2,400,000	195
49.	Sensitivity Analysis with Drilling and Well Completion Cost = \$2,600,000	196

LIST OF FIGURES (CONT'D)

		<u>Page</u>
50.	Sensitivity Analysis with Drilling and Well Completion Cost = \$2,800,000	196
51.	Sensitivity Analysis with Drilling and Well Completion Cost = \$3,000,000	197
52.	Sensitivity Analysis with Surface Equipment and Facilities Cost = \$1,250,000	197
53.	Sensitivity Analysis with Surface Equipment and Facilities Cost = \$2,750,000	200
54.	Sensitivity Analysis with Steam Generator Cost = \$1,100,000	200
55.	Sensitivity Analysis with Treated Water Cost = \$0.10/bbl	204
56.	Sensitivity Analysis with Treated Water Cost = \$0.50/bbl	204
57.	Sensitivity Analysis with Natural Gas Cost = \$1.00/Mcf	205
58.	Sensitivity Analysis with Natural Gas Cost = \$1.50/Mcf	205
59.	Sensitivity Analysis with Inflation Factor = 0.045	209
60.	Sensitivity Analysis with $S_{or} = 0.10$	209
61.	Sensitivity Analysis with $S_{or} = 0.30$	210
62.	Sensitivity Analysis of Cumulative Fractional Recovery with $S_{or} = 0.10$	210
63.	Sensitivity Analysis of Cumulative Fractional Recovery with $S_{or} = 0.30$	211
64.	Sensitivity Analysis of Oil Production Rate with $S_{or} = 0.10$	211
65.	Sensitivity Analysis of Oil Production Rate with $S_{or} = 0.30$	212
66.	Best Case Scenario for Determining Economic Potential of West Sak	212

LIST OF FIGURES (CONT'D)

	<u>Page</u>
67. Worst Case Scenario for Determining Economic Potential of West Sak	216
<u>CHAPTER FIVE</u>	
1. Schematic of the Steam/Solvent Flood Apparatus	233
2. Schematic of the Density Measurement Apparatus	236
3. Cumulative Recovery vs. Pore Volumes Injected (Equivalent Water) for Runs 1 and 2	242
4. Cumulative Water/Oil Ratio vs. Pore Volumes Injected for Runs 1 and 2	242
5. Cumulative Recovery vs. Pore Volumes Injected for Steam and High-Temperature CO ₂ /Steam Runs (Runs 1, 3, 4 and 5)	244
6. Cumulative Water/Oil Ratio vs. Pore Volumes (Runs 1, 3, 4 and 5)	244
7. Cumulative Recovery vs. Pore Volumes Injected for High-Temperature and Low Temperature CO ₂ /Steam Runs (Runs 4, 5, 6 and 7)	246
8. Cumulative Water/Oil Ratio vs. Pore Volumes Injected for (Runs 4, 5, 6 and 7)	246
9. Distillation Experiments for Steam and High-and-Low-Temperature 1:3 Molar Ratio of CO ₂ /Steam	247
10. Percentage of C ₇ -C ₁₇ in Produced Oil Samples for Runs 1, 5 and 7	251
11. Percentage of C ₁₈ -C ₂₉ in Produced Oil Samples for Runs 1, 5 and 7 ...	251
12. Effect of Temperature on Oil Density for One Pore Volume Effluent Oil Sample from Run 1	253
13. Cumulative Recovery vs. Pore Volumes Injected for Steam and Nitrogen Runs (Runs 8 and 9)	255

LIST OF FIGURES (CONT'D)

	<u>Page</u>
14. Cumulative Water Oil Ratio vs. Pore Volumes Injected (for Runs 8 and 9)	255
15. Cumulative Recovery vs. Pore Volumes Injected for High and Low-Temperature Methane/Steam Runs (Runs 10 and 11)	256
16. Cumulative Water Oil Ratio vs. Pore Volumes Injected (for Runs 10 and 11)	256
17. Temperature Profile for Run 1 (Steam Alone)	258
18. Pressure Drop Profile for Run 1	258
19. Temperature Profile for Run 4 (1:3 Molar Ratio of CO ₂ /Steam @ 660°F)	259
20. Pressure Drop Profile for Run 4	259
21. Temperature Profile for Run 8 (1:4 Molar Ratio of Nitrogen/Steam)	261
22. Pressure Drop Profile for Run 8	261
23. Temperature Profile for Run 9 (1:3 Molar Ratio of Nitrogen/Steam)	262
24. Pressure Drop Profile for Run 9	262
25. Temperature Profile for Run 10 (1:3 Molar Ratio of Methane/Water)	263
26. Pressure Drop Profile for Run 11	263
 <u>CHAPTER SIX</u>	
1. Model Configuration	266
2. Cross-Section of the Core Flood Model	270
3. Effect of Diffusivity Ratio on Heat Frontal Movement	280

LIST OF FIGURES (CONT'D)

	<u>Page</u>
4. Varying the Inner Layer Biot Number	281
5. Varying the Outer Layer Thickness	282

LIST OF TABLES

	<u>Page</u>
<u>CHAPTER ONE</u>	
1. Log-Derived Data For Selected Wells in the West Sak Sands	8
2. Petrophysical Properties of West Sak Upper Sands	8
3. Petrophysical Properties of West Sak Lower Sands (Sand 1)	8
4. Petrophysical Properties of West Sak Lower Sands (Sand 2)	8
5. Petrophysical Properties of West Sak Lower Sands (Sand 3)	9
6. Petrophysical Properties of West Sak Lower Sands (Sand 4)	9
<u>CHAPTER TWO</u>	
1. Constant Composition Expansion of West Sak Crude at 80°F	31
2. Differential Expansion of West Sak Crude at 80°F	33
3. West Sak Oil Density at 80°F	34
4. West Sak Crude Viscosity Measurements at 80°F	35
5. Constant Composition Expansion of 60 Mol% CO ₂ - 40 Mol% West Sak Crude Mixture at 80°F	40
6. Constant Composition Expansion of 80 Mol% CO ₂ - 20 Mol% West Sak Crude Mixture at 80°F	43
<u>CHAPTER THREE</u>	
<u>PART I</u>	
1. Compositions (Mol%) of Recombined West Sak Crude, Prudhoe Bay Natural Gas (PBG) and Natural Gas Liquids (NGL)	64
2. Summary of Slim Tube Displacement Tests For West Sak Crude With CO ₂ as Solvent at 100°F	65
3. Summary of Slim Tube Displacement Tests For West Sak Crude With N-Butane as Solvent	65

LIST OF TABLES (CONT'D)

	<u>Page</u>
4. Summary of Slim Tube Displacement Tests For West Sak Crude With Mixtures of PBG and NGL as Solvent	68
<u>PART II</u>	
1. Overall Compositions of CO ₂ - West Sak Crude Mixtures	87
2. Composition of Mixture of 20% NGL/80% Prudhoe Bay Gas with West Sak Crude	95
<u>PART III</u>	
1. Experimental Results on Static Asphaltene Precipitation Tests For West Sak (Tank) Oil-A	105
2. Compositional Changes (Mol%) and Density Changes in West Sak Crude After Asphaltene Precipitation by N-Pentane and N-Butane	106
3. Experimental Results on Static Asphaltene Precipitation Tests For West Sak (Tank) Oil-B	107
4. Effect of Amount of N-Heptane Used for Washing Asphalts on the Resin Dissolution	109
5. Effect of CO ₂ Addition to Recombined West Sak Oil A on the Asphaltene Precipitation (at 1705 psia, 80°F)	111
6. Effect of Pressure on Amount of Asphaltene Precipitation 30 Mol% CO ₂ : 70 Mol% West Sak Crude A (Recombined at 1705 psia & 80°F)	112
7. Effect of Pressure on Amount of Asphaltene Precipitation 50 Mol% CO ₂ : 50 Mol% West Sak Crude A (Recombined at 1705 psia & 80°F)	113

LIST OF TABLES (CONT'D)

	<u>Page</u>
<u>CHAPTER FOUR</u>	
1. Estimated Costs Used in Initial Sensitivity Analysis	164
2. Predicted Oil Recovery for Various Steam Qualities and Injection Rates	164
3. Preliminary Results Indicating Required Price Range of Oil for Economic Feasibility in West Sak	183
4. Results From Sensitivity Analysis of Windfall Profits Tax and Possible Values of ELF	188
5. Results From Sensitivity Analysis of Drilling and Well Completion Costs	198
6. Results From Sensitivity Analysis of Surface Equipment and Steam Generator Costs	202
7. Results From Sensitivity Analysis of Treated Water and Fuel Costs for Generating Steam	206
8. Results From Sensitivity Analysis of Inflation	208
9. Results From Sensitivity Analysis of Residual Oil Saturation Values ...	214
10. Results From Best and Worst Case Scenarios For Steamflooding in West Sak	214
<u>CHAPTER FIVE</u>	
1. West Sak Crude Oil Properties	238
2. Composition (Mol%) of Recombined and Dead West Sak Crude	238
3. Flooding Experimental Variables	240
4. Analysis of the Produced Oil Samples From Run #1 (steam 660°F)	249

LIST OF TABLES (CONT'D)

	<u>Page</u>
5. Analysis of the Produced Oil Samples From Run #5 (1:4 Molar Ratio at 660°F)	249
6. Analysis of the Produced Oil Samples From Run #7 (1:4 Molar Ratio at 570°F)	250
7. Effect of CO ₂ on the Density of Produced Oil Samples From (Run 1)	250
 <u>CHAPTER SIX</u>	
1. Dimensionless Parameters for Program Validation (After Ref. 2)	279
2. Rock Thermal Conductivity Data	284

EXECUTIVE SUMMARY

This report summarizes three years of research efforts on thermal and miscible processes for recovery of heavy oil from West Sak reservoir, which was jointly funded by the U.S. Department of Energy (Morgantown Energy Technology Center) and the University of Alaska Fairbanks (Petroleum Development Laboratory).

West Sak reservoir located on the North Slope of Alaska is a mega-giant and the largest known heavy oil accumulation in the United States. It is estimated to contain up to 25 billion barrels of heavy oil in place. West Sak sands extend over 260 square miles area within the Kuparuk River Unit (KRU) and outside of the KRU northeast boundaries in to the Milne Point Unit (MPU) at depths ranging from 2300 feet to 4500 feet below the surface. Due to close proximity of West Sak sands to overlying permafrost, the reservoir temperatures are very low (45 to 100°F). Degradation of crudes at shallow depths and low reservoir temperatures make the West Sak crude very viscous. The high degree of variation in the oil gravity (14 to 22.5°API) and oil viscosity (50-3000 cp.) in these highly heterogeneous, unconsolidated, fine-grained sands; presence of clay minerals; low permeabilities (10 to 140 milidarcies); highly faulted structure; and proximity to the overlying permafrost, make the West Sak reservoir, a unique, special heavy oil reservoir. The possibility of sharing of Kuparuk River Unit facilities which currently exist makes the development and production of West Sak reservoir, a near-term target.

The absence of natural drive mechanism in the reservoir demonstrated by ARCO Alaska Inc.'s waterflood pilot in 1984-86, and high viscosities of West Sak oil make the reservoir, a target for enhanced oil recovery processes. A single enhanced oil recovery method may not be sufficient to produce this huge resource in an effective manner. For example, thermal recovery processes may be more applicable to heavier crudes in the shallower sand members, while miscible processes may be

more suitable for the recovery of lighter crudes in the deeper sections of the West Sak reservoir.

Based on the analysis of well log data, a reservoir description of West Sak sands is presented in the first chapter. Understanding of the West Sak reservoir framework and structural characteristics is a pre-requisite for design, development and application of any enhanced oil recovery process. Such understanding will include the knowledge of the basinal analysis, the source and origin of hydrocarbons, the migrational path and attributes, the spatial distribution and continuity of sand members, the microscopic and macroscopic heterogeneities, the depositional environment and the variation of reservoir rock and fluid properties. Cross-sectional study shows that the West Sak sands and lower West Sak sands. The upper West Sak sands are further divided into two sand members and the lower West Sak sands into four sand members. For each sand member, petrophysical properties such as water saturation, porosity and pay zone thickness were obtained. Contour maps, cross-sectional correlations and 3-D surface plots were used to describe the spatial distribution of these parameters within the pay zones. Correlations of the SP, GR and resistivity logs were used to determine lateral and vertical gradients of the dominant lithofacies. The spatial variation within each lithofacies distribution were used to interpret the depositional environment of these sands. West Sak sands were deposited during a major regressive sea with minor cyclic sea level fluctuations. The lower West Sak sand members were lesser sorting and increased fine particles suggest inner shelf deposition; while the upper sands with coarser nature show on increasing energy of deposition. The West Sak reservoir description presented helps to address some of the problems concerning the reservoir heterogeneity, the continuity of pay zone, presence of local structures such as folds, faults etc. Generation of database, development of 3-D reservoir model for West Sak based on

flow units to be used for reservoir simulation studies are some of the aspects on which currently further work is in progress.

The second chapter of this report describes experimental work conducted to measure PVT properties of West Sak oil, study phase behavior of CO₂-West Sak crude mixtures and to determine effect of gas solubility on viscosity of West Sak crude at various pressures and temperatures. PVT data gathered includes constant composition expansion and differential expansion at 80°F. CO₂-West Sak crude phase behavior data were gathered from the viewpoint of CO₂ flooding feasibility study. Results show that CO₂ reduces oil viscosity by 75% and swells West Sak crude by 10% at reservoir conditions (1705 psia and 80°F). Presence of three phase region (liquid-liquid-vapor) and deposition of black organic residue were also observed. The visual observation indicates that precipitation is greater at higher pressures and for high CO₂ contents in the CO₂-oil mixtures. Viscosity measurements were compared with various correlations reported in literature. The experimental PVT and fluid property measurements obtained for West Sak crude are useful in equation of state predictions, compositional reservoir simulation studies and in studies of miscible and thermal recovery processes.

Rest of the report describes studies pertaining to miscible and thermal recovery processes which are considered feasible based on the preliminary EOR screening criteria. These processes include miscible flooding with enriched hydrocarbon gas solvent, carbon dioxide injection, steamflooding and gas additives (CO₂, N₂, CH₄) to steam.

Slim Tube Displacement (STD) tests were conducted to evaluate the ability of various solvents such as CO₂, n-butane and enriched hydrocarbon gas mixtures (Prudhoe Bay natural gas enriched by natural gas liquids) to achieve miscibility with West Sak oil. In order to understand mechanism of displacements, equation of state

predictions were performed. Equation of state predictions include determination of pressure-composition diagram and thermodynamic compositional path in a multi-contact process for a given solvent mixture. Results indicate that CO₂ can not generate multi-contact miscibility with West Sak crude at reservoir conditions. The compositional path followed by immiscible CO₂ drive indicates a combined vaporizing-condensing mechanism. Displacements with n-butane (thermodynamically first contact miscible solvent) at 80°F showed 80% oil recovery at 1.2 pv injection. In order to evaluate effect of thermal enhancement of miscible displacement process, displacements with n-butane at 250°F were conducted and showed 74% oil recovery at 1.2 pv injection. STD tests with enriched hydrocarbon gas mixtures (PBG enriched by NGL) were interpreted by technique of methane spike disappearance phenomena. EOS predictions indicate that displacements with PBG/NGL mixtures (enriched hydrocarbon gas solvent) are condensing-vaporizing type. EOS predictions were used to determine minimum enrichment of Prudhoe Bay natural gas (PBG) by natural gas liquids (NGL) to achieve dynamic miscibility with West Sak crude at reservoir conditions.

In processes such as water alternating gas (WAG) for miscible or immiscible displacement, significant amount of water is injected into the reservoir. In light of this, EOS predictions were performed to understand the effect of presence of water on the phase behavior and miscibility conditions for West Sak crude - solvent mixtures. Results indicate that presence of water can possibly change the volumes and compositions of existing phases. The degree of change in the phase diagrams is function of the water contents of overall mixtures of solvent-water-crude. Results also indicate that presence of water is beneficial in that it reduces the minimum enrichments required to achieve dynamic miscibility between PBG-NGL mixtures and West Sak crude.

Asphaltene precipitation during miscible flooding has been known to be problematic specifically for low permeability reservoirs. Asphaltene precipitation can cause reduction in solvent injectivity or oil productivity due to permeability reduction and result in lower recoveries. For this reason, asphaltene precipitation tests were conducted for various solvents such as CO₂, ethane, propane, n-butane, n-pentane, n-heptane, PBG and NGL. From the solids precipitated, asphaltenes and resins were separated and measured. Effect of solvent/oil dilution ratio on the amount of precipitation was studied. Gas chromatographic analysis shows precipitation of asphaltene alters crude oil composition. This indicates that EOS predictions to calculate minimum miscibility pressure or enrichments should incorporate asphaltene precipitation effect. Currently, further work is in progress in this direction. Effects of pressure and CO₂ mol% on the amount of asphaltene precipitation for CO₂-West Sak crude mixtures were also studied.

A simplified steamflood performance prediction model was developed, validated and integrated with an economic model to study feasibility and recovery potential of steamflooding for West Sak reservoir. A sensitivity analysis was conducted to determine optimum conditions necessary for a steamflood. Results of this study indicate a minimum price range of \$18-25/bbl is necessary for steamflooding to be economic in the West Sak reservoir. The analysis is based on a simplified model and does not consider reservoir heterogeneity or other aspects such as swelling of clays at high temperatures.

Laboratory displacement studies with one dimensional (linear) sand packs were undertaken to evaluate the effects of addition of non-condensable gases such as CO₂, N₂ and methane to steam on the recovery of West Sak oil. Conclusions of this experimental work are as follows:

- Addition of CO₂, N₂ or methane to steam improves recovery, rate of recovery and decreases heat input (or steam injection temperature) over steam injection alone.
- CO₂/steam injection runs indicate that there is optimum CO₂/steam ratio. 1:1 molar ratio increases recovery by 5.5% where as, 1:3 molar ratio increases recovery by 12.8% over steam alone.
- N₂/steam injection runs also indicate that there is optimum N₂/steam ratio. 1:3 molar ratio increases recovery by 2.8% whereas, 1:4 molar ratio increases recovery by 8% over steam alone.
- The presence of a free gas phase reduces the ultimate recovery of a conventional steamflood.
- The addition of CO₂ to steam at the same temperature increases the yield for the same amount of water distilled.

Since the recovery efficiency of the steam-solvent process is a function of phase behavior, it is desirable to conduct laboratory displacement experiments at the same pressures and temperatures existing in the reservoir. To accomplish this goal, a one-dimensional heat transfer model was developed to describe the temperature distribution and heat frontal movement in the linear reservoir and in laboratory displacement experiments.

CHAPTER ONE

WEST SAK RESERVOIR DESCRIPTION

A. Introduction

West Sak reservoir located on the North Slope of Alaska is a megajant and the largest known heavy oil accumulation in the United States. The West Sak sands occur above the Kuparuk sands and these oil bearing sands were discovered in 1969 at Chevron Kaveavak Point Well #1. The West Sak reservoir is estimated to contain up to 25 billion barrels of heavy oil in place (Werner, 1985). The high degree of variation in the oil gravity (14 to 22.5°API) in these highly heterogeneous, unconsolidated, fine-grained sands; presence of clay minerals; low permeability; highly faulted structure; and close proximity to the overlying permafrost, makes it a unique, special heavy oil reservoir. West Sak sands extend over 260 square miles area within and outside Kuparuk River Unit boundaries at a depth ranging from 2300 to 4500 feet below surface. Due to close proximity to overlying permafrost, the reservoir temperatures vary between 45 - 100°F. Degradation of crude at shallower depths and low reservoir temperatures makes the West Sak crude viscous. The viscosity of crude varies between 50-1000 cp, the salinity of formation water varies in the range of 1,500 - 35,000 ppm and gross pay varies between 200 - 450 feet (Werner, 1985). These sands have a gentle dip of 1 - 2° (130 feet per mile) from north to northeast.

Understanding of the reservoir framework and structure is a prerequisite for design and application of any enhanced oil recovery process. Such understanding will require knowledge of the basinal analysis, the source and origin of the hydrocarbons, the migrational attributes, the migrational path, the spatial distribution and continuity of sand members, the microscopic and macroscopic

heterogeneities, the depositional environment and the variation of reservoir rock and fluid properties.

Based on the analysis of well log data, a reservoir description of West Sak sands is presented (Panda et al, 1989). Petrophysical properties such as water saturation, porosity and pay zone thickness are obtained from well logs. Contour maps, cross-sectional correlations and 3-D surface plots are used to determine the spatial distribution of these parameters within the pay zones. Correlations of the Spontaneous Potential (SP), Gamma Ray (GR) and resistivity logs of several wells from the West Sak field are used to determine the lateral and vertical gradients of the dominant lithofacies of the West Sak. The spatial variation within each lithofacies distributions are used to interpret the depositional environment of these sands.

B. Geology of Alaskan North Slope

The major oil fields of the state of Alaska lie in the northeastern part of the 65,000 square miles of the North Slope region (Figure 1). This area is located on the northern coast of Alaska between the National Petroleum Reserves - Alaska (NPRA) and the Arctic National Wildlife Refuge (ANWR). In terms of oil-bearing reservoirs, the North Slope region can be divided into two major units - - the Prudhoe Bay Unit and the Kuparuk River Unit (Figure 2). The geology of this region has been studied by several investigators (Jamison et al, 1980; Carman and Hardwick, 1983; Molenaar, 1983; van Poolan and associates, 1978; and Werner, 1985). A summary of the published literature on the geology of North Slope is provided to facilitate understanding of the reservoir description discussed later.

The Barrow Arch and the Colville Trough (east-west oriented geosyncline), are the dominant features in the North Slope region. The thickness of the sediment varies from 25,000 feet at Point Barrow to 30,000 feet at the deepest region (Carman

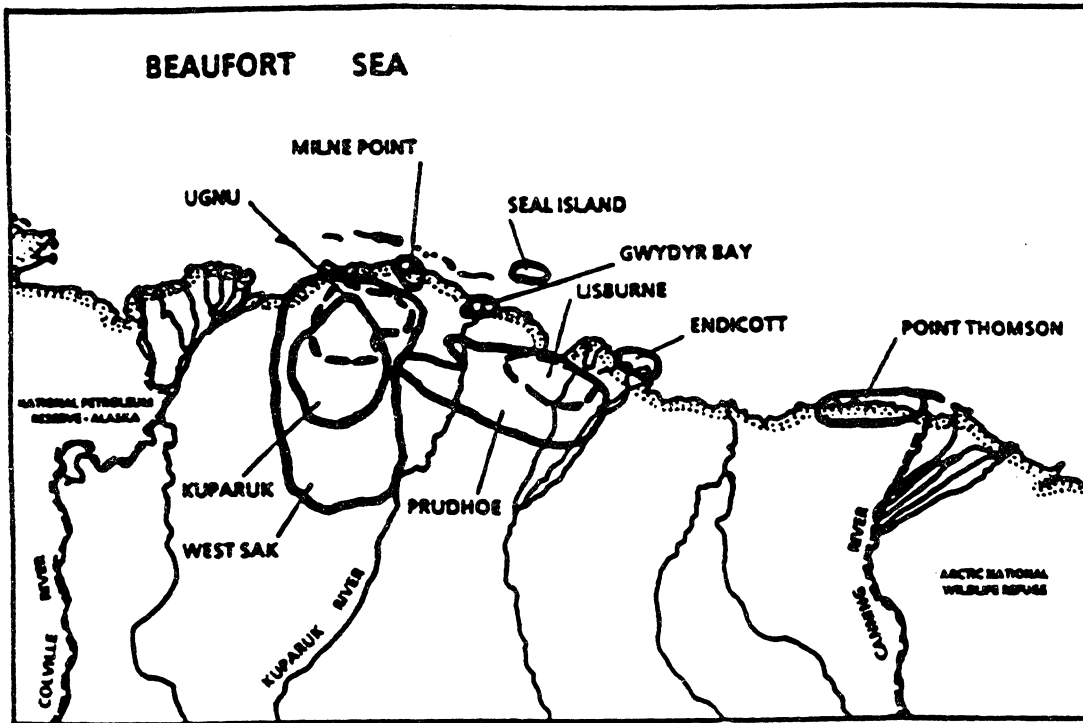


Figure 1: Location Map of Major Oil Fields in Alaskan North Slope

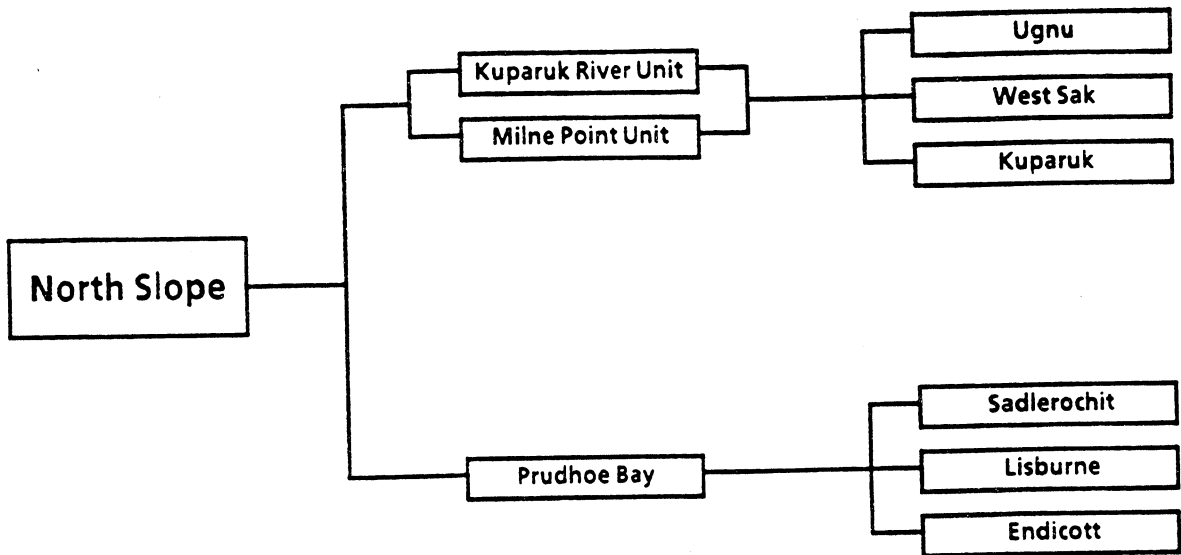


Figure 2: A Schematic Showing the Hierarchy of the Major Reservoir Units of the Alaskan North Slope

and Hardwick, 1983). The lithological sequence can be described as follows. The non-productive basement rocks consists of the argellites and the quartzetic grey wackes of Pre-Mississippian Neuruokpuk Formation. The upper surface is termed the Colville Trough towards the Brooks Range. The Mississippian and overlying rocks through the lower most Cretaceous rocks are termed the Ellesmerian Sequence. The Brookian Sequence (Lower Cretaceous through Tertiary) overlies the Ellesmerian Sequence.

The carbonate and elastic formations of the Ellesmerian Sequence can be described in ascending order as Endicott, Lisburne, Sadlerochit Group, Shublik Formation, Sag River Formation, Kingkak Shale and Kuparuk River Formation. It has been suggested that these formations have their source in the north. The Kuparuk River formation conformably overlies the Kingkak Shale and is unconformably overlain by the Dot River Sands and shales of the Late Cretaceous. The Kuparuk River Formation is the uppermost unit of the Ellesmerian Sequence. There is a pronounced unconformity between the Ellesmerian Sequence and the Brookian Sequence.

The Brookian Sequence can be described as Okpikmak Formation, Torok Formation and Nanushack Group (all Lower Cretaceous), Colville Group (Upper Cretaceous) and Saga Vanirktak Formation (Tertiary). The source of sediments for Brookian Sequence is in the south. Formations in the Brookian Sequence are thick in the south and thin out gradually towards north. On the other hand, the Upper Cretaceous and Tertiary Units progressively thicken to the north-east across the eastern North Slope due to the north-eastward progression of the depocenters.

The comprehensive study of the stratigraphic and structural framework of the heavy oil bearing sands has been done by several investigators (Jamison et al; 1980; Carman and Hardwick, 1983). These geologic studies provide a basis for further delineation of these shallow sands.

The "shallow sands" strata comprises a portion of the Late Cretaceous and Early Tertiary Shallow Marine and Deltaic complex which occurs in the Kuparuk River area. Figure 3 is a generalized stratigraphic column for the Kuparuk River area showing West Sak, Ugnu and other shallow oil bearing intervals. The stratigraphy of this sequence is discussed in detail by Molenaar (1983).

Carman and Hardwick's (1983) geochemical work indicates that crude oil in the shallow sands has the same source of oil as in the deeper Kuparuk, Sadlerochit and Lisburne reservoirs, but are biodegraded. They postulate that the mid-to-late Tertiary regional tilting which reduces the amount of original closure on the Prudhoe Bay Sadlerochit structure spilled the hydrocarbons to the west towards shallower reservoirs. This secondary migration accounts for the most of the volume of oil in the shallow sands.

Werner's (1985) description of West Sak Sands is briefly summarized here. West Sak Sands are divided into two major sand groups. These are the Upper West Sak Sands and the Lower West Sak Sands. These Late Cretaceous Sands have a gentle dip of 1-2° (130 feet per mile) from north to northeast and lie at a depth between 2300 and 4100 feet below the surface. These sands consist of a very fine to fine-grained sands and silty sands interbedded with silts and muds. Sand grains consist of quartz, lithic rock fragments and feldspar with traces of mica and glauconite. They are unconsolidated and friable. They are classified as litharenites and lithic wackes.

The thickness of these sands varies from 450 feet in the south-west to 200 feet in the north-east. These sands represent a transition from inner shelf deposition for the lower sand group to delta front deposition for the upper sand group. These sands are intersected by N-S trending faults. The throw on these faults may range from 50 to 150 feet. The general trapping condition of oil in West Sak sands is due to combination of faults and stratigraphy (Werner, 1985; Carman and Hardwick, 1983; and Molenaar, 1983). Core studies indicate that the porosity in the West Sak Sands

ERA	SYSTEM	SERIES	GROUP	FORMATIONS Members	HEAVY OIL ZONES KUPARUK AREA
CENOZOIC	QUAT.	HOLOCENE / PLEISTOCENE		GUBIK FM.	
	TERTIARY	PLIOCENE		SAGAVANIRKTOK FORMATION	
		MIOCENE			
		OLIGOCENE			
		EOCENE			
		PALEOCENE			
MESOZOIC	CRETACEOUS	UPPER	COLVILLE GROUP (1)	PRINCE CREEK FM.	Lower Ugnu Sands
				SCHRADER BLUFF FM.	West Sak Sands
				SEABEE FORMATION	
		LOWER		UGNURAVIK GROUP (3)	
	KALUBIK FM.				
	KUPARUK FM.				
	JURASSIC				MILUVEACH FM.
				KINGAK SHALE	

Figure 3: A Generalized Stratigraphic Column for Kuparuk River Area Depicting Heavy Oil Bearing Sands

can be as high as 35% and horizontal air permeability ranges between 10-140 millidarcy.

C. Classification and Spatial Distribution of the West Sak Sands and Petrophysical Properties

West Sak reservoir description presented here is based on the well log analysis study conducted at the University of Alaska Fairbanks. The detailed description of this work are provided in the following references (Panda, 1988; Panda et al. 1989, Zhang, 1989). The log-derived data presented here were obtained from the thirteen wells in the West Sak field. A computer-aided well log data interpretation procedure was developed using the LOGCALC computer programs written by Scientific Software Intercomp (SSI, 1986). Well log traces were normalized by applying the interactive graphical techniques of histogram and parameter crossplotting built into the log analysis software. Data smoothing and bed boundary determination were performed with the aid of Walsh functions also included in the computer programs (Panda et al, 1989).

The results of well log data analysis from the selected wells in West Sak reservoir are summarized in the Table 1. Table 1 shows the potentially hydrocarbon-bearing interval for which the log responses were analyzed, the average porosity, average water saturation and the net pay thicknesses. By visual inspection of all the well log traces, the depth of occurrence of hydrocarbon-bearing zones at various depths in the West Sak sands was determined. Tables 2 through 6 give the top and bottom depths of each individual hydrocarbon-bearing sand as they occur at different well locations. In some wells certain sand members are absent. This may be due to truncation of sand bodies or may be due to inadequate log data.

To define the spatial distribution of the West Sak sands, two stratigraphic cross-sections were made. The cross-section lines AA' (SW-NE) and BB' (NW-SE) shown in

Table 1: Log-Derived Data For Selected Wells in the West Sak Sands

Well Name	Interval* (ft)	Weighted Mean Effective Porosity (%)	Weighted Mean Water Saturation (%)	Net Pay Thickness (ft)	Net to Gross Ratio
West Sak No 1	3746-4044	34.6	32.5	116	0.39
West Sak No 2	3304-3530	28.7	19.0	84	0.37
West Sak No 3	2628-2882	29.95	33.6	41	0.16
West Sak No 5	3332-3428	26.8	18.0	12	0.13
West Sak No 9	2678-2930	35.5	42.2	50	0.20
West Sak No 8-10	2695-3174	37.6	41.9	55	0.11
West Sak No 11	2324-2694	28.6	44.3	27	0.07
West Sak No 17	3516-3620	15.8	31.3	17	0.12
West Sak No 18	2526-2720	36.3	38.3	13	0.07
East Ugnu No 1	3386-3654	32.6	44.2	27	0.10
Kuparuk No 1G-7	3408-3638	24.8	34.6	64	0.28
Kuparuk No 3B-14	2538-3025	38.3	41.0	136	0.28
Milne Pt. No. N-1B	3555-3806	24.2	24.1	56	0.22

* Represents interval that is potentially hydrocarbon bearing. Properties of individual West Sak sand members are listed in Tables 2 & 6.

Table 3: Petrophysical Properties of West Sak Lower Sands (Sand 1)

Well Name	Interval (ft)	Net Pay (ft)	Average ϕ (%)	Average Sw (%)
West Sak No 1	3860-3874	11	35.6	38.7
West Sak No 2	3428-3434	5	28.3	16.5
West Sak No 3	2753-2772			
West Sak No 5	No log data	available		
West Sak No 9	2852-2860	6	33.5	40.5
West Sak No 8-10	2934-2945	3	33.7	45.3
West Sak No 11	2566-2575		23.9	59.3
West Sak No 17	3714-3722		16.9	79.8
West Sak No 18	2526-2536	4	36.4	35.4
East Ugnu No. 1	3511-3530	5	31.6	42.2
Kuparuk No 1G-7	3533-3540	2	21.1	46.2
Kuparuk No 3B-14	2698-2740	37	39.8	40.5
Milne Pt. No. N-1B	3677-3684	4	16.9	37.1

Table 2: Petrophysical Properties of West Sak Upper Sands

Well Name	Interval (ft)	SAND 1				SAND 2			
		Net Pay (ft)	Average ϕ (%)	Average Sw (%)	Net Pay (ft)	Average ϕ (%)	Average Sw (%)		
West Sak No 1	3746-3784	32	33.3	26.4	3810-3844	34	34.8	32.9	
West Sak No 2	3304-3334	30	29.2	9.1	3364-3404	37	29.2	13.8	
West Sak No 3	2628-2672	18	30.3	27.6	2706-2734	10	25.2	36.6	
West Sak No 5	3332-3374	10	27.0	18.1	3410-3428	1	24.5	17.5	
West Sak No 9	2628-2716	33	36.5	43.0	2770-2786	9	33.6	39.7	
West Sak No 8-10	2695-2747	7	35.4	37.5	2804-2840	12	38.1	40.1	
West Sak No 11	2324-2364	17	27.7	43.5	2402-2432	9	30.7	45.2	
West Sak No 17	3516-3558	4	17.8	27.5	3597-3620	8	14.8	33.5	
West Sak No 18	No log data	available			No log data	available			
East Ugnu No. 1	3386-3424	8	34.0	42.5	3459-3490	14	31.6	45.5	
Kuparuk No 1G-7	3408-3455	23	28.1	36.6	3477-3512	27	21.9	30.7	
Kuparuk No 3B-14	2538-2559	21	40.0	37.1	2575-2613	36	39.1	42.8	
Milne Pt. No. N-1B	3555-3570	10	21.3	32.1	3582-3617	20	32.8	19.0	

Table 4: Petrophysical Properties of West Sak Lower Sands (Sand 2)

Well Name	Interval (ft)	Net Pay (ft)	Average ϕ (%)	Average Sw (%)
West Sak No. 1	3930-3940	9	36.7	33.2
West Sak No. 2	3456-3460	4	31.8	18.4
West Sak No. 3	2796-2806	4	31.8	38.1
West Sak No. 5	No log data	available		
West Sak No. 9	2892-2904	1.5	35.4	47.9
West Sak No. 8-10	3048-3076	20	37.9	41.2
West Sak No. 11	2630-2638		20.7	67.7
West Sak No. 17	3770-3790		16.9	79.8
West Sak No. 18	2612-2618	3	35.5	42.0
East Ugnu No. 1	3622-3654	2	31.6	47.7
Kuparuk No. 1G-7	3588-3605	5	26.8	38.3
Kuparuk No. 3B-14	2774-2807	29	39.8	42.7
Milne Pt. No. N-1B	3719-3750	12	17.2	26.1

Table 5: Petrophysical Properties of West Sak Lower Sands (Sand 3)

Well Name	Interval (ft)	Net Pay (ft)	Average ϕ (%)	Average S_w (%)
West Sak No. 1	3972-3984	6	39.2	42.0
West Sak No. 2	3472-3476	4	28.9	20.3
West Sak No. 3	2815-2824	1	29.6	46.1
West Sak No. 5	No log data	available		
West Sak No. 9	2918-2930	0.5	31.3	44.8
West Sak No. B-10	3112-3132	11	37.7	45.8
West Sak No. 11	2688-2694	2	27.8	47.5
West Sak No. 17	3836-3844	-	18.3	79.8
West Sak No. 18	2692-2720	6	36.7	38.5
East Ugnu No. 1	-	-	-	-
Kuparuk No. 1G-7	3637-3658	8	24.6	35.6
Kuparuk No. 3B-14	2898-2907	2	26.6	49.8
Milne Pt. No. N-1B	3786-3806	11	21.3	26.3

Table 6: Petrophysical Properties of West Sak Lower Sands (Sand 4)

Well Name	Interval (ft)	Net Pay (ft)	Average ϕ (%)	Average S_w (%)
West Sak No. 1	4032-4044	4	27.6	45.8
West Sak No. 2	3524-3530	4	29.8	14.5
West Sak No. 3	2872-2882	8	31.3	41.3
West Sak No. 5	No log data	available		
West Sak No. 9	-	-	-	-
West Sak No. B-10	3167-3174	4	45.2	43.8
West Sak No. 11	2726-2730	-	18.9	67.3
West Sak No. 17	3969-3974	-	13.4	91.3
West Sak No. 18	-	-	-	-
East Ugnu No. 1	-	-	-	-
Kuparuk No. 1G-7	-	-	-	-
Kuparuk No. 3B-14*	2941-2969	6	26.8	42.8
Milne Pt. No. N-1B	3888-3905	-	10.1	71.0

* Only this well has Sand #5 in the interval 3007-3026 ft with net pay of 6 ft, average porosity of 25% and average water saturation of 35.9%

Figure 4 refer to the stratigraphic cross-sections in Figures 5 and 6, respectively. Only these wells that showed reasonably porous and permeable sands within the range of 2300-4500 feet were included in these cross-sections. Based on these cross-sections, the West Sak sands are classified as follows:

- (1) Upper West Sak Sands
 - Sand 1 (top)
 - Sand 2 (bottom)
- (2) Lower West Sak Sands
 - Sand 1 (top)
 - Sand 2
 - Sand 3
 - Sand 4 (bottom)

These sand beds are shown in the SW-NE and NW-SE cross-sections presented in Figures 5 and 6 respectively. Note the unit along the x-axis is the grid unit. One grid unit is equivalent to six miles. To further enhance the spatial distribution of West Sak Sands, contour maps of various parameters are presented. The data used for the contour maps and 3-D surface plots are summarized in Tables 2 through 6. Figures 7 through 12 present isopach maps for each major sand member. In addition, the areal distribution of porosity is depicted in Figures 13A and 13B and the areal distribution of water saturations is depicted in Figures 14A and 14B.

A close examination of the contour maps and the cross sections show that the West Sak sands rise to a shallower depth towards south-east region of the Kuparuk River Unit. In the north-east and east region, the West Sak sands occur at greater depths. For example, the top of West Sak Upper Sand 1 occurs in West Sak No. 3 well at 2628 feet, whereas this sand is encountered at 3746 feet in West Sak No. 1. The isopach map (Figure 7) indicate thinning of West Sak Upper Sand 1 occurs towards the northwest and southwest. The SW-NE cross-section further suggests that the West

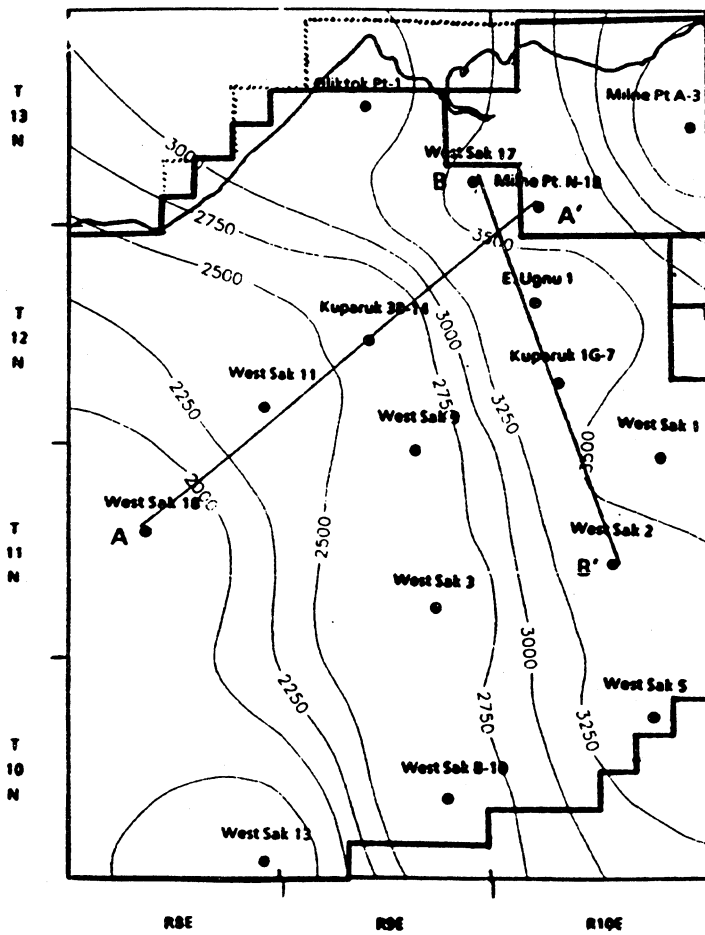


Figure 4: Contour Map Showing Depths to the Top of West Sak Upper Sand 1 (AA': SW-NE Cross-Section, BB': NW-SE Cross-Section)

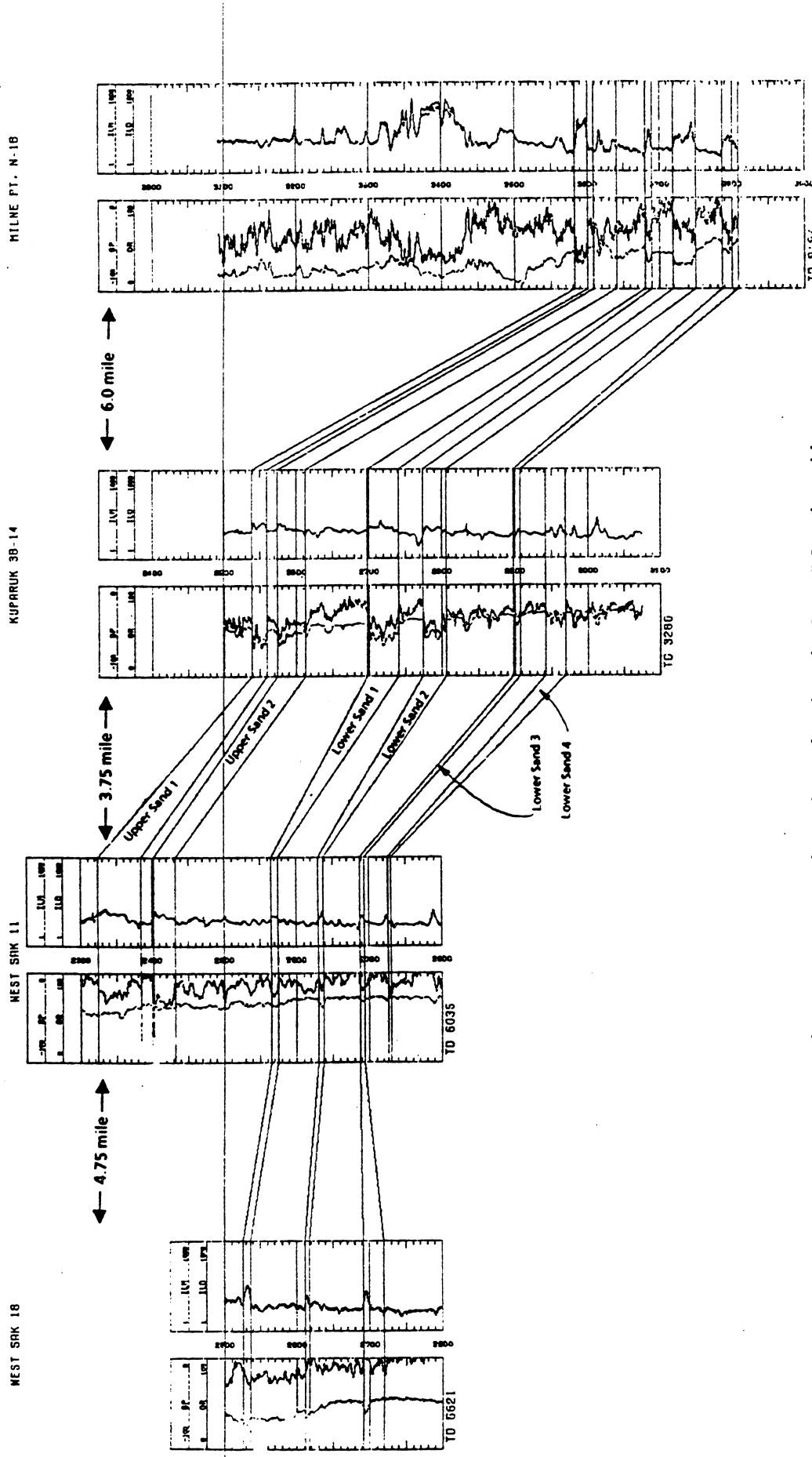


Figure 5: West Sak Sands Depicted on the SW-NE Stratigraphic Cross-Section AA'

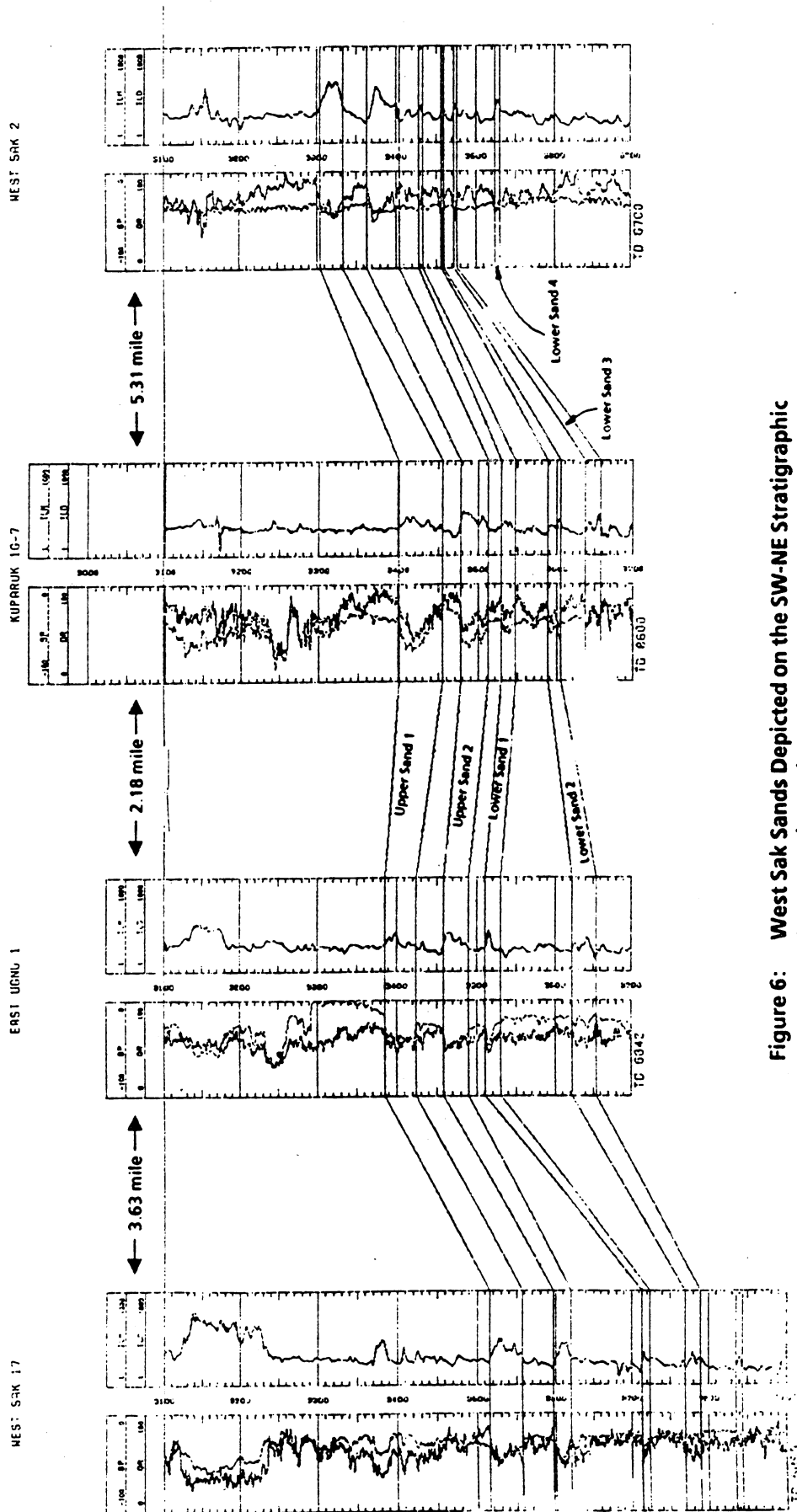


Figure 6: West Sak Sands Depicted on the SW-NE Stratigraphic Cross-Section BB'

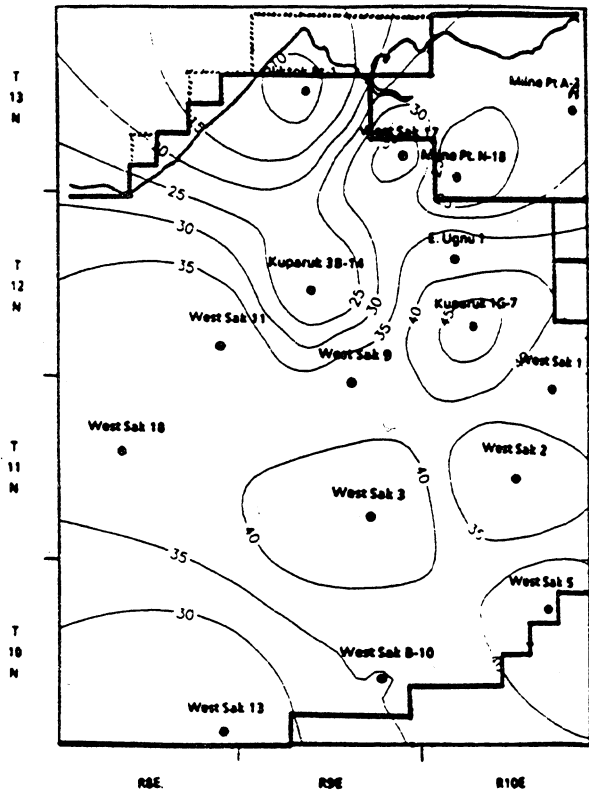


Figure 7: West Sak Upper Sand 1 Gross Pay Zone Thickness Contour Map

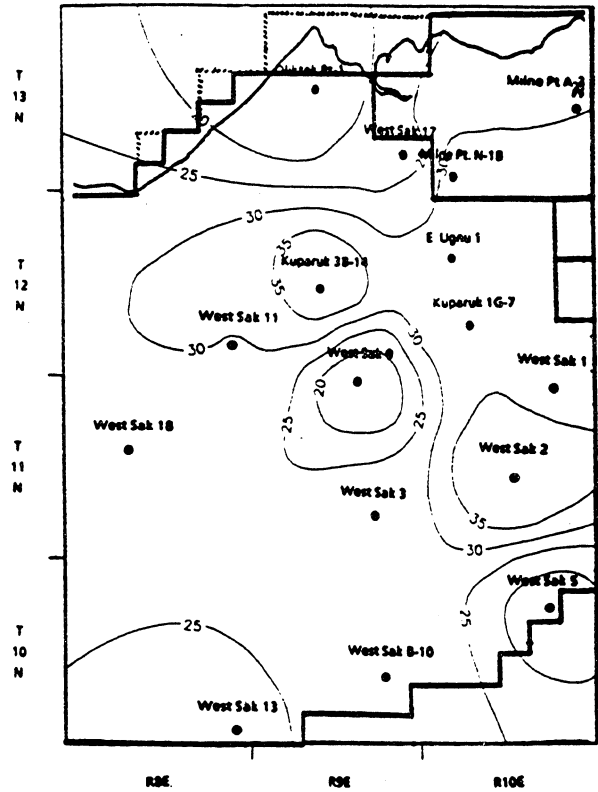


Figure 8: West Sak Upper Sand 2 Gross Pay Zone Thickness Contour Map

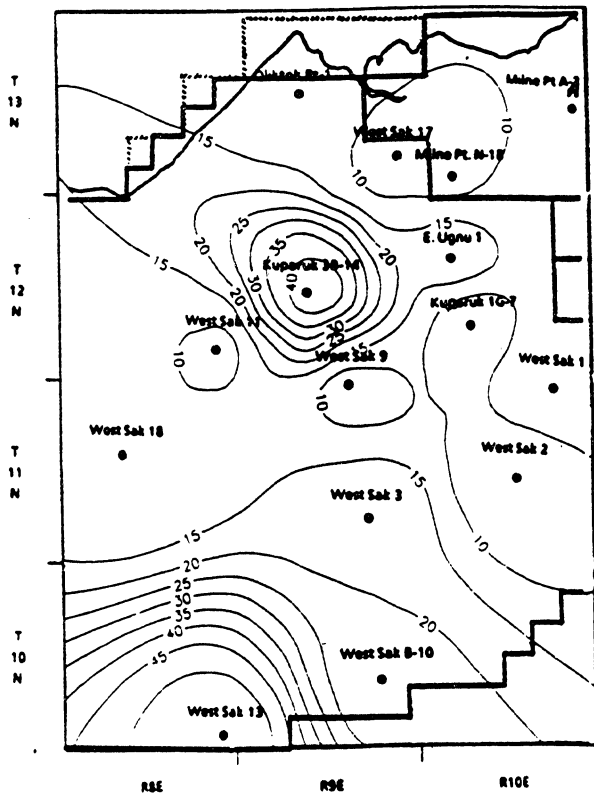


Figure 9: West Sak Lower Sand 1 Gross Pay Zone Thickness Contour Map

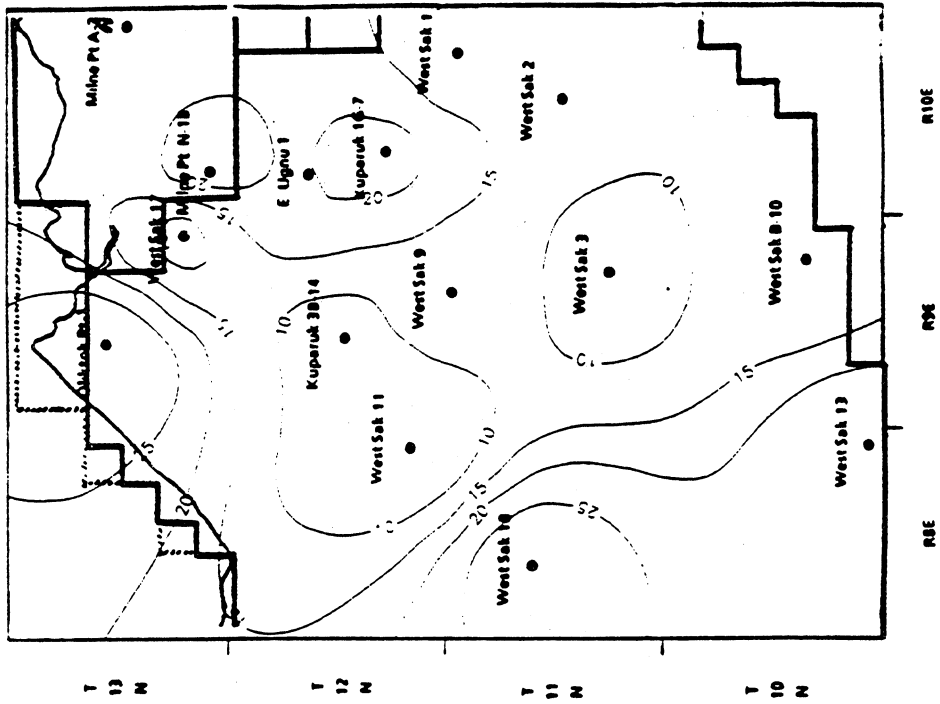


Figure 10: West Sak Lower Sand 2 Gross Pay Zone Thickness Contour Map

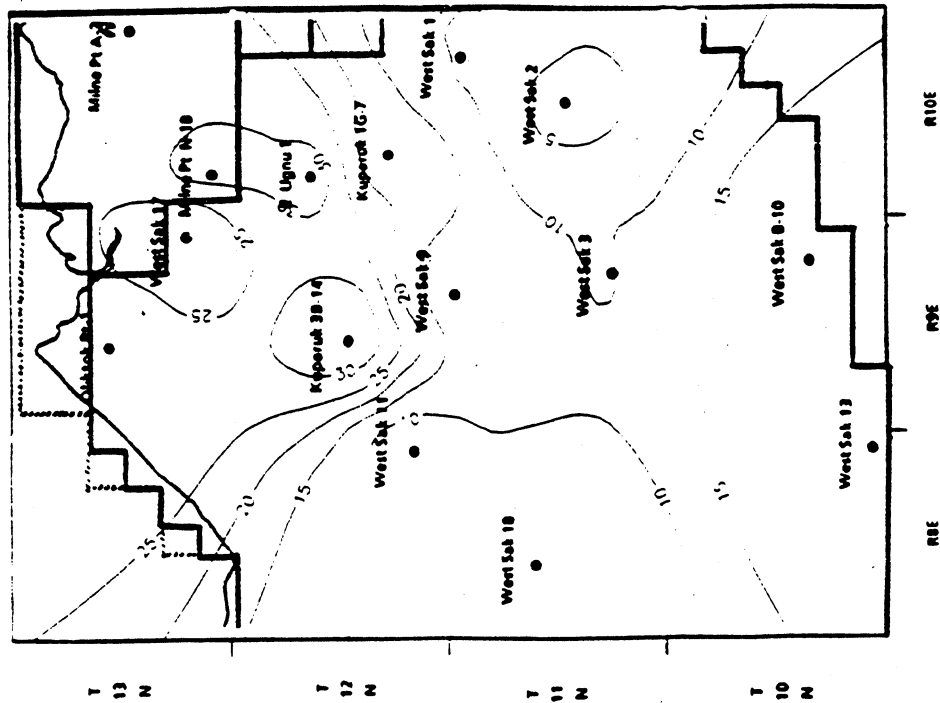


Figure 11: West Sak Lower Sand 3 Gross Pay Zone Thickness Contour Map

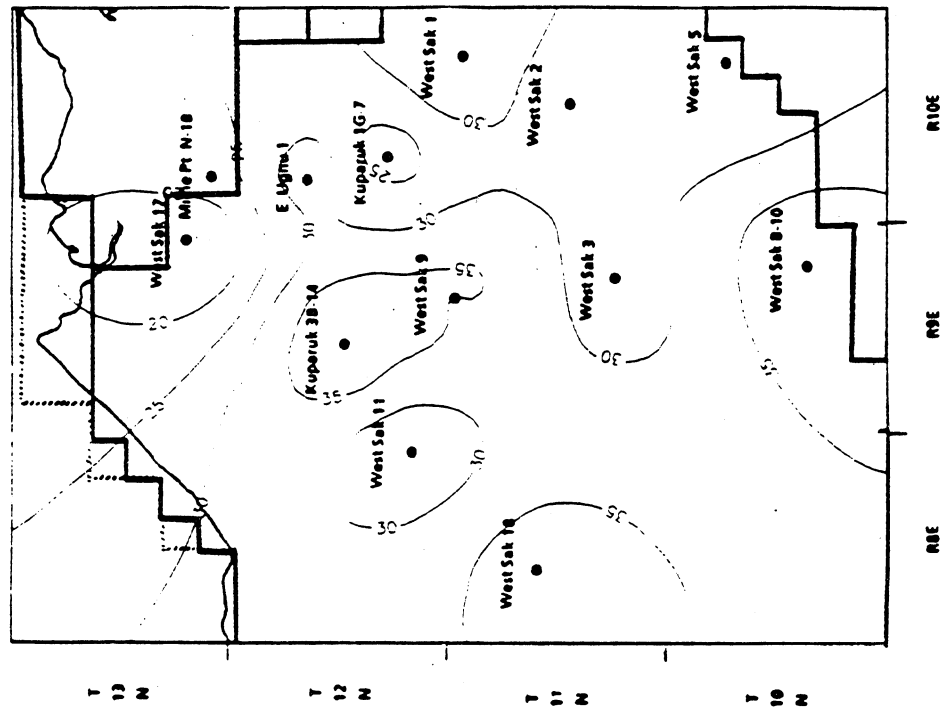


Figure 12: West Sak Lower Sand 4 Gross Pay Zone Thickness Contour Map

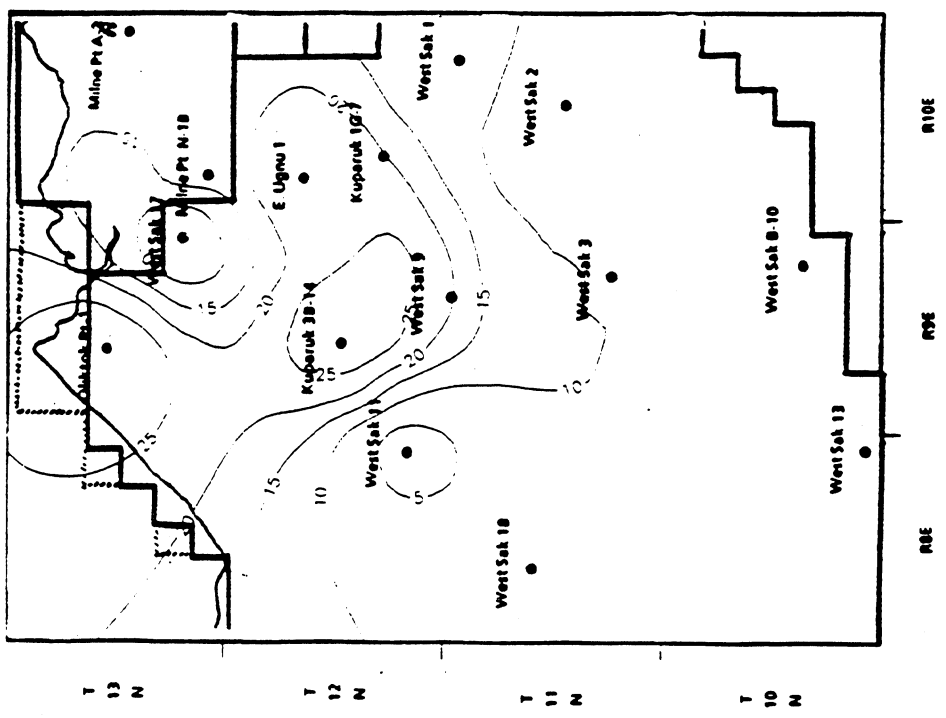


Figure 13A: Iso-Porosity Contour Map of West Sak Sands

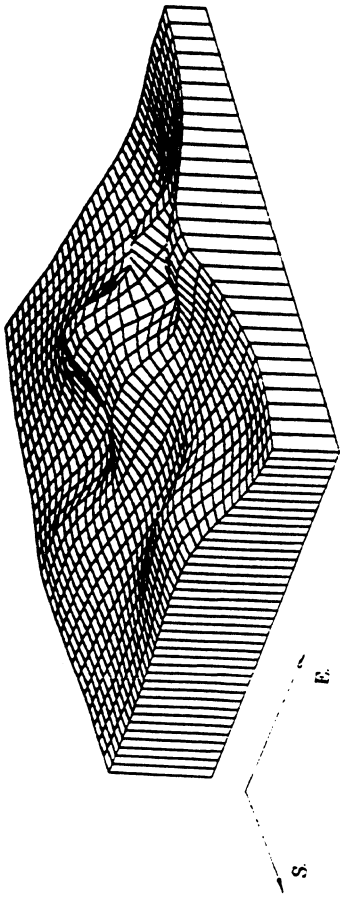


Figure 13B: 3-D Plot Illustrating Porosity Distribution in West Sak Sands

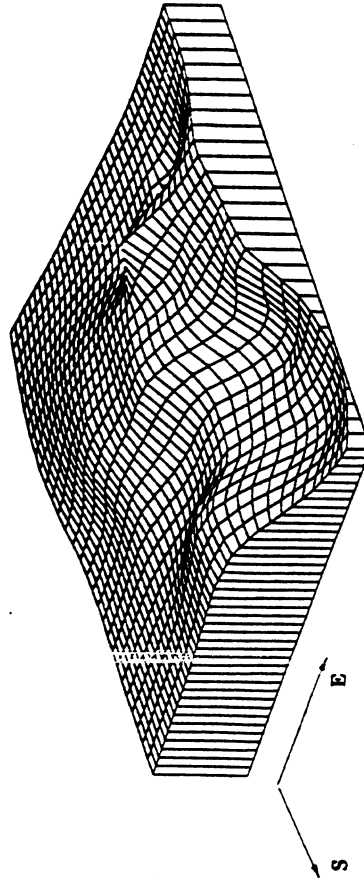


Figure 14B: 3-D Plot Illustrating Water Saturation Distribution

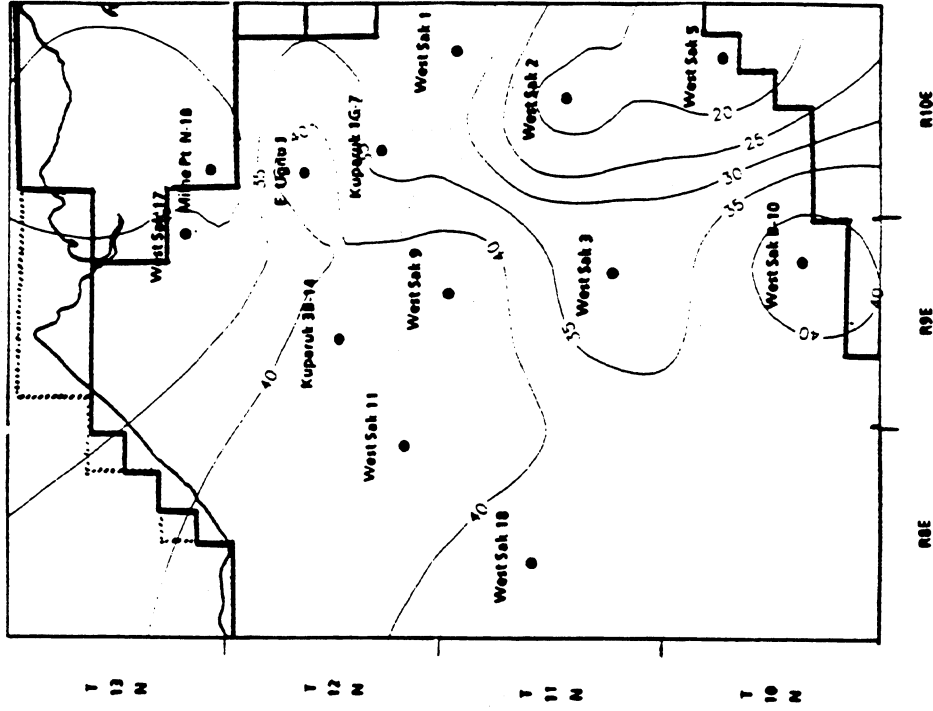


Figure 14A: Iso-Water Saturation Map of West Sak Sands

Sak sands are truncated in the south-west and west direction. This can be interpreted as a lateral facies change in this direction. Presence of various basinal depocenters observed in the isopach maps along with the facies change (evident from the change in porosity displayed in Figures 13A and 13B) suggest that a combination of structural and stratigraphic traps play major role in creating the enclosure for the pay horizons in the West Sak reservoir.

D. Depositional Environment

The SP (Spontaneous Potential) and resistivity traces of various wells shown in Figures 5 and 6 suggest that the West Sak sands were deposited during a major regressive sea with minor cyclic sea level fluctuations. The lower sand members with lesser sorting and increased finer particles suggest innershelf deposition, while the upper members with coarser sands show an increasing energy environment of deposition. Core studies presented by van Poolan indicate that the distribution of coarse grains toward shallower depths; i.e. towards the southwest further supports the deposition environments for these sands.

Evidence for a regressive sea towards the north can be seen in West Sak No. 18 well, where Upper West Sak sands are absent. Non-deposition of the upper unit suggests movement of the shoreline northeast of West Sak No. 18 and southwest of West Sak No.3 at that time. There is a distinct shale baseline change between the upper sand unit and underlying sand units indicating a distinct unconformity; thus suggesting partial erosion of upper sand units in West Sak No. 18 well. The coarsening upward sequence in beds is indicated by the funnel shape of the SP curves which are either smooth or serrated. The egg shaped SP curves suggest many cyclical sequences.

This indicates a depositional energy environment gradually increasing towards the NE direction. In other words, towards the south-west direction the sand bodies

are much better sorted compared to the sands in north eastern direction. This would also indicate an increasing heterogeneity towards the basin center.

The progradational deposition of the West Sak sands would indicate that the ratio of vertical permeability to horizontal permeability should be more than it is commonly found in sandstone reservoirs. This also suggests that if an EOR flooding process is undertaken, fingering, overlaying of the oil by the injected fluid, may occur due to the coarsening of the grains upward as reported by Werner and van Poolan.

The reservoir description presented helps to address some of the problems concerning the reservoir heterogeneity, the continuity of pay zone, presence of local structures like the folds and faults, etc. Reservoir description also helps in determining the degree of sorting of the potential pay zones. Reservoir continuity and the presence of structures are important parameters needed for planning an EOR project, e.g., determining the number of wells to be drilled and the injection pattern to be used.

E. References

1. Carman, G.J. and Hardwick, P., "*Geology and Regional Setting of Kuparuk Oil Field, Alaska,*" AAPG Bulletin, Vol. 67, No. 6 (June 1983).
2. Kamath and Sharma, "*Summary of Petroleum Resources on the North Slope, Alaska and Their Recovery,*" In-House Report, Petroleum Development Laboratory, University of Alaska Fairbanks (1986).
3. Lanning, E.N. and Johnson, D.M., "*Automated Identification of Rock Boundaries: An Application of the Walsh Transforms to Geophysical Well-Log Analysis,*" Geophysics, Vol. 48, No. 2 (1983).

4. Molenaar, C.M., "*Depositional History and Seismic Stratigraphy of Lower Cretaceous and Lower Tertiary Rocks, North-Eastern Alaska*," AAPG Bulletin, (Dec. 1983).
5. OGJ Report, "*North American Arctic*," Oil and Gas Journal, (1984).
6. Panda, M.N., "*Reservoir Description and A Feasibility Study of Enhanced Oil Recovery Applications to West Sak Field*," M.S. Thesis, University of Alaska Fairbanks (Dec. 1988).
7. Panda, M.N., Zhang, M., Ogbe, D.O., Kamath, V.A., and Sharma, G.D., "*Reservoir Description of West Sak Sands Using Well Logs*," SPE Paper #18759, Proceedings of SPE California Regional Meeting held in Bakersfield, CA (April 5-7, 1989).
8. Scientific Software - Intercomp, 1986, Logcalc and Z-values, Users' Manual, Version 2.4, (Sept. 1986).
9. van Poolan and Associates, "*In-Place Hydrocarbon Determination: Kuparuk River Formation and Prudhoe Bay Field*," A report prepared for the State of Alaska by van Poolan and Associates, Inc., and the State of Alaska Division of Oil and Gas, (Oct. 1978).
10. Werner, M.R., "*West Sak and Ugnu Sands - Low Gravity Oil Zones of Kuparuk Area, Alaskan North Slope*," AAPG Bulletin, Vol. 23, (1985).
11. Zhang, M., "*Characterization and Description of Lower Ugnu and West Sak Reservoirs Using Well Logs*," M.S. Thesis, University of Alaska Fairbanks (Dec. 1989).

CHAPTER TWO

PHASE BEHAVIOR AND FLUID PROPERTIES MEASUREMENTS

A. Abstract

This experimental study is divided into three phases. In the first phase, PVT measurements were obtained for West Sak crude. Constant composition expansion and differential liberation tests were conducted using oil samples recombined with methane to a bubble point pressure of 1704.7 psia at 80°F. In the second phase, effect of addition of CO₂ to West Sak crude was studied. Live oil was subjected to single contacts with CO₂. Constant composition expansion tests were conducted at 80°F for 60 mol% CO₂ - 40 mol% West Sak crude mixture and 80 mol% CO₂ - 20 mol% West Sak crude mixture. Data for 60/40 (mol% CO₂/mol% live oil) at 1704.7 psia and 80°F showed oil swelling of 9.9%, oil viscosity reduction by 75% and the solubility of CO₂ in oil phase 1.5 times that of methane. Data for 80/20 (mol% CO₂/mol% live oil) showed maximum oil swelling of 13% or greater near or below the lower pressure limit of a liquid/liquid/vapor phase region. Small amounts of a black (asphaltene) precipitate were observed for systems with CO₂ at pressures below 1704.7 psia.

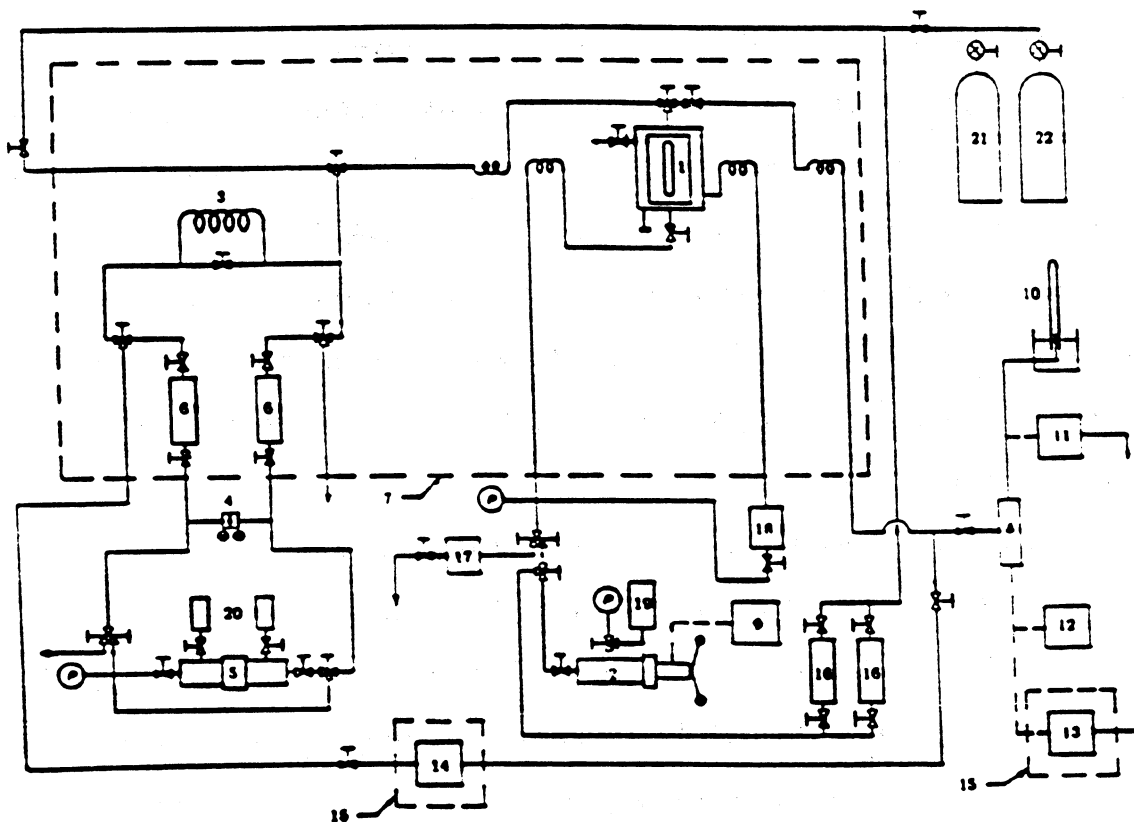
In the third phase, effect of gas solubility on viscosity of West Sak crude at various pressures and temperatures were determined. Viscosity measurements were done with a rolling ball viscometer and density measurements were done with densitometer. The experimental data were used to compare various oil viscosity correlations reported in literature.

B. Experimental PVT Apparatus

The experimental PVT apparatus consists of individual equipment components assembled to allow measurement of West Sak oil/CO₂ vapor/liquid physical properties including density, viscosity, vapor/liquid ratios, formation volume factors

and phase compositions. Visual observations of the fluids at reservoir conditions also facilitated determination of conditions which produce complex phase behavior. The major equipment components include a phase behavior cell with sight glass, cathometer, rocking mechanism, capillary tube viscometer, Fann rotational viscometer, temperature control oven, high pressure density meter, atmospheric pressure density meter, flash separator, atmospheric pressure gas collection tubes, temperature controlled oil bath, gas chromatograph, back pressure regulator, and positive displacement pumps. The following discussion refers to the equipment diagram shown in Figure 1.

Item (1) in Figure 1, is a phase behavior cell manufactured by D.B. Robinson & Associates Ltd. The cell is rated for operating pressures up to 10,000 pounds per square inch and temperatures to 390°F. The cell may be agitated by an electric motor (not shown in Figure 1) for rapid attainment of thermodynamic equilibrium and to allow the recombination of live oil samples. The fluids under study were contained within a transparent glass cylinder that can withstand a maximum differential pressure of 2,000 psi. The glass cylinder is pressurized by injecting mineral oil into one end with a hand pump (2). An isolation piston prevents contamination of the process fluid by the injected mineral oil. The glass cylinder is enclosed in a stainless steel shell fitted with full length tempered Pyrex sight glass windows to allow visual observation of fluids at reservoir temperature and elevated pressures. The space between the sight glass windows and the glass tube is filled with a clear mineral oil which exerts an overburden stress on the outside of the glass tube equal and opposite to the pressure on the process fluid side. The glass sample cylinder-overburden pressure system is designed to maintain the sample volume dimensionally constant throughout the cell's operating pressure range of 0 to 10,000 psi so that only a single volume calibration is needed at operating temperature.



- | | |
|---|---|
| (1) PHASE BEHAVIOR CELL | (12) SCALE |
| (2) HAND PUMP | (13) ATMOSPHERIC PRESSURE DENSITY METER |
| (3) CAPILLARY TUBE | (14) HIGH PRESSURE DENSITY METER |
| (4) PRESSURE TRANSDUCER | (15) CONSTANT TEMPERATURE BATH |
| (5) PROGRAMMABLE CONSTANT RATE PUMP | (16) SAMPLE CYLINDER |
| (6) MERCURY/SAMPLE VESSEL | (17) BACK PRESSURE REGULATOR |
| (7) TEMPERATURE CONTROL OVEN | (18) SEPARATION VESSEL |
| (8) FLASH SEPARATOR | (19) MINERAL OIL RESERVOIR |
| (9) DIGITAL PUMP DISPLACEMENT INDICATOR | (20) MERCURY RESERVOIRS |
| (10) GRADUATED GAS COLLECTION TUBE | (21) METHANE CYLINDER |
| (11) GAS CHROMATOGRAPH | (22) CARBON DIOXIDE CYLINDER |

Figure 1: Experimental Apparatus for PVT and Phase Behavior Studies

A mirror image of the phase behavior cell contents was viewed through a cathometer (not shown in Figure 1), which allowed visual measurement of phase volumes within the cell. The cathometer consists of a sliding scope mounted on a linear scale which can be read to 5 significant digits for volume determinations. A cell calibration constant of 0.83897 cm^3 per cathometer unit (for readings with a decimal point inserted before the next to last digit) was obtained by comparing visual readings with the weight of distilled water displaced from the cell. The cell volume calibration data at 80°F are shown in Figure 2. The average of several visual readings yielded an isolation piston thickness of 27.47 cathometer units.

Viscosity measurements were conducted for both live oil at reservoir conditions and dead oil at stock tank conditions. The dead oil viscosity was measured at temperatures between 60° and 80°F using a Fann plumb and bob rotational viscometer (not shown in Figure 1). Factory calibration of the rotational viscometer was validated with two certified viscosity standards; a 137.5 centipoise fluid at 68°F and a 286.0 centipoise fluid at 68°F . Live oil viscosity measurements were conducted by displacing samples through a capillary tube (3) at constant rate and measuring the resulting steady state pressure drop with a pressure transducer (4). A constant displacement rate was achieved with a programmable opposed piston constant rate pump (5) using mercury as the displacing fluid. Large diameter lines were installed between the viscometer pump (5) and the mercury/oil vessels (6) to minimize the pressure drop in the portion of the system that flows mercury, and thus maintain linearity in the viscometer system response. Pressure was maintained above the sample bubble point at the downstream side of the pump during displacements to prevent the liberation of solution gas. The downstream pressure was monitored by deducting the digital pressure transducer calibration constant of 23.184 psi per indicated digital unit value was obtained with a Ruska dead weight gauge for a transducer indicator span setting of 4.50 with a Validyne 4-64 transducer diaphragm

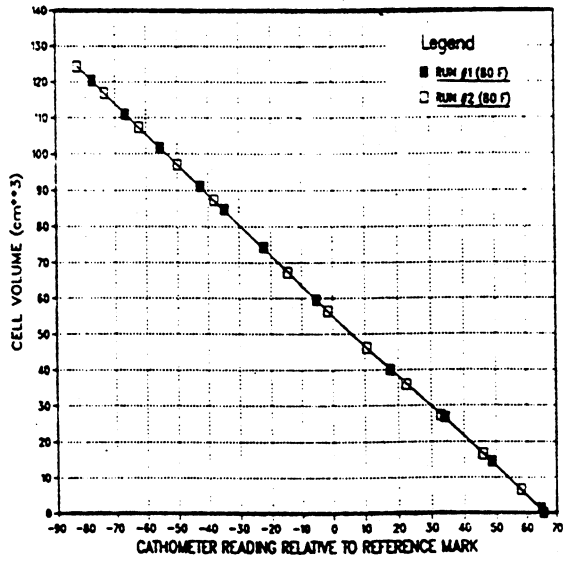


Figure 2: PVT Cell Volume Calibration Chart

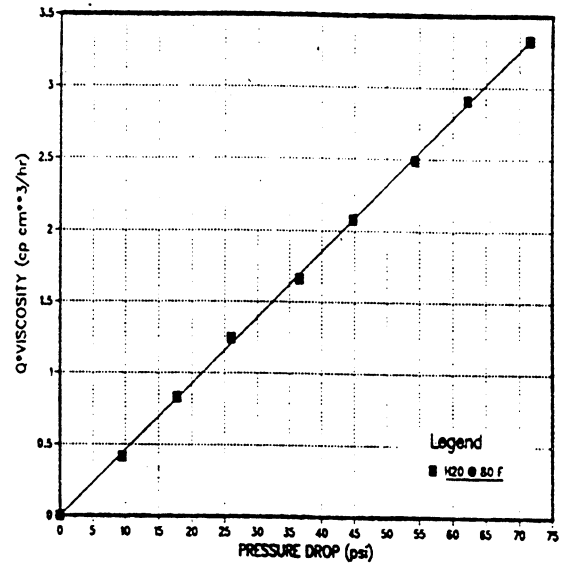


Figure 3: Viscometer Constant at Low Pressures

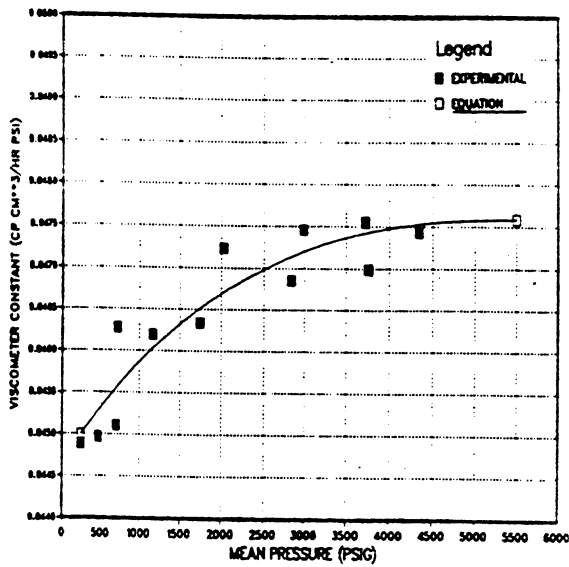


Figure 4 Shifting of Viscometer Constant with Pressures

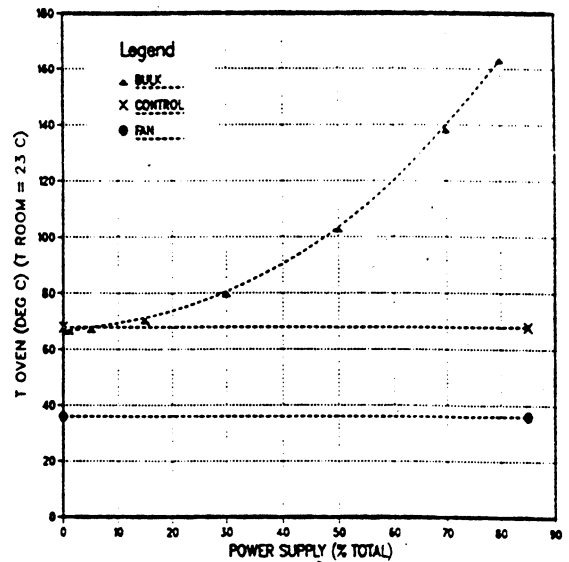


Figure 5 Heating Element Calibration

(differential pressure rating of 0 to 3,000 psi) installed. The transducer readings were influenced by hysteresis of the zero reading, and by changes in the head of mercury in the viscometer vessels (6) during operation. These effects were accounted for by deducting a static pressure drop reading (determined by stopping the viscometer after recording the steady state pressure drop) from the steady state flowing value.

The capillary tube viscometer was calibrated by pumping distilled water at various rates below the critical rate for the onset of laminar instability, and noting the steady state pressure drop. The geometrical viscometer constant for operation near atmospheric pressure was determined as the slope from a plot of flow rate times calibrating fluid viscosity vs. steady state flowing pressure drop. Since the viscometer constant is theoretically proportional to the fourth power of the capillary tube diameter as expressed by Poiseuille's equation, shifting of the viscometer constant due to tube expansion at higher operating pressures was also investigated. The viscometer constant calibration data was regression fit to the cubic polynomial expression shown below to allow programming of the data reduction calculations. Figure 3 illustrates the determination of a viscometer constant near atmospheric pressure, and Figure 4 compares the higher pressure viscometer constants with values calculated from the regression equation. The magnitude of the shift in the viscometer constant when going from atmospheric pressure to 5,000 psig is approximately 6.5%.

$$\mu (cp) = C \frac{\Delta P (psi)}{Q (cm^3/hr)} \dots\dots\dots (1)$$

where for

$$0 \leq \bar{P} (psig) \leq 5,000 \dots\dots\dots (2)$$

$$C = 0.044528 + 1.6507 \times 10^{-6} \bar{P} - 2.9730 \times 10^{-10} \bar{P}^2 + 1.6456 \times 10^{-14} \bar{P}^3 \quad \dots\dots\dots (3)$$

The phase behavior cell and capillary viscometer are enclosed in a D.B. Robinson forced air circulation oven (7) for temperature control. The oven is equipped with two heating elements; a 1,500 watt main bulk heating coil, and a 250 watt heating coil activated by a temperature controller. Two thermocouples are provided; one linked to the temperature controller which senses the air bath temperature, and a second which is inserted into the overburden fluid at the bottom of the phase behavior cell. These thermocouples received a two point calibration with distilled water at the boiling and fusion temperatures. Manual temperature control was required for the work at 80°F, however, because the heat from the air circulation fan motor was found to warm the oven in excess of 80° with both heating elements switched off. Manually controlled heating was provided by a 100 watt light bulb positioned near the oven viewing window, with the air circulation fan ran intermittently as needed. The oven heating coils were calibrated at the start of this study, and the results are shown in Figure 5.

Reservoir samples were flashed to stock tank conditions in a gas/oil separator (8). The flashing process was equivalent to a constant pressure displacement in the phase behavior cell, which allowed the reservoir volume of the flashed fluid to be obtained from a digital readout (9) of the distance traveled by the pump piston with a volumetric calibration factor of 20.0290 cm³/inch which was determined during the cell volume calibration. Graduated gas collection tubes (10) were used to determine the volume of flashed or liberated gas samples at atmospheric pressure, and gas composition was determined by transferring 0.5 ml samples to a gas chromatograph (11) with a syringe. The gas chromatograph was calibrated before collecting data for the pure West Sak oil, and again before collecting data on systems with CO₂ since

a higher detector sensitivity setting was used for these latter measurements. Volumes of residual oil were determined from the weight of the separator plus dead oil reading from a Metler balance (12), and the dead oil density measured with an electrically excited oscillating U-tube atmospheric pressure density meter (13). The atmospheric pressure density meter was calibrated at 60° and 80°F with air and distilled water, which bracket the density range of interest.

Live oil density was measured with a second U-tube density meter (14) rated for pressures up to 6,000 psi. The high pressure density meter was also calibrated with air and water at atmospheric pressure to obtain the required instrument constants for operation at 60° and 80°F. In addition, shifting of the density meter constants with increasing pressure was quantified by linear least squares regression fits of calibration data collected at 150°F. Temperature control for both density meters was provided by a Magni Whirl constant temperature oil bath (15) modified by adding an immersion cooler and stir motor to allow data collection at 60° and 80°F.

Two sample cylinders (16) fitted with isolation pistons were charged with dead oil, toluene (wash solvent), or CO₂ as needed. A back pressure regulator (17) was installed to allow controlled throttling of the overburden fluid from the cell when charging target volumes of CO₂ from a sample cylinder (16) with the hand pump (2). Component (18) is a separation vessel to allow the use of mercury as a displacing fluid in the hand pump (2). Because the sample cylinders (16) were fitted with isolation pistons, we were able to use mineral oil rather than mercury in the hand pump, so vessel (18) contained only mineral oil during the experimental runs.

C. Experimental Procedure

Since the West Sak sands contain several potentially productive zones of large areal extent at depths ranging from 2,000 to 5,000 feet subsurface, variations in reservoir and crude oil properties are expected. Werner (1985) reported the

existence of crude oil at reservoir temperatures of 45° to 100°F, with API gravities ranging from 16° to 22°. Experimental data were first collected to quantify the phase behavior properties of the crude oil samples, available for use by the University of Alaska Fairbanks, and the effects of carbon dioxide addition to the oil were then investigated. Crude oil samples were recombined with methane at 80°F to a bubble point of 1,704.7 pounds per square inch absolute pressure. Because it is likely that enhanced oil recovery methods will be necessary from startup of the field in order to recover the West Sak crude economically, carbon dioxide was added to the live crude oil which had been previously recombined to the same bubble point pressure of 1,704.7 psia.

Oil samples were recombined with methane by charging dead oil into a sample cylinder equipped with an isolation piston, and displacing it to the phase behavior cell with the hand pump. A methane cylinder was then tapped, and a methane bubble corresponding to approximately 10% of the oil volume was placed on top of the oil at the bubble point pressure. The phase behavior cell was turned on its side to promote intimate contacting of the oil and gas, and the cell was agitated with a 1/3 hp electric motor. The cell pressure was periodically restored to the bubble point with the hand pump because pressure decreased during the recombination process as gas entered into solution in the oil. When the cell pressure stabilized, the cell was allowed to sit undisturbed for several hours in an upright position to promote separation of any phases present. If a gas phase could be seen at the top of the phase behavior cell after allowing time for phase separation, the recombination was considered complete. Otherwise, additional methane was added and the procedure repeated until no more gas could be forced into solution in the oil at the desired bubble point pressure. Gas remaining on top of the recombined oil was then throttled out of the phase behavior cell while maintaining a constant cell pressure with the hand pump. In order to minimize the loss of any hydrocarbon components

stripped from the oil phase, only small methane samples were introduced into the phase behavior cell at any one time so that very little gas remained to be purged after recombining the oil. The recombination procedure required approximately 17 to 25 hours for each oil sample.

Systems consisting of 60 and 80 mole percent CO₂ in CO₂ - West Sak oil mixtures were prepared by initially recombining stock tank oil samples with methane to a bubble point pressure of 1,704.7 psia as described above. A sample cylinder containing an isolation piston was then charged with CO₂. The hand pump was used to displace target volumes of carbon dioxide into the phase behavior cell with the live oil at constant pressure by throttling overburden fluid from the cell under controlled conditions through a back pressure regulator. The valve connecting the mineral oil below the phase behavior cell isolation piston to that on the outside of the glass tube was left open during CO₂ addition to minimize pressure differentials across the glass that could damage the tube or produce leaks across the glass tube end seals.

D. Constant Composition Expansion Data

The results of an isothermal constant composition expansion experiment for live West Sak crude at 80°F are listed in Table 1, and are displayed in Figures 6 and 7. These data include visually determined equilibrium measurements of the total volume of oil and gas present as a function of pressure (Figure 6), as well as the volume fraction occupied by liquid below the bubble point pressure (Figure 7). The total volume data are expressed relative to the original bubble point oil volume present at the start of the experiment. Above the bubble point pressure (1704.7 psia), the change in total volume with pressure is relatively small since only a single liquid phase is present in the cell. The slope of this plot above 1704.7 psia represents the compressibility of the live oil. An abrupt change in slope occurs due to the

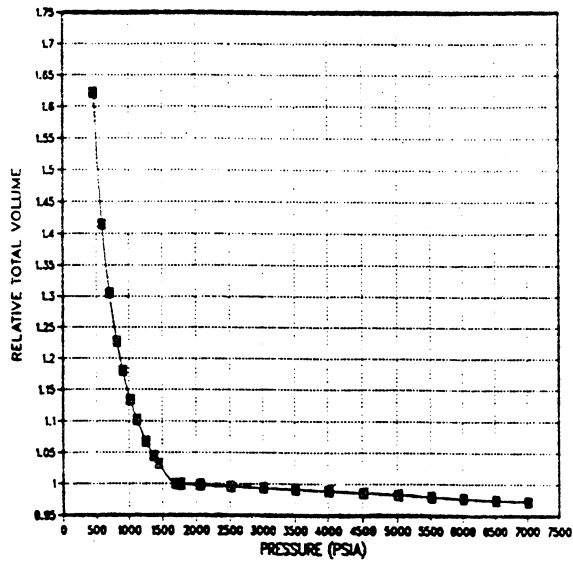


Figure 6 Relative Total Volume Versus Pressure (Constant Composition Expansion of West Sak Crude at 80°F)

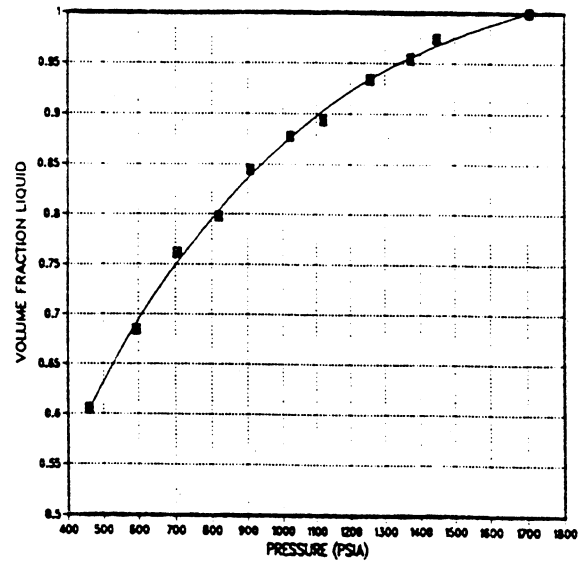


Figure 7 Volume Fraction Liquid Versus Pressure (Constant Composition Expansion of West Sak Crude at 80°F)

Table 1: Constant Composition Expansion of West Sak Crude at 80°F

Pressure (psia)	Relative Total Volume	Volume Fraction Liquid
7014.7	.972	
6514.7	.974	
6014.7	.977	
5514.7	.980	
5014.7	.983	
4514.7	.986	
4014.7	.989	
3514.7	.991	
3014.7	.994	
2514.7	.996	
2064.7	.998	
1764.7	.9996	
1714.7	.9999	
1704.7	1.000	1.000
1447.7	1.032	.974
1372.7	1.045	.954
1258.7	1.067	.934
1120.7	1.102	.894
1021.7	1.134	.876
907.7	1.180	.844
818.7	1.227	.798
705.7	1.305	.762
594.2	1.415	.685
460.2	1.622	.605

liberation of free gas from solution when pressure is reduced below the bubble point of 1,704.7 psia.

E. Differential Expansion Data

Experimental results obtained by differentially liberating a live West Sak oil sample at 80°F from the bubble point to atmospheric pressure in pressure steps of approximately 200 psi are given in Tables 2 through 4, and are displayed graphically in Figures 8 through 17.

Table 2 contains measured volumetric properties of the oil and gas, and properties of the incrementally liberated gas that were calculated from the experimentally measured gas phase compositions. Values in columns 2 through 4 are expressed relative to the residual stock tank oil volume at 60°F, where the stock tank oil volumes were obtained from the weight of the residual oil collected with the experimental dead oil density of 0.9407 g/cm³ measured at 60°F. Gas volumes at standard conditions refer to a stock tank temperature of 60°F and a pressure of 14.65 psia.

F. Single Contact Tests with CO₂ - West Sak Crude Mixtures

CO₂ was added to live West Sak crude to investigate the systems phase behavior, and to measure resulting phase properties. Two single contact mixtures were studied, namely 60 mol% CO₂ - 40 mol% West Sak crude and 80 mol% CO₂ - 20 mol% West Sak crude.

F1. 60 Mol% CO₂ - 40 Mol% West Sak Crude Mixture

A constant composition expansion experiment was conducted on this (60/40) mixture at 80°F, to investigate the possibility of complex phase behavior, and to quantify the system volumetrics including any oil swelling

Table 2: Differential Expansion of West Sak Crude at 80°F

Pressure (psia)	Solution Gas/Oil Ratio (SCF/STB)	Relative Oil Volume (RB/STB)	Relative Total Volume (RB/STB)	Incremental Gas Gravity	Gas Deviation Factor	Gas Formation Volume Factor (ft ³ /SCF)
1704.7	207	1.070	1.070			
1514.7	187	1.062	1.096	.571	.831	.00834
1314.7	165	1.055	1.129	.579	.843	.00976
1114.7	144	1.047	1.185	.567	.866	.01182
914.7	124	1.040	1.270	.568	.887	.01475
714.7	96	1.033	1.406	.568	.909	.01936
514.7	70	1.026	1.703	.574	.933	.02757
314.7	42	1.019	2.343		.951	.04555
114.7	11	1.012	5.403	.575	.985	.13060
14.7	0	1.008		.661		

Table 3: West Sak Oil Density at 80°F

Oil Bubble Point Pressure (psia)	Pressure (psia)	Oil Density (g/cm ³)
1704.7	1704.7	0.9119
	2014.7	0.9138
	2514.7	0.9167
	3014.7	0.9192
	3514.7	0.9220
	4014.7	0.9246
	4514.7	0.9269
	5014.7	0.9292
1114.7	1114.7	0.9165
	2014.7	0.9214
	3014.7	0.9266
	4014.7	0.9316
	5014.7	0.9363
914.7	914.7	0.9187
	1014.7	0.9194
	2014.7	0.9248
	3014.7	0.9299
	4014.7	0.9347
	5014.7	0.9391
714.7	714.7	0.9209
	1014.7	0.9225
	2014.7	0.9277
	3014.7	0.9325
	4014.7	0.9373
	5014.7	0.9416
14.7	14.7	0.9370

Table 4: West Sak Crude Viscosity Measurements at 80°F

Oil Bubble Point Pressure (psia)	Pressure (psia)	Measured Oil Viscosity (Centipoise)	Extrapolated Bubble Point Oil Viscosity (Centipoise)	Calculated Gas Viscosity (Centipoise)	Oil/Gas Viscosity Ratio
1704.7	1704.7		45.2		
	2674.4	55.5			
	2850.1	58.1			
	3464.0	64.7			
	4245.0	75.5			
	4970.4	84.7			
1514.7	1514.7		50.2	.0143	3510
	2276.9	59.5			
	2981.9	72.0			
1314.7	1314.7		51.8	.0137	3780
	2158.7	66.1			
	2469.9	70.2			
1114.7	1114.7		59.3	.0132	4490
	2118.7	79.1			
	2590.4	86.0			
914.7	914.7		68.6	.0127	5400
	2107.3	94.2			
	2447.7	100.7			
714.7	714.7		83.4	.0124	6730
	2128.0	115.7			
	2556.5	127.8			
514.7	514.7			.0120	
114.7	114.7			.0115	
14.7	14.7	272.7		.0110	24800

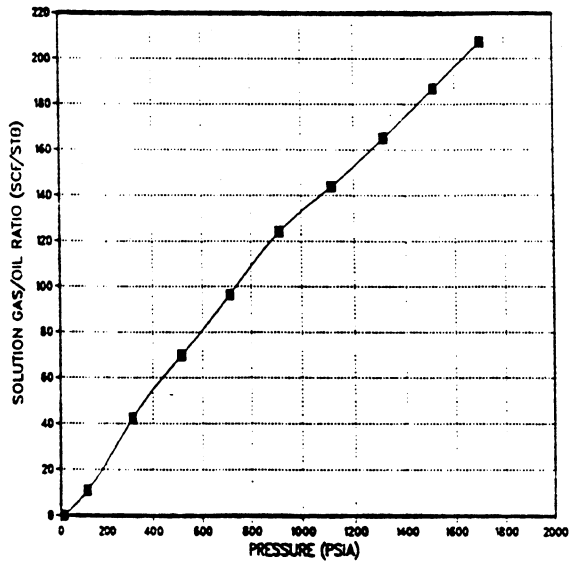


Figure 8 Solution GOR Versus Pressure (Differential Liberation of West Sak Crude at 80°F)

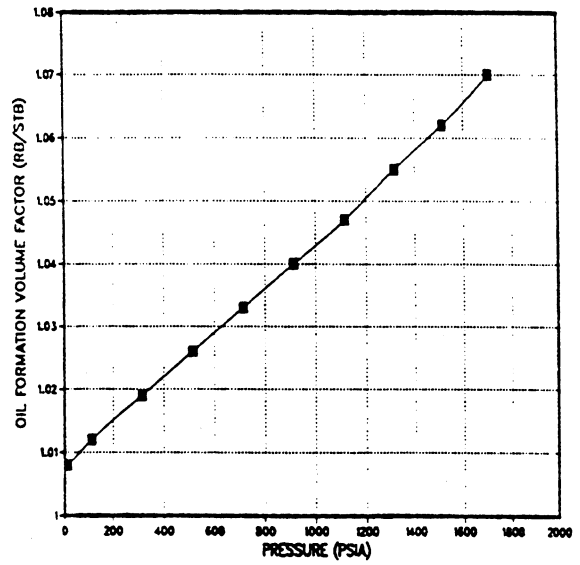


Figure 9 Oil FVF Versus Pressure (Differential Liberation of West Sak Crude at 80°F)

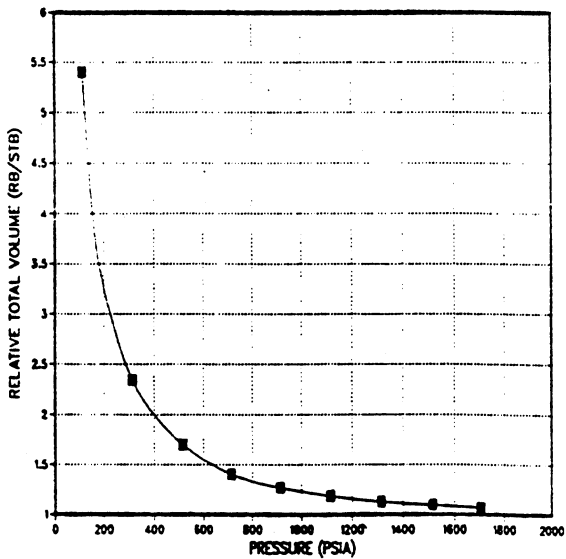


Figure 10 Relative Total FVF Versus Pressure (Differential Liberation of West Sak Crude at 80°F)

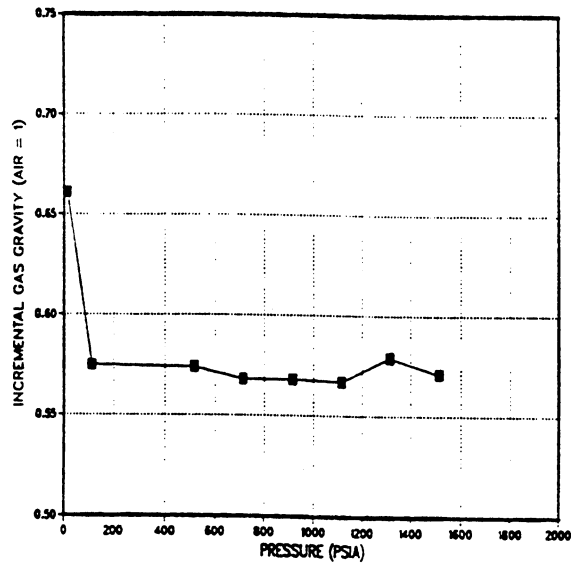


Figure 11 Incremental Gas Gravity Versus Pressure (Differential Liberation of West Sak Crude at 80°F)

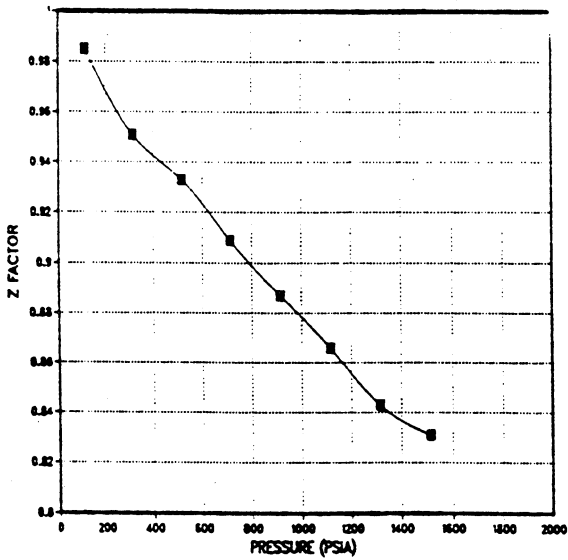


Figure 12 Gas Deviation Factor Versus Pressure (Differential Liberation of West Sak Crude at 80°F)

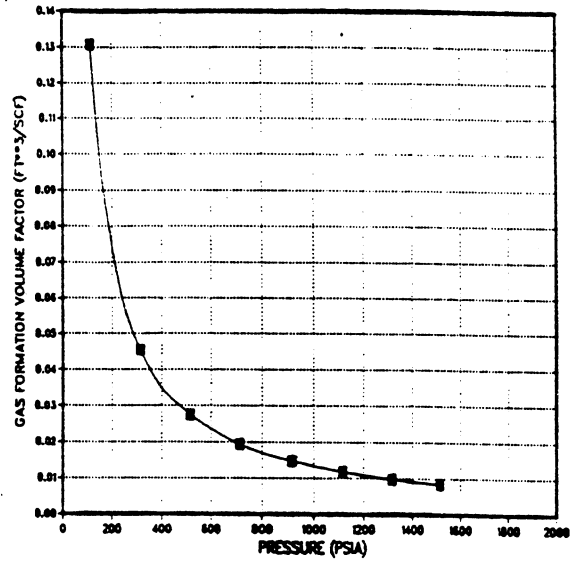


Figure 13 Gas FVF Versus Pressure (Differential Expansion of West Sak Crude at 80°F)

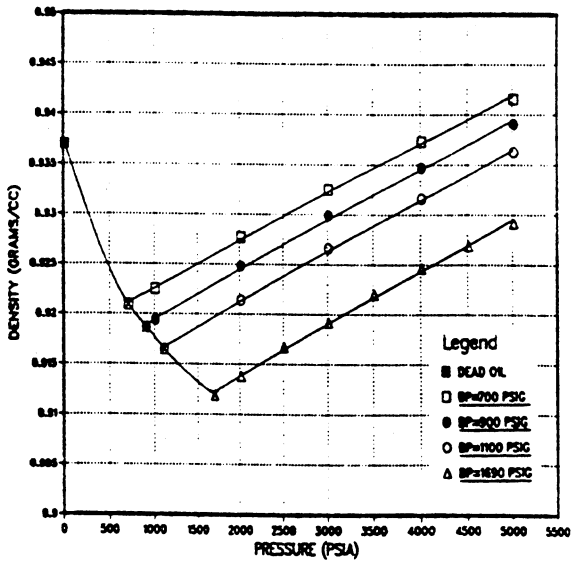


Figure 14 Oil Density Versus Pressure (80°F)

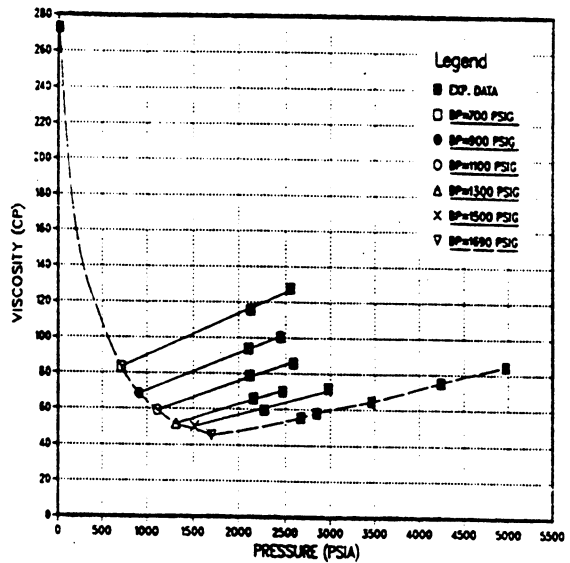


Figure 15 Oil Viscosity Versus Pressure (80°F)

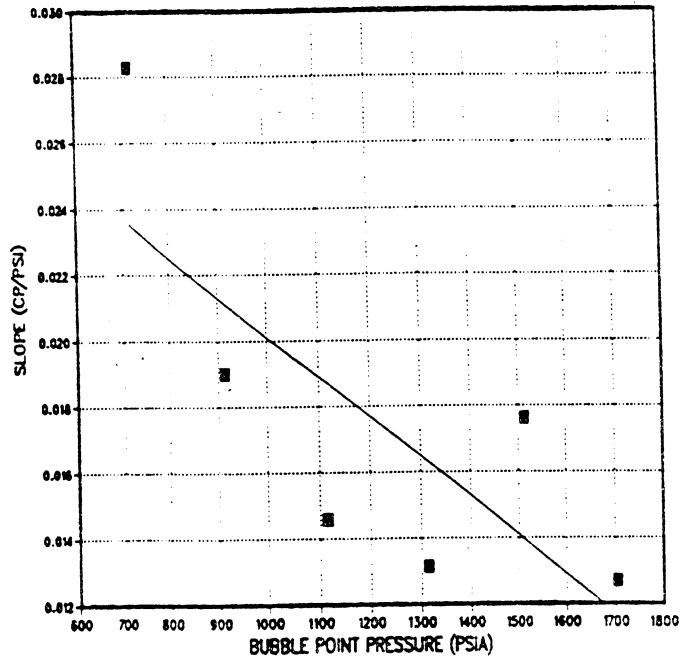


Figure 16 Analysis of Oil Viscosity Data (80°F)

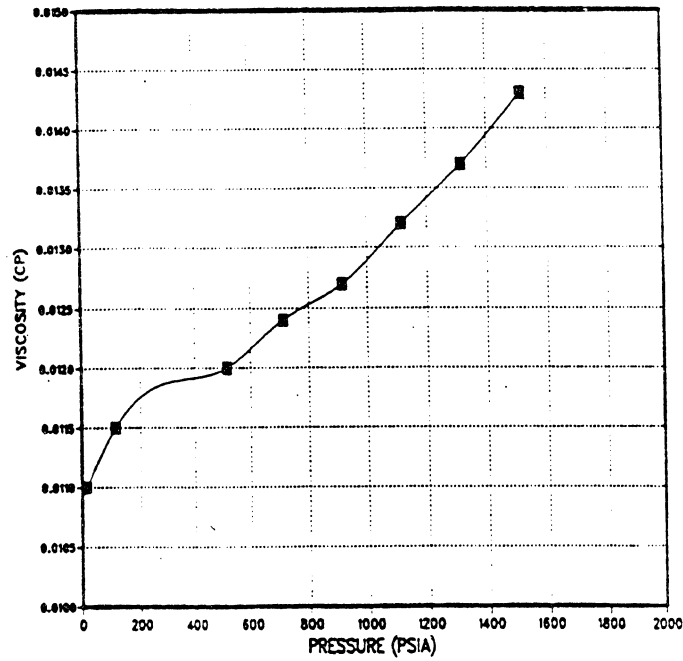


Figure 17 Viscosity of Incremental Gas at 80°F (Calculated)

effect. The oil rich and CO₂ rich phases were sampled, and the oil rich phase viscosity was measured at the original CO₂ free bubble point pressure.

Table 5 lists the results of the constant composition expansion. These results are shown graphically in Figures 18 through 20. The total volumes listed in column 2 of Table 5 and plotted in Figure 18 are expressed relative to the bubble point oil volume at 1,704.7 psia and 80°F prior to the addition of CO₂ to the system. The volume fraction oil rich liquid data tabulated in column 3 and plotted in Figure 19 indicate that the system remains in the two phase region to a pressure well in excess of 7,000 psia. The pressure obtained by extrapolating this plot to a y-axis value of 1.0 is so high that it likely represents a dew point rather than a bubble point. The swelling index values (defined as the ratio of the oil rich phase volume to the CO₂ free live oil volume at the same temperature and pressure) listed in column 4 and shown in Figure 20 were determined from visual cathometer readings, and indicate a 9.9 percent expansion of the reservoir oil at the original CO₂ free bubble point pressure of 1704.7 psia. A maxima on the swelling index plot normally occurs at a pressure near the minimum miscibility pressure in cases where vaporization of oil components by CO₂ begins to dominate over increasing CO₂ solubility in the oil phase with increasing pressure. No local maxima occurred on the swelling index plot between 1,274.7 and 7,000 psia for the first contact mixture of 60 mole percent CO₂ with the live reservoir oil. Thus, efficient extraction of intermediate hydrocarbon components as is needed for the development of vaporizing gas drive miscibility is not indicated by the first contact data in this pressure range. The trend of increased oil swelling with increasing pressure suggests that CO₂ solubility in the oil phase also increases at higher pressures.

Two equilibrium fluid phases as well as a black precipitate were observed in the windowed cell at the tabulated pressure points. A gummy resin-like

Table 5: Constant Composition Expansion of 60 Mol% CO₂ - 40 Mol% West Sak Crude Mixture at 80°F

Pressure (psia)	Relative Total Volume	Volume Fraction Oil Rich Liquid	Swelling Index
7014.7	1.207	.9645	1.197
6014.7	1.215	.9446	1.175
5014.7	1.228	.9333	1.166
4014.7	1.239	.9129	1.144
3014.7	1.254	.8944	1.129
2514.7	1.269	.8794	1.121
2014.7	1.297	.8535	1.109
1704.7	1.342	.8184	1.099
1514.7	1.436	.7598	1.094
1391.7	1.527	.7186	1.096
1274.7	1.652	.6575	1.089

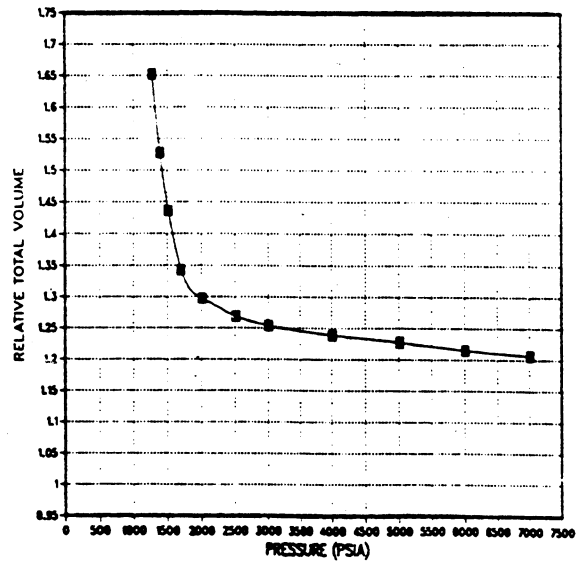


Figure 18: Relative Total Volume Versus Pressure (Constant Composition Expansion at 80°F for 60 Mol% CO₂ - 40 Mol% West Sak Crude)

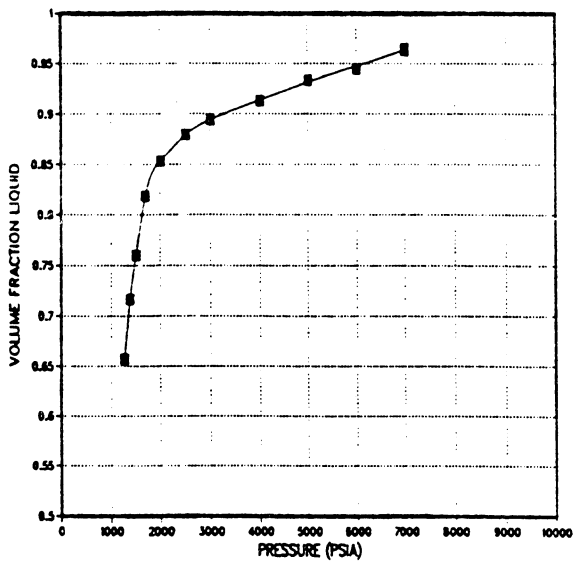


Figure 19: Volume Fraction Oil-Rich Liquid Versus Pressure (Constant Composition Expansion at 80°F for 60 Mol% CO₂ - 40 Mol% West Sak Crude)

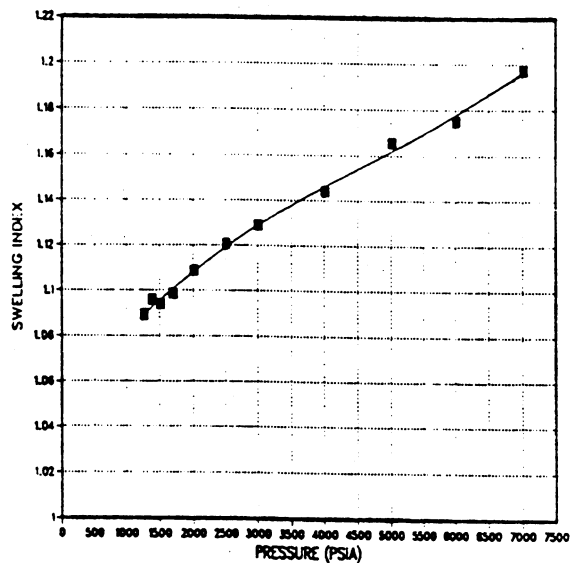


Figure 20: Oil Swelling Index Versus Pressure (60 Mol% CO₂ - 40 Mol% West Sak Crude at 80°F)

black precipitate was observed adhering to the glass tube wall after increasing the pressure to 7,000 psia. Most of this black precipitate redissolved or stopped adhering to the glass when lowering the cell pressure during the expansion, and only a small amount remained on the glass tube at pressures below the original oil bubble point pressure. Some of the black substance was seen running down the side of the glass tube during pressure reductions.

The phase samples were collected and the oil rich phase viscosity was measured at 1,704.7 psia and 80°F. The compositions of the CO₂ rich phase and the solution gas contained in the oil rich phase were measured. Viscosity of the CO₂ - swelled oil is compared with CO₂ - free oil viscosity in Figure 21. The oil density increase due to the addition of CO₂ is shown in Figure 22.

The results indicate that a single equilibrium contact between the live oil and 60 mole percent CO₂ at the original reservoir temperature and pressure will reduce the live oil viscosity by roughly 75%. This viscosity reduction may significantly improve the fractional flow of oil during subsequent water injection if water is used to chase a CO₂ slug through the reservoir, or if a waterflood is conducted after sustained CO₂ injection.

F2. 80 Mol% CO₂ - 20 Mol% West Sak Crude Mixture

The results of a constant composition expansion experiment for this mixture at 80°F are listed in Table 6, and are plotted in Figures 23 through 26. At pressures up to 1,119.7 psia, the system consisted of an oil rich liquid phase, a clear to slightly straw colored CO₂ rich liquid phase, a lower oil rich liquid phase, a CO₂ rich vapor phase and small amounts of a black solid precipitate which adhered to the wall of the glass tube. Four equilibrium phases were observed in the pressure range from 1,119.7 to 1,214.7 psia; a clear CO₂ rich vapor phase, and small amounts of the solid precipitate. At pressures above 1,214.7 psia, CO₂ rich liquid was observed on top of oil rich liquid. View of the

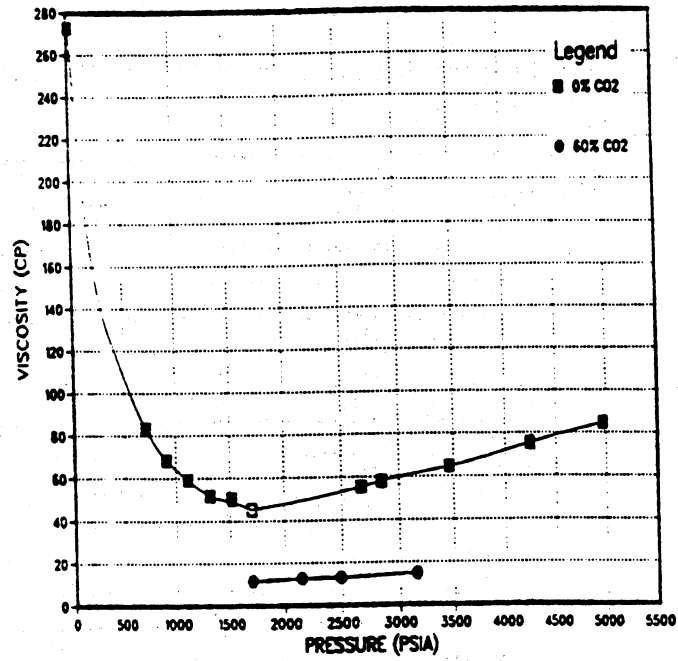


Figure 21: Oil Viscosity Reduction By CO₂ at 80°F

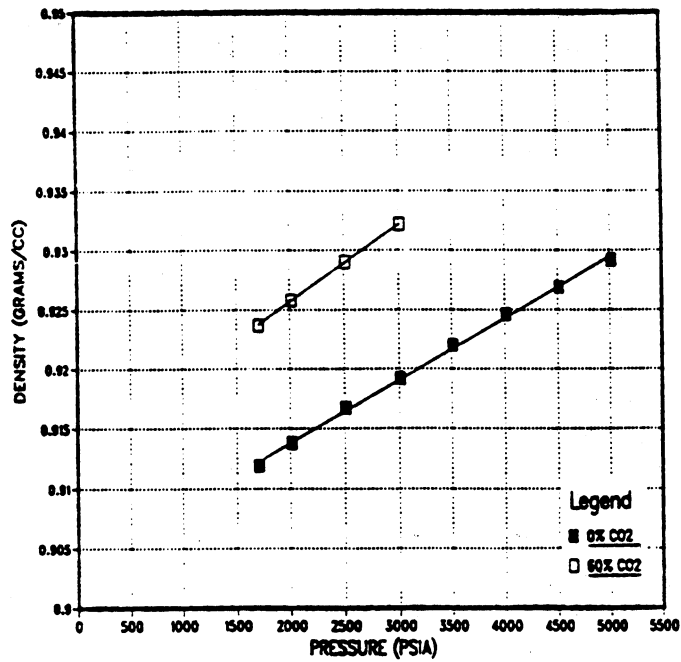


Figure 22: Oil Density Increase By CO₂ at 80°F

Table 6: Constant Composition Expansion of 80 Mol% CO₂ - 20 Mol% West Sak Crude Mixture at 80°F

Pressure (psia)	Relative Total Volume	Volume Fraction Oil Rich Liquid	Swelling Index	$\frac{V_{UL}}{V_{UL} + V_{UV}}$
5014.7	1.673	.6308	1.074	
4014.7	1.696	.6253	1.072	
3014.7	1.731	.6118	1.065	
2014.7	1.792	.5951	1.068	
1704.7	1.827	.5833	1.066	
1514.7	1.864	.5722	1.075	
1314.7	1.953	.5477	1.085	
1284.7	1.982	.5419	1.091	
1214.7	2.194	.4934	1.102	.5486
1184.7	2.265	.4776	1.102	.3903
1148.7	2.632	.4177	1.122	.0462
1128.7	2.668	.4126	1.124	.0342
1119.7	2.738	.4043	1.131	

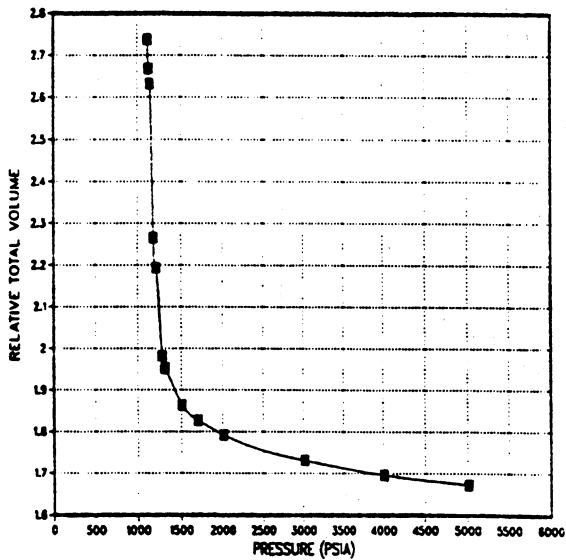


Figure 23: Relative Total Volume Versus Pressure (Constant Composition Expansion at 80°F For 80 Mol% CO₂ - 20 Mol% West Sak Crude)

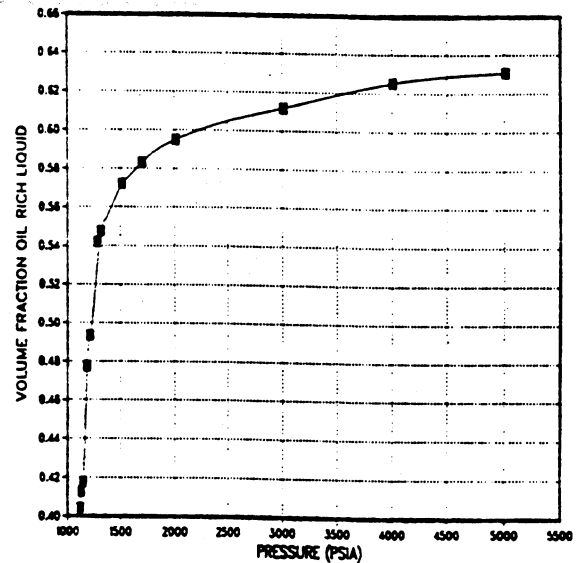


Figure 24: Volume Fraction Oil-Rich Liquid Versus Pressure (Constant Composition Expansion at 80°F For 80 Mol% CO₂ - 20 Mol% West Sak Crude)

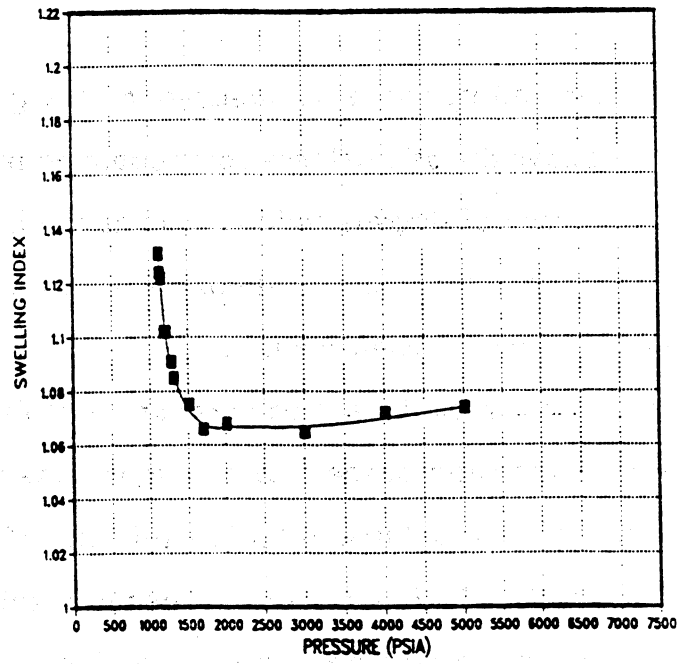


Figure 25: Oil Swelling Index Versus Pressure (80 Mol% CO₂ - 20 Mol% West Sak Crude)

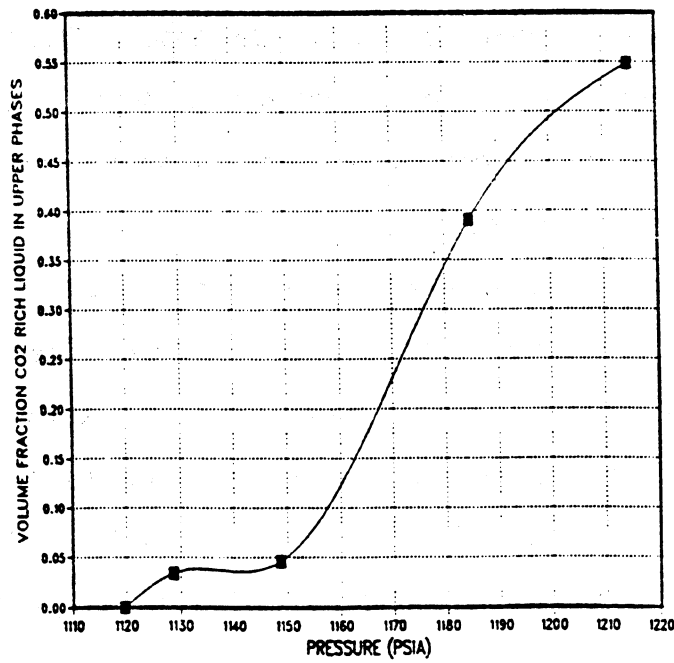


Figure 26: Three Phase Region at 80°F (Constant Composition Expansion For 80 Mol% CO₂ - 20 Mol% West Sak Crude)

cell contents was obscured by the black precipitate to a greater degree for increasing pressures above the original reservoir bubble point. The precipitate phase appeared to consist of discrete solid chunks at the high pressure data points with 80/20 mixture in the phase behavior cell, in contrast to the gummy resin-like appearance noted for 60/40 mixture.

The relative total volume values listed in column 2 of Table 6 and plotted in Figure 23 represent the ratio of the total system volume for 80/20 mixture the CO₂ free bubble point oil volume at 1,704.7 psia and 80°F. For pressures between 5,014.7 psia and 1,704.7 psia, the phase behavior cell contained a CO₂ rich liquid phase in equilibrium with an oil rich liquid. The relative total volume plot is approximately linear in this pressure range since the liquid phases exhibit low compressibility, but shows some curvature which is probably due to small increases in the solubility of CO₂ in the oil phase with increasing pressure. A rapid increase in the system volume occurs as the cell pressure is reduced below 1,704.7 psia because of a rapid decrease in CO₂ solubility in the oil, because of the liberation of natural gas from solution in the oil, and because of any system expansion associated with the transition from an upper CO₂ rich liquid phase to CO₂ rich vapor.

The volume of oil rich liquid divided by the total cell volume at each pressure is given in column 3 of Table 6, and is graphed in Figure 24. This parameter increases rapidly with increasing pressure for lower equilibrium pressures as additional CO₂ and natural gas are forced into solution in the oil phase, as the CO₂ rich vapor phase is condensed into a CO₂ rich liquid, and as the densities of the CO₂ rich phases are increased. At higher pressures, the plot flattens out indicating that little additional solubility of CO₂ in the oil phase is gained by further pressure increases. The plot is essentially horizontal at

5,014.7 psia, and gives no indication of approaching a dew point at attainable pressures.

Figure 25 is a plot of oil swelling index (the swelled oil volume) divided by the CO₂ free live oil volume at the same temperature and pressure, which are listed in column 4 of Table 6. The swelling index is approaching a local maxima near or below a pressure of 1,119.7 psia, where CO₂ has swelled the live oil by 13%. This pressure corresponds to the lower limit of the three phase region where the CO₂ rich liquid phase first appears. The swelling index declines rapidly with increasing pressure in the range from 1,119.7 psia to 1,700 psia. Since the solubility of CO₂ in the oil rich phase generally increases with increasing pressure, this rapid decrease in the swelling index likely identifies a region where extraction of hydrocarbons into the CO₂ rich phases is causing an oil rich phase volume reduction that overwhelms any oil rich phase expansion due to the solution of additional CO₂. This region of probable efficient hydrocarbon extraction by CO₂ occurs at pressures where the transition from CO₂ rich vapor to dense CO₂ rich liquid takes place. The swelling index remains approximately constant for pressures from 1,700 to 5014.7 psia, which indicates that oil swelling from the solution of CO₂ in the oil rich phase is about balanced by oil shrinkage due to compaction and extraction of hydrocarbons by dense CO₂ in this region. This swelling behavior is different from that observed for 60/40 mixture. There is no indication that the development of vaporizing gas drive miscibility (which requires efficient vaporization/extraction of oil components by CO₂ at the flood front) is likely unless local CO₂ concentrations in excess of 60 mole percent can be established in the porous media at the front during a CO₂ flood.

Column 5 of Table 6 lists the volume fraction of the upper CO₂ rich phases that consists of CO₂ rich liquid for the data points collected in the three phase

region. These values are plotted in Figure 26 in order to define the range of pressures over which three immiscible equilibrium phases occur for the first contact mixtures of the live West Sak oil with 80 mole percent CO₂ at 80°F. Extrapolation of this plot to a y-axis value of zero indicates that 1,119.7 psia is a good estimate of the lower pressure limit for occurrence of the liquid/liquid/vapor phase region. No attempt was made to extrapolate the higher pressure data points to the upper limit of the three phase region, because repeated observations at pressures a few psi above 1,214.7 psia revealed only the liquid/liquid phase region. In addition, the interface between the CO₂ rich liquid and vapor phases was found to be quite unstable at 1,214.7 psia. The interface was observed to break up, fade out of view, and reappear several times during extended observation periods. Thus, the best estimate of the upper pressure limit for occurrence of the three phase region is 1,214.7 psia.

G. Effect of Gas Solubility on West Sak Crude Viscosity

The primary objective of this study was to correlate the viscosity of gas saturated West Sak crude as a function of solution gas (or pressure) and to compare the experimental results with various viscosity correlations reported in the literature. Viscosity measurements were done with a rolling ball viscometer and density measurements were done with densitometer. The details of the experimental set up, procedures and used and the experimental results are given by Siddiqui (1989).

A total of four sets of experimental runs were conducted. In the first two runs, viscosity of dead West Sak crude versus pressure data were gathered at 100°F and 150°F respectively. The next two sets of experiments were conducted using the recombined samples of West Sak crude with methane. In these runs, viscosity data for the live oil sample were collected by differentially liberating sample at 100°F and

150°F. Viscosity correlations most commonly used in the industry were used to compare experimental results. Beggs and Robinson correlation, Chew and Connally correlation, Lohrenz, Bray and Clark's correlations were used for comparison.

Following correlations were developed using least square fitting to the experimental data:

At 100°F

$$\mu_d = 104.1 + 0.02654 p \quad \dots\dots (4)$$

$$\frac{\mu_{ob}}{\mu_d} = 0.2834 + 0.2259 \left(\frac{p_{b_i} - p_b}{p_{b_i}} \right) + 0.0352 \left(\frac{p_{b_i} - p_b}{p_{b_i}} \right)^2 + 0.4709 \left(\frac{p_{b_i} - p_b}{p_{b_i}} \right)^3 \quad \dots\dots (5)$$

$$\mu_{ob} = 120.4 - 190.3 R_s + 140.9 R_s^2 - 36.87 R_s^3 \quad \dots\dots (6)$$

At 150°F

$$\mu_d = 28.68 + 0.0053 p \quad \dots\dots (7)$$

$$\frac{\mu_{ob}}{\mu_d} = 0.5085 + 0.1135 \left(\frac{p_{b_i} - p_b}{p_{b_i}} \right) - 0.1873 \left(\frac{p_{b_i} - p_b}{p_{b_i}} \right)^2 + 0.577 \left(\frac{p_{b_i} - p_b}{p_{b_i}} \right)^3 \quad \dots\dots (8)$$

$$\mu_{ob} = 25.98 - 34.61 R_s + 33.3 R_s^2 - 11.47 R_s^3 \quad \dots\dots (9)$$

where:

- p = pressure (psia)
- μ_d = Dead West Sak Crude Viscosity in (cp)
- μ_{ob} = Live West Sak Crude Viscosity in (cp)

p_{b_i} = Bubble point pressure of fully saturated West Sak crude

p_b = Bubble point pressure of partially saturated West Sak crude

R_s = Solution gas-oil ratio in (SCF/Bbl)

Comparison of the experimental viscosity data with reported literature viscosity correlations showed that while Chew and Connally's correlation gives fairly good agreement with the data at 100°F, the Lohrenz, Bray and Clark and Beggs-Robinson correlation provide better agreement with experimental viscosity data at higher temperatures.

H. Conclusions

The PVT and fluid property measurements obtained for West Sak crude sample are useful in Equation of State predictions and in miscible and thermal studies described later in this report. It should be noted however, the type of West Sak crude used in all the experimental studies presented in this report is not necessarily representative of only one type of oil.

Effect of addition of CO₂ on West Sak crude properties and phase behavior of CO₂ - West Sak crude mixtures was investigated. The results for 60 mol% CO₂ - 40 mol% West Sak crude mixture indicate a) two phase region up to pressures of 7000 psia, b) CO₂ addition reduces live oil viscosity by 75% at CO₂ free oil bubble point pressure, c) CO₂ addition causes 9.9% oil swelling at reservoir pressure, d) CO₂ addition to oil single contact does not extract/vaporize intermediates, as needed for the development of dynamic miscibility. The results for 80 mol% CO₂ - 20 mol% West Sak crude mixture indicate, a) two phase, V/L₁ region occurs below 1120 psia, b) three phase, V/L₁/L₂ region occurs 1120-1215 psia, c) two phase L₁/L₂ region occurs above 1215 psia.

Both CO₂ - West Sak crude mixtures showed precipitation of black solids (asphaltene) for pressure range investigated in this study. Visual observations

indicate that amount of precipitation increases is greater as CO₂ mol% in the overall mixture increases and pressure increases.

Finally, experimental data were used to correlate the viscosity of West Sak crude as a function of gas solubility.

I. **References**

1. Roper, M.K., "An Experimental Study of CO₂/West Sak Crude Oil Phase Behavior," M.S. Thesis, University of Alaska Fairbanks, (1989).
2. Siddiqui, N., "Effect of Gas Solubility on Viscosity of West Sak Crude," M.S. Thesis, University of Alaska Fairbanks (1989).

CHAPTER THREE
MISCIBLE DISPLACEMENT STUDIES

PART I: Determination of Minimum Miscibility Pressures and Mechanism of Miscibility Development For Enriched Gases

A. Abstract

The API gravity and viscosity of oil in the West Sak sands varies considerably from horizon to horizon. Thus, a single enhanced oil recovery method may not be sufficient to produce this huge resource. For example, thermal processes may be more applicable to heavier crude in the shallower sections, while miscible processes may be more suitable to lighter crude in the deeper sections of West Sak reservoir. The available natural gas on the North Slope which currently is not marketed can be enriched to provide injection gas for miscible flooding in West Sak.

In this study, slim tube displacement (STD) tests supported by equation of state (EOS) predictions were used to evaluate the ability of various solvents such as CO₂, n-butane and various mixtures of Prudhoe Bay natural gas (PBG) and natural gas liquids (NGL), to achieve miscibility with West Sak oil. Equation of state predictions were used to understand the mechanism of dynamic miscibility development (a multi-contact process) for enriched gas drive (i.e. for PBG/NGL mixtures).

Results indicate that CO₂ was unable to develop dynamic miscibility with West Sak crude at reservoir pressure and temperature conditions. N-Butane, even though thermodynamically first contact miscible (FCM) solvent, showed only up to 80% oil recovery in STD tests. MMP - enrichment correlation was obtained for PBG/NGL mixtures.

B. Introduction

The API gravity and viscosity of oil in the West Sak sands varies considerably from horizon to horizon. Thus, a single enhanced oil recovery method may not be sufficient to produce this huge resource. For example, thermal processes may be more applicable to heavier crude in the shallower sections, while miscible processes may be more suitable to lighter crude in the deeper sections of West Sak reservoir. The available natural gas on the North Slope which currently is not marketed can be enriched to provide injection gas for miscible flooding in West Sak. Currently, miscible flood is underway in Prudhoe Bay Unit and a similar one based on NG/NGL type solvent is planned for Kuparuk River pool of the Kuparuk River Unit.

Slim tube displacement (STD) tests are usually performed to determine minimum enrichment (ME) requirements at reservoir conditions to achieve multi-contact miscibility (MCM) between enriched solvents and light crudes. In this study, STD tests were conducted to evaluate characteristics and applicability of this method when applied to heavy crudes. The emphasis of this study was placed on evaluating various solvents such as CO₂, n-butane, various mixtures of Prudhoe Bay natural gas (PBG) and natural gas liquids (NGL) for the ability to achieve dynamic miscibility with West Sak crude. In addition, the study also emphasized on understanding the mechanism of displacement and how it helps to interpret STD tests. Equation-of-state predictions were performed to compare the results of STD tests and to gain further insight into the mechanism of displacement.

Phase behavior of solvent-crude mixtures are the most important tools in understanding the mechanism of miscibility development in either CO₂ drives or enriched hydrocarbon solvent drives. Pseudo-ternary diagrams have been often used to explain the mechanisms of oil displacement by vaporizing gas drives or condensing gas drives⁽¹⁾. For past three decades, it has been considered that enriched hydrocarbon miscible displacement occurs via condensing mechanism⁽²⁾ and

high pressure lean miscible hydrocarbon gas⁽³⁾ displacement occurs via vaporizing mechanism. In condensing gas drives, the in-situ generation of miscibility occurs due to gradual enrichment of reservoir fluids in intermediate components of solvent to a point where it becomes fully miscible with the injected solvent. In the vaporizing drives on the other hand, the in-situ generation of miscibility occurs due to extraction of intermediate components of the reservoir fluid by the solvent and its gradual enrichment with these intermediates as it flows in the reservoir. The displacement by any mechanism is further characterized with the help of pseudo-ternary diagram as immiscible (IMM), multi-contact miscible (MCM) and first contact miscible (FCM)⁽⁴⁾. In 1960, Benham *et al.*,⁽⁵⁾ proposed a method of predicting minimum miscibility pressure (MMP) or minimum enrichment (ME) required to achieve multi-contact miscibility by constructing pseudo-ternary diagrams and determining limiting tie-line intersections with the light-intermediate component axis. This method has been used ever since, although it has been updated slightly in recent years^(6,7).

However the work of Stalkup⁽⁸⁾ and Zick⁽⁹⁾ challenged this traditional concept for some rich gas displacements. Zick⁽⁹⁾ provided evidence indicating that the mechanism of enriched gas drives is not condensing type but it is both simultaneous vaporizing and condensing types.

Recently, Novosad and Costain⁽¹⁰⁾ using STD tests and EOS calculations showed that in Canadian reservoir rich gas projects the principal mechanism is liquid extraction drive and provided further interpretation of this process.

Other two recent studies on investigation of dominant mechanism of miscible displacement are reported by Mansoori and Gupta⁽¹¹⁾ and Lee *et al.*,⁽¹²⁾.

Mansoori and Gupta⁽¹¹⁾ presented the results of a compositional simulation investigating the relationship between the displacement mechanism, the minimum enrichment requirement, and the oil recovery efficiency for a rich gas system. They

used three approaches in their study. The first approach was to simulate slim tube displacement. The second approach was based on Hutchinson and Braun's⁽¹⁾ multiple contact mixing, and the third approach was based on numerical, 1-D simulation of displacement behavior at the limit of zero dispersion. They concluded that the displacement mechanism over a wide range of solvent enrichment was governed by a condensing/vaporizing process; however the relative importance of the condensing or vaporizing mass transfer processes and their impact on the overall displacement efficiency, was a function of the enrichment level. For displacements at or above the slim tube ME; recovery was very high and the process behavior was similar to a classical condensing mechanism. Displacements simulated below slim tube ME were less efficient; however, both condensing and vaporizing mass transfer processes contributed to the overall recovery efficiency. At enrichment levels far above the slim tube ME, the effect of the condensing mass transfer process on displacement was less significant and the behavior approached that of a classical vaporizing mechanism.

Lee et al.,⁽¹²⁾ also studied mechanism of rich gas displacement by performing experimental slim tube displacements and 1-D compositional simulation. They concluded that, the dominating mechanism depends upon pressure, temperature, and solvent - oil compositions. They also stated that the solvent density can be a useful parameter for preliminary screening of solvent compositional requirement.

The experimental STD test results and EOS predictions presented here support the dual drive mechanism proposed by Zick's study and infer on implications of this dual mechanism on interpretation of STD results and minimum enrichment determination. The results also provide various apparent limitations of pseudo-ternary diagram method when used for minimum enrichment determination by assuming condensing drive mechanism. A more rigorous procedure for determining minimum enrichment (ME) or minimum miscibility pressure (MMP) in case of dual

drive mechanism calls for proper characterization of reservoir fluid and solvents, determination of compositional path followed by solvent-reservoir fluid mixtures in a multi-contact test calculations, and use of solvent-reservoir fluid, pressure-composition isothermal diagrams. This procedure was used to determine solvent enrichments and comparison of ensuing values with those predicted from pseudo-ternary diagrams are provided.

C. Slim Tube Miscibility Set-Up

To obtain accurate data in laboratory flow experiments, it is essential that certain requirements are met. Extremely accurate flow control must be maintained at all pressures. Reliable pressure readings should be monitored frequently throughout the experimental run. Accurate and constant back pressure must be kept throughout the run. A reliable method for measuring volumes of fluids under high pressures and at atmospheric conditions must be available. In order to meet these requirements and assure the reproducibility of the resulting data, the high pressure high temperature miscibility apparatus designed by D.B. Robinson and Assoc. was modified, assembled and used in the laboratory to determine MMP relations. This assembly is schematically shown in Figure 1. The major components of this assembly consist of the following:

1. Motorized positive displacement pump.
2. Slim-tube.
3. Two forced air temperature controlled ovens.
4. High pressure capillary sight glass.
5. Three digital pressure gauges.
6. Differential pressure transducer.
7. Calibrated glass receiver and optical liquid measuring device.
8. Precision 40 liter gasometer.

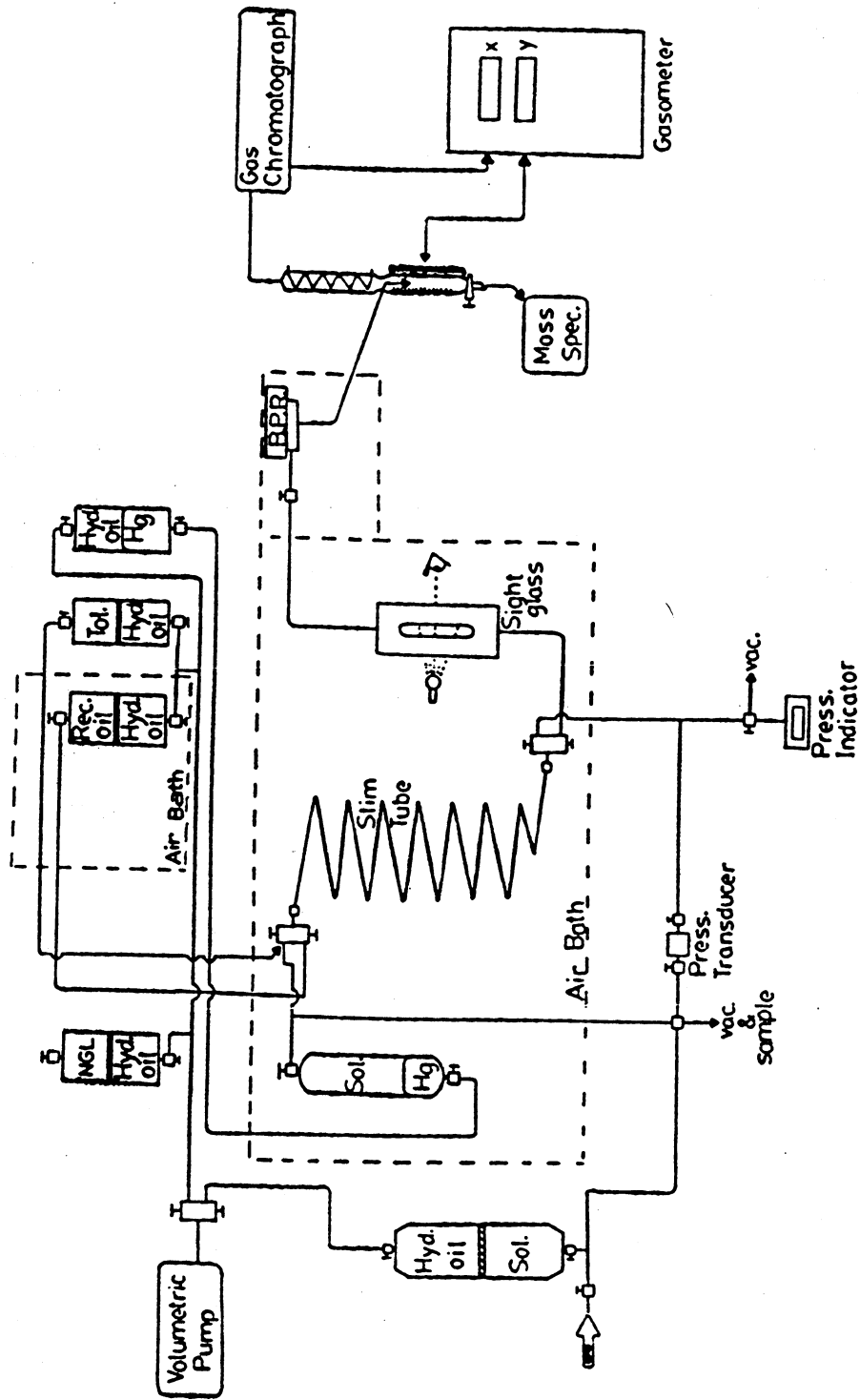


Figure 1: Slim Tube Miscibility Apparatus

9. Six transfer cells.
10. Gas chromatograph.
11. Recombination cell and shaking device.
12. Dome type back pressure regulator.
13. High volume vacuum pump.
14. Constametric pump.
15. Immersion cooler.

The equipment was designed for operation at pressures up to 10,000 psi and temperatures to 200°C. The motorized JEFRI positive displacement pump was used throughout the experiment to accurately meter, feed and proportionately displace liquids and gases under high pressure. More specifically, it effectively had four functions.

1. Provide constant pressure while recombining West Sak Crude samples.
2. Compress and transfer gases and NGL's during the solvent mixing process.
3. Drive recombined oil to saturate the slim-tube before each run and drive solvents to clean the slim-tube after each run.
4. Inject the gas solvent mixture during each run.

The pump was equipped with a DC servo motor and chain drive which in turn was controlled by a microprocessor indexer. This allowed the pump to either displace fluids at constant flow rates from 1 to 1000 cc/hr, or to maintain a constant pressure, regardless of the direction of flow, at variable speeds. Pump operation could be monitored throughout the run with the use of high and low pressure limit alarms.

The slim-tube itself was composed of a 12 meter section of 6.4 mm O.D. high pressure stainless steel tubing which was packed with Ottawa sand and coiled to a diameter of approximately one foot. The porosity of slim tube was 35.2% and

permeability was calculated to be 5.0 darcies, using pure toluene as the test fluid of known viscosity.

The slim-tube and recombination cell were enclosed in a windowed, forced air, temperature controlled oven. Oven temperature was controlled through the simultaneous heating of a main bulk heating coil and a smaller microprocessor controlled heating coil. The main bulk heater was set with a simple rheostat and was the main heat source for the oven, while smaller coils were used to control the oven's temperature within 0.2°C of the desired set point.

At the effluent end of the slim-tube, a JEFRI high pressure capillary sight glass was used to visually observe displaced fluids during the dynamic miscible process. The sight glass consisted of a Pyrex capillary tube, 4.390 inches in length with a 7.5 mm O.D. and 1.5 mm I.D., mounted within a windowed overburden cell. In the overburden cell, distilled water was compressed by a hand operated pressure generator to a pressure approximately 300 psi. greater than that within the capillary tube. While maintaining this pressure differential it was possible to visually observe the fluids at operating conditions of up to 200°C and 10,000 psi. The passage of the miscible front was photographed using a 35 mm camera.

The overall operating pressure of the slim-tube system was controlled by a gas driven, dome type back pressure regulator. Operating on the principle of balanced pressure, a stainless steel diaphragm separated the effluent pressure from the pressure exerted by the operator's set point. A pressure reaction chamber allowed for precise pressure imbalance control thus maintaining predetermined run pressures.

Once the effluent is flashed to atmospheric conditions, through the back pressure regulator, the resulting gas and liquid components were collected and measured volumetrically. The gas was measured by a JEFRI precision gasometer using a calibrated stainless steel cylinder and piston fixed to a threaded rod which

was linked to an electric motor. As gas entered the cylinder, atmospheric pressure was maintained in the gasometer by a system which moved the piston to expand the cylinder's volume. Such volume control was achieved using an oil filled manometer equipped with a pair of optical interrupter switches. An increase in pressure within the cylinder was indicated by a change in manometer fluid meniscus level. Any such change in meniscus level was noted by the optical sensors, and a signal was sent to the motor drive which increased the volume of the cylinder to accommodate the additional gas. Piston location was measured and displayed by an optical linear encoder, and converted through a calibrated constant to standard cubic centimeters.

A specially designed glass cylinder collected the condensed liquid after it passed through a condenser. An optical sensor, similar to that used in the gasometer, was mounted on a motor driven lead-screw. As the opaque oil meniscus rose up the glass cylinder it interrupted the path of the laser sighted optical sensor, which in turn signaled the motor to raise it according to the level of the air liquid interface. Once again, a linear encoder measured the calibrated sensor level which was converted into cubic centimeters of oil.

While traveling to the gasometer, effluent gases passed through a glass sample bottle equipped with a diaphragm which permitted gas sampling with a calibrated syringe. The samples were analyzed in a standard Hewlett Packard 5790 gas chromatograph, equipped with a thermal conductivity detector.

During the run, the upstream pressure was monitored by a precision pressure transducer linked to the motorized pump's microprocessor, while the downstream pressure was monitored by a digital Heise pressure gauge. An external Heise gauge was also linked into the system to monitor gas pressures during solvent mixing. A validyne differential pressure transducer was used to monitor the differential pressure across the slim-tube during the displacement process. The external Heise

gauge was calibrated using a dead weight tester and was then used to calibrate the other gauges.

Six cells, five of them with pistons and one without a piston, were used to recombine oil, mix solvents, and transfer fluids during each experiment. Two of the pistoned cylinders, manufactured by Temco, were used to compress gas for solvent mixtures and the back pressure regulator, as well as drive cleaning solvents through the slim-tube. The remaining JEFRI cylinders were used to recombine oil, transfer NGL's, and drive final solvent mixtures during each experimental run.

Each piece of equipment was connected with 1/8 and 1/16 inch high pressure 316 stainless steel tubing and HIP fittings. Generally, lines containing liquid were of the larger 1/8 inch O.D. to accommodate the fluid's higher viscosity, while gas lines were constructed of 1/16 inch tubing. Whenever possible, it was important to reduce line size and length to minimize dead volume in the apparatus.

When transferring fluids from one cell to another through stainless steel tubing, it was necessary to thoroughly evacuate the system to maintain compositional purity and avoid contamination. This was accomplished with the use of a Sargent-Welch high volume vacuum pump capable of inducing effective vacuums down to 50 microns. Generally, less than 200 microns were achieved before transferring oil, solvents, or gases.

D. Experimental Procedures

Toluene calibration allowed a precise slim-tube pore volume determination and also initially wet the system, making it operational. All lines, including the slim-tube, were evacuated to approximately 50 microns. A pistoned cylinder filled with toluene was fitted to the positive displacement pump and pressurized to an arbitrary pressure far above the vapor pressure of toluene at room temperature (2000 psi). While maintaining its vacuum, the slim-tube pore volume, from the inlet valve

(including the sight glass) to the back pressure regulator inlet, was separated from the rest of the system by closing the appropriate valves. Toluene at 2000 psi was primed up to the slim-tube inlet and an initial pump reading was taken. The inlet valve was opened slightly, pumping toluene into the slim-tube under the displacement pump's constant pressure option. After the slim-tube pressure equilibrated at the initial 2000 psi, a final pump reading indicated the volume of toluene displaced into the slim-tube under constant pressure. This was in fact the pore volume of the slim-tube (69.4 cc + 0.2 cc dead volume of BPR).

It was necessary to calibrate the main bulk heater for high as well as low temperature runs. From this initial data calibration temperature settings were maintained within 0.2°C of the desired set point. The rheostat setting was set according to the calibrated curve and the same set point entered into the digital controller. An upper alarm was set 0.2°C above the set point, effectively shutting down both coils should the oven temperature rise above this point.

Prior to each run certain tasks were routinely performed to set up the apparatus for data collection. Perhaps the most critical of these was the gas solvent preparation, especially when NGL mixtures were required. Care was taken to maintain the solvent mixture in the single phase.

The dead oil samples were recombined with methane at 1705 psia in the recombination cell. The recombined oil was pumped at 3 cc/hr through valve 5 into the slim-tube; the crude was never allowed to flash. This continued over a period of approximately 48 hours until over 2 pore volumes had been injected. Distinct color changes of the fluids passing through the sight glass indicated the degree of slim-tube saturation. Once the recombined oil had completely displaced all traces of toluene from the slim-tube, the apparatus was ready to run.

Once the slim-tube was saturated with crude the pump was stopped and sufficient time was allotted to allow the slim tube inlet and outlet pressures to

equilibrate. The pressure was balanced across the pressure transducers to initialize a starting point (time zero). Solvent pressure was raised 50 psi above the pressure at the inlet of the slim-tube to assure positive flow and solvent injection was started at 3 cc/hr. Progress throughout the run was monitored by recording several variables, including photographic records of visual sight glass observations. Initial readings were taken at one to two hour intervals, while the intervals between later readings decreased to 30 minutes or less as the miscible front passed through the sight glass. Following the miscible front, large gas volumes were flashed into the gasometer, signaling the production of the injected solvent. Generally, after 1.2 PV had been injected, or when three consecutive unchanging recovery readings at one hour intervals were obtained, the run was terminated.

Following the run, it was necessary to clean the slim-tube for consecutive experiments. The presence of asphaltene precipitates and the high water content of West Sak crude complicated this process considerably. When using this heavy crude, a method was developed using a series of two cleaning solvent slugs. The first slug consisted of 2 to 3 pore volumes of toluene, which effectively dissolved all precipitants and cleaned the slim-tube of all residual hydrocarbons. The toluene slug, however, was ineffective in complete removal of residual water pockets from the miscible bank. It was necessary to develop a cleaning slug which would remove water while not contributing to further precipitation from any small fractions of residual oil. Pure acetone, although effective in displacing water, was highly immiscible with West Sak crude. Various mixtures of solvents and alcohols were tested until a solvent consisting of 60% benzene, 20% methanol, and 20% acetone was found to work effectively. The system was charged with an additional 2 pore volumes of this mixture until no pockets of residual water were present in the sight glass. Once the slim-tube was eluted with sufficient cleaning solvents, the oil

recombination cell was connected to the slim-tube inlet and the system was saturated with recombined oil for the next run.

E. Experimental Results

Table 1 shows the compositional analysis of the recombined West Sak oil, Prudhoe Bay natural gas and natural gas liquids.

E1. Carbon Dioxide as Solvent

The first solvent tested was carbon dioxide for its apparent advantages. Three STD tests were conducted at 100°F and at increasingly higher pressures of 1750, 4000 and 6650 psia. The results of these three tests are given in Table 2. Figure 2 shows a typical plot of cumulative % oil recovery versus PV of CO₂ injected for 1750 psia pressure test. All the three tests clearly indicated immiscible displacement behavior such as observation of two phases in sight glass, early breakthrough, increase in breakthrough and ultimate oil recovery versus pressure and very low (45.1 to 54.7%) ultimate oil recoveries. The EOS predictions also indicated CO₂ to be immiscible at these pressures as described later.

E2. N-Butane as Solvent

It was quite apparent from CO₂ STD tests that heavier solvents would be required to achieve miscibility with West Sak crude. For this reason, liquid solvent such as pure n-butane was chosen to study displacement behavior of West Sak crude. Three STD runs at 80°F and pressures of 3600, 2375 and 1775 psia and three STD runs at 250°F and pressures of 4800, 4050 and 2625 psia were conducted. Runs at 80°F were conducted to simulate reservoir temperature and runs at 250°F were conducted to investigate the effect of thermal enhancement on STD recoveries. The results of these STD tests are summarized in Table 3. The bubble point pressures of the West Sak crude at

Table 1: Compositions (Mol%) of Recombined West Sak Crude, Prudhoe Bay Natural Gas (PBG) and Natural Gas Liquids (NGL)

Component	Recombined West Sak Crude	Prudhoe Bay Natural Gas (PBG)	Natural Gas Liquids (NGL)
N ₂	0.03	trace	0.02
CO ₂	0.02	12.73	trace
C ₁	38.33	72.80	trace
C ₂	0.86	7.44	trace
C ₃	0.36	3.94	1.50
C ₄	0.18	2.29	50.50
C ₅	0.06	0.80	29.13
C ₆	0.20		18.85 (C ₆ +)
C ₇	0.02		
C ₈	0.01		
C ₉	0.82		
C ₁₀	1.50		
C ₁₁	1.72		
C ₁₂	0.35		
C ₁₃	0.50		
C ₁₄	0.80		
C ₁₅	0.94		
C ₁₆	0.80		
C ₁₇	0.57		
C ₁₈	1.80		
C ₁₉	2.47		
C ₂₀	2.84		
C ₂₁ +	38.82		
Mol. wt of + Fraction	455		96

Table 2: Summary of Slim Tube Displacement Tests For West Sak Crude With CO₂ and Solvent at 100°F

Test #	Pressure (psia)	Breakthrough Recovery (%)	Ultimate Recovery (%)	Sight Glass Observations	Conventional Interpretation*	New Interpretation**
1	1750	39.8	45.1	Two phase	Immiscible	Immiscible
2	4000	43.4	52.0	Two phase	Immiscible	Immiscible
3	6650	50.0	54.7	Two phase	Immiscible	Immiscible

- * Conventional interpretation is based on traditional pseudo-ternary diagram construction using 3-component model.
- ** New interpretation is based on p-x (solvent-oil) diagram and compositional path in multi-contact test calculations using 23-component model.

Table 3: Summary of Slim Tube Displacement Tests For West Sak Crude With N-Butane as Solvent

AT 80°F

Test #	Pressure (psia)	Breakthrough Recovery (%)	Ultimate Recovery (%)	Sight Glass Observations	Conventional Interpretation*	New Interpretation**
1	1775	78.0	79.8	Single phase	FCM	FCM
2	2375	79.2	81.3	Single phase	FCM	FCM
3	3600	79.8	81.0	Single phase	FCM	FCM

AT 250°F

4	2625	73.0	74.0	Single phase	FCM	FCM
5	4050	73.4	73.8	Single phase	FCM	FCM
6	4800	74.2	75.0	Single phase	FCM	FCM

- * Conventional interpretation is based on traditional pseudo-ternary diagram construction using 3-component model.
- ** New interpretation is based on (solvent-oil) p-x diagram and compositional path in multi-contact test calculations using 23-component model.

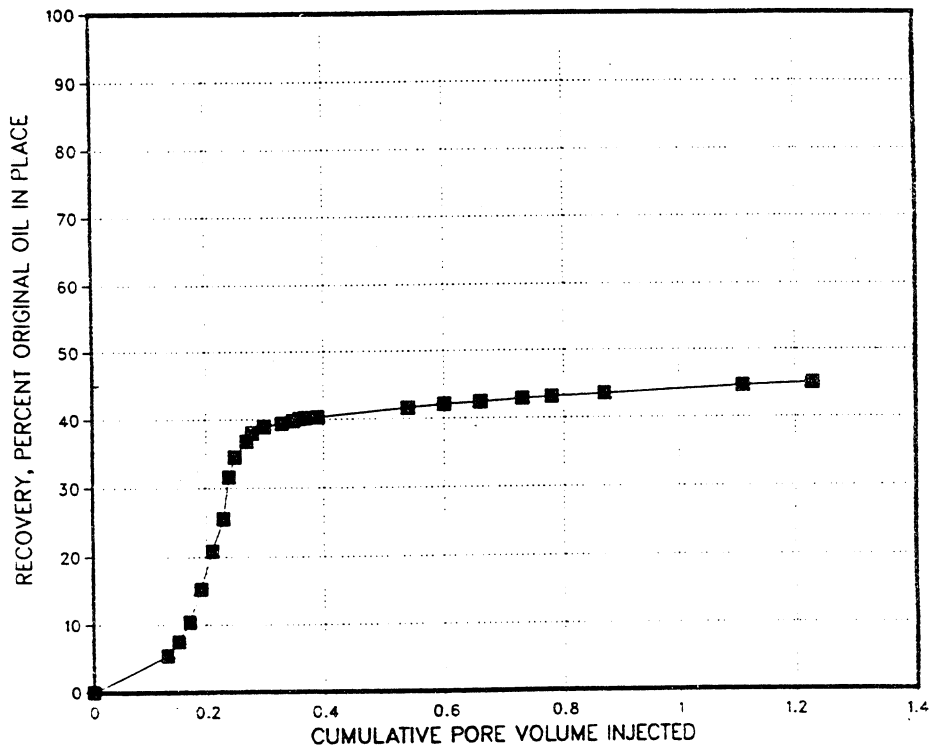


Figure 2: Slim Tube Oil Recovery Versus PV of CO₂ Injected (1750 psi, 100°F)

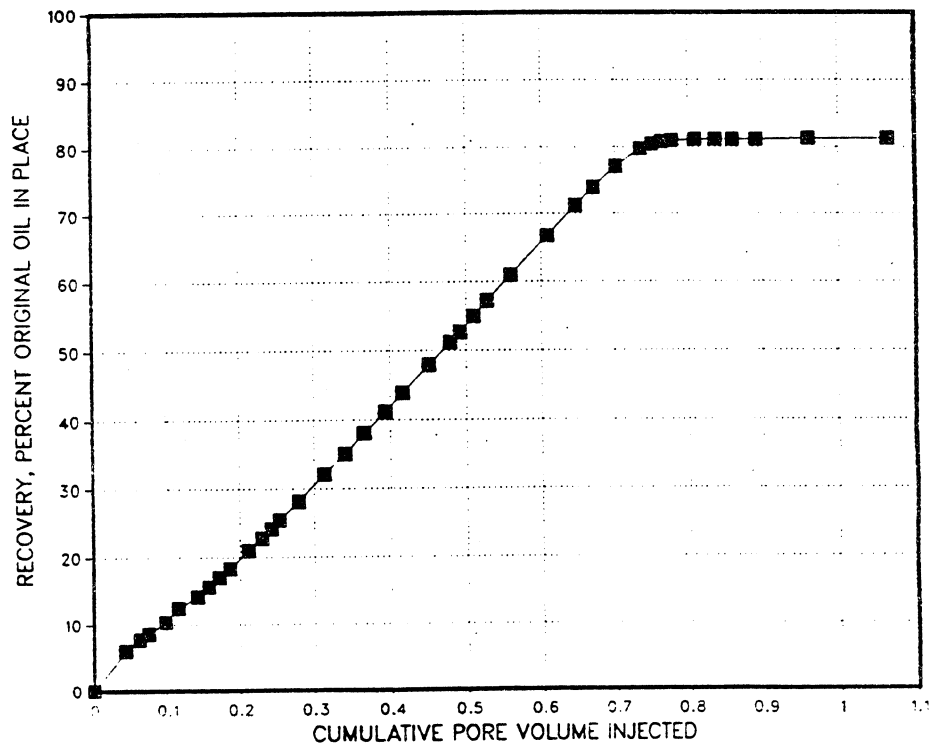


Figure 3: Slim Tube Oil Recovery Versus PV of N-Butane Injected (2375 psia, 80°F)

80°F and 250°F are 1700 and 2500 psia respectively. A typical STD plot for 2375 psia is given in Figure 3. All six runs clearly indicated miscible displacement as noted by insignificant ultimate oil recovery change with pressure, distinct color changes, and single phase in sight glass observations. It was not clear, however, from STD runs whether the displacement was FCM or MCM. It was also surprising to see very low ultimate oil recoveries (74 to 81.3%) despite clear miscible displacement behavior. EOS predictions conducted subsequently revealed that the process was FCM as described later.

E3. NGL/PBG Mixtures as Solvent

After gaining experience with CO₂ and butane solvents no further tests were conducted with pure solvents, instead from more practical standpoint, STD tests were conducted with various mixtures of natural gas liquids (NGL) and Prudhoe Bay natural gas (PBG). 5/95 (mol% NGL/mol% PBG), 17.6/82.4 and 35/65 solvents were tested. The results of these STD tests are given in Table 4. The typical STD plots for solvent mixtures, 5/95 (2500 psia), 17.6/82.4 (2500 psia), 35/65 (3500 psia) are given in Figure 4. The compositions of NGL and PBG are shown in Table 1.

A leaner solvent (5/95) mixture clearly indicated immiscible displacement behavior in STD tests at 2500 and 3500 psia as noted by very low oil recoveries, two phases in sight glass and increase in ultimate oil recovery with pressure. The displacement behavior for (17.6/82.4) solvent mixture however was more difficult to distinguish especially since sight glass observations indicated two phase where as the effect of pressure on breakthrough or ultimate oil recoveries (see Table 4) were insignificant. The richer solvent (35/65) mixture showed miscible displacement in STD test although it was not clear whether the displacement was MCM or FCM. The further interpretation of these STD tests is provided in the later section.

**Table 4: Summary of Slim Tube Displacement Tests For West Sak Crude
With Mixtures of PBG and NGL as Solvent**

Test #	Mol% NGL in Solvent	Temp. (°F)	Pressure (psia)	Breakthrough Recovery (%)	Ultimate Recovery (%)	Effluent Methane Spike (t)	Sight Glass Observations	Conventional Interpretation*	New Interpretation**
1	5.0	80	2500	37.3	39.7	34.6	Two phase	Imm.***	Imm.
2	5.0	80	3500	53.7	63.1	31.9	Two phase	Imm. - MCM	Imm.
3	17.6	80	1900	-	73.8	27.3	Two phase	Imm. - MCM	Imm.
4	17.6	80	2350	70.3	74.7	26.3	Two phase	MCM	Imm.
5	17.6	80	2500	69.1	73.6	26.0	?	MCM	Imm.
6	17.6	80	2775	72.7	75.3	24.4	?	MCM	Imm.
7	17.6	250	4050	45.9	54.7	25.1	Two phase	MCM	Imm.
8	35.0	80	3500	-	78.1	0.1	Single phase	FCM	MCM

* Conventional interpretation is based on traditional pseudo-ternary diagram construction using 3-component model.
 ** New interpretation is based on (solvent-oil) p-x diagram and compositional path in multi-contact test calculations using 23-component model.
 *** Imm - Immiscible.
 † Methane concentration (mol%) in effluent gas minus methane concentration in solution gas.

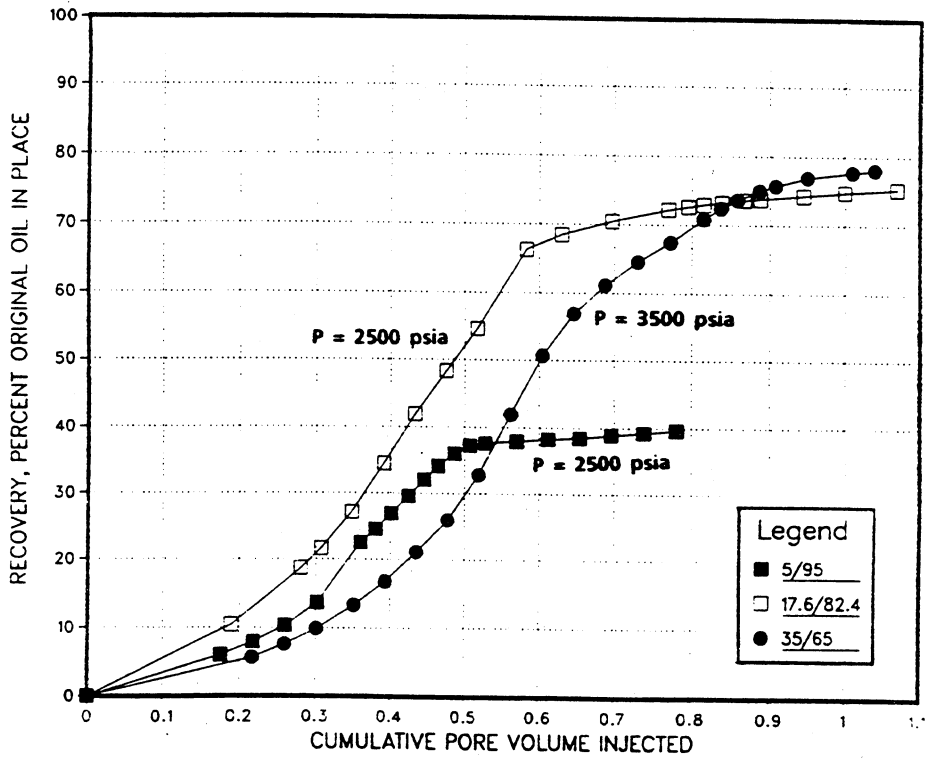


Figure 4: Slim Tube Oil Recovery Versus PV of NGL/PBG Injected

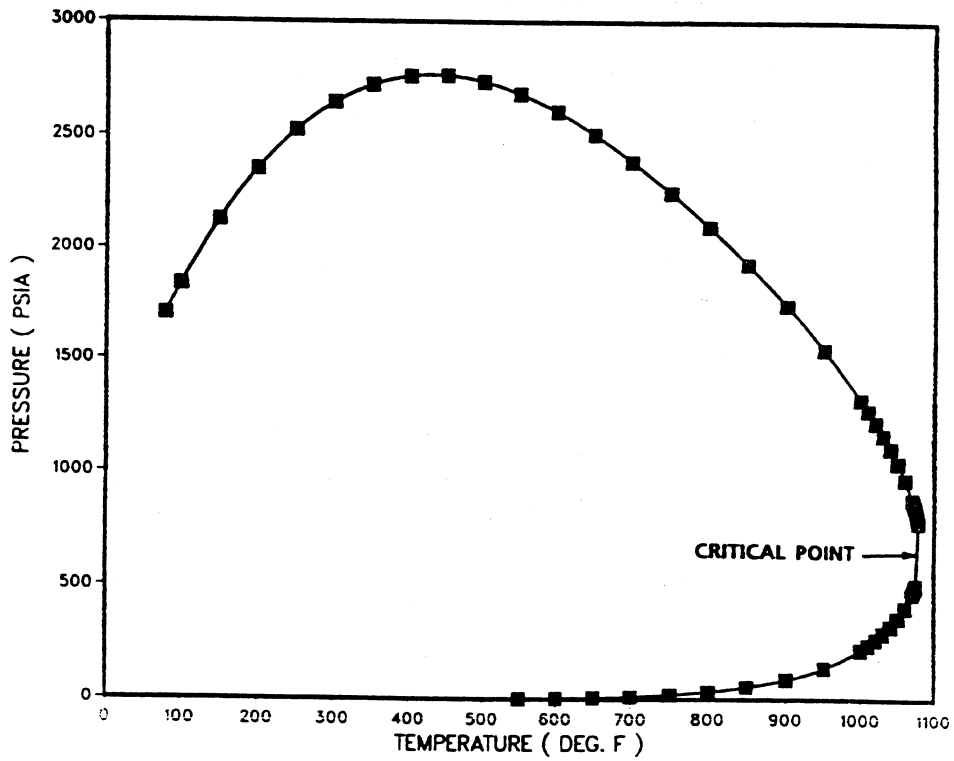


Figure 5: EOS Predicted P-T Envelope for West Sak Crude

F. EOS Predictions

To gain insight into the understanding of mechanism of miscibility development for the solvents studied and for the interpretation of STD results it was necessary to use EOS calculations. All of the phase behavior calculations were derived using the Peng-Robinson EOS. The West Sak PVT and phase behavior data were used in tuning EOS constants. For all EOS predictions except for the one used in pseudo-ternary diagram construction, we used 23 component fluid model as shown in Table 1. The first set of predictions included complete P-T envelope for West Sak fluid as shown in Figure 5. The bubble point curve on this diagram ranged from (80°F, 1705 psia) to (1076°F, 709 psia). Next, the P-T envelopes for various NGL/PBG mixtures were determined (see Figure 6). These curves were helpful for preparing mixture of solvents so that the solvent remained in single phase. It should be noted that solvent mixtures between (0/100) and (11/89) are gases where as solvent mixtures between (12/88) to (40/60) are liquids at 80°F. In other words, solvent mixtures between (11/89) and (12/88) have critical temperatures close to 80°F.

F1. Limitations of Pseudo-Ternary Diagram Method

Even though the inherent approximations in representing phase behavior of multi-component systems in terms of three pseudo-components are well known, these diagrams are often used to interpret processes of miscibility development, to determine compositional path of oil-solvent mixtures in a multi-contact process, and to determine MMP or solvent enrichment needed to achieve MCM. For construction of two phase envelope in the pseudo-ternary diagram, arbitrary mixtures of three pseudo-components are flashed at given pressure and temperature⁽¹⁰⁾. In another method⁽⁷⁾ mixtures of fixed solvent/oil ratio with increasingly rich solvent are flashed. The resulting liquid and gas compositions are plotted as tie-lines.

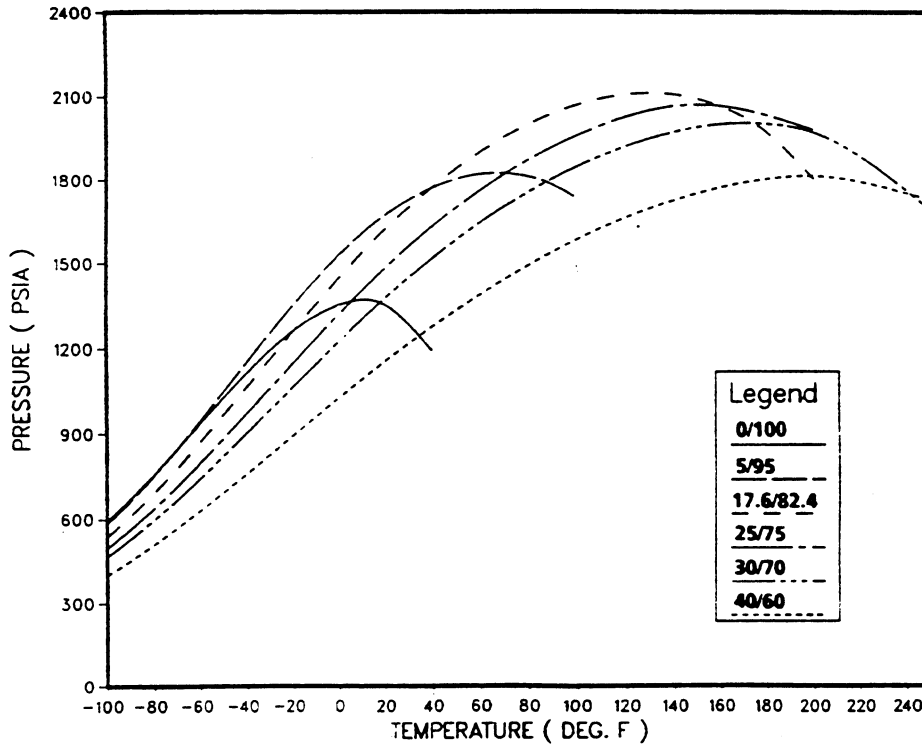


Figure 6: P-T Envelopes for Various Mixtures of Prudhoe Bay Gas (PBG) and Natural Gas Liquids (NGL)

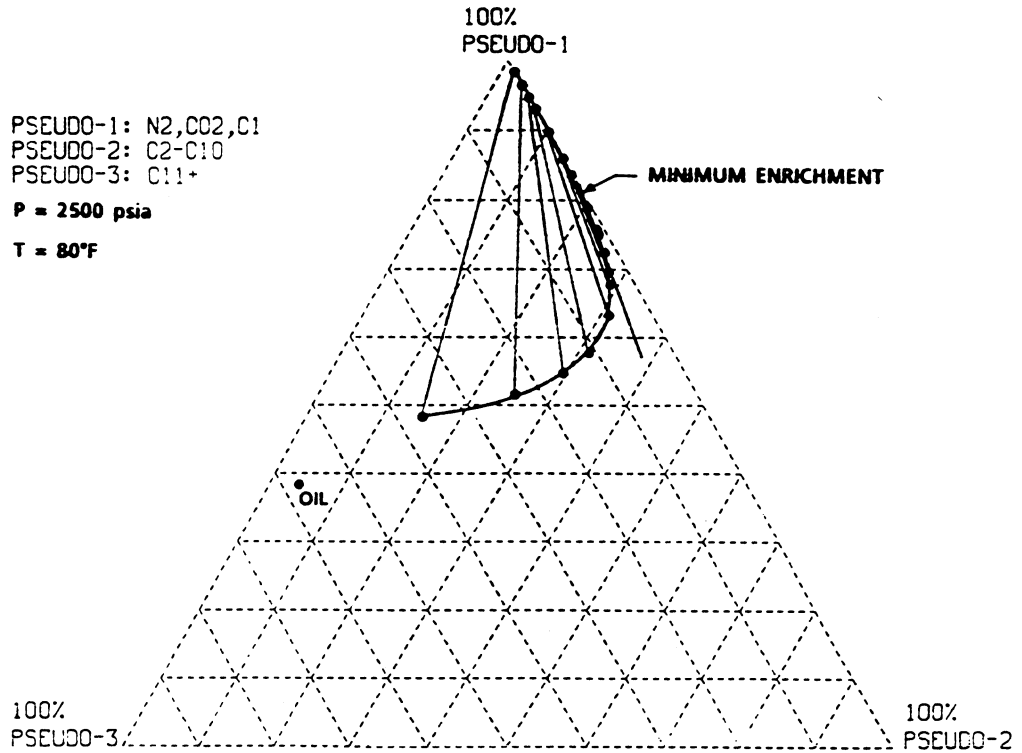


Figure 7: Ternary Diagram Developed Using Three Pseudo-Component Flashing Technique

To demonstrate how misleading the use of three pseudo-component model in phase behavior calculations can be, we used pseudo-ternary limiting tie-line method to determine pressure-enrichment correlation (MMP for a given enrichment). All oil-solvent mixtures were represented by three pseudo-components namely; $PC_1 = CO_2 + N_2 + C_1$, $PC_2 = C_2$ to C_{10} and $PC_3 = C_{11+}$. Figure 7 shows the 2-phase envelope generated by flashing technique using these 3-pseudo-components at 80°F and 2500 psia.

For CO_2 solvent, this technique predicted immiscibility with West Sak crude at all STD test conditions showing agreement with the STD results. However, the multi-contact process indicated vaporizing mechanism which is incorrect. For n-butane also, this technique showed agreement with STD results indicating first contact miscibility.

For NGL/PBG solvent, minimum enrichment required for MCM versus pressure were determined using limiting tie-line method at 60°F, 80°F, 150°F and 250°F. Also minimum enrichment required for FCM at these temperatures were obtained. Figure 8 shows the MMP-ME correlation obtained in above manner. Clearly, these results disagree with STD results. For example, STD tests for 5/95 mixture at 3500 psia and 80°F, 17.6/82.4 mixture at 1900, and 2320 psia indicated two phase in sight glass observations while limiting tie-line method (Figure 8) showed these to be multi-contact miscible.

Limitations of pseudo-ternary diagram construction using 3-component model are summarized as follows:

1. For enriched gas drives, this method predicts condensing drive mechanism resulting in dynamic miscibility while in reality the mechanism is condensing-vaporizing process.
2. For CO_2 drives, this model predicts vaporizing process mechanism while in reality the mechanism is condensing-vaporizing process.

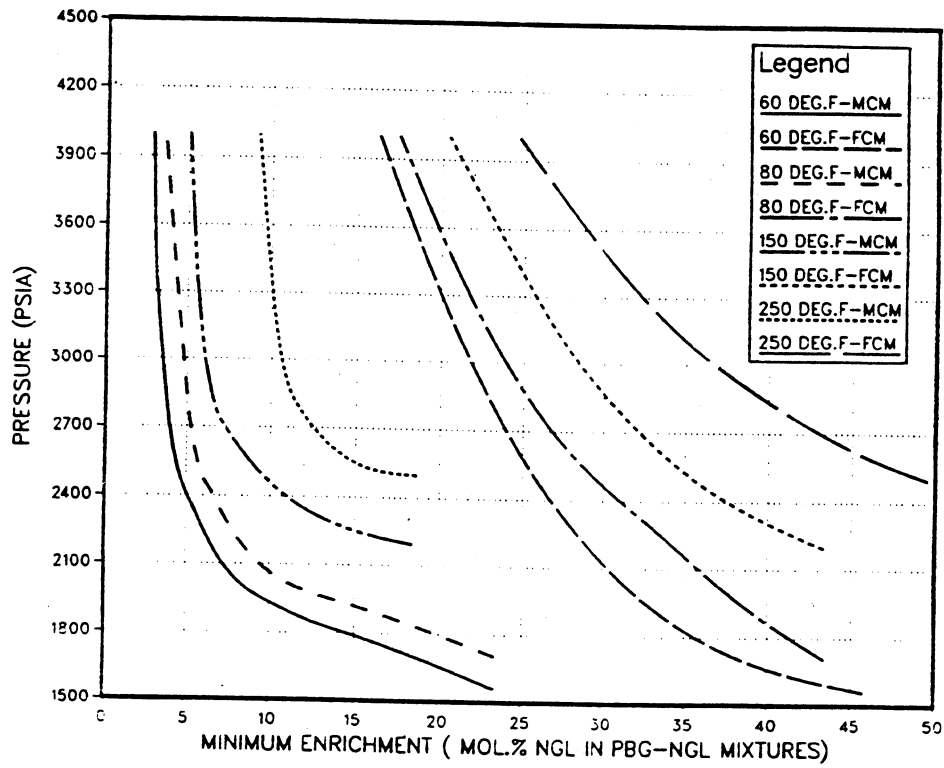


Figure 8: Pressure-Enriched Correlation For West Sak Crude (Pseudo-Ternary Tie Line Method)

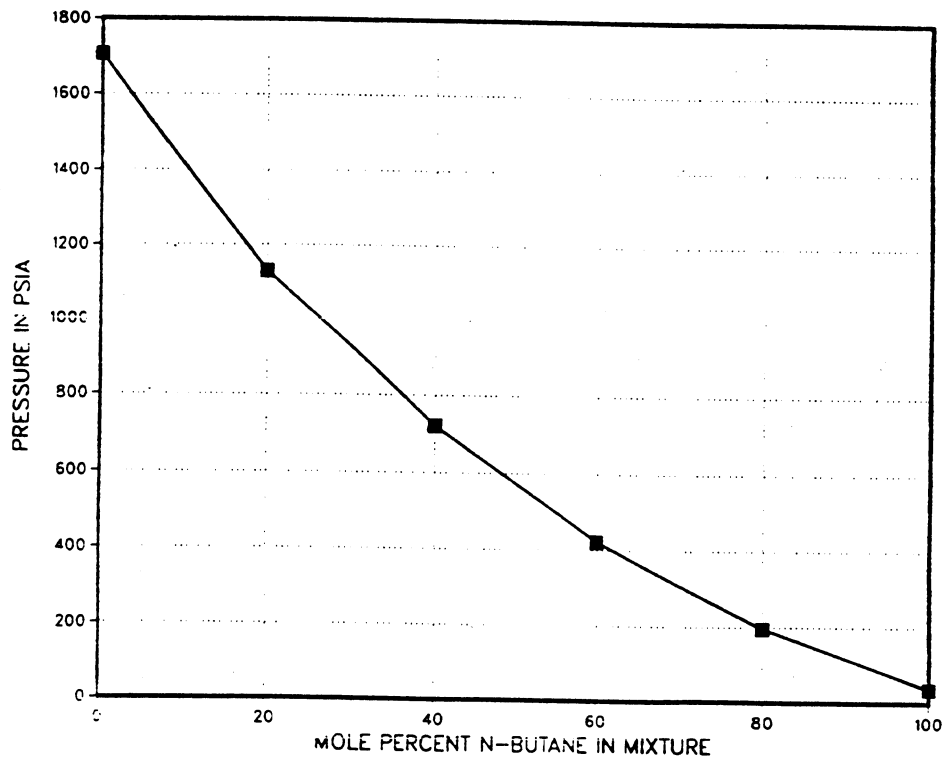


Figure 9: P-X Diagram For West Sak Crude/N-Butane Mixtures at 80°F

3. This method provides incorrect interpretation of STD tests and minimum enrichment.
4. The compositional path followed by oil-solvent mixtures in multi-contacts predicted by this method is clearly different than the actual compositional path.
5. This method develops one two-phase envelope at fixed pressure and temperature irrespective of solvent and oil compositions. However, in reality the shape of the two-phase envelope is also a function of solvent-oil combination.

F2. Solvent-Crude Oil Pressure-Composition Diagram

The solvent-crude oil pressure-composition isothermal diagrams are important for understanding the mechanism in miscibility development. However, care should be taken while characterizing oil-solvent mixtures into number of components. It was observed that 3-pseudo-component model resulted in completely different p-x diagram (much lower cricondenbar pressure) than that obtained by 23-component model. Thus, in all calculations for p-x diagram generation a 23-component model was used.

For CO₂ - West Sak crude mixtures at 80°F, p-x diagram (not shown) showed that for compositions greater than 60 mol% CO₂, the cricondenbar pressures were very high (greater than 17000 psia).

For n-butane - West Sak crude mixtures at 80°F, the p-x diagram (Figure 9) showed neither cricondenbar nor critical point and therefore the curve indicating first contact miscibility. Similar behavior was also observed at 250°F.

The most interesting p-x diagrams as shown in Figure 10 are for the (NGL/PBG) solvent - West Sak crude mixtures at 80°F. This figure includes diagrams for (5/95), (17.6/82.4), (25/75), (30/70), (35/65), and (40/60) mixtures of NGL/PBG with West Sak crude. The cricondenbar pressure in this figure

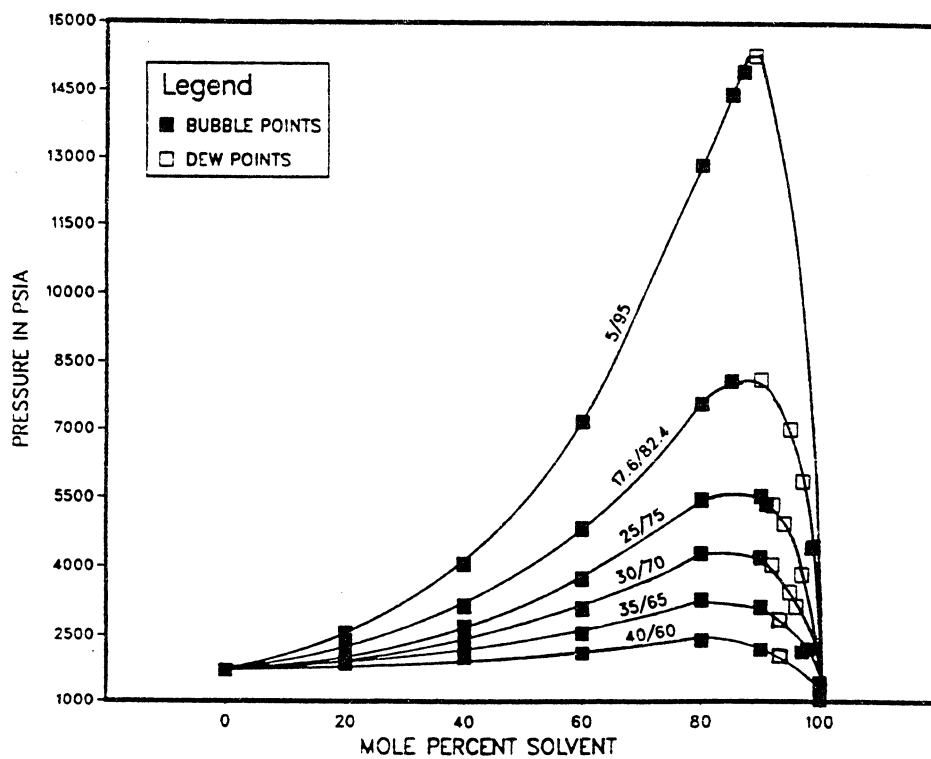


Figure 10: P-X Diagram For West Sak Crude/(NGL/PBG) Solvent Mixtures at 80°F

represents pressure at which the solvent is FCM with West Sak crude. The 5/95 mixture solvent is dew point gas at 1360 psia and the mixtures of this solvent and West Sak crude have a critical point at 15,000 psia, (88 mol% solvent, dew point). Novosad and Costain⁽¹⁰⁾ suggested that if the cricondenbar is dew point then process of achieving multi-contact miscibility is vaporizing drive. However, on the contrary, the compositional path in multi-contact test calculations for this mixture (see Figure 11a) showed both condensing and vaporizing mechanisms.

The solvent mixtures richer than (12/88) at 80°F above their respective saturation pressures are in liquid phase. Thus in Figure 10, mixtures (17.6/82.6), (25/75), (30/70), (35/65) and (40/60) are shown as bubble point liquid. In such cases, the p-x diagram shows two critical points and the interpretation of p-x diagram becomes more complex.

F3. Determination of Thermodynamic Compositional Path

To determine the thermodynamic compositional path followed by oil-solvent mixtures for achieving dynamic miscibility, it is necessary to conduct multi-contact tests either experimentally or using EOS predictions. (Note that actual compositional path in the reservoir under flowing conditions would be different and would be dependent upon the relative permeabilities of solvent rich and oil rich phases and the rate of mass transfer.) The compositional path directly determines the mechanism of achieving dynamic miscibility. Even though, MCT calculations were performed for all the STD tests, for the brevity only compositional path at 2500 psia and 80°F for solvents 5/95 (Figure 11a), 17.6/82.4 (Figure 11b), 30/70 (Figure 11c), 35/65 (Figure 11d), 40/60 (Figure 11f) and for solvent 35/65 (Figure 11e) at 3000 psia and 80°F are shown. For MCT calculations, a 23 component model was used. The equilibrium phase compositions at each contact were then lumped into three components such as

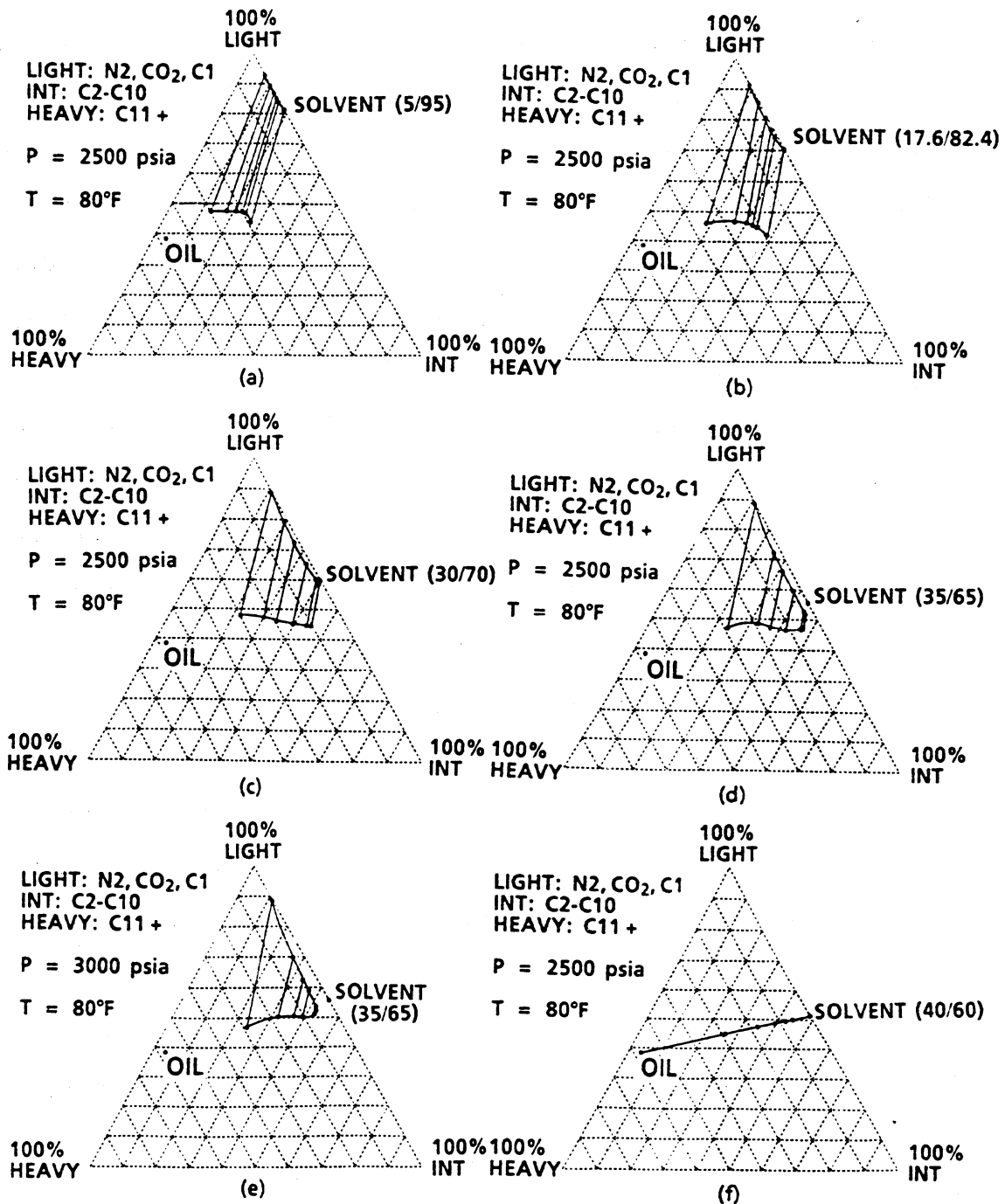


Figure 11: Compositional Path of West Sak Crude/(NGL/PBG) Solvent Mixtures at 80°F Using 23-Component Model

$PC_1 = C_1 + N_2 + CO_2$, $PC_2 = C_2 - C_{10}$ and $PC_3 = C_{11+}$. The resulting phase envelopes by this method are dependent on solvent composition as opposed to independent of solvent composition in pseudo-ternary 3-component flashing technique. Thus, the compositional path illustrated by later method (Figure 8) is not correct. The compositional path represented in Figures 11a-e show simultaneous condensing-vaporizing drive mechanism. This mechanism is discussed in detail by Zick⁽⁹⁾ and will not be repeated here. Figures 11a, 11b, 11c and 11d show that at 2500 psia and 80°F, solvents leaner than (including) 35/65 mixture are immiscible. Figure 11e, however, shows at 3000 psia and 80°F the 35/65 solvent mixture becomes multi-contact miscible with West Sak crude. The actual MMP for 35/65 mixture is 2725 psia and the cricondenbar pressure (or pressure at which 35/65 mixture is FCM) is 3300 psia. Thus at the pressures between 2725 and 3300 psia, 35/65 solvent is MCM with West Sak crude. Therefore, there is a range of pressures or enrichment at which the process can be multi-contact miscible. The MCT calculations for CO₂ at STD test conditions also showed dual mechanism without achieving dynamic miscibility with West Sak crude.

Figure 11f for 40/60 solvent (richer) shows the compositional path between oil and solvent is straight line and all points represent liquid phase and no two phase appear. Similar behavior was also observed for n-butane at all STD test conditions. This indicates first contact miscibility. The STD tests were re-evaluated using multi-contact test calculations and the new interpretation of STD test versus old interpretation of STD tests using pseudo-ternary approach are shown in Tables 2 to 4. Using this new technique, MMP versus solvent enrichments of NGL/PBG mixtures were plotted at 80°F and 250°F and are shown in Figure 12.

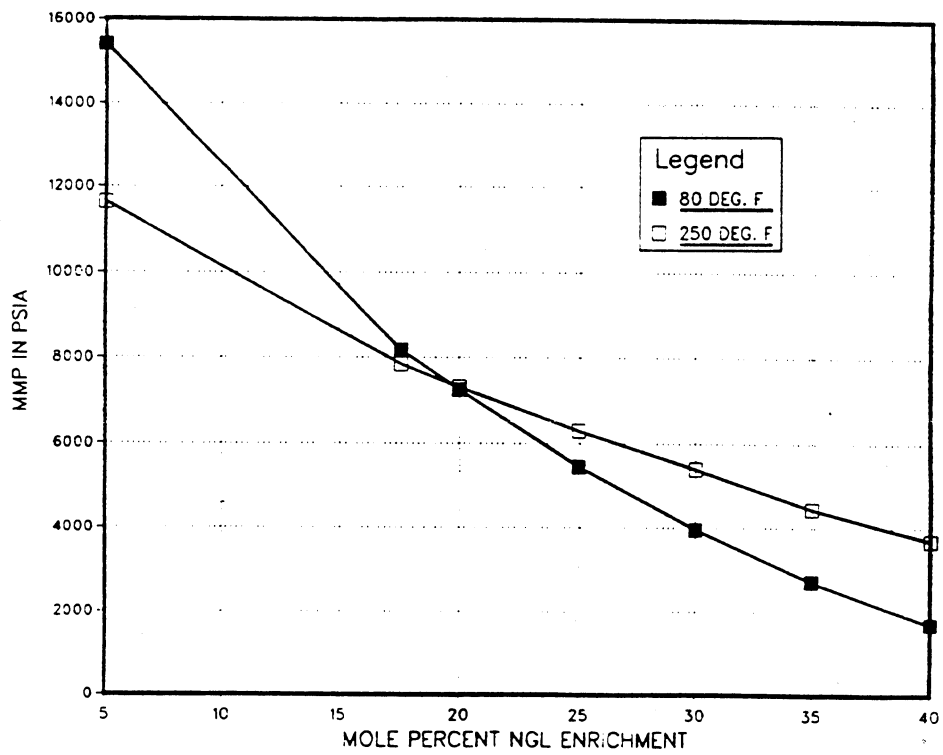


Figure 12: Pressure-Enrichment Correlation For West Sak Crude (23-Component Model)

The results shown in Figure 8 obtained by pseudo-ternary limiting tie-line approach show significantly leaner solvents to be MCM when compared with Figure 12. One way of identifying the condensing-vaporizing mechanism in STD tests is to observe a minima in liquid density and maxima in gas density⁽⁹⁾. For interpretation of STD tests in terms of miscibility for the case of condensing-vaporizing drive, it is necessary to determine methane spike in the slim tube effluent⁽⁹⁾. Methane spike is defined as the concentration of methane in effluent gas minus the concentration of methane in solution gas. In the presence of a methane spike the process is immiscible. In the absence of methane spike the process is miscible. In other words, if miscibility is developed the miscible zone represents plait point composition with k-value of unity for each component. Using this criteria, STD runs for NGL/PBG solvent mixtures in Table 4 were interpreted in terms of miscibility and agreed well with sight glass observations.

Normally, in STD runs the ultimate oil recovery versus pressure is plotted to determine minimum miscibility pressure for a given solvent at reservoir temperature. The breakover point is considered as the MMP. The increase in ultimate oil recovery with pressure indicates immiscible and ultimate oil recovery in relation to pressure flattens out after minimum miscibility pressure is exceeded.

The STD tests for 17.6/82.4 solvent mixture at 80°F for pressures between 1900 to 2775 psia (Table 4) resulted only in slight increase in ultimate or breakthrough oil recovery with increase in pressure; even though these runs were immiscible. This indicates that the criteria of breakover point was violated for this solvent-oil mixture. Another point to note is that for 35/65 mixture (a MCM solvent) at 3500 psia the ultimate recovery (78.1%) is slightly higher than ultimate recovery for 17.6/82.4 solvent (immiscible solvent) at 2775 psia (75.3). This indicates that an immiscible drive can be as efficient (displacement wise) as miscible drive.

Finally, butane STD runs (FCM) and 35/65 solvent STD runs (MCM) showed lower ultimate recoveries (78-81%) despite of being miscible. This reduction in ultimate oil recovery may be due to asphaltene precipitation. Study of asphaltene precipitation during addition of solvents to West Sak crude are discussed later in this chapter.

G. Conclusions

1. STD tests combined with EOS predictions indicate that the CO₂ was unable to generate multi-contact miscibility with West Sak crude at 80°F and pressures up to 6650 psia. The compositional path followed by immiscible CO₂ drive indicates a combined vaporizing-condensing mechanism.
2. STD tests and EOS predictions indicate that n-butane is first contact miscible with West Sak crude.
3. In EOS predictions, care should be taken in characterizing oil-solvent mixtures in order to determine correct, thermodynamic compositional path and mechanism of dynamic miscibility development.
4. The traditional pseudo-ternary diagram construction and limiting tie-line method for determining either MMP or ME are not always valid and can lead to recommending solvents which are too lean or too rich.
5. Results of this study indicate that multi-contact miscibility can be developed for enriched gas drives by condensing - vaporizing mechanism.
6. An immiscible solvent mixture containing 17.6% (mol%) NGL and 82.4 (mol%) PBG showed as high displacement efficiencies in STD tests as that for a MCM solvent (35/65) mixture.

H. References

1. Hutchinson, C.A. Jr. and Braun, P.H.: "Phase Relations of Miscible Displacement in Oil Recovery," AIChEJ. (1961) vol. 7, 64-72.
2. Clark, N.J., Schultz, W.P., and Shearin, H.M.: "Condensing Gas Drive, Critical Displacement Process - New Injection Method Affords Total Oil Recovery," Pet. Eng. (Oct. 1956) vol. 28, B-45.
3. Slobod, R.L. and Koch, H.A. Jr.: "High Pressure Gas Injection - Mechanism of Recovery Increase," Drill and Proc. Prac. API (1953) 82.
4. Stalkup, F.I. Jr.: "Miscible Displacement," Henry L. Doherty Series Monograph, vol. 8, SPE - AIME, New York (1983).
5. Benham, A.L., Dowden, W.E., and Kunzman, W.J.: "Miscible Fluid Displacement - Prediction of Miscibility," Trans. AIME (1960) vol. 219, 229-237.
6. Williams, C.A., Zana, E.N., and Humphrys G.E.: "Use of The Peng-Robinson Equation-of-State to Predict Hydrocarbon Phase Behavior and Miscibility for Fluid Displacement," SPE 8817, A paper presented at the SPE/DOE Symposium on Enhanced Oil Recovery at Tulsa, OK (April 20-23, 1980).
7. Wu, R.S., Batycky, J.P., Harker, B., and Rancier, D.: "Enriched Gas Displacement: Design of Solvent Compositions," J. Can. Pet. Tech. (May - June, 1986) vol. 25, 55-59.
8. Stalkup, F.I.: "Using Phase Surfaces to Describe Condensing - Gas - Drive Experiments," SPEJ (Sept. 1965), 186-188.
9. Zick, A.A.: "A Combined Condensing/Vaporizing Mechanism in the Displacement of Oil by Enriched Gases," SPE 15493, A paper presented at the 61st Annual Technical Conference and Exhibition SPE, New Orleans, Louisiana, (Oct. 5-8, 1986).

10. Novasad, Z. and Costain, T.: *"New Interpretation of Recovery Mechanisms in Enriched Gas Drives,"* J. of Can. Pet. Tech. (March - April 1988) vol. 27. No. 2, 54-60.
11. Mansoori, J. and Gupta, S.P.: *"An Interpretation of the Displacement Behavior of Rich Gas Drive Using an Equation-of-State Compositional Model,"* SPE 18061, presented at 63rd Annual Technical Conference and Exhibition SPE in Houston, TX (Oct. 2-5, 1988).
12. Lee, S.T., Lo, H., Dharmawardhana, B.T.: *"Analysis of Mass Transfer Mechanisms Occurring in Rich Gas Displacement Process,"* SPE 18062, presented at the 63rd Annual Technical Conference and Exhibition SPE in Houston, TX (Oct. 2-5, 1988).

PART II: Effect of Presence of Aqueous Phase on Phase Behavior and Miscibility Conditions for Solvent - West Sak Crude Mixtures

A. Abstract

Water is always present in the reservoir either as a connate water or as a mobile water in a previously waterflooded portions of the reservoir. Also, in processes such as water alternating gas injection (WAG) for miscible or immiscible displacement, significant amount of water is injected into the reservoir. In light of this, this work was conducted to understand the effect of presence of water on the phase behavior and miscibility conditions (minimum miscibility pressure for a given solvent composition or minimum enrichment calculations at reservoir conditions) for West Sak crude - solvent mixtures.

An equation of state based four phase flash calculation algorithm developed by Enick et al. (1987) was used in this work. The original model used Peng-Robinson equation of state. The model was modified to include ZIRK equation of state. The model was tuned to obtain EOS parameters by matching the PVT data for West Sak crude and then used to predict phase behavior of mixtures of West Sak crude with gases such as CO₂, n-butane and mixtures of Prudhoe Bay natural gas (PBG) and natural gas liquids (NGL) both in absence and presence of water. Results indicate that presence of water can possibly change the volumes and compositions of existing phases. The degree of change in the phase diagrams is function of the water contents of overall mixtures of gas-water-crude. Results also indicate that presence of water reduces the minimum enrichments required to achieve dynamic miscibility between PBG/NGL mixtures and West Sak crude.

B. Introduction

Enick et al. (1987) developed a technique for predicting one to four phase flash equilibrium conditions for multi-component systems containing water. Due to the ability of this model to handle systems containing water, it was chosen to accomplish the objectives of this study. This model uses Peng-Robinson equation of state to describe aqueous, CO₂ and hydrocarbon vapor and liquid phases along with accelerated - stabilized successive substitution method to obtain convergence in the near critical region. They also incorporated a new mixing rule for asymmetric systems to handle strongly polar compounds like water. A comprehensive search strategy incorporated in this model allows checking for additional or disappearance of aqueous and hydrocarbon phases and considers eleven general classifications of the systems which may result from the introduction of water into one, two and three phase water-free (gas and oil mixtures) systems.

In this study, the above model was modified to include an additional equation of state, namely, Zudkovitch-Joffe modification of Redlich-Kwong equation of state (ZJRK). Prior to use of this model for prediction of phase behavior and miscibility conditions for West Sak crude - solvent and West Sak crude - solvent - water systems, it was tuned using PVT properties of West Sak crude provided earlier in this report. The details of the model equations and search strategy are given in Enick et al. (1987). The details of the model tuning and validation along with predictions are described by Bhandari (1988). Only relevant results are summarized here.

C. Model Predictions and Discussion

For tuning of EOS parameters and phase behavior predictions, 23-component characterization was used for West Sak crude. In phase behavior calculations, the overall mixtures of crude oil and solvent were flashed at various pressures and temperatures to determine the number of equilibrium phases present, phase

volumes and phase compositions. The solvents considered were CO₂, n-butane and various mixtures of Prudhoe Bay natural gas (PBG) and natural gas liquids (NGL). These calculations were then repeated for above systems in presence of water component in the overall mixtures. The amount of water in overall mixtures was varied in each prediction.

For minimum miscibility pressure predictions, first 23-component mixtures of Prudhoe Bay natural gas - natural gas liquids with West Sak crude were flashed to obtain equilibrium compositions of vapor and liquid phases. The two phase envelope was then plotted on a pseudo-ternary diagram. In pseudo-ternary diagram, the light fractions were represented by N₂, CO₂ and methane, the intermediate fractions by C₂-C₁₀ and the heavy fractions by C₁₁₊. The limiting tie line method was used to determine enrichment versus pressure. These calculations were repeated for same gases in presence of varying amount of water. After flashing, the phase compositions were normalized by excluding water and then pseudoized to determine enrichment versus pressure.

First the flash calculations for different mixtures of CO₂ and West Sak crude, i.e. 0%, 20%, 40%, 60% and 80% (mol%), were performed at four different temperatures (80, 150, 250 and 700°F). Table 1 lists the overall compositions of different CO₂ - West Sak crude mixtures. Figures 1, 2, and 3 show the pressure versus volume % liquid for CO₂ - West Sak mixtures at 80°F, 250°F and 700°F respectively. The results also showed that CO₂ is not multi-contact miscible with West Sak crude at reservoir conditions (Bhandari, 1988). The phase behavior predictions for different mixtures of CO₂ and West Sak crude were repeated in presence of water. Figure 4 shows phase volumes versus pressure for West Sak crude in presence of 0%, 10% and 90% water. The figure shows that there is slight lowering of bubble point pressure of West Sak crude in presence of water and increase in mol% water in the overall mixture, decreases the bubble point pressure of West Sak crude. Figure 5 shows

Table 1: Overall Composition of CO₂ - West Sak Crude Mixtures

Component	0%CO ₂	20%CO ₂	40%CO ₂	60%CO ₂	80%CO ₂
CO ₂	0.016	20.013	40.010	60.006	80.003
N ₂	0.032	0.026	0.019	0.013	0.006
C ₁	38.333	30.666	23.000	15.333	7.667
C ₂	0.857	0.686	0.514	0.343	0.171
C ₃	0.359	0.287	0.215	0.144	0.072
C ₄	0.179	0.143	0.107	0.072	0.036
C ₅	0.064	0.051	0.038	0.026	0.013
C ₆	0.200	0.016	0.012	0.008	0.004
C ₇	0.016	0.013	0.010	0.006	0.003
C ₈	0.008	0.006	0.005	0.003	0.002
C ₉	0.823	0.658	0.494	0.329	0.165
C ₁₀	1.496	1.197	0.898	0.598	0.299
C ₁₁	1.720	1.376	1.032	0.688	0.344
C ₁₂	1.346	1.077	0.808	0.538	0.269
C ₁₃	1.496	1.197	0.898	0.598	0.299
C ₁₄	1.795	1.436	1.077	0.718	0.359
C ₁₅	1.944	1.555	1.166	0.778	0.389
C ₁₆	1.795	1.436	1.077	0.718	0.359
C ₁₇	1.570	1.256	0.942	0.628	0.314
C ₁₈	1.795	1.436	1.077	0.718	0.359
C ₁₉	2.468	1.974	1.481	0.987	0.494
C ₂₀	2.841	2.273	1.705	1.136	0.568
C ₂₁₊	39.037	31.222	23.416	15.611	7.805

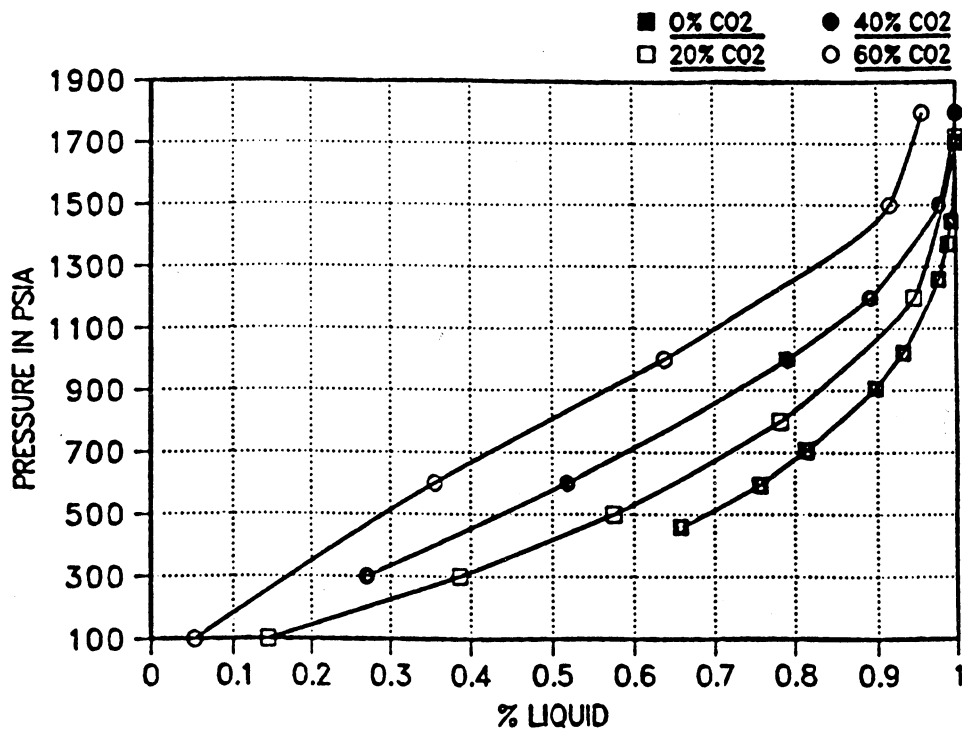


Figure 1: Phase Behavior of CO₂ - West Sak Crude Mixture at 80°F

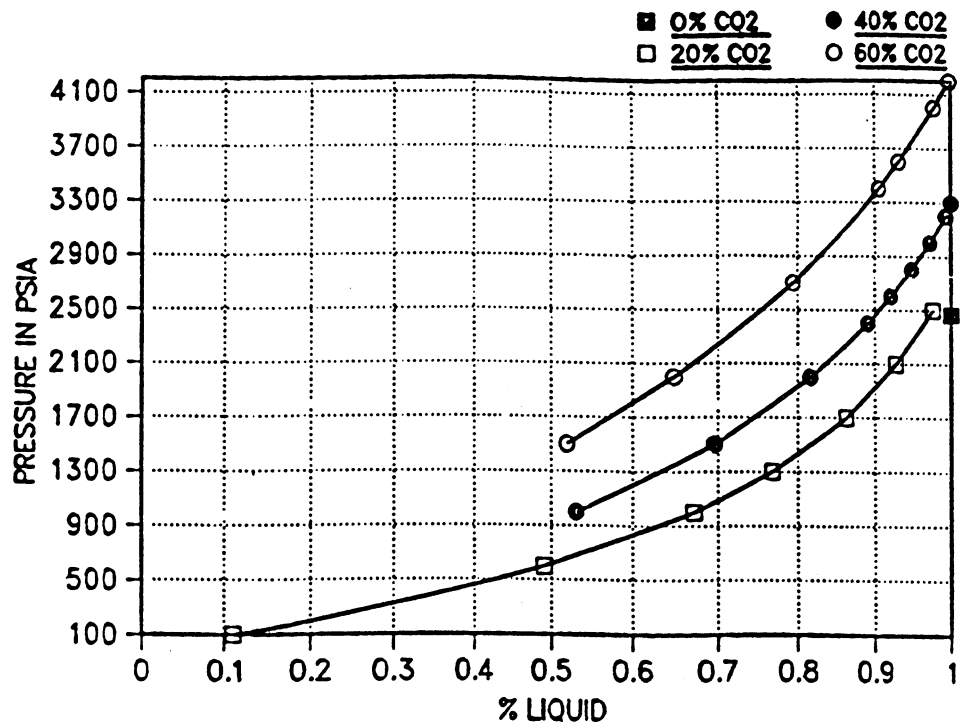


Figure 2: Phase Behavior of CO₂ - West Sak Crude Mixture at 250°F

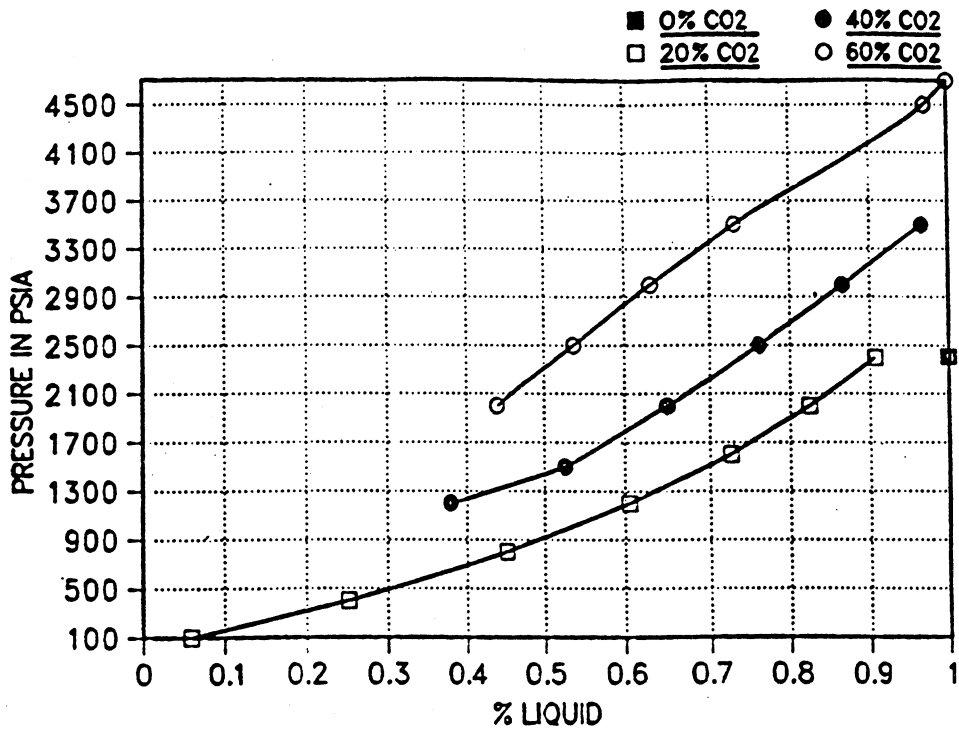


Figure 3: Phase Behavior of CO₂ - West Sak Crude Mixture at 700°F

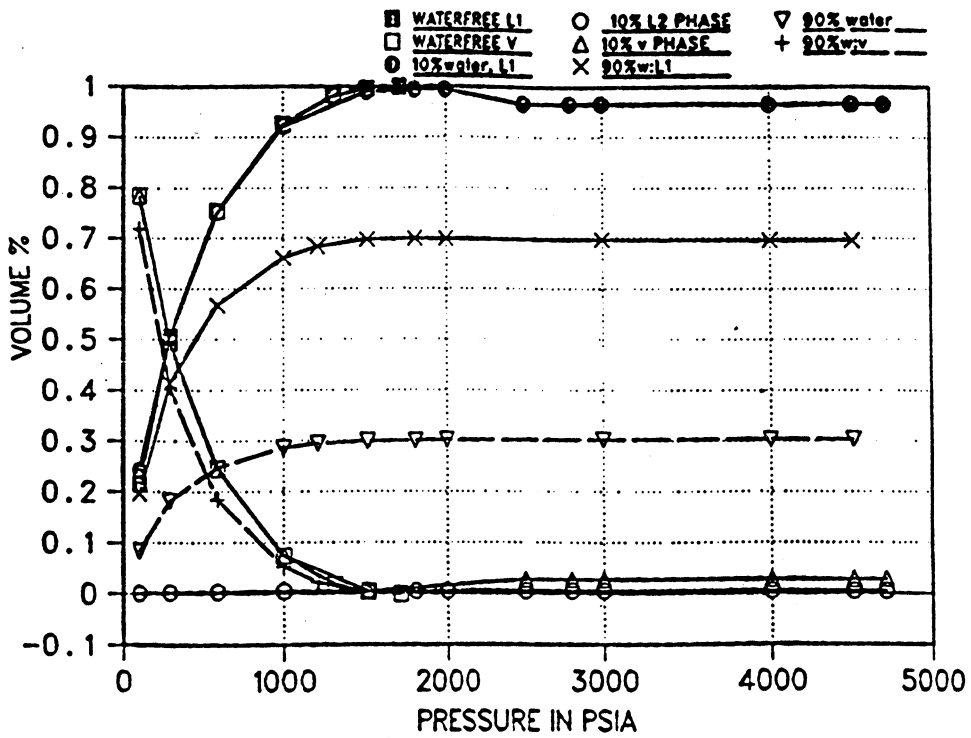


Figure 4: Phase Behavior of West Sak Crude in the Presence of Water at 80°F

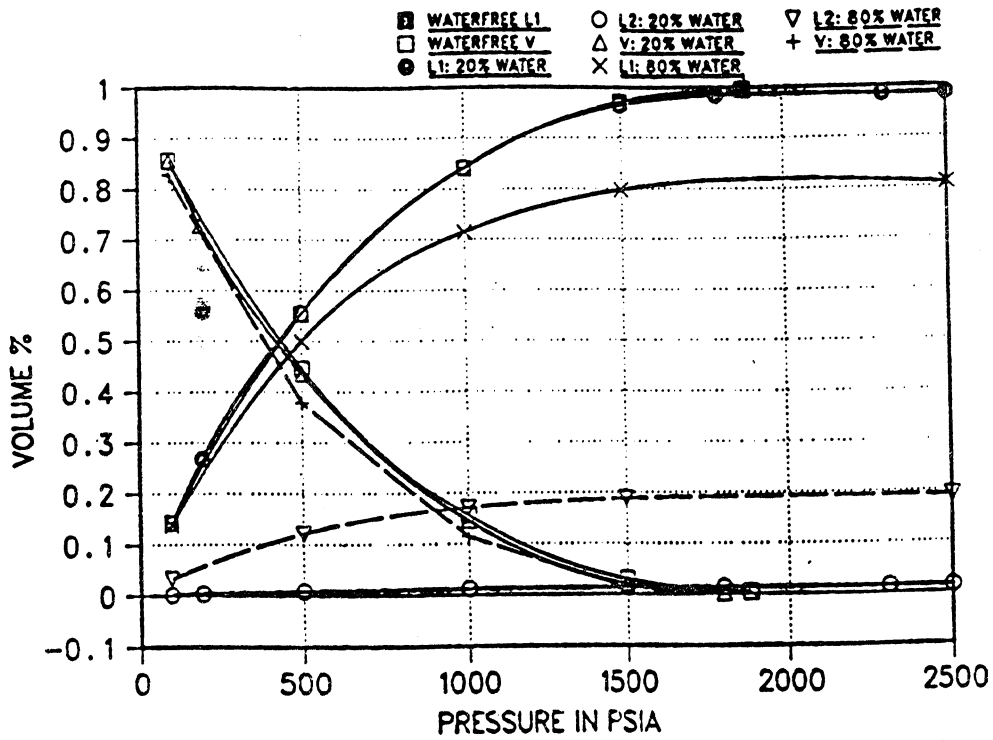


Figure 5: Effect of Water on Phase Behavior of 20% CO₂ - 80% West Sak Crude Mixture at 80°F (Water Included)

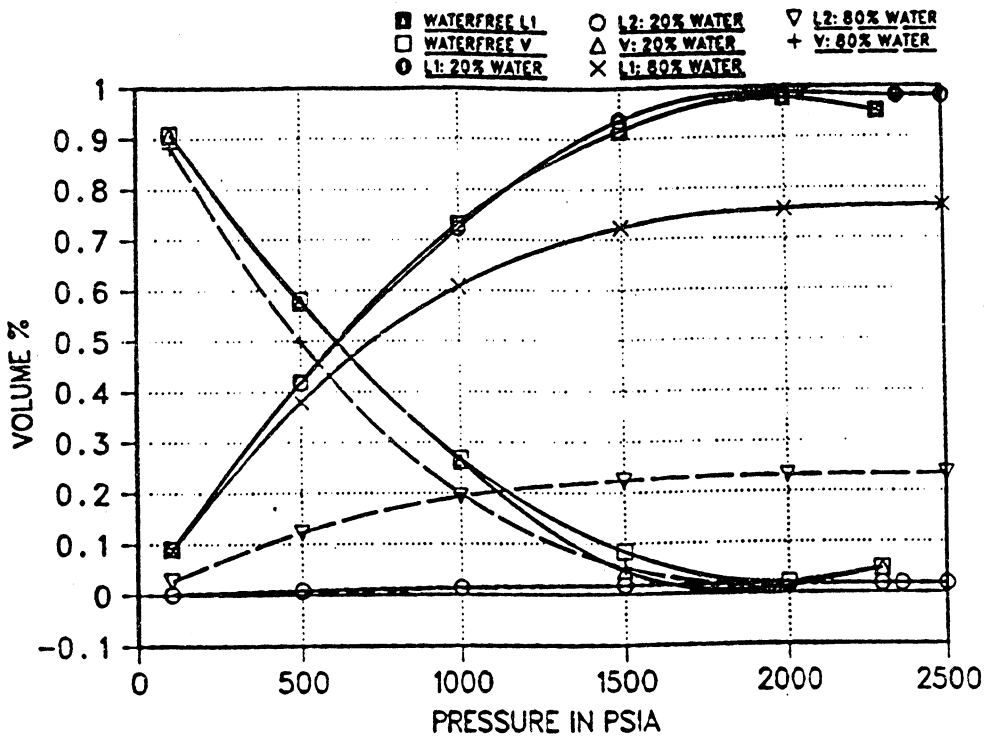


Figure 6: Effect of Water on Phase Behavior of 40% CO₂ - 60% West Sak Crude Mixture at 80°F (Water Included)

effect of 0, 20 and 80% water on phase behavior of 20 mol% CO₂ - 80% mol% West Sak crude mixture at 80°F. Figures 6 and 7 show effect of water on phase behavior of 40/60 and 60/40 mixtures of CO₂ and West Sak crude respectively. While all the results in Figure 5, 6 and 7 show absence of CO₂ - rich liquid phase, the increase in water content causes greater lowering of vapor phase volume. To correctly understand the effect of water on phase behavior, the Figures 5, 6 and 7 were reconstructed (see Figures 8, 9 and 10 respectively) after exclusion of water phase volume and renormalization of vapor and liquid hydrocarbon phase volumes. The results in Figures 8, 9, and 10 show that the degree of lowering of bubble point pressure due to water increases with increase in water content and increase in CO₂ content. In presence of water, CO₂ is still not multi-contact miscible with West Sak crude at reservoir conditions, but increase in water content decreases the shape of CO₂ - oil phase envelope.

For n-butane - West Sak crude mixtures, the results show first contact contact miscibility in absence or presence of water (Bhandari, 1988), since for all n-butane mol fractions in the mixtures vapor phase was found to be absent at pressures above reservoir pressure, and increase in mol fraction of n-butane decreased the bubble point pressure of the n-butane - West Sak crude mixtures. Increase in water content causes further lowering of the bubble point pressure (see Figure 11).

Finally, effect of water on phase behavior and minimum miscibility pressures for Prudhoe Bay natural gas (PBG)/natural gas liquid (NGL) with West Sak crude was studied. Effect of water on phase behavior of mixture of (80 mol% PBG - 20% NGL) with West Sak crude is illustrated in Figure 12. Table 2 shows the composition of solvent (80/20 mixture of PBG/NGL) - West Sak crude mixtures. From Figures 13 and 14, it is evident that increase in water content of overall mixture reduces the minimum miscibility pressure for a given solvent mixture of PBG/NGL or reduces the

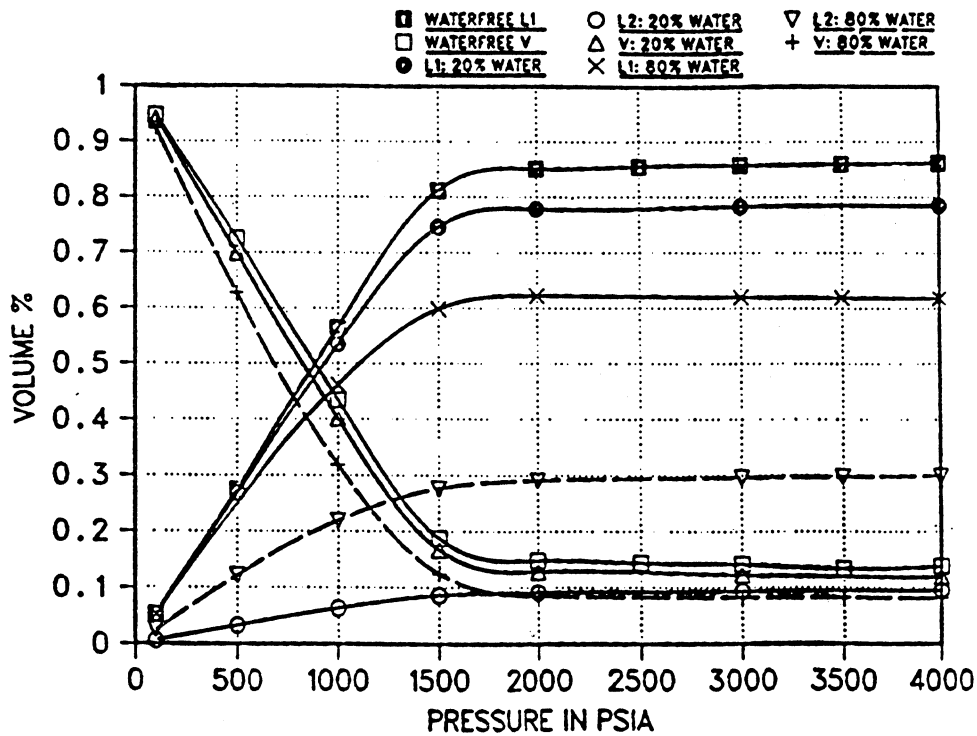


Figure 7: Effect of Water on Phase Behavior of 60% CO₂ - 40% West Sak Crude Mixture at 80°F (Water Included)

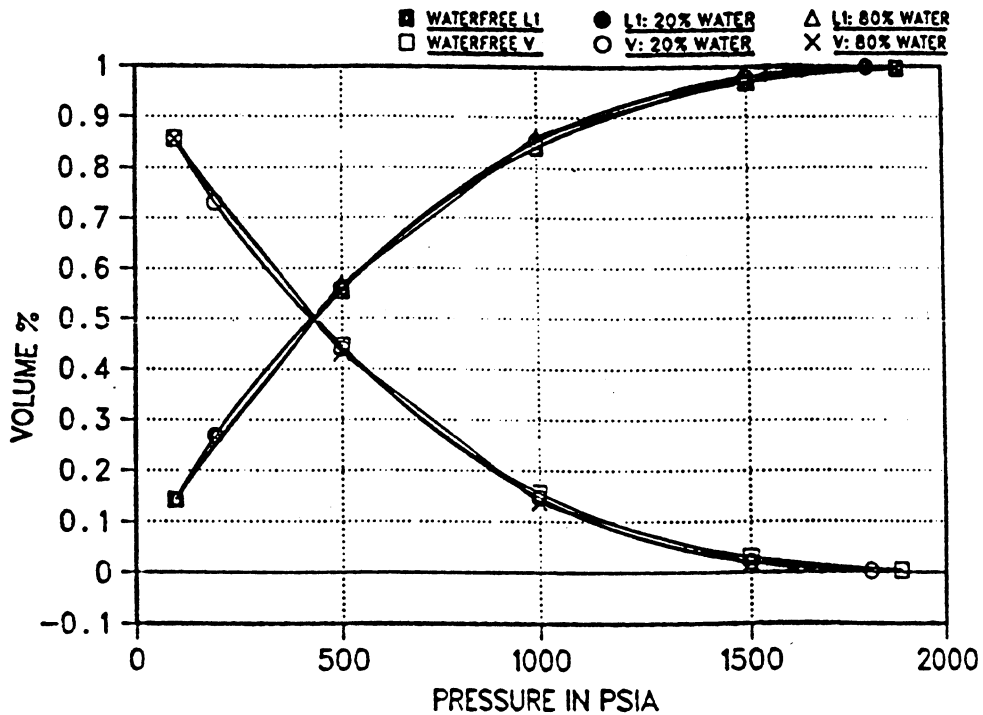


Figure 8: Effect of Water on Phase Behavior of 20% CO₂ - 80% West Sak Crude Mixture at 80°F (Water Excluded)

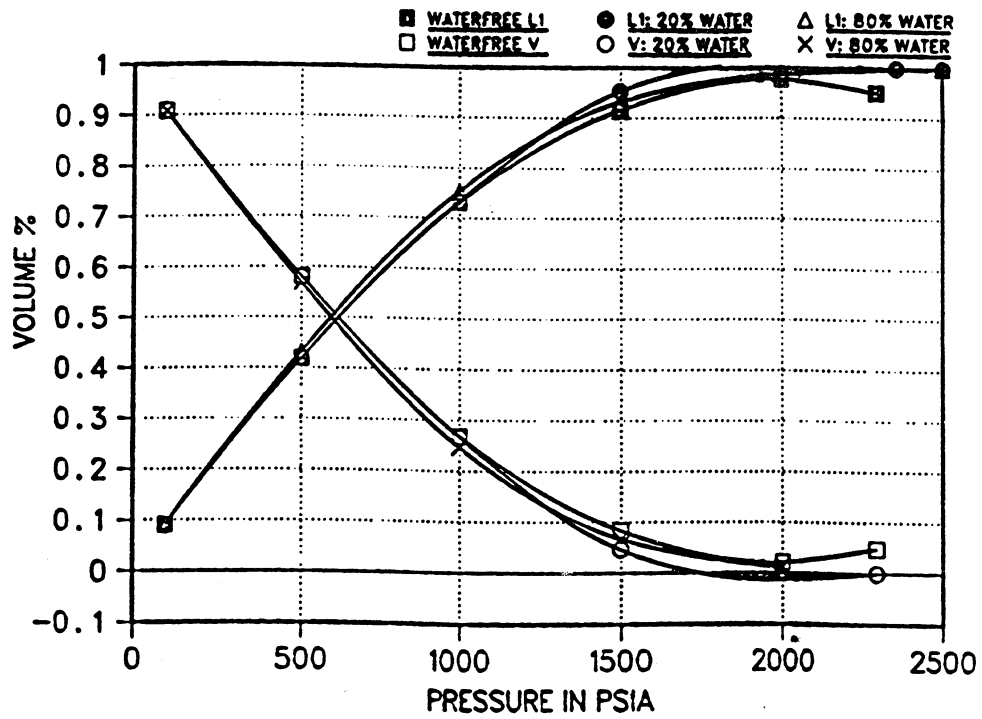


Figure 9: Effect of Water on Phase Behavior of 40% CO₂ - 60% West Sak Crude Mixture at 80°F (Water Excluded)

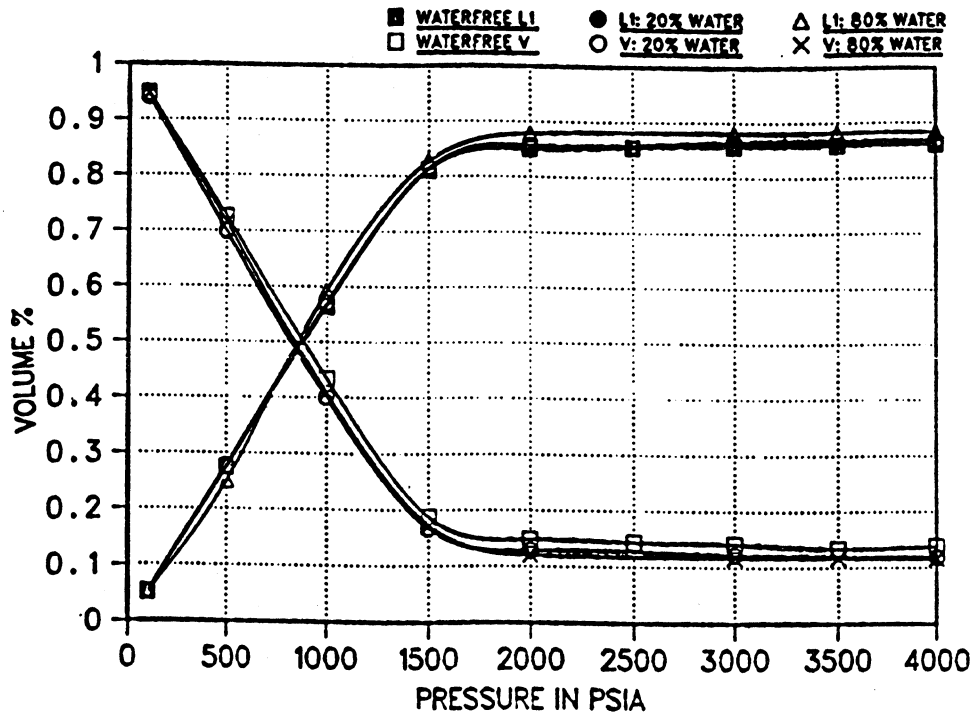


Figure 10: Effect of Water on Phase Behavior of 60% CO₂ - 40% West Sak Crude Mixture at 80°F (Water Excluded)

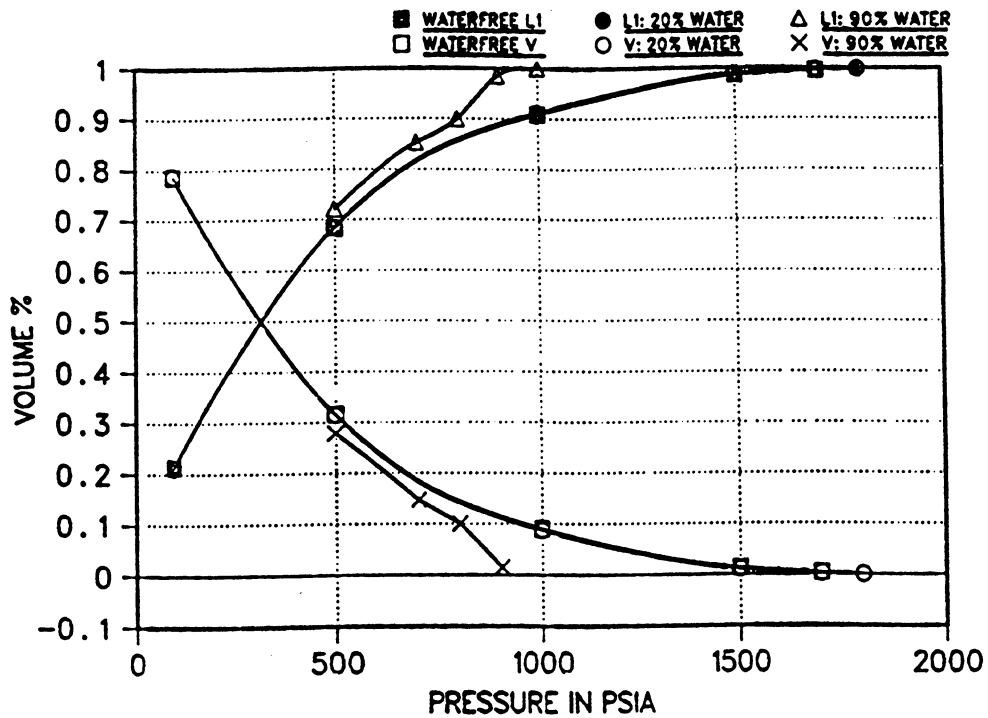


Figure 11: Effect of Water on the Phase Behavior of N-Butane - Crude Mixture at 80°F (Water Excluded)

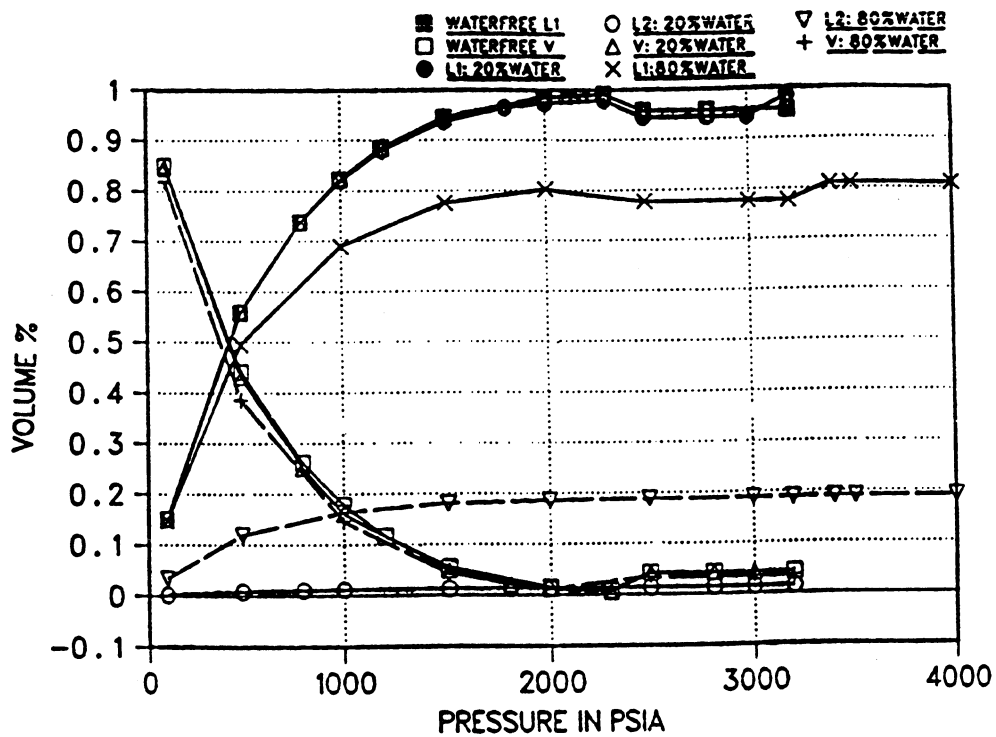


Figure 12: Effect of Water on the Phase Behavior of (80 Mol% PBG/ 20 Mol% NGL) - West Sak Crude Mixture at 80°F (Water Included)

Table 2: Composition of Mixture of 20% NGL/80% Prudhoe Bay Gas with West Sak Crude

Compt.	20%Solv.	40%Solv.	60%Solv.	80%Solv.	90%Solv.
CO ₂	1.7552	3.4944	5.2336	6.9728	7.8424
N ₂	0.1400	0.2480	0.3560	0.4640	0.5180
C ₁	43.7128	49.0926	54.4724	59.8522	62.5421
C ₂	1.4584	2.0598	2.6612	3.2626	3.5633
C ₃	0.5584	0.7578	0.9572	1.1156	1.2563
C ₄	2.2144	4.2498	6.2852	8.3206	9.3383
C ₅	1.2804	2.4968	3.7132	4.9296	5.5378
C ₆	0.4184	0.8168	1.2152	1.6136	1.8128
C ₇	0.1888	0.3616	0.5344	0.7072	0.7936
C ₈	0.1804	0.3528	0.5252	0.6976	0.7838
C ₉	0.6584	0.4938	0.3292	0.1646	0.0823
C ₁₀	1.1968	0.8976	0.5984	0.2992	0.1496
C ₁₁	1.3760	1.0320	0.6880	0.3440	0.1720
C ₁₂	1.0768	0.8076	0.5384	0.2692	0.1346
C ₁₃	1.1968	0.8976	0.5984	0.2992	0.1496
C ₁₄	1.4360	1.0770	0.7180	0.3590	0.1795
C ₁₅	1.5552	1.1664	0.7776	0.3888	0.1944
C ₁₆	1.4360	1.0770	0.7180	0.3590	0.1795
C ₁₇	1.2560	0.9420	0.6280	0.3140	0.1570
C ₁₈	1.4360	1.0770	0.7180	0.3590	0.1795
C ₁₉	1.9744	1.4808	0.9872	0.4936	0.2468
C ₂₀	2.2728	1.7046	1.1364	0.5682	0.2841
C ₂₁₊	31.2216	23.4162	15.6108	7.8054	3.9027

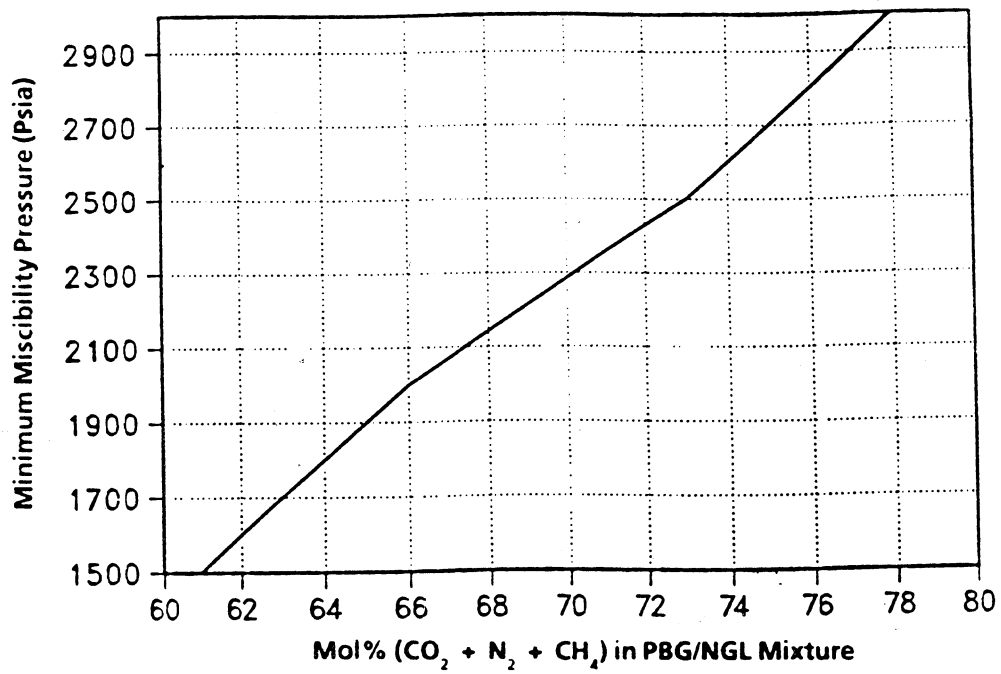


Figure 13: Effect of 20% Water on Minimum Miscibility Pressures for PBG/NGL Mixtures

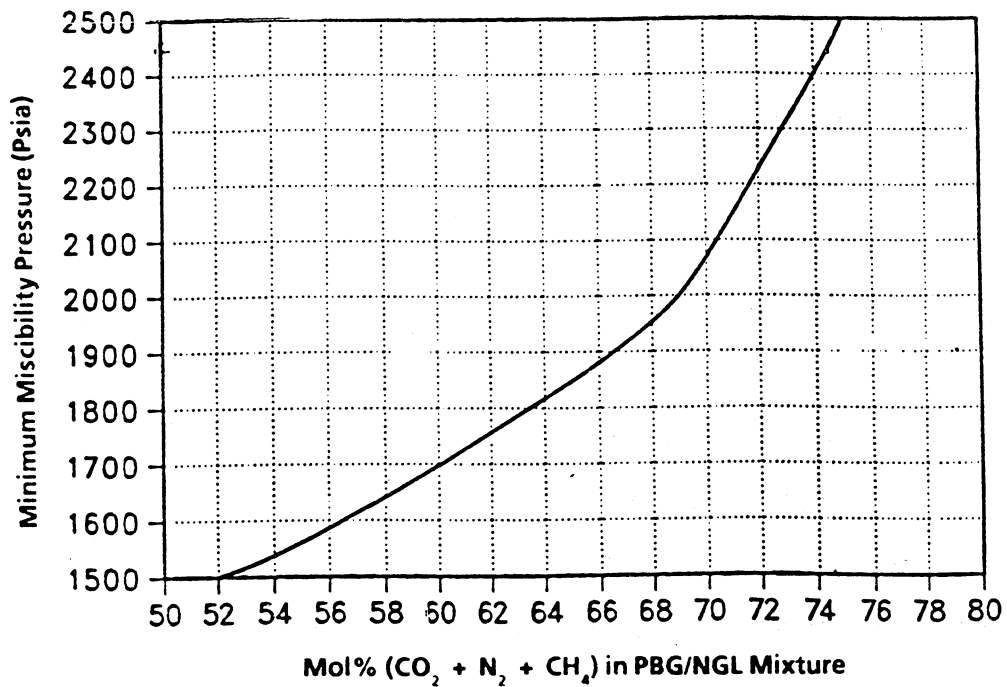


Figure 14: Effect of 80% Water on Minimum Miscibility Pressures for PBG/NGL Mixtures

minimum enrichment of PBG by NGL required to achieve multi-contact miscibility with West Sak crude.

D. Conclusions

Effect of presence of water on phase behavior and miscibility conditions for West Sak crude - solvent mixtures was studied. Results indicate that increase in water volume in the overall mixture of solvent - crude system decrease the minimum miscibility pressures for given PBG/NGL mixtures. Thus, presence of water is not detrimental in that it does not destroy the miscibility between solvent and crude. This conclusion is valid, strictly from thermodynamic viewpoint, and does not consider displacement effects.

E. References

1. Bhandari, R.P.S., "*Prediction of Phase Behavior and Miscibility Conditions For West Sak Crude - Solvent Mixtures,*" M.S. Thesis, University of Alaska Fairbanks (1988).
2. Coats, K.H. and Smart, "*Application of a Regression - Based EOS - PVT Program to Laboratory Data,*" SPE Paper #11197, Proceedings of Annual Technical Conference and Exhibition of SPE (1982).
3. Enick, R.M., Holder, G.D., and Mohamed, R.S., "*Four Phase Flash Equilibrium Calculations Using the Peng-Robinson Equation of State and a Mixing Rule for Asymmetric Systems,*" SPE Reservoir Engineering (Nov. 1987) pp. 687-694.

PART III: Study of Asphaltene Precipitation During Addition of Solvents to West Sak Crude

A. Abstract

Experimental study was conducted to measure the amount of asphaltene during addition of solvents such as carbon dioxide and hydrocarbon gases and liquids to West Sak crude. The solvents used in this study include: carbon dioxide, ethane, propane, n-butane, n-pentane, n-heptane, Prudhoe Bay natural gas (PBG), and natural gas liquids (NGL).

In the first set of experiments, solids (asphaltenes and resins) precipitated by addition of various solvents to the tank oil were measured. Two types of West Sak tank oils were used. Resins were then separated from asphaltenes by dissolution of resins in n-heptane. The effect of solvent type and solvent/oil dilution ratio on the amount of asphaltene precipitation was studied. Asphaltene precipitation altered the crude oil composition, which was determined from the oil chromatographic analysis.

In the second set of experiments, the tank oil was first recombined at 1705 psia pressure and 80°F temperature. Two types of tests were conducted with the recombined crude. In the first test, CO₂ was added to the crude in various proportions at reservoir conditions and the effect of CO₂ to oil ratio on the amount of asphaltene precipitation was determined. In the second test, at fixed CO₂/oil ratio, effect of pressure on the amount of asphaltene precipitation was determined.

The data gathered in this work will be useful to determine solubility parameters in Flory-Huggins polymer solution theory which can be used to model the solubility of asphaltenes in the oil and to predict amount of asphaltene precipitation upon addition of a solvent to oil at any pressure and temperatures.

This will enable further understanding of effect of asphaltene precipitation on the minimum miscibility pressures.

B. Introduction

Asphaltene deposition during production and processing of crude oils is considered as one of the costliest technical problems. Asphaltene deposition can occur during primary (natural depletion) process. In such instances, asphaltene deposition has been reported to occur around the wellbore, well tubings, flow-lines, separators, pumps, tanks and other equipments (Mansoori, 1988). Asphaltene deposition is specifically the biggest problem in miscible floods (CO₂ or hydrocarbon injection) and also in caustic floods (caustic injection). Asphaltene deposition also occurs during acid stimulation tests. Refinery is another example where asphaltene deposition can be biggest problem during crude processing.

On many occasions, asphaltene deposition problem has threatened the economic recovery of the oil or increased considerably the cost of producing it. Such cases were reported in the Princess Field, Greece (Adialalis, 1982), the Mata-Acema Field, Venezuela (Lichaa, 1977), the Hassi-Messahoud Field, Algeria (Haskett and Tartera, 1965), and the Ventura Field, California (Tuttle, 1983). In most of these instances, asphaltene deposition problem was not foreseen either during exploration or even during developmental stage. As a result, the operator company became aware of the problem after a very large portion of the capital expenditure was spent making it difficult from an economic standpoint to quit the project. So it is important to evaluate any potential asphaltene problems and its implications prior to development of the field.

Asphaltenes are polar, aromatic-based, high molecular weight hydrocarbons of amorphous structure and they exist in crude oils in the form of colloiddally dispersed fine particles and in part as dissolved compounds. Although, the exact chemical

structure of asphaltenes is unknown and will be function of type of crude, their chemical structure consists of aromatic ring structures with oxygen, nitrogen and sulphur present in heterocyclic side chains and oxygen in alkyl side chains. For practical purposes, they are described as the n-heptane insoluble fraction of crude oil obtained by conducting the IP-143 test. According to Long (1981), asphaltenes exist in a broad distribution of sizes, polarities and molecular weights. The molecular weight of asphaltenes range from 1,000 - 500,000 with a density of approximately 1.2 g/cc and a spherical shape 30 to 65^oA in diameter (Witherspoon and Munir, 1960).

Resins are also polycyclic aromatic-based compounds, somewhat lower molecular weight (250 - 1000) than asphaltenes. They are non-polar compared to polar asphaltenes. Resins are easily adsorbed in common adsorbents like clay or silica gel. Resins are defined as the fraction of crude oil insoluble in ethyl acetate but soluble in n-heptane. According to Margusson (1931), there is a close relationship between high molecular weight polycyclic aromatic hydrocarbons, asphaltenes and resins which may exist in a crude. The heavy polycyclic aromatic compounds upon oxidation gradually form neutral resins, while asphaltenes form as a result of further oxidation of neutral resins. The physicochemical properties of resins are completely different from asphaltenes. Resins are the primary cause of keeping asphaltene particles from coagulation and agglomeration.

The term asphalt is used as a general term to designate the mixture that flocculates out of oil and contains asphaltene particles surrounded by resins, oil and other liquid entities in the crude oil that are trapped in the flocculated mass.

Asphaltene deposition as a result of flocculation of finer asphaltene particles is a complex phenomena and not well understood. Some of the recent studies (Leontaritis and Mansoori, 1987; Hirshberg et al., 1984) provide more comprehensive description on the causes of asphaltene deposition.

Asphaltene are lyophobic with respect to low molecular weight paraffinic hydrocarbons and lyophilic with respect to aromatics and resins. That is why resin molecules are adsorbed on the surface of asphaltene particles or micelle (onion skin model). As a result, when asphaltene particles are completely surrounded by resin molecules, they remain in the fine colloidal suspension and do not agglomerate or precipitate. This process is called as "peptization". The degree of dispersion of asphaltenes in crude oils depends upon the chemical composition of crude. In heavy, highly, aromatic crudes, the asphaltenes were well dispersed; but in presence of paraffinic hydrocarbons they flocculate and precipitate. Also, in crudes with high resin contents the degree of asphaltene precipitation is less.

Makey et al. (1978) suggested that the ratios "polar to non-polar" and "heavy to light" molecules in a crude are particularly important in keeping mutual solubility of the compounds in the crude. By the addition of a solvent to the crude, this ratio is altered. The heavy and polar (asphaltene) molecules separate from the mixture either in the form of another liquid phase or to a solid precipitate. Hydrogen bonding and the sulfur (and/or the nitrogen) containing segments of the separated (asphaltene) molecules start to aggregate (or polymerize) and as a result produce the irreversible asphaltene deposits which are insoluble in solvents.

In general, any action of chemical, mechanical or electrical nature which depeptizes the asphaltene micelle can lead to precipitation of the asphaltenes from the crude oil - asphaltene suspension. The amount of resins adsorbed on the surface of the asphaltenes is essentially a function of the concentration of the resin in the liquid phase of the oil. Processes which depletes or dilute the resin concentration in the oil may lead to asphaltene precipitation. For example when miscible solvents (CO_2 or lighter hydrocarbons) are added to asphaltene containing crudes, the resin concentration may be so depleted that the entire surfaces of the asphaltene micelles

cannot be covered. The result is flocculation of the asphaltenes and sludging or precipitation.

Asphaltene deposition problems upon natural depletion (primary recovery) have been encountered in the well tubing of the Hassi-Messahoud Field in Algeria (Haskett and Tartera, 1965) and the Ventura Field in California (Tuttle, 1983). In both fields the crude was strongly undersaturated with respect to gas. At Hassi-Messahoud, heavy asphaltene precipitation took place in a 450m region of the tubing located just below the level at which bubble point was reached. Furthermore, upon gas injection, a reduced injectivity (factor of two) was experienced in the first period of field development until 1970. However, once the reservoir pressure reached the bubble point, the wells produced without trouble of asphaltenes.

Reduction in well injectivity or productivity by a factor of 2 to 3 during several CO₂ flood field projects (Stalkup, 1978) and water alternating gas drives (Dyes et al, 1972; Harvey et al, 1977) have been caused by asphaltene deposition.

The asphaltene deposition problems have also been reported for the Little Creek CO₂ injection EOR pilot in Mississippi (Tuttle, 1983).

Asphaltene have an electrical charge and thus their precipitation is possible by the application of electric field. Stream potential experiments conducted by Preckshot (1943) demonstrated that crude oil flowing through sand produces a potential and this appears to be responsible for the formation of precipitated asphaltenes in the flow of crude oil through porous reservoir rock. This same phenomena is thought to be responsible for asphaltene deposition in the slotted liners of low gravity wells in California.

Asphaltene deposition also occurs during release of low molecular weight hydrocarbons from the crude below its bubble point. There appears to be controversy over the issue whether asphaltene precipitation is reversible or irreversible mechanism, especially due to lack of sufficient experimental evidence.

Hirshberg et al (1984) provides some proof as to reversibility in asphaltene deposition. It however makes sense to consider asphaltene precipitation phenomenon as reversible because adsorption of resins on asphaltene micelle follows reversible Langmuir type phenomenon. It is not quite clear however if the asphaltene deposition caused by flow of crude through porous media (rather than caused by chemical alteration of resin concentration in oil phase) is reversible or not.

C. Asphaltene Precipitation From Tank Oils Upon Addition of Solvents

Asphaltene precipitation tests were conducted for two different types of West Sak (tank) oil and eight different solvents. "Oil A" refers to West Sak crude from the Milne Point Unit, whereas "Oil B" refers to West Sak crude from the Kuparuk River Unit. Eight different solvents were used. These include: carbon dioxide, ethane, propane, n-butane, n-pentane, n-heptane, Prudhoe Bay natural gas and natural gas liquids.

Following experimental procedure was used for asphaltene precipitation tests with tank oils. Initially, a known amount of tank oil (i.e. dead oil with no solution gas) was taken in a cell. In case of liquid solvents such as pentane and heptane, the known amount of solvent was directly added to the tank oil in the cell. In case of volatile solvents such as carbon dioxide, ethane, propane, n-butane and natural gas liquids, the solvents were first condensed to liquid state and then known amount of solvents were added to the tank oil in the cell. After preparation of a solvent-oil mixture in the cell, the cell contents were continuously agitated with the rocking mechanism for several hours at room temperature. The solvent-oil mixture was then flashed and remaining liquid was filtered to separate precipitated solids (asphalts). The filter paper was then dried thoroughly and total solid asphalts (asphaltenes + resins) left on the filter paper were weighed. N-heptane was then added to total solids precipitated to redissolve resins leaving only asphaltenes on the filter paper.

The amount of asphaltenes were then weighed. These experiments were repeated for each solvent to measure asphaltene/asphalt precipitation for varying solvent to oil dilution ratio.

Table 1 shows the experimental results obtained for West Sak (tank) Oil A. The results indicate that increase in the solvent to oil dilution ratio increases the amount of precipitation of asphaltenes which levels off after certain solvent to oil dilution ratio. In these experiments the onset of asphaltene precipitation could not be determined. The results also indicate that the total amount of solids (asphalts) precipitated increase with the decrease in the molecular weight of solvent. However, no such trend was found for asphaltene precipitation.

In two of the precipitation tests, the asphalts were first precipitated by addition of n-butane and n-pentane to the tank Oil-A. The asphaltene-crude mixture was then filtered to separate asphalts and crude. The deasphalted crude was then analyzed using liquid chromatography. The results of alteration of crude oil composition due to asphalt precipitation are shown in Table 2. The results in Table 2 indicate that higher the amount of asphaltene precipitation the greater is the change in crude oil composition. The deasphalted crude is much lighter than the original crude. This indicates that in miscible processes, asphaltene precipitation can change the composition of crude oil which may result in altered phase behavior, compositional path and miscibility conditions for solvent - oil systems.

Table 3 shows the experimental results obtained for West Sak (tank) Oil B. Again, for this oil, the general trend of increase in asphaltene precipitation with increase in solvent to oil dilution ratio followed by leveling of the asphaltene precipitation at high dilution ratios for all solvents is observed. Also, for normal paraffinic solvents, the increase in molecular weight of solvent resulted in decrease in total solids (asphalt) precipitation. This is due to increase in solubility of resins with increase in molecular weight of n-paraffinic solvent.

**Table 1: Experimental Results on Static Asphaltene Precipitation Tests
For West Sak (Tank) Oil-A**

Solvent Used	Solvent/Oil Ratio By Weight	Wt% Solid (Asphalts) Precipitated	Wt% Asphaltenes	Wt% Resins
Ethane	2.96	-	5.14	-
	13.31	-	5.28	-
	-	45.6	12.80	32.80
CO ₂	3.60	-	5.56	-
	6.00	36.8	-	-
	13.62	-	5.80	-
	15.31	-	5.89	-
Propane	4.68	31.0	-	-
	4.71	36.2	8.87	27.33
	4.81	29.0	-	-
	7.79	34.4	8.60	25.80
	16.25	38.9	9.07	29.83
Prudhoe Bay Gas	1.73	29.80	7.40	22.40
N-Butane	-	20.00	-	-
	2.00	28.16	6.22	21.94
	4.44	33.00	17.40	15.60
	13.30	24.55	6.45	18.10
N-Pentane	2.01	13.42	1.79	11.63
	7.03	16.30	6.20	10.10
	12.52	13.60	6.30	7.30
	20.20	16.48	6.69	9.79
NGL	3.24	17.50	5.73	11.77
	7.64	22.80	8.80	14.00
	9.87	23.85	8.88	14.97
N-Heptane	2.00	3.83	3.83	0.00
	7.26	5.34	5.34	0.00
	13.50	7.50	7.50	0.00
	20.10	7.32	7.32	0.00

Table 2: Compositional Changes (Mol%) and Density Changes in West Sak Crude After Asphaltene Precipitation by N-Pentane and N-Butane

Component	Original Dead Oil	After Prec. with N-Butane	After Prec. with N-Pentane	Component	Original Dead Oil	After Prec. with N-Butane	After Prec. with N-Pentane
C1-C6	-	-	-	C23	1.87	1.73	2.13
C7	1.27	1.19	0.16	C24	1.22	1.67	1.39
C8	1.05	2.01	0.28	C25	1.75	2.06	0.96
C9	1.35	2.03	0.75	C26	1.60	1.84	1.58
C10	1.47	2.11	1.41	C27	1.25	1.46	1.52
C11	1.94	2.74	1.94	C28	1.23	1.59	0.72
C12	1.97	3.27	2.85	C29	1.55	1.21	0.91
C13	2.49	3.45	3.28	C30	0.69	1.17	0.90
C14	2.67	3.49	3.53	C31	2.11	1.38	1.10
C15	2.30	3.20	3.42	C32	2.11	3.02	2.55
C16	2.35	3.29	3.64	C33	2.52	2.70	2.33
C17	2.80	3.74	4.28	C34	1.45	3.22	2.12
C18	2.55	3.34	3.89	C35	2.63	1.14	1.90
C19	2.44	3.10	3.54	C36	4.14	3.62	2.72
C20	1.90	2.38	2.68	C37+	40.41	27.01	35.86
C21	2.43	2.55	2.79		100.00	100.00	100.00
C22	1.98	2.75	2.87	Sp. gravity	0.9390	0.9125	0.9242

**Table 3: Experimental Results on Static Asphaltene Precipitation Tests
For West Sak (Tank) Oil-B**

Solvent Used	Solvent/Oil Ratio By Weight	Wt% Solid (Asphalts) Precipitated	Wt% Asphaltenes	Wt% Resins
Ethane	2.93	36.60	2.90	33.70
	7.34	42.91	4.96	37.95
	21.00	43.92	5.44	38.48
CO ₂	2.09	-	4.20	-
	2.69	36.00	4.70	31.30
	19.33	-	4.85	-
	20.93	42.50	5.50	-
Propane	2.44	24.00	8.00	16.00
	6.85	33.71	9.79	23.92
	21.15	41.68	9.00	32.68
Prudhoe Bay Gas	1.99	33.00	7.00	26.00
	17.26	30.75	8.32	22.43
N-Butane	4.34	24.40	11.40	13.00
	10.49	18.50	11.68	6.82
N-Pentane	2.50	6.60	3.00	3.60
	12.52	12.80	5.30	7.50
	20.00	9.90	6.70	3.20
N-Heptane	2.00	5.10	5.10	0.00
	10.50	6.54	6.54	0.00
	20.00	5.70	5.70	0.00
NGL	1.95	18.47	6.82	11.65

Table 4 shows the effect of amount of n-heptane used to wash asphalts precipitated (to dissolve resins) by adding n-pentane to West Sak tank Oil-B in ratio of 12.52:1. The results show that it is necessary to add more than 150 cm³ of n-heptane to dissolve all the resins leaving behind only asphaltenes. This effect was studied only to determine how much n-heptane addition is necessary for conducting all the experiments. Thus in all the experiments, 200 cm³ of n-heptane addition was considered appropriate.

D. Asphaltene Precipitation Test with Recombined (Live) Oils

While the experimental data on asphaltene precipitation with tank oils are useful in determination of solubility parameters, the experimental data on asphaltene precipitation with recombined (live) oils are more appropriate in gas injection (miscible or immiscible) projects.

Keeping this in mind, experimental apparatus was assembled and procedures were developed to conduct asphaltene precipitation tests at high pressures. Figure 1 is a schematic diagram of the experimental apparatus used. The major equipment components of the apparatus include: 1) JEFRI positive displacement pump, 2) recombination cell, 3) solvent transfer cell, 4) stainless steel in-line filter, 5) air bath equipped with temperature controller and rocking mechanism. Positive displacement pump was used either to inject methane into recombination cell to recombine oil or to inject CO₂ at constant pressure into the recombination cell to prepare desired CO₂-recombined oil mixture. Initially, the known amount of tank oil was taken into the recombination cell. Dead oil was then recombined with methane at 1705 psia and 80°F. The solvent (CO₂) was then injected from the solvent transfer cell into the recombination cell (which acted also as asphaltene cell) at constant pressure. The amount of CO₂ injected was determined from the pump reading. The resulting CO₂-oil mixture was rocked for several hours to achieve good mixing. The

Table 4: Effect of Amount of N-Heptane Used for Washing Asphalts on the Resin Dissolution

Wt% Asphalts Precipitated by Adding N-Pentane to Oil B in 12.52 to 1 Ratio	Amount of N-Heptane Used for Asphalt Wash (ml.)	Wt% Asphaltenes Remaining After Heptane Wash
12.8	200	5.3
13.0	150	5.2
12.3	100	5.4
12.7	50	6.6

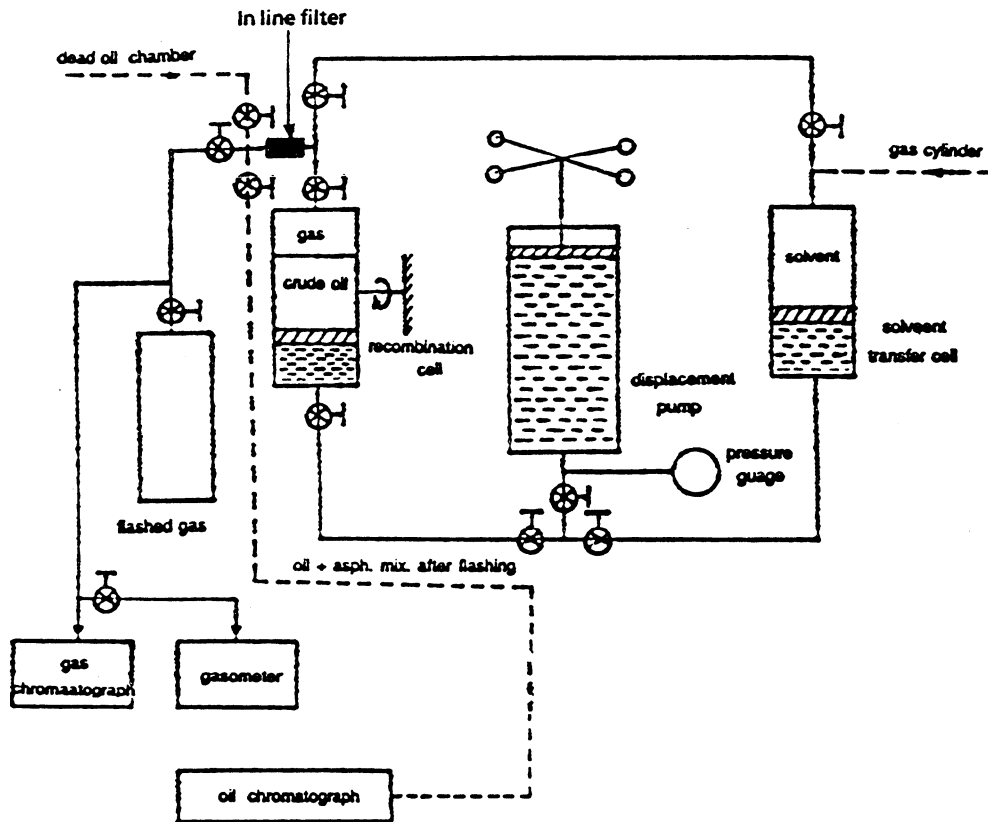


Figure 1: Schematic of Experimental Apparatus for Asphaltene Precipitation Studies

mixture was then passed through a stainless steel in-line filter to trap precipitated solids and allowing the filtrate to pass through. The resulting mixture was then flashed into a oil-gas separator. The amount of asphaltenes in the filter and oil were measured.

The first set of experiments were conducted to measure the amount of asphaltene precipitation that resulted from adding CO₂ to West Sak crude at 1705 psia and 80°F. The results are shown in Table 5 and Figure 2. The increase in amount of CO₂ in CO₂-oil mixture causes increase in the amount of deposition of asphaltenes.

The effect of pressure on asphaltene precipitation due to addition of fixed amount of CO₂ to Oil A was studied. Table 6 and Figure 3 show the results for mixture containing 30 mol% CO₂ and 70 mol% Oil A. Table 7 and Figure 4 show the results for mixture containing 50 mol% CO₂ and 50 mol% Oil A. Asphaltene precipitation seem to be highest at the bubble point pressure and decreases with increase in pressure above the bubble point pressure and decreases with decrease in pressure below the bubble point pressure.

E. Conclusions

Limited experimental study was undertaken to measure asphaltene precipitation from both live and tank West Sak crudes using various solvents. Following conclusions are drawn from this study.

1. Asphaltene precipitation changes the crude oil composition which may change the compositional path of solvent-oil mixtures in a miscible flood and may change the minimum miscibility pressures.
2. The amount of asphalt (asphaltenes plus resins) precipitation increases with decrease in molecular weight of n-paraffinic solvents.
3. Increase in solvent/oil dilution ratio increases the amount of asphaltene precipitation until a certain value of dilution ratio and then level off.

Table 5: Effect of CO₂ Addition to Recombined West Sak Oil A on The Asphaltene Precipitation (at 1705 psia, 80°F)

Mol% CO ₂ in CO ₂ /Oil Mixture	Predicted Bubble Point Pressure (Psia)	Wt% Asphaltenes
0	1705	3.14
20	1884	3.23
40	2364	3.99
60	11445	4.79
80	(Too High)	5.89

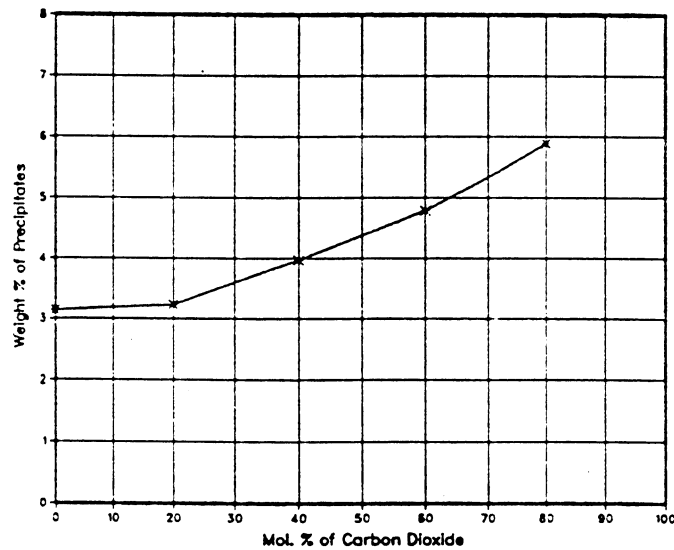
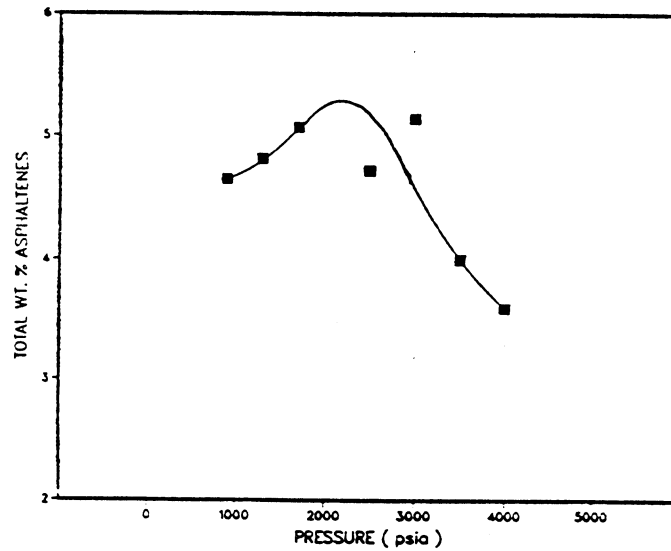


Figure 2: Effect of CO₂ Addition to West Sak Crude Oil A on Asphaltene Deposition at (1705 psia and 80°F)

**Table 6: Effect of Pressure on Amount of Asphaltene Precipitation
30 Mol% CO₂ - 70 Mol% West Sak Crude A
(Recombined at 1705 psia and 80°F)**

Pressure (Psia)	Wt% Asphaltenes in the In-Line Filter	Wt% Asphaltenes in the Oil	Total Wt% Asphaltenes
900	0.177	4.472	4.649
1300	0.183	4.631	4.814
1705	0.197	4.873	5.070
2500	0.151	4.569	4.720
3000	0.179	4.963	5.142
3500	0.183	3.817	4.000
4000	0.212	3.389	3.601



**Figure 3: Effect of Pressure on Asphaltene Precipitation
(30 Mol% CO₂: 70 Mol% Oil A)**

**Table 7: Effect of Pressure on Amount of Asphaltene Precipitation
50 Mol% CO₂ - 50 Mol% West Sak Crude A
(Recombined at 1705 psia and 80°F)**

Pressure (Psia)	Wt% Asphaltenes in the In-Line Filter	Wt% Asphaltenes in the Oil	Total Wt% Asphaltenes
1000	0.140	4.170	4.310
1705	0.192	6.430	6.622
3000	0.156	4.750	4.906
4000	0.108	4.510	4.618

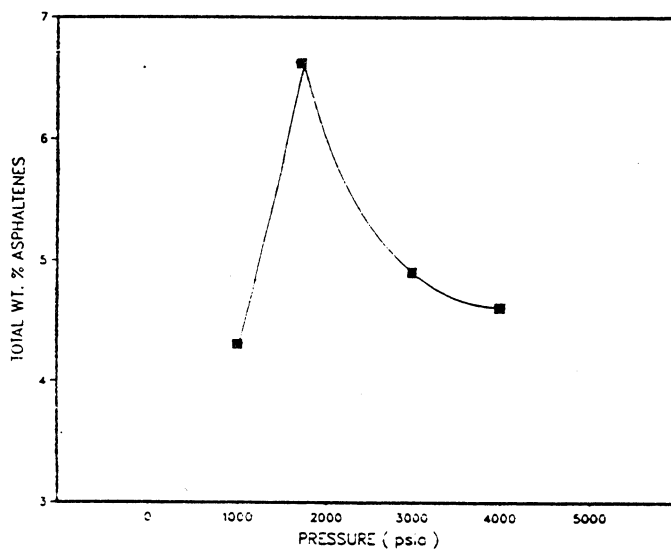


**Figure 4: Effect of Pressure on Asphaltene Precipitation
(50 Mol% CO₂: 50 Mol% Oil A)**

4. For recombined crudes, the increase in CO₂ content of CO₂-oil mixture results in increase in asphaltene precipitation.
5. For a fixed solvent to oil ratio, the asphaltene precipitation increases with pressure up to bubble point pressure and then decreases with further increase in pressure.

Further work is in progress to gather more experimental data on asphaltene precipitation from Prudhoe Bay gas and natural gas liquids addition to West Sak crude and to determine effect of asphaltene precipitation on miscibility conditions.

F. References

1. Adialalis, S., "*Investigation of Physical and Chemical Criteria as Related to the Prevention of Asphalt Deposition in Oil Well Tubings*," M.Sc. Thesis, Petroleum Eng. Dept., Imperial College of the University of London, London (Sept. 1982).
2. Danesh, A., Krinis, D., Henderson, G.D., and Peden, J.M., "*Asphaltene Deposition in Miscible Gas Flooding of Oil Reservoirs*," Chem. Eng. Res. Des., Vol. 66, No. 7 (1988) pp. 339-344.
3. Dyes, A.B. et al, "*Alternate Injection of HPG and Water - A Two Well Pilot*," SPE Paper #4082, Proc. of 1972 SPE Annual Meeting held in San Antonio, Texas (Oct. 8-11, 1972).
4. Flory, P.J., "*Thermodynamics of High Polymer Solutions*," J. Chem. Phys. Vol. 12 (1942) p. 51.
5. Harvey, M.T. Jr., Shelton, L.J., and Kelm, C.H., "*Field Injectivity Experiences with Miscible Recovery Projects Using Alternate Rich Gas and Water Injection*," J. Pet. Tech (Sept. 1977) pp. 1051-55.
6. Haskett, C.E. and Tartera, M., "*A Practical Solution to the Problem of Asphaltene Deposits - Hassi Messahoud Field, Algeria*," J. Pet. Tech. (April 1965) pp. 387-391.

7. Hirshberg, A., deJong, L.N.J., Schipper, B.A., and Meijer, J.G., "Influence of Temperature and Pressure on Asphaltene Flocculation," SPEJ, No. 6 (1984) pp. 283-293.
8. Huggins, M., "Some Properties of Solutions of Long-Chain Compounds," J. Phys. Chem. Vol 46 (1942) p. 151.
9. Leontaritis, K.J. and Mansoori, G.A., "Asphaltene Flocculation During Oil Recovery and Processing: A Thermodynamic - Colloidal Model," SPE Paper #16258, Proc. of 1987 SPE Symposium on Oil Field Chemistry (1987).
10. Lichaa, P.M., "Asphaltene Deposition Problem in Venezuela Crudes - Usage of Asphaltene in Emulsion Stability Oil Sands," Soc. of Pet. Eng. J. (1977) pp. 609-624.
11. Long, R.B., "The Concept of Asphaltene," The Advances in Chemistry Series, No. 195 (1981) p. 17.
12. Mansoori, G.A., "Asphaltene Deposition: An Economic Challenge in Heavy Petroleum Crude Utilization and Processing," OPEC Review (Spring 1988) pp. 103-113.
13. McKay, J.F., Amend, P.J., Cogswell, T.E., Harnsberger, P.M., Erickson, R.B., and Latham, D.R.: "Analytical Chemistry of Liquid Fuel Sources," Adv. in Chemistry Series 170, Chap. 9, ACS, Washington, D.C. (1978) pp. 128-142.
14. Preckshot, G.W. et al, "Asphaltic Substances in Crude Oils," Trans AIME No. 151 (1943) pp. 188-194.
15. Sharma, A.K., Patil, S.L., Kamath, V.A., and Sharma, G.D., "Miscible Displacement of Heavy West Sak Crude By Solvents in Slim Tube," SPE Paper #18761, Proc. of 1989 SPE California Regional Meeting held in Bakersfield, CA (April 5-7, 1989).
16. Stalkup, R.I., "Carbon Dioxide Flooding: Past, Present and Outlook for the Future," J. Pet. Tech. (Aug. 1978) pp. 1102-12.

17. Tuttle, R.N., "*High Pour Point and Asphaltic Crude Oils and Condensates*," J. Pet. Tech. (June 1983) p. 1192.

CHAPTER FOUR
FEASIBILITY OF STEAMFLOODING FOR WEST SAK

A. Abstract

In this study, a simplified model was developed based upon available analytical solutions in the literature to simulate a steamflood process in a heavy oil reservoir. Validation of the steamflood model was made by comparing the results obtained from the model with available field data in the literature. An economic model was then developed and integrated with the steamflood model to determine economic feasibility. The steamflood performance prediction and economic models were then applied to the West Sak reservoir. A sensitivity analysis was conducted to determine the optimum conditions necessary for a steamflood. Results from this study indicate a minimum oil price range of \$18-25/bbl for steamflooding to be economic in the West Sak reservoir. The analysis is based on a simplified model and does not consider reservoir heterogeneity or other aspects such as swelling of clays at high temperatures.

B. Introduction

Because of the size of West Sak reservoir the economics for an EOR project is more favorable than for smaller fields given the same recovery potential. Perhaps the biggest economic advantage in the development of a supergiant field is that because oil reservoirs are highly heterogeneous there can be a wide variance in the reservoir and fluid properties and this wide variance will result in development of the more favorable portions of this field leaving the less favorable portions of the field to be developed at a later time when the economics is more attractive. In this situation, the economics would become more favorable due to the "sunken costs" made in the earlier development of the more favorable portions of the reservoir.

Basically, this is because in a larger field much of the development costs (i.e. production and surface facilities) do not have to be duplicated, and also since transportation costs would be the same, the larger field gets an advantage because these costs can be "spread-out". The cost of drilling the initial wells for either a large field or a small field would be approximately equal, however, the larger field would gain an advantage in savings on transportation (distance as well as time) costs of the required drilling rigs during development of the larger field.

Steamflooding was considered because of the fact that steam displacement is a relatively stable and efficient process and more suitable for heavier, viscous oils. More than one third of oil in West Sak reservoir is very heavy and viscous and thus more suitable for a thermal process. Thus, a feasibility study of steam drive for West Sak was undertaken. Steam drives are not conducive to the formation and growth of viscous fingers in the reservoir. "Small steam fingers, if formed, tend to lose heat at relatively high rates, ultimately resulting in condensation and disappearance of the steam and, thus the finger" (Prats, 1982). Steam drives are also more efficient in performance than a hot water drive and this is due primarily to the presence and effects of condensing vapor formed by the steam drive. Previous laboratory and field studies reported in literature have shown that very low residual oil saturations have been attained with a steam drive, thus indicating a high displacement efficiency.

C. Model Description

For this study, an analytical model was developed for predicting the oil recovery by steam drive. An analytical model was chosen because they are in general simpler in concept than numerical simulators and many simplified models have predicted cumulative oil recoveries that are within ten to fifteen percent of the results generated from a numerical simulator. Such results are good enough to

make a judgment of whether or not further study in the area of consideration is warranted.

Some of the previous steamflood models such as those of Aydelotte, Pope and Williams, et al. have included simple economic models to be used with the results obtained from the steamflood portion of the model to evaluate the economics of the steamflood. However, the Tax Reform Act of 1986 produced changes in the basic tax structure and in the methods which companies could make deductions such as the elimination of the investment tax credit which is no longer valid. Prior to the Tax Reform Act, the federal tax rate for large companies was forty-six percent; after the reform act the tax rate was thirty-four percent. These recent changes in the tax structure would necessitate the modification of these models developed prior to the Tax Reform Act of 1986 for current application.

As an incentive to oil companies because development costs are so high in Alaska, the state of Alaska developed a provision referred to as the statutory economic limit factor (better known as ELF) which reduces the severance tax as well productivity declines during production. This statutory economic limit factor is unique to the state of Alaska and has been included in the economic model developed for this study to determine its sensitivity on the rate of return analysis.

In most models the basic approach to finding the economic feasibility of a given thermal or enhanced oil recovery project has been to determine the rate of return based on known operating and maintenance costs for the steam generator and a best current estimate of the market price of oil. Additional factors of importance in determining economic feasibility are the various taxes which are placed on oil production in addition to federal and state income taxes, including severance taxes and windfall profit taxes. Currently two popular methods are used in the industry for depreciating tangible capital used in the production of oil; sum of years-digits depreciation and double declining (or variations of) balance

depreciation. Under the 1986 Tax Reform Act, a new depreciation system for the Accelerated Cost Recovery System (ACRS) allows most tangible capital equipment used in oil production to be depreciated by 200 percent declining balance over seven years, compared with the 150 percent declining balance method over five years under the previous law. The model used in this study uses the current double declining (200 percent) balance method over seven years for depreciating capital.

C1. Steamflood Performance Prediction Model

The steamflood model used in this study is basically composed of three main sections: prediction of heat and pressure losses in the surface lines and in the wellbore; prediction of steam zone advance and oil recovery; prediction of economic constraints based on steamflood performance. This chapter outlines the equations and modifications used in developing both the steamflood and the economic performance models. Development of the steamflood predictive performance model was derived by combining what were considered the best features from the previous models examined during the literature search into one model; similarly the economics portion of the steamflood model was derived through reviewing previous models and modifying what was considered the most pertinent sections for application in this model.

C1.1 Prediction of Heat and Pressure Losses

As steam is injected from the steam generator and down through the wellbore into the reservoir, pressure and heat losses will be encountered which will affect the rate at which heat can be injected into the reservoir. These losses are due to both friction and conduction within the surface lines and injection tubing of the steam injection system. The equations used in this model are derived from the Earlougher equation for estimating pressure drop over a known distance [Aydelotte and Pope, 1983]:

$$\Delta P = 1.219 \times 10^{-13} \frac{f m_t^2 v_t \Delta L}{r_s^5} \dots\dots\dots (1)$$

where:

- f = single phase Moody friction factor
- m = mass flow rate of injected fluid, lbm/hr
- v_t = specific volume of steam, ft³/lbm
- r_s = inner radius of surface pipe, ft
- ΔL = length of surface pipe, ft

The single phase friction factor is derived from the Reynolds Number which is a dimensionless number used to identify if a fluid system is experiencing laminar or turbulent flow conditions. For the purposes of this study the Reynolds Number can be expressed as:

$$N_{Re} = 0.8267 \frac{m_t}{r_s \mu_l H_l \mu_v [1 - H_l]} \dots\dots\dots (2)$$

$$H_l = \frac{(1 - X) v_t}{v_t} \dots\dots\dots (3)$$

where:

- μ_l = viscosity of liquid phase
- μ_v = viscosity of vapor phase
- X = injected steam quality

H_l , the Hagedorn and Brown liquid hold-up factor represents the volume fraction of liquid in the injected fluid assuming no slippage. Laminar or turbulent flow is determined by the magnitude of the Reynolds Number (N_{Re}). When it is less than 2000 it is considered laminar flow, above 4000 it is termed turbulent, and when it is between 2000 and 4000 the flow is

considered a mixed boundary condition. The following equations are expressions for the Moody friction factor (f) in relation to the classification of the fluid flow system.

$$f_t = \frac{64}{N_{Re}}, \text{ for laminar flow when } N_{Re} \leq 2000 \quad \dots\dots\dots (4)$$

For turbulent flow conditions, an iterative procedure derived from the Colebrook equation is used to find the turbulent friction factor.

$$\frac{1}{\sqrt{f_2}} = 1.14 - 2(0.43429) \ln \left[\frac{e}{24 r_s} + \frac{9.34}{N_{Re} \sqrt{f_2}} \right] \quad \dots\dots\dots (5)$$

where:

e = pipe roughness factor

If the flow condition that exists is a mixed boundary type, than an interpolation based on the previous equations for finding the friction factor is used:

$$f = f_1 + \frac{(N_{Re} - 2000)(f_2 - f_1)}{2000} \quad \dots\dots\dots (6)$$

C1.1.1 Surface Heat Losses

Surface heat losses (Q_{surf}) are found from general heat and mass transfer relationships knowing the surface area of the pipe exposed, thermal resistance of the surface pipe, and mean annual temperature difference.

$$Q_{surf} = 2 \pi r_s \Delta L U_{surf} \Delta T_s \quad \dots\dots\dots (7)$$

where:

Q_{surf} = surface heat losses, Btu/hr

U_{surf} = heat transfer coefficient of surface pipe

ΔT_s = $T_{stm} - T_{mast}$

$$U_{surf} = \left[\left(\frac{R_{ti} \ln \left(\frac{R_{to}}{R_{ti}} \right)}{K_{pipe}} \right) + \left(\frac{R_{ti} \ln \left(\frac{R_{ins}}{R_{to}} \right)}{K_{ins}} \right) \right]^{-1} \dots\dots\dots (8)$$

where:

R_{ti} = inner radius of tubing, ft

R_{to} = outer radius of tubing, ft

R_{ins} = thickness of insulation, ft

K_{pipe} = thermal conductivity of pipe, Btu/ft hr °F)

K_{ins} = thermal conductivity of insulation, Btu/(ft hr °F)

Changes in the steam quality at the end of the surface line may be found through the enthalpy changes knowing the pressure losses which occur within the system.

$$X_{j+1} = \frac{S_{surf} (h_{vj} - h_{lj}) + h_{lj} - h_{lj+1} - Q_{surf}/m_t}{h_{vj+1} - h_{lj}} \dots\dots\dots (9)$$

where:

X_{surf} = steam quality at surface

X_{j+1} = steam quality at end of surface line

h_t = enthalpy of fluid phase, Btu/lbm

h_v = enthalpy of vapor phase, Btu/lbm

C1.1.2 Wellbore Heat and Pressure Losses

The pressure drop in the wellbore is calculated in much the same manner as the surface lines but in the wellbore the Earlougher

form of the Bernoulli equation is used which accounts for the pressure change due to changes in the kinetic energy and an increase in pressure due to the weight of the fluid column.

$$\begin{aligned}
 p_{stin} = p_{surf} + [1.687 \times 10^{-12} (v_{tj} - v_{tj+1}) m_i^2 / r_{ri}^4] \\
 + \left[6.944 \times 10^{-3} \frac{\Delta Z}{v_{tj}} \right] - \Delta p_f
 \end{aligned}
 \dots\dots (10)$$

$$\Delta p_f = 4.219 \times 10^{-13} \frac{f m_i^2 v_t \Delta Z}{r_{ti}^5}
 \dots\dots (11)$$

where:

- p_{surf} = surface steam injection pressure, psia
- p_{stin} = reservoir steam injection pressure, psia
- r_{ti} = inner radius of injection tubing, ft
- ΔZ = reservoir depth, ft
- Δp_f = frictional pressure drop, psia

Once the pressure drop in the wellbore is known, the temperature of the steam in the wellbore can be obtained by interpolation through a steam table. The next step in the program is to calculate the approximate hot water depth point of the steam injected. If the hot water depth point lies above the reservoir depth, then the conditions are considered not feasible, whereas if the hot water point lies below the reservoir, then it is known that steam still exists in the wellbore at reservoir depth. Steam quality being injected in the wellbore as well as the hot water depth point is found using the method outlined by Satter (1965) for finding the heat losses from

the wellbore relates the change in steam quality to reservoir depth (Z), steam injection rate, and rate of heat transferred to the surrounding reservoir. Steam quality for a given depth is expressed as the following:

$$X_{inj} = X_{j-1} + \frac{a Z^2}{2 A'} + \frac{A' B' + T_{mean} + a Z - T_{stm}}{2 A'} \dots\dots (12)$$

$$A' = \frac{m_i L_v_j (K_{ob} + R_{ti} U_{ti} f(t))}{2\pi R_{ti} U_{ti} K_{ob}} \dots\dots (13)$$

$$B' = \frac{1}{778 L_v} \dots\dots (14)$$

$$R_{ti} U_{ti} = \left[\left(\frac{\ln R_{to} / R_{ti}}{K_{tube}} \right) + \left(\frac{\ln R_{ci} / R_{to}}{K_{ins}} \right) + \left(\frac{\ln R_{co} / R_{ci}}{K_{cas}} \right) + \left(\frac{\ln R_w / R_{co}}{K_{cem}} \right) \right]^{-1} \dots\dots (15)$$

where:

$f(t)$ = Ramey's time function for transient heat conduction

X_{inj} = injected steam quality at reservoir depth

a = geothermal gradient, °F/ft

Z = depth, ft

T_{mean} = mean annual surface temperature, °F

T_{stm} = surface temperature of injected steam, °F

- L_v = latent heat of vaporization, Btu/lbm
- K_{ob} = thermal conductivity of overburden, Btu/ft hr °F)
- K_{tube} = thermal conductivity of tubing, Btu/(ft hr °F)
- R_{ci} = inner radius of casing, ft
- R_{co} = outer radius of casing, ft
- R_w = radius of wellbore, ft
- $R_{ti}U_{ti}$ = Overall convective heat transfer coefficient, Btu/hr-ft-°F

In the case of saturated steam, as in this study, the percent loss using Satter's approach is expressed in the following manner:

$$F_{wb} = \frac{\left[(X_{inj} - X_{surf}) L_v + \frac{Z}{778} \right] 100}{H_t + X_{inj} L_v - (H_t)_{T_{mean}}} \dots\dots\dots (16)$$

where:

$$F_{wb} = \text{fraction wellbore heat loss}$$

C1.1.3 Underburden and Overburden Heat Losses

The other major source for heat losses which occur during the steam injection period is the heat lost to the overburden and underburden of the reservoir. For this model it was decided that the approach used by Marx and Langenheim would suffice for the purposes of this study. According to Marx and Lengenheim (1959) the total rate of heat loss (Q_{lost}) increases with time as the heated zone grows. Further, they assume that the heat losses from a horizontal reservoir into the adjacent surrounding formations are by vertical conduction only. In their work it was found that the fraction of heat which remains in the reservoir, which is a measure

of the heat efficiency (E_{hs}) does not depend on the injection temperature, rate of fluid injection, or rate of heat injection. So long as the heat input is constant, the heat efficiency is a function of the dimensionless time, t_D , which is defined in the following manner:

$$t_D = 4 (365 \times 24) K_{ob} M_s \frac{t}{h_t^2 M_1^2} \dots\dots\dots (17)$$

where:

M_s = volumetric heat capacity of over and underburden, Btu/(ft³-°F)

M_1 = volumetric heat capacity of reservoir, BTU/(ft³-°F)

Heat loss to the adjacent underburden and overburden formations is given by

$$Q_{lost} = Q_{inj} (1 - e^{-t_D} \operatorname{erfc} \sqrt{t_D}) \dots\dots\dots (18)$$

where:

Q_{lost} = heat lost to the adjacent formation, Btu

Q_{inj} = total heat input into reservoir, Btu

where $\operatorname{erfc}(x)$ is the complementary error function:

$$\operatorname{erfc}(x) = \frac{2}{\sqrt{\pi}} \int_x^\infty e^{-s^2} ds \dots\dots\dots (19)$$

$$= 1 - \frac{2}{\sqrt{\pi}} \int_0^x e^{-s^2} ds \dots\dots\dots (20)$$

$$= 1 - \text{erf}(x) \quad \dots\dots\dots (21)$$

For this model the complementary error function described above is solved using an analytical solution which approximates the value of the function $\text{erfc}(x)$. The solution used is the same as that found in the Jeff Jones model and produces results which correlate well with the published table values for the error function.

$$\begin{aligned} \text{erfc}\sqrt{t_D} = & (0.25482952K - 0.284496736K^2 + 1.42141374K^3 \\ & - 1.453152037K^4 + 1.061405429K^5) e^{-t_D} \quad \dots\dots\dots (22) \end{aligned}$$

$$K = \frac{1}{1 + 0.3275911 \sqrt{t_D}} \quad \dots\dots\dots (23)$$

The total amount of heat which can effectively remain in the reservoir is a function of the isobaric heat capacity of a fluid-filled porous formation, or more simply put the amount of heat required to raise a unit bulk volume by one degree of temperature. This heat required is equal to the product of the effective density and the isobaric specific heat capacity of the bulk formation. In general this term is simply referred to as the volumetric heat capacity of the formation (M_R). The volumetric heat capacity of the formation is equal to the sum of the heat contents of the fluid phases occupying the pore space within the solid rock phase, and it expressed as:

$$M_R = \phi \frac{h_n}{h_t} (S_{o_n} \rho_o C_{p_o} + S_{w_n} \rho_w C_{p_w} + S_{g_n} \rho_g C_{p_g})$$

$$+ \left(1 - \phi \frac{h_n}{h_t} \right) \rho_{rx} C_{p_{rx}} \dots\dots\dots (24)$$

where:

- M_R = volumetric heat capacity of formation, Btu/(ft³-°F)
- ϕ = porosity, fraction
- h_n = net thickness of oil sands in reservoir, ft
- S_{o_n} = initial saturation of fluid phase n in reservoir, fraction
- ρ_o = density of reservoir oil, lbm/ft³
- ρ_g = density of reservoir gas, lbm/ft³
- ρ_{rx} = density of reservoir rock, lbm/ft³
- C_{p_n} = specific heat of phase n , Btu/lbm °F

The amount of heat that will remain in the adjacent or surrounding formation is found from the volumetric heat capacity of the underburden and overburden which are assumed to be equal in this application and is found from the following equation.

$$M_s = \frac{K_{ob}}{\alpha_s} \dots\dots\dots (25)$$

where:

- M_s = volumetric heat capacity of adjacent formation, Btu/(ft³-°F)
- α_s = thermal diffusivity of surrounding formation, ft²

C1.2 Steam Zone Shape Factor

The shape of the steam zone is an important consideration in predicting the production of oil and water as a result of steam injection.

Several analytical solutions have been formulated which describe the approximate shape of the steam zone in the reservoir. In this model, however, the approach taken by van Lookeren is used to predict the steam zone shape of a radial steam drive. van Lookeren found that the shape of the steam zone is controlled mainly by one group of parameters which include steam injection rate, formation and effective permeability to steam. An important consideration in the description of the shape of the steam drive is the steam-liquid interface present in the steam drive, which is dependent upon the steam consumption distribution in the reservoir. For most steam drives the actual steam-liquid interface lies between the two extreme cases of even and concentrated consumption; however, the even steam consumption occurs much more frequently and as a result it can be assumed to be the type of consumption present for most steam calculation purposes, as was done for this model.

van Lookeren developed a dimensionless parameter (A_{RD}) for characterizing the shape of a radially growing steam zone which is dependent upon the viscosity of the injected steam, steam injection rate, reservoir thickness, and density of the fluids.

$$A_{RD} = \left[\frac{\mu_{stm} i_{stm, inj}}{\pi (\rho_o - \rho_{stm}) g h^2 k_{stm} \rho_{stm}} \right]^{1/2} \dots\dots\dots (26)$$

Accounting for field units the equation then becomes:

$$A_{RD} = \left[\frac{(350)(144) \mu_{stm} i_{stm} X}{6.328 \pi (\rho_o - \rho_{stm}) \rho_{stm} K_{stm} h_n^2} \right]^{1/2} \dots\dots\dots (27)$$

where:

A_{RD} = van Lookeren shape factor

- μ_{stm} = viscosity of steam, cp
- i_{stm} = steam injection rate, bbl/day
- ρ_{stm} = density of injected steam, lbm/ft³
- k_{stm} = permeability to steam phase, md

van Lookeren found that if the steam-zone shape factor, A_{RD} is less than 0.6, liquid levels in steam injection wells can indicate steam zone limits. Having found a value of A_{RD} , van Lookeren developed a correlation from the shape factor to find the average steam zone thickness, h_{stm} .

$$h_{stm} = 0.5 A_{RD} h_n \dots\dots\dots (28)$$

C1.3 Areal Sweep Efficiency

Areal sweep efficiency at breakthrough (E_{ABT}) is found from a correlation of steam zone areal sweep efficiency and oil viscosity at 80°F (Aydelotte and Pope, 1984).

$$E_{ABT} = 0.9 - 0.1025 \log(\mu_{oil} @ 80^\circ F) \dots\dots\dots (29)$$

where:

- μ_{oil} = viscosity of oil, cp

After finding the sweep efficiency at breakthrough it is possible to determine the steam zone volume at breakthrough from the following equation:

$$V_{sbt} = 43560 A E_{ABT} h_{stm} \dots\dots\dots (30)$$

where:

- A = effective area of well spacing, Acres
- V_{sbt} = steam zone volume at breakthrough, ft³

C1.4 Critical Time

Determining the critical time in a steamflood is an important aspect in steam-drive processes because it marks an important time change in the heat flow across the condensation front. Before the onset of critical time, heat flow across the condensation front is conductive; after critical time, the heat flow becomes predominantly convective. The dimensionless critical time (t_{CD}) during the steam drive process is found using an approximate solution from the Jeff Jones model.

$$t_{CD} = 0.48 h_D^{1.71} \quad \dots\dots (31)$$

$$h_d = \frac{X_j Lv_j}{(h_{t_j} - h_{t_{res}})} \quad \dots\dots (32)$$

where:

- h_d = effective steam quality at critical time
- Lv_j = latent heat of vaporization at wellbore conditions, Btu/lbm
- h_{t_j} = enthalpy of water of wellbore conditions, Btu/lbm
- $h_{t_{res}}$ = enthalpy of water at reservoir conditions, Btu/lbm

This solution is derived from an earlier work by Mandl and Volek (1969) regarding heat and mass transfer in steam drives, whose original solution for determining critical time is an iterative solution. From the previously defined equation for finding dimensionless time, it is possible to find the actual critical time through back substitutions. Since the critical time marks an important change in the heat flow, the equation used for determining steam zone growth will have to change after the onset of critical time to account for this difference.

C.1.5 Steam Zone Growth

An analytical solution for predicting steam zone growth during a steamflood was first derived by Marx and Langenheim (1959), and their solution remains the basis from which later works were derived such as Mandl and Volek's (1969) solution. For this model steam zone growth is predicted using the method adopted by Myhill and Stegemeier (1978) which is an extension of the solution originally developed in Mandl and Volek's work on heat and mass transport in steam drives. In this solution the steam zone is always related to the fraction of the injected heat remaining (heat efficiency) in the steam zone with that of the total heat injected.

$$V_s = \frac{Q_{inj} E_{hs}}{M_4 \Delta T_4} \dots\dots (33)$$

$$\Delta T_4 = T_{stm} - T_{res} \dots\dots (34)$$

$$V_4 = V_s \dots\dots (35)$$

where:

M_4 = volumetric heat capacity of steam zone, Btu/(ft³-°F)

T_{stm} = surface temperature of injected steam, °F

T_{res} = reservoir temperature, °F

V_s = volume of steam zone, ft³

As mentioned previously the heat efficiency (E_{hs}), is primarily a function of dimensionless time. In this model the expression developed by Myhill and Stegemeier which is based upon the previous works of Mandl and

Volek, and Marx and Langenheim is used for defining the thermal efficiency before critical time.

$$E_{hs} = \frac{1}{t_D} \left(e^{t_D} \operatorname{erfc} \sqrt{t_D} + 2 \sqrt{\frac{t_D}{\pi}} - 1 \right) \dots\dots\dots (36)$$

After the onset of critical time, heat across the condensation front becomes primarily convective and the heat efficiency expression to be used in the model must show this change in heat transfer occurring at the condensate front. An expression which does account for this difference was originally developed by Mandl and Volek, which has since been adopted by others in their models and is also used in this model. In terms of dimensionless time the thermal efficiency equation after critical time becomes:

$$E_{hs} = \left[\left(e^{t_D} \operatorname{erfc} \sqrt{t_D} + 2 \sqrt{\frac{t_D}{\pi}} - 1 \right) - \left(\frac{t_D - t_{CD}}{\pi} \right)^{1/2} \left(\frac{1}{1 + h_D} + (t_D - t_{CD} - 3) \frac{e^{t_D}}{3} \operatorname{erfc} \sqrt{t_D} - \frac{t_D - t_{CD}}{3 \sqrt{\pi t_{CD}}} \right) \right] \frac{1}{t_D} \dots\dots\dots (37)$$

C1.6 Hot Condensate Zone

The volume of the hot condensate zone formed as a result of steam injection is found using an incremental heat balance method, similar to that proposed by Aydelotte and Pope in their model. In this model, however, an energy balance based on the previously calculated steam zone is implemented knowing that the heat remaining within the steam and condensate zones is equal to the cumulative heat input minus the rate of the heat losses in the steam and hot condensate zones.

$$\Delta(V_4 M_4 \Delta T_4)^n + \Delta(V_3 M_3 \Delta T_3)^n = Q_{inj} - Q_4^n - Q_3^n \quad \dots\dots\dots (38)$$

$$Q_k^n = \frac{(V_k^n - V_k^{n-1})}{h_{stm}} q_k^n \Delta t^n \quad \dots\dots\dots (39)$$

$$q_k^n = \frac{K_{ob} \Delta T_k}{\sqrt{\pi \alpha t^n - t^{n-1}}} \quad \dots\dots\dots (40)$$

where:

- Q_k = cumulative heat absorbed in zone k
- q_k = heat loss rate in zone k , Btu/ft²-day
- α = thermal diffusivity of reservoir, ft²/hr
- Δt = time step, days

In the development of the above equations it was assumed that all fronts act as shock fronts, and for describing the fluid saturations in the steam zone, a relationship to describe the rate of heat arrival the steam front was used.

$$vel_4 M_4 \Delta T_4 = U_4 (f_{w4} \rho_{w4} C_{p_{w4}} \Delta T_4 + f_{g4} \rho_{g4} C_{p_{g4}} \Delta T_4) \quad \dots\dots\dots (41)$$

where:

- vel_4 = velocity of steam front, ft/day
- f_{w4} = fractional flow of water in steam zone
- f_{g4} = fraction flow of gas in steam zone

The volumetric flux, U_4 , in the steam zone, is defined assuming that the residual oil phase to steam is immobile.

$$U_4 = \frac{m_{sti}}{f_{w4} \rho_{w4} + f_{g4} \rho_{g4}} \frac{1}{2 \pi r_4 h_n} \dots\dots\dots (42)$$

where:

U_4 = volumetric flux in steam zone, ft/day

r_4 = radial extent of steam zone, ft

Steam zone velocity (vel_4) in the above equation is found knowing the volume of the steam zone and its rate of growth assuming a vertical steam-hot water interface and radial flow.

$$vel_4 = \frac{\Delta r_4}{\Delta t} \dots\dots\dots (43)$$

Water saturation in the steam zone is found by back substitution of the volumetric heat capacity equation assuming that the only unknowns are the liquid saturations which can all be expressed in terms of one another.

$$S_{o4} = S_{or} f_{o4} = 1 - S_{w4} - S_{or} f_{g4} = 1 - f_{w4} \dots\dots\dots (44)$$

$$S_{w4} = \frac{\left[M_4 - \left(1 - \phi \frac{h_n}{h_t} \right) \rho_{rx} C p_{rx} \right]}{\phi \frac{h_n}{h_t} \rho_w C p_w} - \frac{S_{or} \rho_o C p_o + S_{g4} \rho_{g4} C p_{g4}}{\rho_w C p_w} \dots\dots\dots (45)$$

where:

S_{or} = residual oil saturation, fraction

Once the liquid saturations in the steam zone are known, the fractional flow terms are found from the following equation.

$$f_j = \frac{\frac{K_{rj}}{\mu_j}}{\frac{K_{ro}}{\mu_o} + \frac{K_{rw}}{\mu_w} + \frac{K_{rg}}{\mu_g}} \dots\dots\dots (46)$$

In the above equation subscript *j* refers to the respective fluid phase. The relative permeabilities required in the above equation are calculated using a correlation based upon Stone's three phase relative permeability model using the calculated saturation values. After the fractional flow terms in the steam zone have been obtained the volumetric flux, U_4 , in the steam zone is then calculated.

The volumetric flux in the condensate zone (U_3) is found by a mass balance on the steam zone shock front, which is the approach developed in Aydelotte and Pope's model, and the result is expressed as:

$$U_3 = U_4 \left(f_{w4} \frac{\rho_{w4}}{\rho_{w3}} + f_{g4} \frac{\rho_{g4}}{\rho_{g3}} \right) - \phi vel_4 \left(S_{o4} \frac{\rho_{o4}}{\rho_{o3}} + S_{w4} \frac{\rho_{w4}}{\rho_{w3}} + S_{g4} \frac{\rho_{g4}}{\rho_{g3}} - 1 \right) \dots\dots\dots (47)$$

where:

U_3 = volumetric flux in condensate zone, ft/day

Subscript 3 denotes condensate zone.

Subscript 4 denotes steam zone.

After determining the volumetric flux in the condensate zone, the water saturation in the condensate zone is required in order to determine the heat capacity within this zone. Continuing with the approach developed

by Aydelotte and Pope, the following relationship describing the fractional flow of water in the condensate zone has been developed:

$$f_{w3} = a_3 S_{w3} + b_3 \quad \dots\dots (48)$$

$$a_3 = \frac{\phi vel_4}{U_3} \quad \dots\dots (49)$$

$$b_3 = 1 + a_3 \left(S_{o4} \frac{\rho_{o4}}{\rho_{o3}} - 1 \right) \quad \dots\dots (50)$$

In the condensate zone it is further assumed that there is no gas phase present; therefore oil saturation is simply:

$$S_{o3} = 1 - S_{w3} \quad \dots\dots (51)$$

Using the heat capacity of the steam zone as an approximation for that of the condensate zone, an approximate value for the water saturation in the condensate zone is obtained. As with the steam zone calculations the fractional flow terms are found after obtaining the liquid saturations. From the fractional flow terms found, a new water saturation value is obtained using the equations just defined, and the new saturation values are then used to find the volumetric heat capacity of the condensate zone. One of the assumptions made with regards to calculating the fluid properties (i.e. density) within the condensate zone, in this model, is the temperature of the condensate zone. It has been observed in previous studies that the temperature in the condensate zone gradually decreases from the steam zone temperature to the reservoir temperature. In the

work conducted by Rhee and Doscher (1980) it was found that for most engineering applications a linear temperature profile as an approximate temperature distribution for the condensate zone can be used. As an initial guess for the temperature in the condensate zone this approach was used in the model, with T_m representing the condensate zone temperature.

$$T_m = \frac{T_{stm} - T_{res}}{2} \dots\dots\dots (52)$$

From this value, T_m , obtained for the condensate zone temperature, a new value for the volumetric heat capacity M_3 , in the condensate zone is calculated. Also, the energy balance equation can now be implemented to get an initial prediction for the condensate zone volume using the above defined equations. Rearranging some terms and solving the heat balance for the condensate zone yields:

$$\Delta V_3 = \frac{(Q_{inj} - Q_4 - \Delta(V_4 M_4 \Delta T_4))}{(M_3 \Delta T_3 + q_3 \Delta t / h_{stm})} \dots\dots\dots (53)$$

$$\Delta(V_4 M_4 \Delta T_4) = (V_4^n M_4^n - V_4^{n-1} M_4^{n-1}) \Delta T_4 \dots\dots\dots (54)$$

From the predicted volume of the condensate zone a new temperature for this zone is calculated based upon the velocity of the steam and condensate zone advancement in the reservoir. The radial extent of the condensate zone is found using the same equation for the steam zone calculation. The resultant temperature drop which occurs across the condensate zone is related to the advancement of the steam and condensate fronts from the following equation:

$$dT_3 = \left(\frac{vel_4}{vel_4 + vel_3} \right) \frac{M_4}{M_3} \Delta T_4 \quad \dots\dots (55)$$

$$T_3 = dT_3 + T_{res} \quad \dots\dots (56)$$

An average temperature (T_{con}) equal to the following

$$T_{con} = \frac{T_m + T_3}{2} \quad \dots\dots (57)$$

is then used to find the new condensate zone volume prediction in this model. When the total volumes of both the steam and condensate zones exceeds the steam zone volume at breakthrough, calculated earlier, a provision in the model is made to readjust the volume of oil displaced from the condensate zone to account for this. In this provision if the combined steam and condensate volumes are greater than the breakthrough volume, the condensate volume is recalculated to be equal to the difference between the breakthrough volume and the steam zone volume. The volume which exceeds the breakthrough volume becomes what is referred to as the secondary or "pseudo"-condensate volume (V_2), which is to be considered in calculating the volume of water displaced by the steam drive. Using this provision a boundary condition is thus imposed on the steam and condensate zone advancement.

$$Sum V_4 V_3 = V_4 + V_3 \quad \dots\dots (58)$$

$$V_3 = V_{sbt} - V_4 (Sum V_4 V_3 < V_{sbt}, \text{ and } V_4 < V_{sbt}) \quad \dots\dots (59)$$

$$V_2 = \text{Sum}V_4 V_3 - V_{sbt} \quad \dots\dots\dots (60)$$

where:

$\text{Sum}V_4 V_3 =$ combined steam and condensate zone volumes, ft³

$V_2 =$ pseudo-condensate volume, ft³

When the steam zone volume is greater than or equal to breakthrough volume than the following condition regarding the condensate volume is considered.

$$V_2 = V_3 \quad (V_4 \geq V_{sbt}) \quad \dots\dots\dots (61)$$

The condensate volume, V_3 , is set equal to zero regarding oil displaced, this condition is indicative of the entire condensate volume existing outside the boundary of the reservoir specified earlier.

C1.7 Pressure Drop in the Reservoir

Pressure drop in the reservoir between the injector and the producer is found as a function of the mobility and size of the steam and condensate zones, and summing the pressure drop across each zone to find the total pressure drop. No pressure drop is calculated for the condensate zone after it has achieved breakthrough which indicates that the zone has advanced past the producing well.

$$dPr = \frac{U_4 r_{stm} \ln\left(\frac{r_{stm}}{r_{stm3}}\right)}{K\lambda_4} + \frac{U_3 r_{stm3} \ln\left(\frac{r_{stm3}}{r_{sbt}}\right)}{K\lambda_3}$$

$$\lambda = \frac{Kro_j}{\mu_{oj}} \quad \dots\dots\dots (62)$$

where:

- dPr = pressure drop across reservoir, psi
- λ = mobility ratio of oil phase in reservoir
- K_{ro} = relative permeability to oil phase

C1.8 Calculation of Fluids Displaced

Having predicted the advancement of the steam and condensate zone volumes within the reservoir and the fluid saturations in the respective zones, the volume of oil and water displaced by the advancing steam front is then calculated. The following equation was used for estimating oil production as a result of steam injection in the reservoir:

$$N_p = \frac{\phi \frac{h_n}{h_t} [\Delta V_4 (S_{oi} - S_{or}) + \Delta V_3 (S_{oi} - S_{o3})]}{5.615 B_{oi}} \dots\dots\dots (63)$$

where:

- N_p = oil displaced by steam injection, bbl
- B_{oi} = oil formation volume factor, bbl/bbl

A similar equation was then used for estimating water production by substituting the respective values of water saturation found for both the steam and condensate zones in the above equation.

The sequence of equations presented are then repeated for each time step until the specified time period to be predicted is reached. At the end of the prediction period the model developed for this study then calculated the rate of return of the steam drive project based on the performance prediction from the equations just derived.

C1.9 Model Validation

The steamflood model used in this study was verified by considering only the steamflooding predictive portion of the model and considering

this portion to be composed of two distinct sections. One distinct section is the prediction of the wellbore heat losses and condensation of the injected steam, and other section is composed of the analytical equations used in determining the predicted cumulative oil and water recovery of the injected steam as a function of time. The cumulative fluid volume predictions were examined for verification because it is the ultimate oil production which determines economic feasibility of an enhanced oil recovery project.

C1.9.1 Wellbore Heat Losses

Since the steamflood model employs Satter's (1965) approach for modeling wellbore heat losses to determine the condensation of steam during injection of the fluid, verification of this portion of the model was made using the same data Satter had used in his original work to model the wellbore heat losses under varying circumstances. A comparison of the predicted fractional wellbore heat losses from the steamflood and the results obtained by Satter's model were then analyzed. Data used for Satter's results were obtained by extrapolating points from the figures of interest provided in his paper. For the purpose of model validation, the case examined corresponds to Figure 8 of Satter's (1965) paper which had the following conditions: injection rate of 5000 lb/hr, injection pressure of 500 psia, saturation temperature of 467°F, and an injection depth of 3000 feet.

In examining the plotted data (Figure 1) obtained from the steamflood model with the data reported in Satter's paper it is easily recognized that the wellbore heat loss profiles of both curves are very similar in appearance. There is a displacement difference

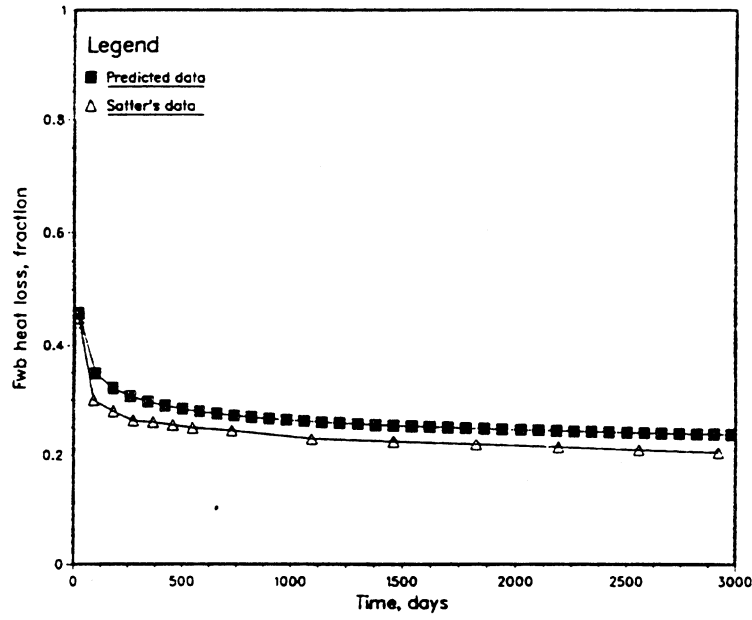


Figure 1: Comparison of Predicted Wellbore Heat Losses

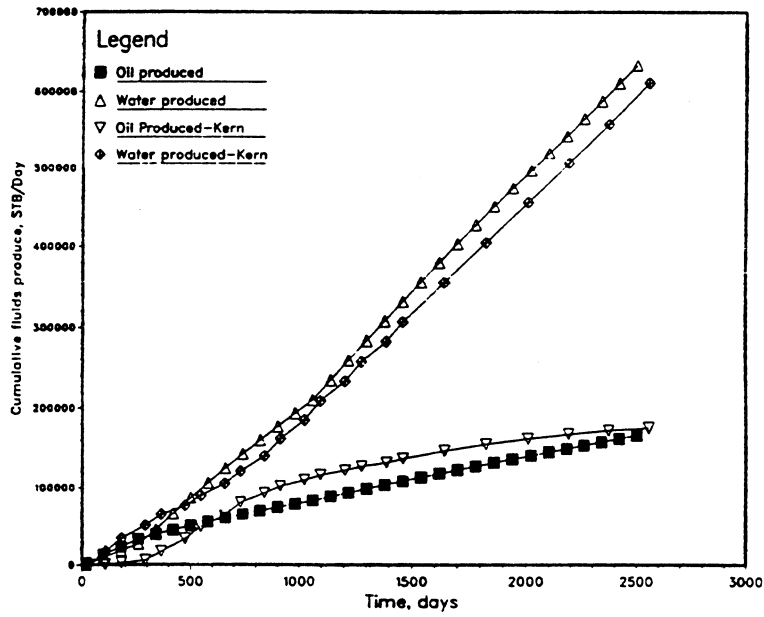


Figure 2: Comparison of Predicted Kern River Simulated Steamflood

between the two curves, with the steamflood model used in this study predicting a slightly greater heat loss than Satter's curve. The average difference in displacement in the predicted heat losses between the two curves is approximately four percent. One explanation for this observed difference may arise from the fact that the steamflood model is also taking into account the heat losses which occur in the surface lines from the steam generator to the injectors. The additional heat losses encountered at the surface should easily account for the higher predicted heat losses from the steamflood model when compared to the results obtained from Satter's (1965) model which only considers wellbore heat losses. With this in consideration, and upon further examination of the results obtained from the steamflood model, it would appear that the prediction of heat losses in the wellbore are in general agreement with the data obtained from Satter's model. Also, it should be noted that the data from Satter's paper had to be interpolated from the figures used in his paper since the actual numerical results from his studies were not available in the paper.

C1.9.2 Prediction of Oil and Water Produced

Verification of the predictive phase of the steamflood model was determined by comparing with the results obtained from another model for the same reservoir conditions. For this verification the model used for comparison is that of Aydelotte and Pope (1983). That model was used to simulate a steamflood in Kern River, California; the results from that simulation were compared to the results predicted from the steamflood model used in this study. Data for the results of this simulation run were obtained from a

report submitted by Aydelotte and Pope (1984) to the Department of Energy entitled "Development and Verification of Simplified Predictive Models for Enhanced Oil Recovery Application." Basic reservoir data and steam injection conditions for the Kern River simulation were also included in this report and provided the necessary data used in the steamflood model verification.

A comparison of the results obtained from the steamflood with those of Aydelotte's model can be found in Figure 2. In reference to this figure, it is obvious that the predicted cumulative produced volumes of both the water and oil from the model do not match exactly with the data plotted from the simulated run. This is not surprising since the models differ in the calculation of the displaced steam volumes which will of course result in different predicted volumes for both the cumulative water and oil produced. Aydelotte and Pope use an iterative heat balance approach to determine the steam and hot condensate zones, while the steamflood model in this study uses the analytic approach of Myhill and Stegemeier to calculate the steam zone, after which a heat balance approach is employed to determine the hot condensate zone. The time frame is one of the most noticeable differences between the two simulation runs, but the objective is to illustrate that the steamflood model developed for this study predicts cumulative recovery that corresponds reasonably well with that of previous steamflood models such as that of Aydelotte and Pope.

The time frame employed in this prediction run spans a period of seven years, although in the model run used for reference a period of ten years was used for the simulation run. Examination of

Figure 2 reveals that during the early history, within the first two years of the steamflood there is a noticeable discrepancy between the predicted cumulative produced volumes of water and oil. The primary reason for this discrepancy, regardless of the different algorithms for determining the displaced steam and hot condensate zones, is the use of different injection rates in the Aydelotte and Pope model, where in the developed steamflood model a fixed steam injection rate of two hundred fifty (250) barrels per day (cold water equivalent) was used; in the model used for verification the injection rate varies for the first two years from 161.7 barrels per day (BPD) to a fixed rate of three hundred barrels per day. This difference in the injection rate would account for the variation in the predicted fluids recovered during the first two years of the steamflood. As should be expected the steamflood predicts a greater cumulative oil recovery during the first six hundred days, while the predicted water produced is less than the reference model (Aydelotte's) for the first five hundred days. This is a result of the higher fixed injection rate having a greater thermal efficiency than the lower initial injection rates used in the reference model. After a period of five hundred days the water production is observed to be consistently greater than that of the reference model, but its profile basically parallels the water production curve of the reference model which would indicate that water production for both models is approximately equal.

With respect to the predicted oil production it is observed that the steamflood model developed predicts cumulative oil production less than that of the reference model by Aydelotte, and as time

progresses the predictions converge toward similar points. Cumulative oil prediction at 2500 days for the developed steamflood model predicts roughly 166,000 barrels, while interpolating values from the simulation for Aydelotte's model yields a value of approximately 175,000 barrels of oil. This results in a difference between the two steamflood predictions of approximately five percent (5.14%). Since the difference between the predicted values are within five percent for a time span of 2500 days, the developed model would appear to be predicting oil recovery in a satisfactory manner. Similarly for the time period of 2500 days, water production from the developed model yields a value of approximately 633,000 barrels, and through interpolation of the results from the Aydelotte and Pope model a value of approximately 591,000 barrels is predicted. The difference between these results is approximately seven (7.12%) percent, which would indicate that the model's prediction of produced water is also in general agreement. From a material balance standpoint if the predicted oil production is less than the reported value in the literature, the water production should also be less than the literature value. However, the differences used to determine the heat losses as well as the steam and condensate volumes could easily contribute to the differences encountered and total fluids injected into the reservoir should be approximately equal to the fluids produced. Thus, to maintain a material balance, if the predicted oil production is less than expected, then the predicted water production should be greater than expected by an equivalent degree. In comparison of the results obtained from the developed

steamflood model with that obtained for the Aydelotte and Pope model for a simulated steamflood of Kern River it would appear that they are in general agreement with each other, and the developed steamflood model's results are verifiable.

C2. Steamflood Economic Model Description

The economic model developed for application in this study is basically a combination of several models. Included among the models reviewed for use in this simulation is the model used by the State of Alaska Department of Revenue for forecasting revenue predictions. The basic outline of the model developed for this study is one that is found in Newnan [1988] and is commonly employed in the industry. In Newnan's model for engineering economic analysis, an outline of the economic analysis technique is to determine the gross revenues, operating costs, depreciation costs, taxes, and other factors used to finally determine the prospective rate of return on the project. As with all projects to be evaluated, the prospective rate of return for a given project determines the ultimate economic feasibility of a project.

C2.1 Gross Revenue and Operating Costs

The gross revenue used for analysis in this model is calculated on a per-year basis, and is found simply by finding the oil produced for a given year and multiplying it by the current delivered market price of oil.

$$Revenue = P\$oil \Delta N_p \dots\dots\dots (64)$$

where:

Revenue = gross income per year from oil produced, \$

P\$oil = market price of oil, \$/bbl

After the gross revenue (income) for a year is found, the various field and operating costs required to operate the steam drive project must be determined in order to estimate the cash flow after operating expenses. Field and operating costs are determined using correlations developed from an economic model used by the State of Alaska Department of Revenue for evaluating North Slope Reservoirs. Using this field cost factor which was expressed in terms of dollars per barrel, the following equation was developed for expressing approximate field costs (C_{field}):

$$C_{field} = C_f \Delta N_p \dots\dots\dots (65)$$

$$C_f = 0.70 \text{ \$/bbl}$$

The primary function of the field cost in the model is a deduction in computing the wellhead value for royalties and includes field functions such as dehydration, cleaning and gathering of lines. "Operating costs are assumed to include all expenses incurred in bringing oil to the surface, and in the gathering, treating, field-processing and field storage. This would include necessary workovers, field engineering, dehydration, cleaning, conditioning, labor, fuel, insurance, repairs and maintenance, and also general administration and overhead costs." [Marks and Moore, 1987] The operating cost factor used in this model was also developed on a per barrel operation cost expression so that the operating cost expression is:

$$Opcost = \Delta N_p E_{oEP} + \Delta N_p TAPS \dots\dots\dots (66)$$

$$E_{oEP} = \$2.14/bbl$$

where:

$Opcost$ = operating costs for producing oil, \$

E_{oEP} = operating cost factor, \$/bbl

Additional operating costs not included in the above correlation are the fuel and water requirements for operation of the steam generator. Cost of fuel is dependent upon the quantity of fuel consumed for generation of steam and the per unit cost of the fuel used. In determining the total amount of fuel required per year it is necessary to calculate the amount of energy required to convert water to steam on a per unit basis.

$$Heatgen = N_{surf} H_i + N_{surf} H_i \quad Btu/lbm \quad \dots\dots\dots (67)$$

where:

$Heatgen$ = required energy to convert water to steam, Btu/lbm

The cost for treated water is not known with accuracy for this area, and as a result the cost of water in this study becomes a variable, subject to a sensitivity analysis to study its effect on the rate of return. The amount of water required is simply the cold water equivalent (CWE) volume of steam being injected, and from this volume the annual cost can also be derived.

$$Stm_{inj} = m_{sti} 365.0 \quad \dots\dots\dots (68)$$

$$Water\$ = Stm_{inj} C\$_{water} \quad \dots\dots\dots (69)$$

where:

Stm_{inj} = annual volume of steam (CWE) to be injected, bbl

$Water\$$ = annual cost of required water for production of steam, \$

$C\$_{water}$ = cost of treated water, \$/bbl

From the annual volume of steam required, and the energy required to convert water to steam the total amount of fuel required by the steam generator can then be calculated.

$$Fuel_{gen} = \left[\frac{350 Stm_{inj} Heat_{gen} - 38}{E_{gen}} \right] / E_{gas} \dots\dots\dots (70)$$

where:

$Fuel_{gen}$ = annual fuel requirement by steam generator, Mcf/yr

E_{gen} = heat efficiency of steam generator

E_{gas} = heat content of Prudhoe Bay natural gas, BTU/Mcf

The annual cost of fuel would then be:

$$Fuel\$ = Fuel_{gen} Gas\$ \dots\dots\dots (71)$$

where:

$Fuel\$$ = annual cost of fuel required for steam generator, \$

$Gas\$$ = cost of Prudhoe Bay natural gas, \$/Mcf

C2.2 Depreciation Schedules and Depletion

Several well known methods are employed by the industry for depreciating the cost of an asset over its depreciable or project life. In this model the double declining balance method of depreciation is used, simply because this is the most common method of depreciation employed by the oil industry today. Prior to the 1986 Tax Reform Act, the 150 percent declining balance depreciation was the most commonly used; however, after the tax reformation act of 1986 the new laws allowed double declining depreciation for seven years (Lucke and Toder, 1987)

which is the depreciation period used in this model. The basic form for double declining balance is:

$$DDB_n = 2 \frac{Cost}{Life} \left(1 - \frac{2}{Life} \right)^{n-1} \dots\dots\dots (72)$$

n = any year

where:

DDB = depreciation allowed by double declining balance, \$

Cost = initial cost of investment, \$

Life = depreciable life of investment, years

For seven year double declining balance depreciation the equation becomes:

$$DDB_n = 2 \frac{Cost}{7} \left(1 - \frac{2}{7} \right)^{n-1} \dots\dots\dots (73)$$

After seven years the cost of the asset (investment) is no longer subject to depreciation, and its salvage value is the residual (book) value after depreciation corrected to a present worth value at the end of the project life. Salvage value at the end of the project life is included in the estimate of incoming cash flow when determining the rate of return. At the end of the project life it is assumed that the depreciable asset can be sold for its salvage value.

The depletion schedule is implemented in the model to account for the depletion of the oil in place due to production and as a result it represents a certain percentage of the gross income from the property. In this model the depletion schedule is based on an allowable percentage

depletion which is limited to not more than fifty percent of the taxable income from the property, computed without the deduction for depletion. From the existing federal tax laws the percentage depletion allowance for oil and gas wells is fifteen percent. In determining the allowable percentage depletion, the deduction from the income is limited to the computed percentage depletion (15% of gross income) or fifty percent of the taxable income whichever is smaller.

C2.3 Royalties, Severances, and Tax Scheduling

An important part of determining the taxable income in this analysis is the computation of the various taxes such as royalty, severance, and windfall profit taxes which are placed on the oil industry in the United States. As stated earlier, petroleum revenues accounted for approximately eighty-four percent of the total state government revenue, and the majority of this income is derived from severance taxes and royalties. In the state of Alaska, oil companies lease the property from which they are producing oil, and must pay a royalty for any oil produced on the leased property to the state. The royalty due to the state is determined from the current royalty rate, oil production, and the wellhead price of the oil.

$$Roy_{inc} = \Delta N_p [Royalty(P\$oil - TAPS - C_f)] \quad \dots\dots\dots (74)$$

where:

Roy_{inc} = annual royalty income, \$

$Royalty$ = royalty rate for determining total royalty

$TAPS$ = Trans Alaska Pipeline System tariff, \$/bbl

In the above equation the wellhead price of oil is determined by subtracting the transportation and field costs from the delivered price of oil.

The calculation of severance taxes which also contribute significantly to Alaska's revenue is somewhat less direct than the calculation of the royalty income. Determination of the severance tax schedule is a function of the royalty rate, oil production, and the statutory economic limit factor, or ELF as it is more commonly referred to. Unique to Alaska, the economic limit factor was originally created to reduce the severance tax rate as the well productivity declines during the life of production in order to make marginal fields appear more attractive. From Marks and Moore the severance tax is expressed in the following way:

$$Sever_{inc} = \Delta Np (1 - Royalty) ELF Sever P \$oil - TAPS + (Royalty C_f) \dots \dots \dots (75)$$

where:

$Sever_{inc}$ = annual severance income to be paid, \$

ELF = statutory economic limit factor

$Sever$ = severance rate for calculation severance income

The statutory economic limit factor ranges in value from zero (0) to one (1), depending on the productivity of the well. The value of the economic limit factor for Prudhoe Bay was one and was recently reduced to 0.7 and is the subject of much recent debate. West Sak, which is a heavy oil reservoir would be expected to have an economic limit factor less than that of Prudhoe Bay in order for the state to make the reservoir more

economically attractive to oil companies seeking to produce from this reservoir.

The windfall profits tax was calculated based on the royalty rate, severance tax rate, current price of oil and a windfall profits tax base price (*Wind*). This tax does not take effect until the current market selling price of oil is greater than the base price established for the Windfall profit tax, at which point the windfall tax becomes another expense to be deducted from the operating income of this economic analysis.

$$Windfall = \Delta Np (P\$oil) (1 - Sever) (1 - Royalty) 0.7 \quad \dots\dots (76)$$

where:

Windfall = annual excise windfall profits tax to be paid, \$

Wind = windfall profits tax base price, \$/bbl

In this model the total net operating costs for a year are composed of the royalty and severance taxes, field operating, water and fuel costs for the steam generator. The yearly operating income is considered to be the yearly gross revenue minus the net operating costs. State taxes are found from the operating income and state corporate income tax rate.

$$IncOp = Revenue - Opcost \quad \dots\dots (77)$$

$$Statax = IncOp State \quad \dots\dots (78)$$

where:

IncOp = annual operating income, \$

Statax = annual state income taxes, \$

State = state corporate income tax rate

The before tax cash flow (BTCF) is calculated to find the yearly taxable income and in this model is defined as:

$$BTCF = IncOp - Statax - Windfall \quad \dots\dots\dots (79)$$

Taxable income is simply the before tax cash flow minus the depreciation of capital for that given year, and the allowed percentage depletion of the gross income.

$$TaxInc = BTCF - DDB - Deplallow \quad \dots\dots\dots (80)$$

where:

TaxInc = annual taxable gross income, \$

Deplallow = allowable annual depletion based on production, \$

For this model the federal income tax to be paid is simply the product of the federal tax rate and taxable income. The federal tax rate used in this model is thirty-four percent (34%) for large corporations as established by the 1986 Tax Reform Act.

$$Tax = TaxInc Fed \quad \dots\dots\dots (81)$$

where:

Tax = annual federal income tax, \$

Fed = assigned federal tax rate

Having determined the amount of federal income tax for a given year, the after tax cash flow (ATCF) available is then defined as the before tax cash flow minus the federal income tax.

$$ATCF = BTCF - Tax \quad \dots\dots\dots (82)$$

The after tax cash flow for the given year of analysis is readjusted to what is called a *year0* value to account for the effect of inflation on the cash flow.

$$Year0 = ATCF Infl \dots\dots\dots (83)$$

$$Infl = (1 + Inflation)^{-1year} \dots\dots\dots (84)$$

where:

Year0 = annual adjusted present worth cash flow, \$

Infl = inflation rate factor to adjust annual cash flow

Inflation = average annual rate of inflation

1year = year in which cash is analyzed

These calculations are repeated for each year in the analysis of the project, and at the end of the project life the salvage value of the initial capital investment (i.e. cost of steam generator and additional surface facilities) is adjusted for inflation, and is also included in the cash flow in determining the project's rate of return. When the after tax cash flow adjusted for inflation, for each year of the entire project life has been found the next step is to find the rate of return. In this model the final rate of return is found through an iterative process until the sum of the present worth cash flow series is approximately equal (tolerance for the difference between values is achieved) to the initial capital invested, then the rate of return used for this successful approximation is the discounted rate of return for the project.

$$Prwrth = Year0 * Pwf \dots\dots\dots (85)$$

$$Pwf = (1 + Pwfactor)^{-1yar} \quad \dots\dots\dots (86)$$

$$SumPrwrth = \sum_{1year=1}^{n=Life} Prwrth_{1year} \quad \dots\dots\dots (87)$$

where:

Prwrth = present worth adjusted year0 cash flow, \$

Pwf = present worth factor to adjust cash flow

Pwfactor = present worth factor

SumPrwrth = sum of present worth series cash flow for the time period analyzed, \$

Initially the present worth factor (*Pwfactor*) is set equal to 0.10 and if the sum of the present worth cash flow does not meet the tolerance set for the difference between the variable *SumPrwrth* and the capital investment than the present worth factor is adjusted. If the value of the *SumPrwrth* variable is greater than the capital investment, the present worth factor is incremented by a factor of one-half, and if it is less than the capital investment it is decremented by a factor of one-half is found which satisfies the tolerance condition specified. This method used for converging on the rate of return is called the interval halving method.

D. APPLICATION OF MODEL TO WEST SAK RESERVOIR

In applying this model to the West Sak reservoir the first step is the creation of a data file to be read by the model. For this model the data file is comprised of two distinct sections; one section is for the parameters required in the steamflood portion and the other section consists of the parameters required for the economic

analysis portion of the model. The data required to be input for the steamflood portion include the basic reservoir properties of the field; fluid injection properties such as quality of the steam, injection pressures, and injection rates; and wellbore design parameters which would include the well radius, casing and tubing sizes, and thermal properties of the casing, tubing, and insulation to be used.

D1. Reservoir Data Used

Basic reservoir data used in this model such as porosity, permeability, and initial fluid saturations were obtained from an earlier study by Panda (1988) which utilized digitized well log data of West Sak. In Panda's study the digitized well log data were interpreted using a computer program to read the digitized well logs from which the values for reservoir porosity, permeability and saturations were then calculated according to the responses measured by the various logging tools used. According to the well logging data given from the various wells drilled in the West Sak reservoir typical porosity values range from 20% to approximately 35%, and initial water saturation values ranging from 21% to about 52%.

A previous thermal recovery pilot project was undertaken by ARCO Alaska to evaluate the West Sak reservoir in the form of a hot waterflood project with an inverted nine-spot pattern and injection rates varying from 1000 to 2500 barrels per day. Injectivity studies indicated that a five spot pattern may not be possible because of the high injection rates required for technical feasibility. A seven-spot pattern with twenty acre spacing was initially implemented in this study with steam injection rates varying from 1000 to 2000 barrels per day of cold water equivalent (CWE) for evaluating the steamflood potential of West Sak.

The time period being investigated in this study for determining the economic analysis and rate of return of a steamflood project in West Sak is ten

years, and represents a typical time frame used by the industry for evaluating the rate of return on a major investment.

In compiling the data file used in this model, physical properties of the wellbore system such as pipe and casing dimensions, and thermal conductivities of the pipe, casing, cement, and insulation to be used are readily available in various literature. Transportation cost data are taken from the "Petroleum Production Revenue Forecast - Quarterly Report" where the reported tariff (based on the TAPS Settlement Methodology ratemaking method) for transporting oil from the Kuparuk field to Valdez is currently (1988) \$4.08/bbl. North Slope wellhead gas prices vary considerably among the producers with the price ranging from \$0.25/Mcf to \$3.43/Mcf. The average market price in 1987 was \$0.46/Mcf and is not expected to vary greatly from this price until the gas line is built or a major gas sale occurs.

Since the West Sak reservoir lies within the Kuparuk River Unit, the costs for drilling and completing a well in West Sak would be expected to be approximately equal on a cost per foot basis for a typical well in the Kuparuk formation. In 1986, a development well in Kuparuk cost \$1,500,000 to complete; since the average depth in the Kuparuk is approximately 6200 feet, the cost to drill on a per-foot basis in this region is approximately 6200 feet, the cost to drill on a per-foot basis in this region is approximately \$242/foot. The surface equipment costs required for this area are not available in sufficient detail; however, it can be assumed that much of the present production and separator facilities already in Kuparuk can also be used for West Sak with only minimal expansion required. The Excess Windfall Profits tax is set at twenty one dollars per barrel in this study which is the oil price limit set for an oil property falling under Property 2 Classification for a newly developed oil field (which West Sak is assumed to be) according to the federal guidelines for oil

property classification (Lucke and Toder, 1987). However, it should be noted that the Windfall Profits Tax is set to be repealed in the near future.

D2. Sensitivity Analysis

A sensitivity study to determine the most likely price required for steamflooding to be economically feasible was performed using the following variables: Drilling Costs, Surface Equipment, Steam Generator Cost, Windfall Tax, Water Cost, Fuel (gas) Cost, and Inflation. All reservoir and wellbore data were fixed for each sensitivity run of the economic variables. Sensitivity analysis of the effect of drilling and well completion cost was performed by keeping all other variables fixed and incrementing the drilling completion cost by \$200,000 for each run. A drilling and well completion cost span of \$1,000,000 to \$3,000,000 was examined. The sensitivity of the other variables was conducted in a similar manner. Water cost was incremented by \$0.010 per barrel. Initially the gas price for steam generator fuel was set at \$0.46/Mcf because this is the average expected market price. In the sensitivity analysis the gas price was increased to one dollar, and then by increments of \$0.50/Mcf.

Recently, inflation in the United States has been steady at around four percent per year. To study the effect of inflation on rate of return this variable was incremented by steps of 0.005 from 0.04 to 0.05, and in increments of 0.01 from 0.05 to 0.07. Since the Windfall Profits Tax is set to be repealed, its effect on the rate of return was found by simply setting this value equal to zero in the data input file.

One of the most important fluid or reservoir properties dictating the success or failure of an enhanced oil recovery method is the value of the residual oil saturation (S_{or}) that can be achieved in the reservoir. Therefore, one of the main objectives of any enhanced oil recovery project is to reduce the residual oil saturation value to as small a value as possible. At the present time

much of the information regarding the pressure, volume, and temperature properties of West Sak crude remains the proprietary information of oil companies and so values for the residual oil saturation of West Sak crude are presently unavailable. The initial oil saturation value is an important facet in determining the initial hydrocarbon pore volume from which estimates of the oil in place in the reservoir are based. Hydrocarbon pore volume is simply a fraction of the reservoir pore volume. Therefore, the residual oil saturation can also be viewed as a fraction of the reservoir pore volume, where the residual oil saturation value is simply the fraction of the pore volume (PV) divided by the initial oil saturation (S_{oi}) value:

$$S_{or} = \frac{PV}{S_{oi}}$$

As an example if the residual oil saturation is twelve percent (12%) of the pore volume with $S_{oi} = 0.60$, then the S_{or} value to be used is:

$$S_{or} = \frac{.12}{0.60} = .20$$

In this study a residual oil saturation value of 0.12 pore volumes was used during the sensitivity analysis of the economic variables in this study. This value was chosen to provide an estimate of S_{or} that would be a slightly pessimistic average in relation to values reported in the literature. A sensitivity analysis was later performed using the values of S_{or} : 0.10, and 0.30 to evaluate the effects of the residual oil saturation on oil recovery and required oil price.

D2.1 Sensitivity of Steam Injection Parameters

A sensitivity analysis for varying steam quality was initially performed with the reservoir variables and other economic variables such as drilling and well completion costs, surface equipment, and steam

Table 1: Estimated Costs Used in Initial Sensitivity Analysis

Drilling & Well Completion	= \$	2,500,000
Surface Equipment	= \$	1,000,000
Steam Generator	= \$	1,000,000
Steam Quality	=	0.60 - 0.90
Windfall Tax Limit	= \$	21.00/bbl
Water Cost	= \$	0.20/bbl
Gas Cost	=	0.46/Mcf
Inflation Factor	=	0.04
ELF	=	0.25

Table 2: Predicted Oil Recovery for Various Steam Qualities and Injection Rates

Steam Quality	1000 BBL/DAY	1250 BBL/DAY	1500 BBL/DAY	1750 BBL/DAY	2000 BBL/DAY
Cumulative Oil Recovered (Stock Tank Barrels)					
0.60	481,768	591,446	701,512	813,824	928,183
0.70	539,214	659,830	781,720	909,773	1,035,118
0.80	594,472	730,724	866,504	999,842	1,136,698
0.90	641,822	785,096	928,766	1,050,325	1,190,358
Pore Volumes Oil Recovered (OOIP) (fractional)					
0.60	0.22753	0.27930	0.33125	0.38426	0.43823
0.70	0.25467	0.31160	0.36913	0.42957	0.48873
0.80	0.28076	0.34507	0.40917	0.47210	0.53669
0.90	0.30312	0.37075	0.43857	0.49594	0.56204

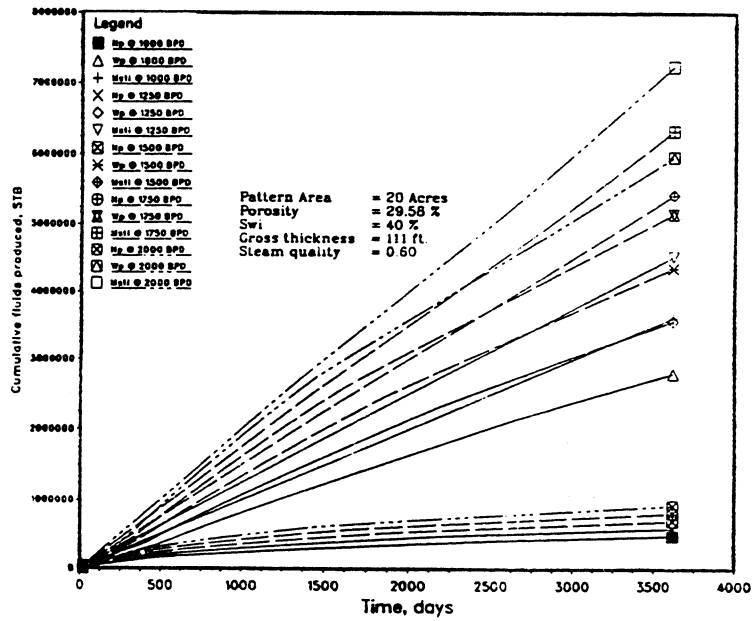


Figure 3: Cumulative Fluids Produced for Injection Rates with Steam Quality = 0.60

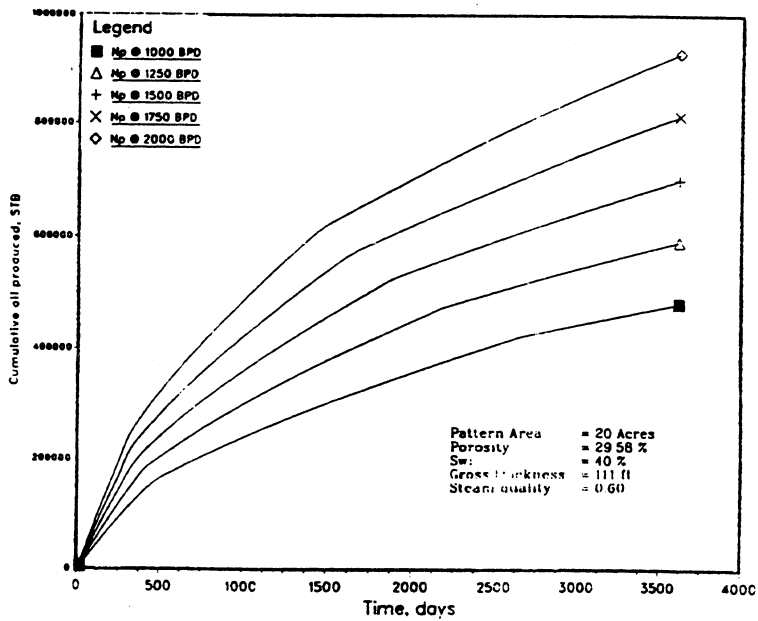


Figure 4: Cumulative Oil Produced for Injection Rates with Steam Quality = 0.60

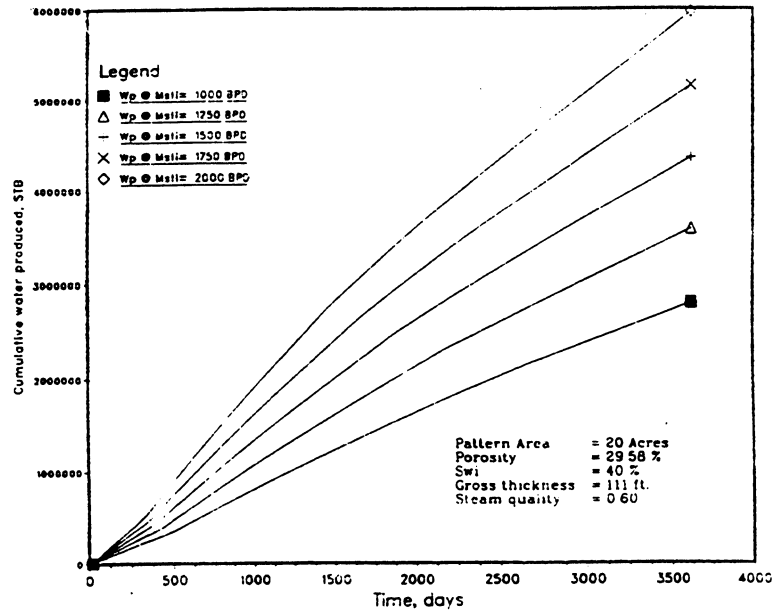


Figure 5: Cumulative Water Produced for Injection Rates with Steam Quality = 0.60

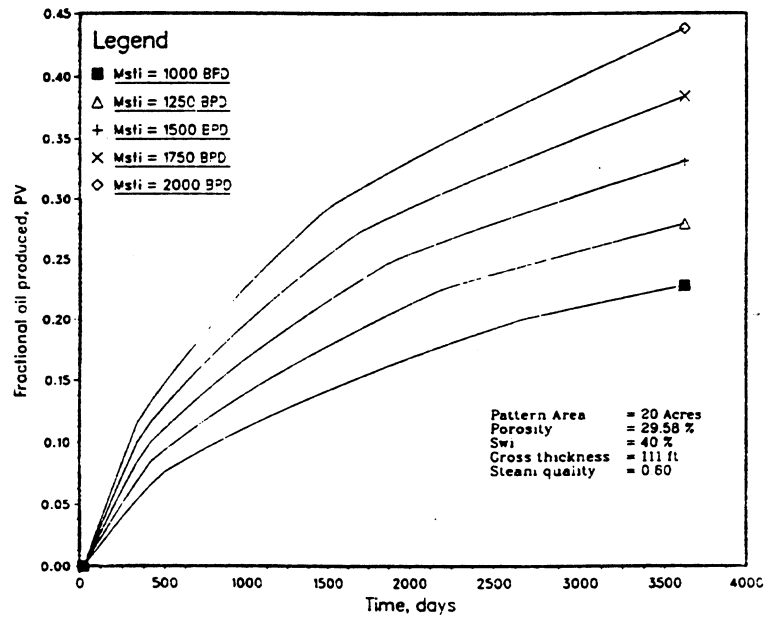


Figure 6: Fractional Oil Produced for Injection Rates with Steam Quality = 0.60

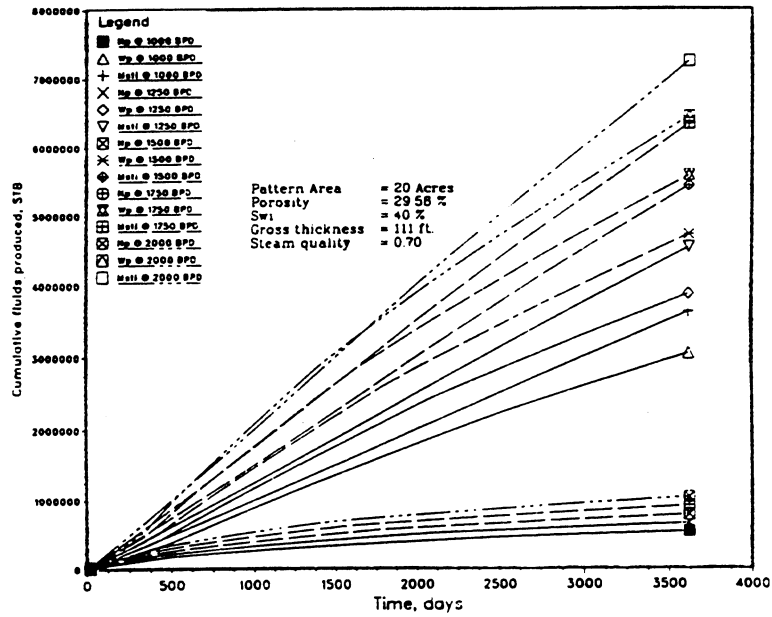


Figure 7: Cumulative Fluids Produced for Injection Rates with Steam Quality = 0.70

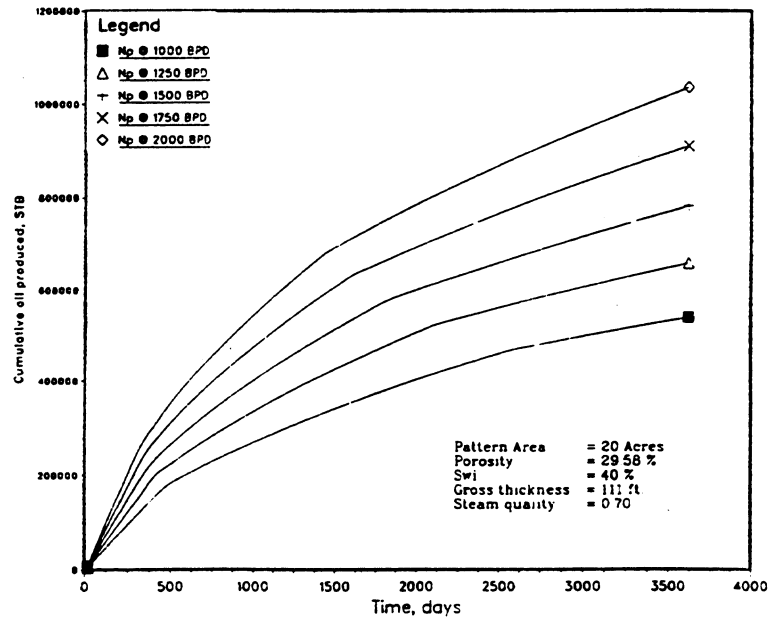


Figure 8: Cumulative Oil Produced for Injection Rates with Steam Quality = 0.70

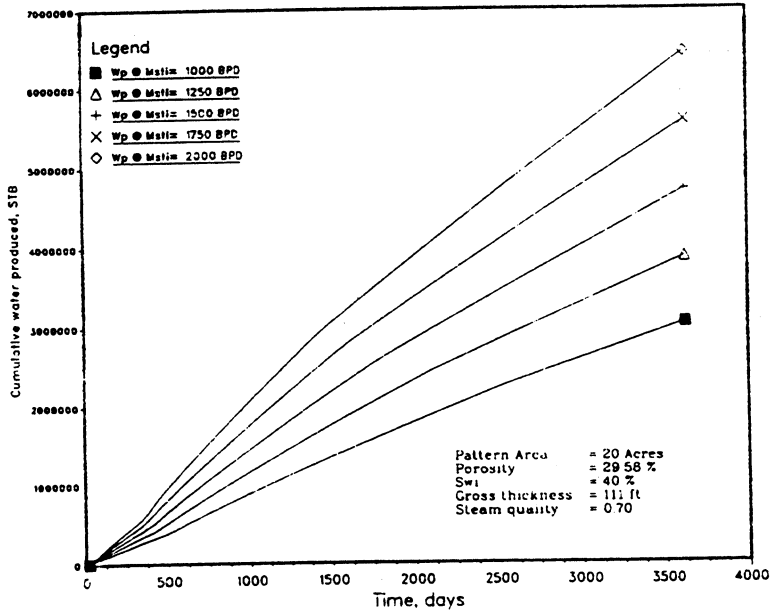


Figure 9: Cumulative Water Produced for Injection Rates with Steam Quality = 0.70

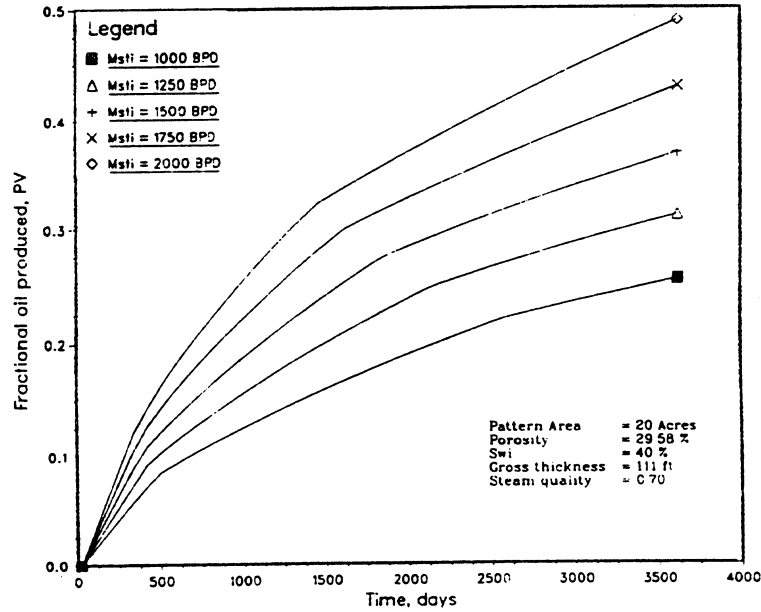


Figure 10: Fractional Oil Produced for Injection Rates with Steam Quality = 0.70

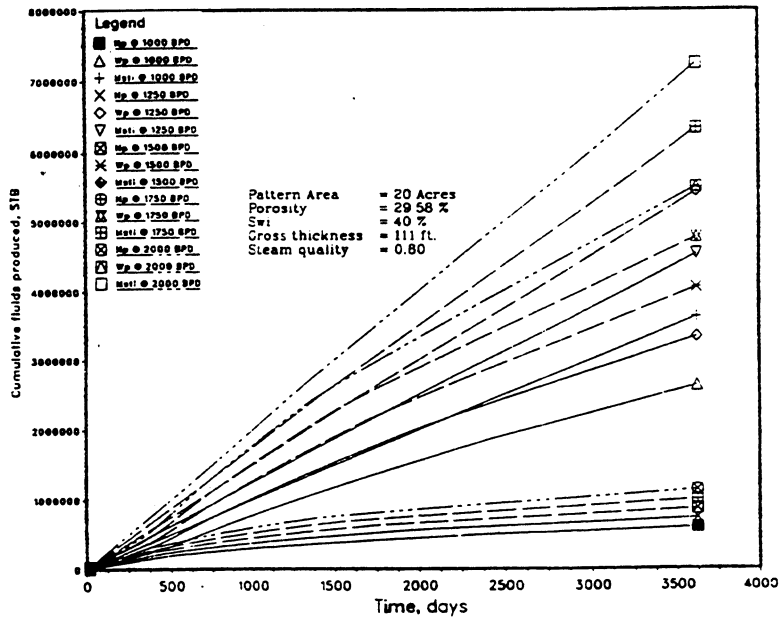


Figure 11: Cumulative Fluids Produced for Injection Rates with Steam Quality = 0.80

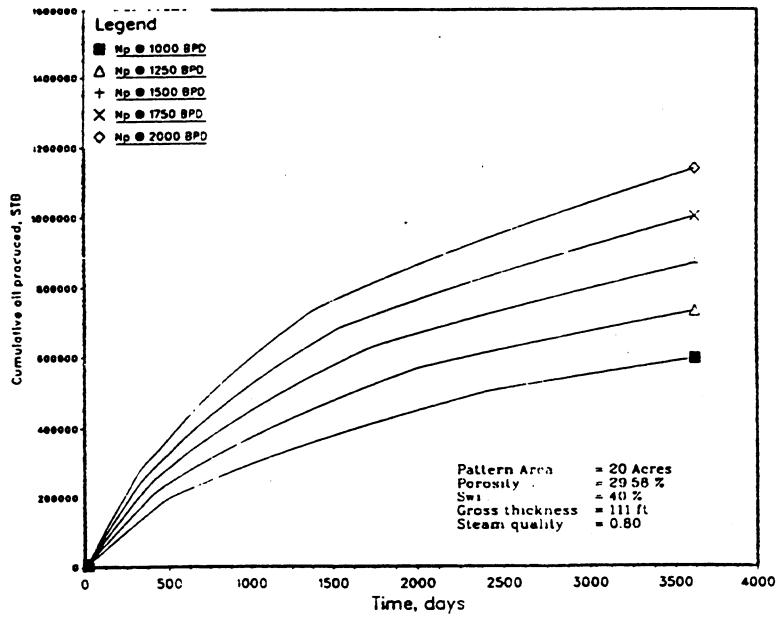


Figure 12: Cumulative Oil Produced for Injection Rates with Steam Quality = 0.80

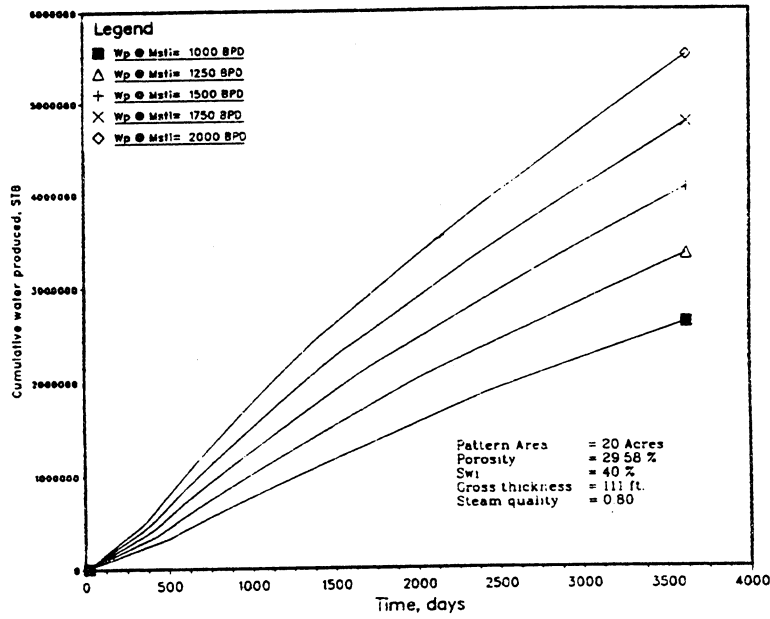


Figure 13: Cumulative Water Produced for Injection Rates with Steam Quality = 0.80

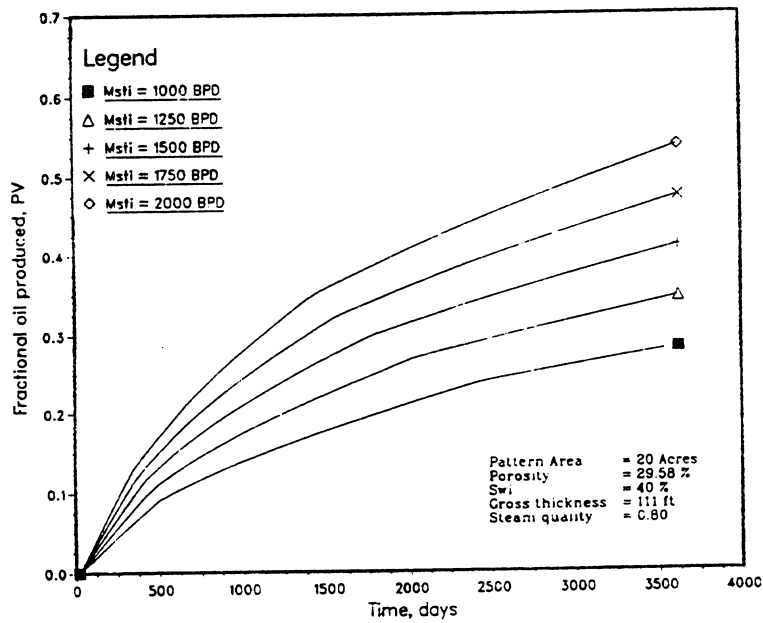


Figure 14: Fractional Oil Produced for Injection Rates with Steam Quality = 0.80

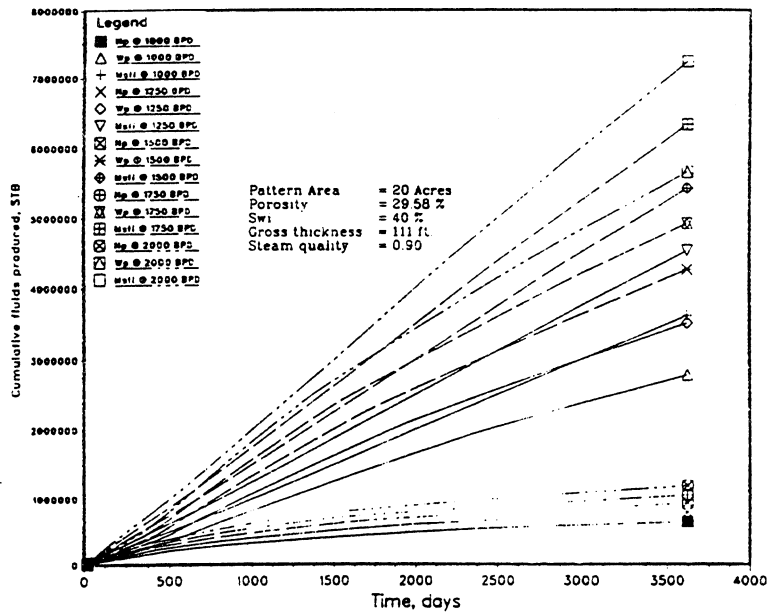


Figure 15: Cumulative Fluids Produced for Injection Rates with Steam Quality = 0.90

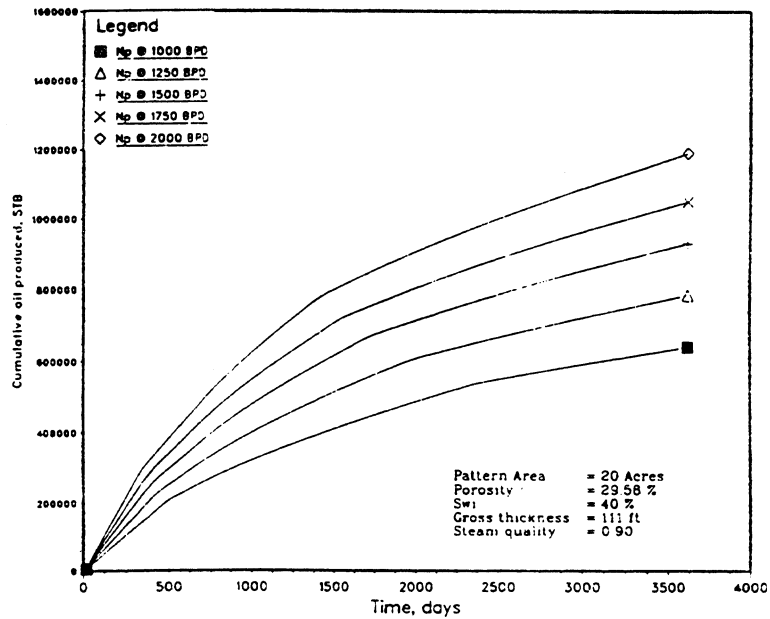


Figure 16: Cumulative Oil Produced for Injection Rates with Steam Quality = 0.90

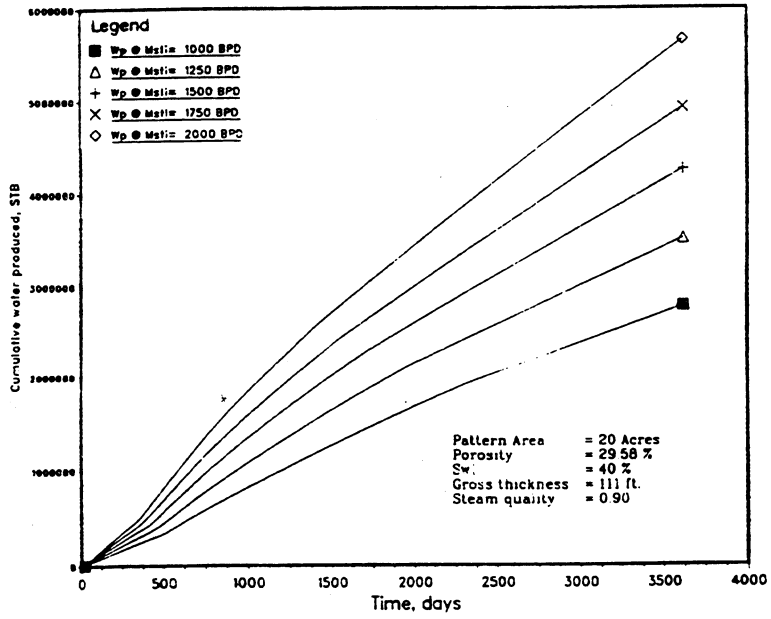


Figure 17: Cumulative Water Produced for Injection Rates with Steam Quality = 0.90

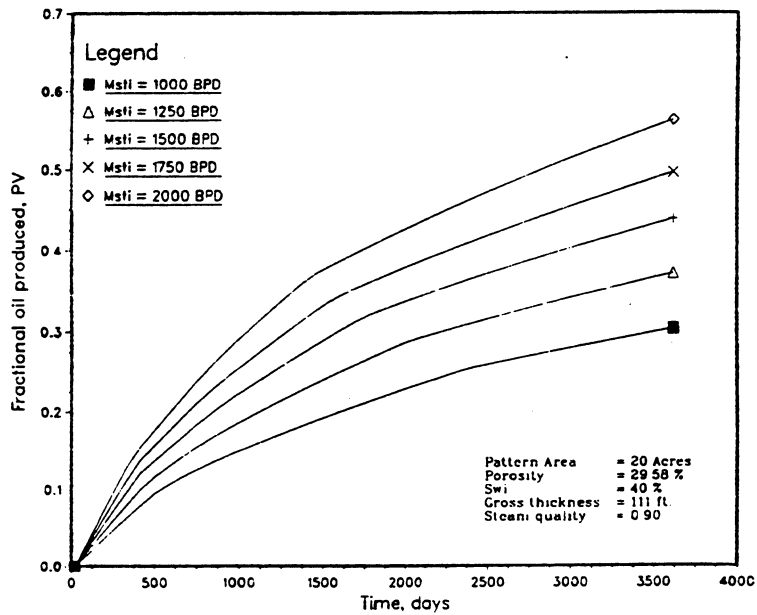


Figure 18: Fractional Oil Produced for Injection Rates with Steam Quality = 0.90

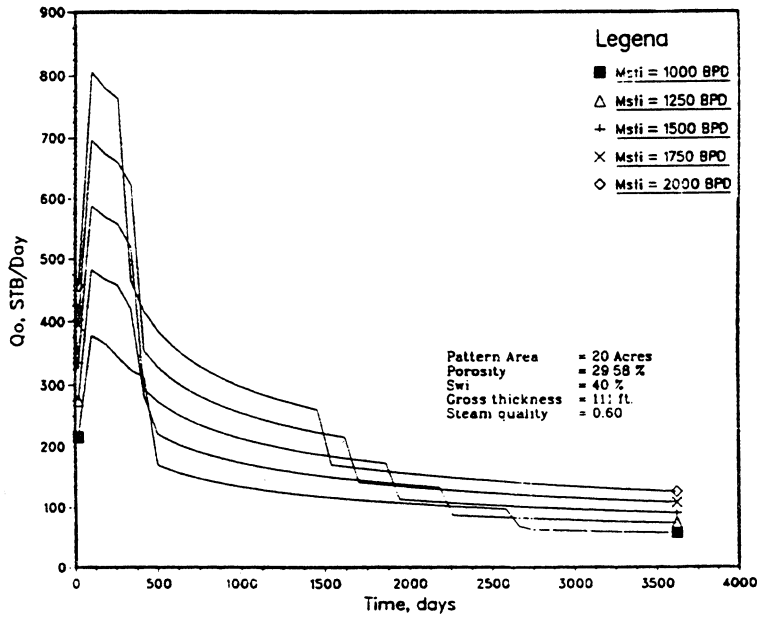


Figure 19: Average Oil Production Rate for Injection Rates with Steam Quality = 0.60

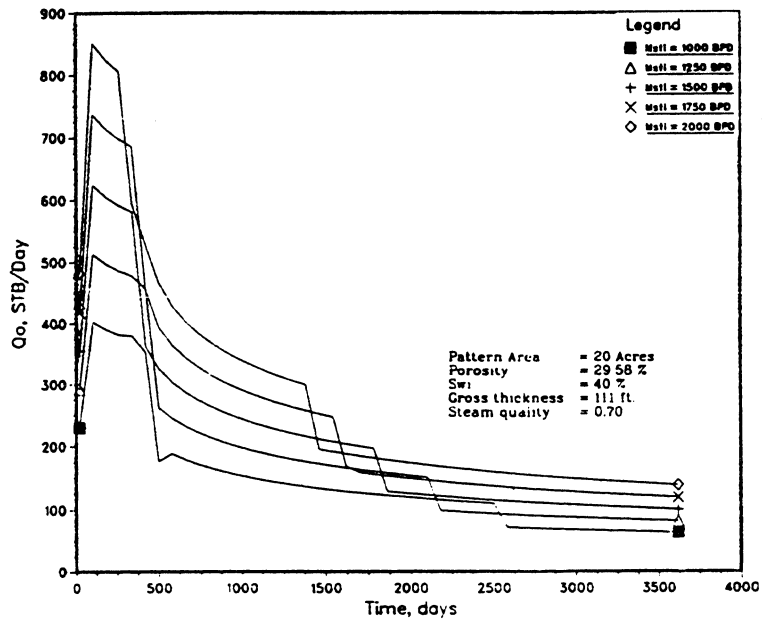


Figure 20: Average Oil Production Rate for Injection Rates with Steam Quality = 0.70

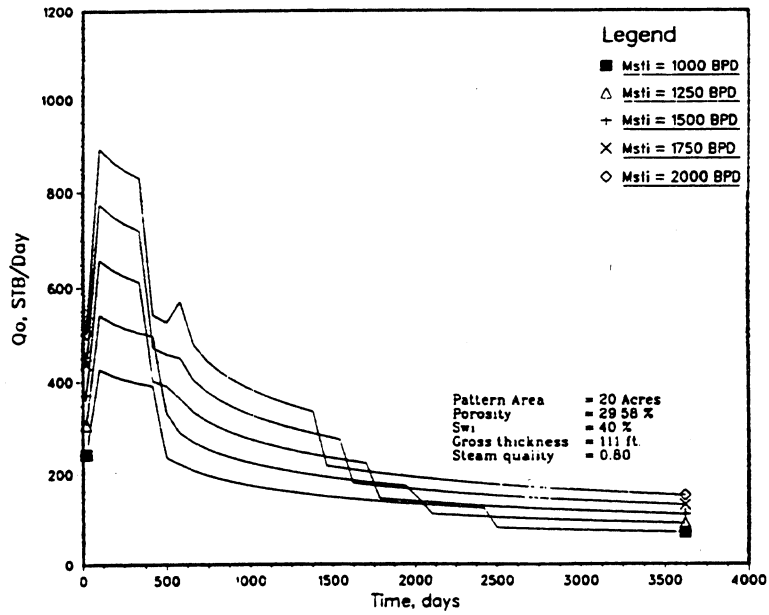


Figure 21: Average Oil Production Rate for Injection Rates with Steam Quality = 0.80

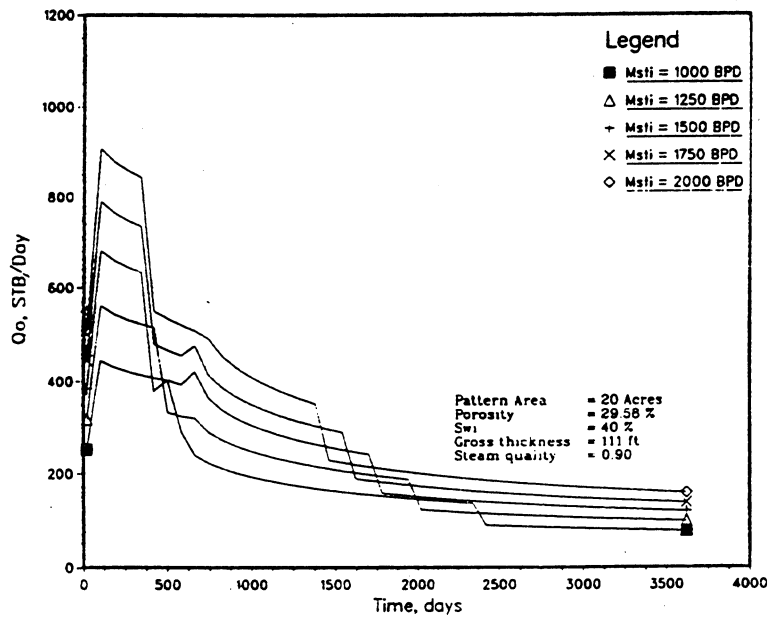


Figure 22: Average Oil Production Rate for Injection Rates with Steam Quality = 0.90

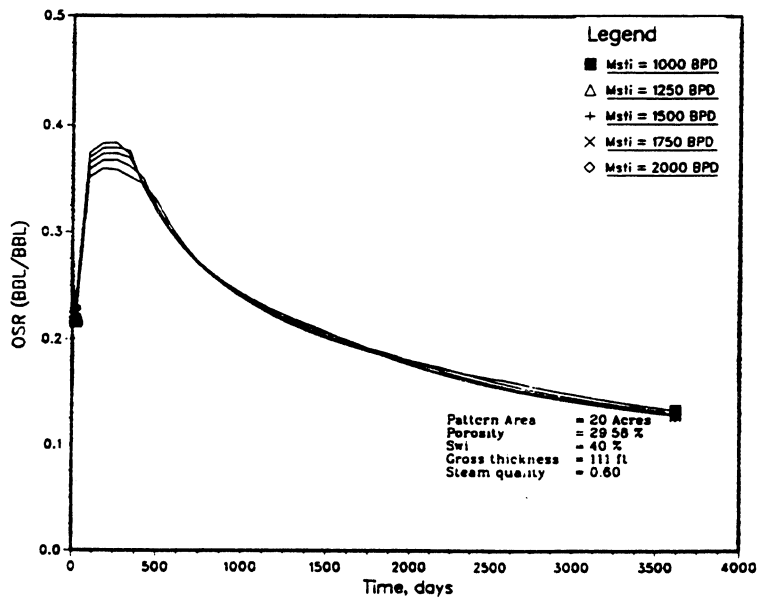


Figure 23: Cumulative Oil Steam Ratios for Injection Rates with Steam Quality = 0.60

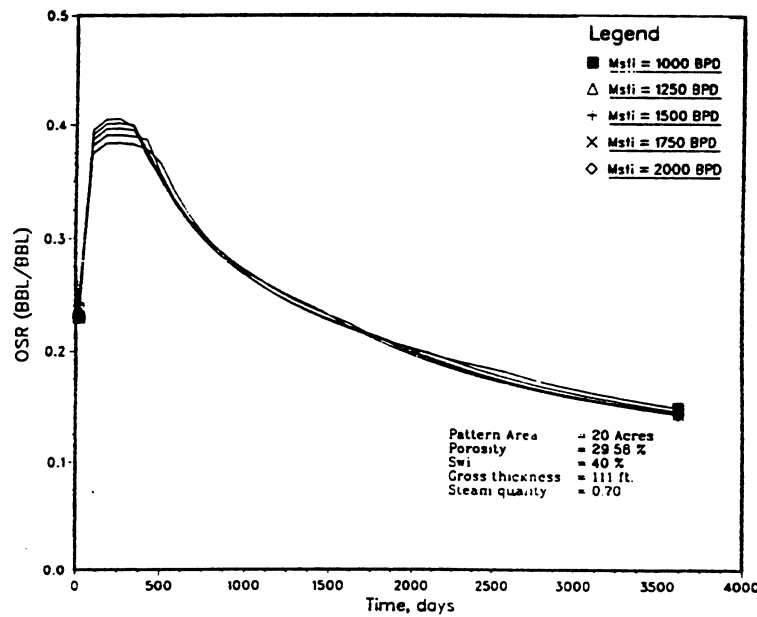


Figure 24: Cumulative Oil Steam Ratios for Injection Rates with Steam Quality = 0.70

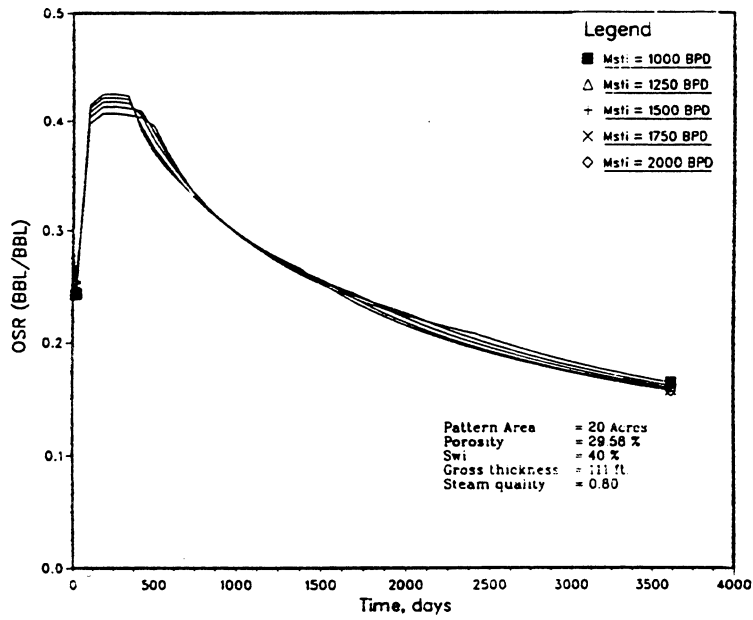


Figure 25: Cumulative Oil Steam Ratios for Injection Rates with Steam Quality = 0.80

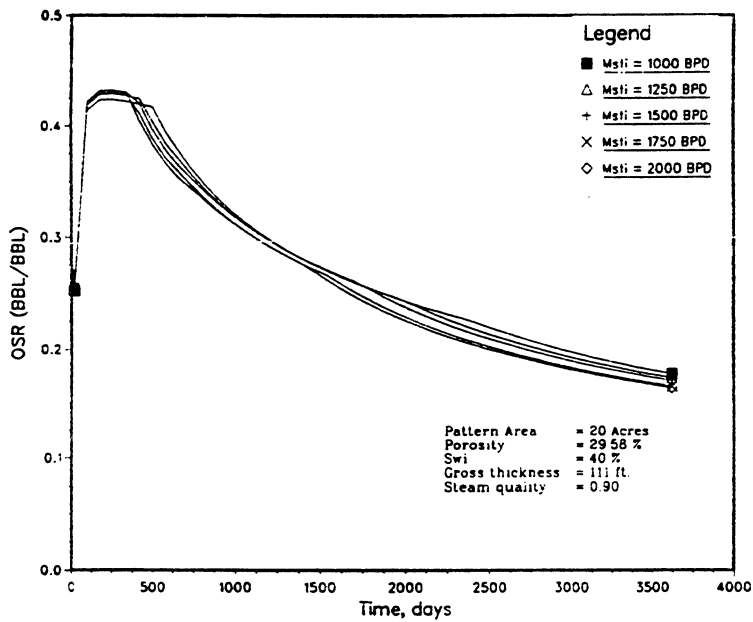


Figure 26: Cumulative Oil Steam Ratios for Injection Rates with Steam Quality = 0.90

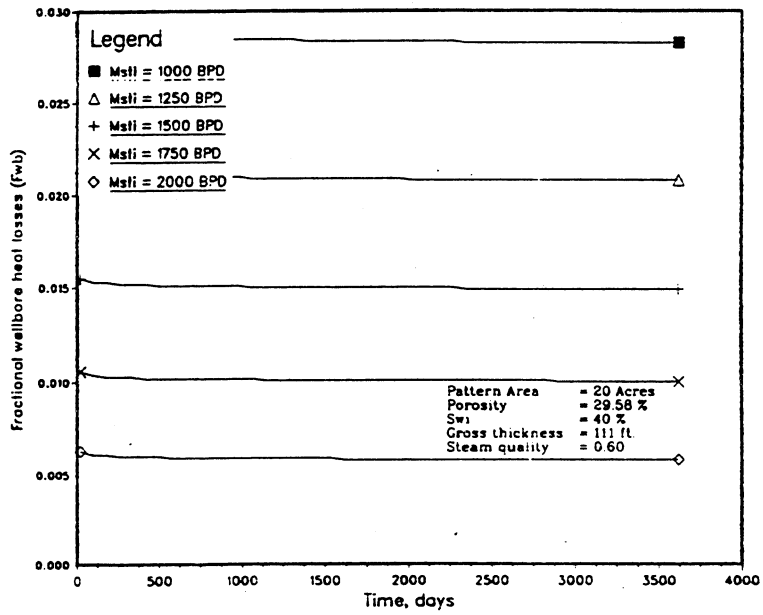


Figure 27: Fractional Wellbore Heat Losses for Injection Rates with Steam Quality = 0.60

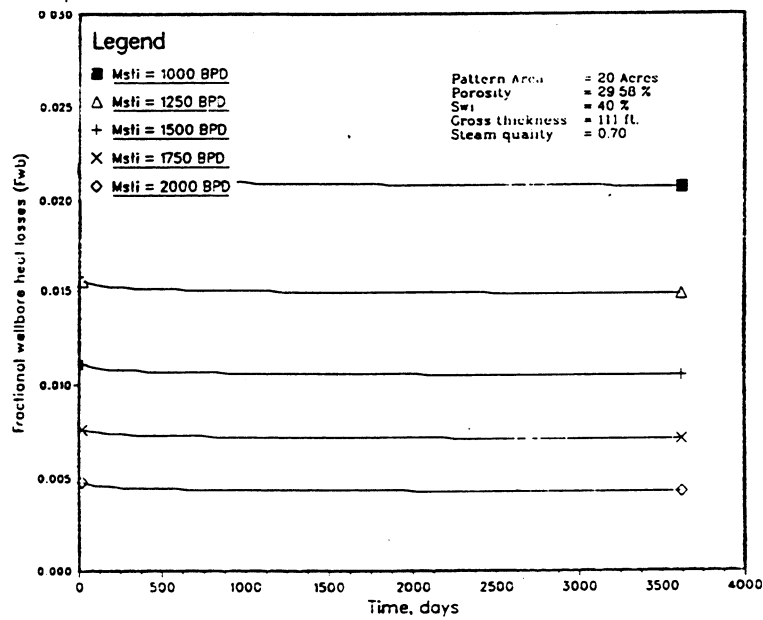


Figure 28: Fractional Wellbore Heat Losses for Injection Rates with Steam Quality = 0.70

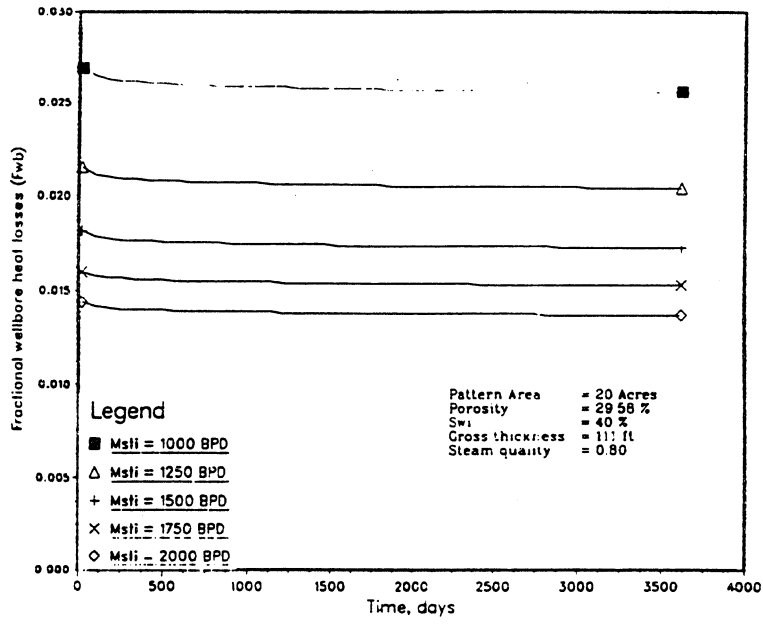


Figure 29: Fractional Wellbore Heat Losses for Injection Rates with Steam Quality = 0.80

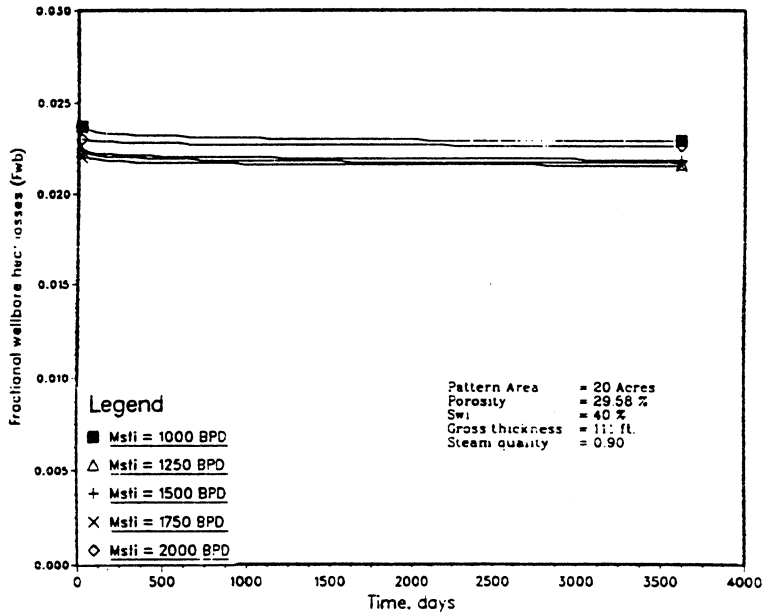


Figure 30: Fractional Wellbore Heat Losses for injection Rates with Steam Quality = 0.90

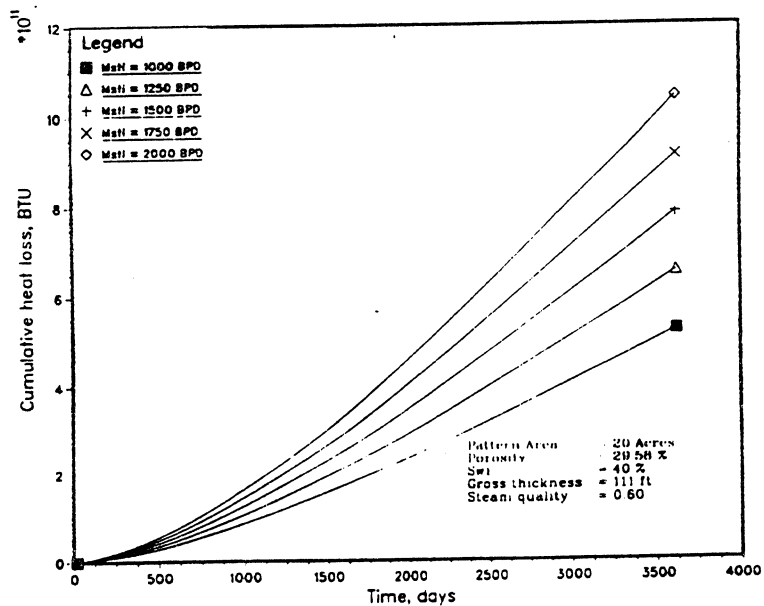


Figure 31: Cumulative Heat Losses to the Reservoir for Injection Rates with Steam Quality = 0.60

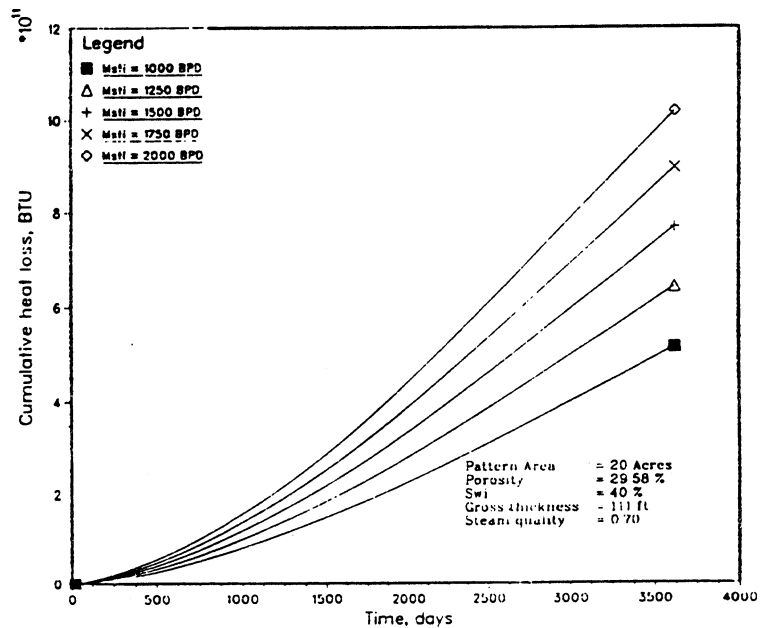


Figure 32: Cumulative Heat Losses to the Reservoir for Injection Rates with Steam Quality - 0.70

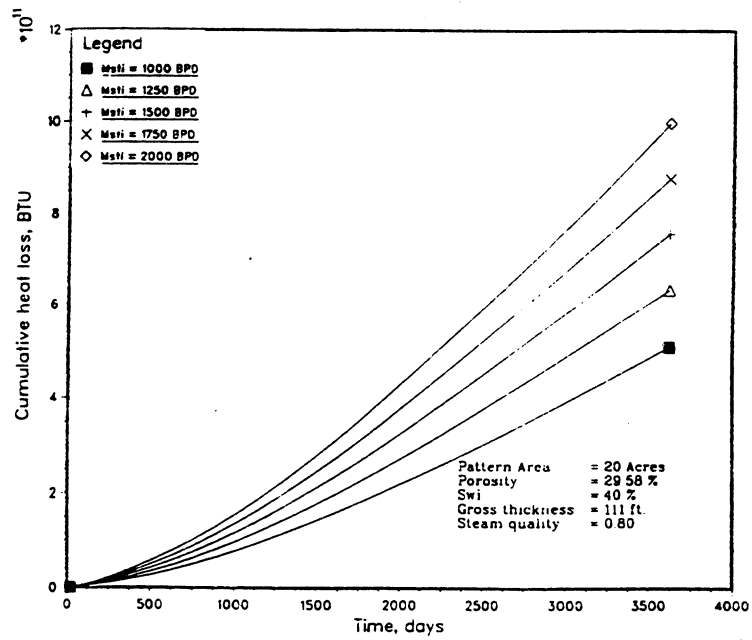


Figure 33: Cumulative Heat Losses to the Reservoir for Injection Rates with Steam Quality = 0.80

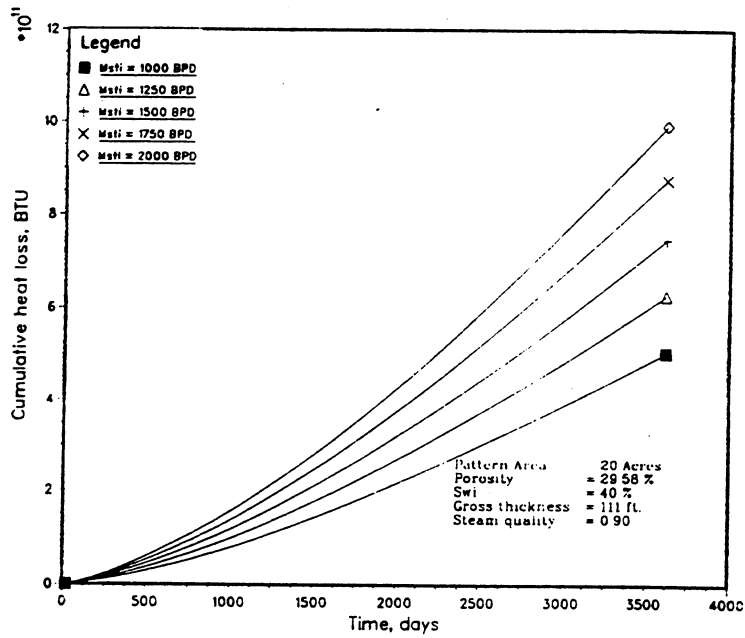


Figure 34: Cumulative Heat Losses to the Reservoir for Injection Rates with Steam Quality = 0.90

generator costs, held constant. The values initially used for each of these variables are listed in Table 1. A series of simulation runs were then performed using the model developed for steam injection rates of 1000, 1250, 1500, 1750 and 2000 barrels per day (CWE) with surface steam qualities of 0.60, 0.70, 0.80, and 0.90. A series of plots (Figures 3 - 34) illustrating cumulative fluids produced, fractional oil recovered, oil production rates, cumulative oil steam ratios, wellbore heat losses, and cumulative heat losses to the underburden and overburden were then constructed. As expected, there was an increase in the cumulative oil recovered for the time period being examined as the amount of steam injected into the reservoir was increased.

A comparison of the plots for the fractional oil recovered and cumulative oil produced more easily illustrates this point, and compiling the data generated by the model produced the results shown in Table 2. Examination of the plots for oil production rates (Figures 18 - 23) as a function of steam quality and injection rates reveals that each follows a similar profile, with oil production rates increasing rapidly during the early stages of the steamflood followed by a gradual decline. During the early stages of the steamflood there is an increase in oil production due to an increase in thermal efficiency as latent heat is being introduced into the reservoir. The first decline appears shortly after the onset of critical time whereupon convective heat effects become important in the transfer of heat from the injected fluids and from the reservoir. At this point there is a change in the thermal efficiency equation used for estimating steam zone growth; fluid production from the condensate zone becomes significant. However, there is still a gradual decline in the oil production rate until steam breakthrough occurs where there is a

sharp decline occurring in the oil production. After steam breakthrough, the oil production rate begins a slow but steady decline.

The plots of the steam ratios (OSR) (Figures 23 - 26) also parallel the oil production rate plots where an increase in the thermal efficiency of the steamflood is illustrated by an increase in the oil steam ratio and then a decline in this ratio after the onset of critical time. The value of the oil steam ratio is in effect a measurement of the overall efficiency of the steamflood, since a higher oil steam ratio mean a greater amount of oil produced per volume of steam. From the plots of fractional wellbore heat losses (Figures 27 - 30) the heat losses are minimal in the wellbore and remain constant throughout the time span being examined. This would indicate that the overall design of the wellbore is sound and there is minimal deterioration in the quality of the steam being injected into the reservoir. A comparison of the plots generated for cumulative heat losses (Figures 31 - 34) to the over and underburden indicates a greater heat loss for increasing steam quality and steam injection rates. This result is to be expected because there is also an increase in the overall heat being introduced into the reservoir and the amount of heat which can be absorbed is limited by the volumetric heat capacity of the reservoir.

While results from the steamflood model indicate that steamflooding in the West Sak reservoir is technically feasible, the more important question remains to be answered is whether steamflooding is economically feasible. A preliminary analysis using the above mentioned injection rates, steam qualities, and values for the economic variables, produced the results in Table 3 which were obtained from the steamflood model developed for this study. The required price range of oil required

Table 3: Preliminary Results Indicating Required Price Range of Oil for Economic Feasibility in West Sak

Steam Quality	1000 BBL/DAY	1250 BBL/DAY	1500 BBL/DAY	1750 BBL/DAY	2000 BBL/DAY
Required Price of oil for 15% ROR - (\$/BBL)					
0.60	50.61	39.07	31.31	25.66	21.37
0.70	43.70	33.66	26.79	21.59	19.68
0.80	39.06	29.83	23.50	20.00	18.59
0.90	35.76	27.39	21.56	19.41	18.11
Required Price of oil for 20% ROR - (\$/BBL)					
0.60	58.24	45.10	36.34	29.26	25.12
0.70	50.37	38.85	31.08	25.56	21.31
0.80	45.19	34.78	27.62	22.13	19.86
0.90	41.55	32.10	25.50	20.81	19.32

for both a 15% and 20% rate of return (ROR) is given for the various injection rates and steam qualities utilized in this study. A series of plots (Figures 35 - 38) was then made comparing the price of oil with the rate of return for steam injection rates of 1000, 1250, 1500, 1750 and 2000 barrels per day. In previous studies the desired rate of return sought for similar enhanced oil recovery projects was fifteen percent, although a less capital intensive investment, such as a secondary recovery tape project, may typically require only a ten percent rate of return. However, because of the anticipated higher costs and higher risks that would be associated with Alaska for an enhanced oil recovery project, a higher rate of return such as twenty percent (20%) would be required for economic feasibility.

From the preliminary results obtained, it would appear that the rate of return on the initial investment improves as the cumulative recovery increases. This occurs as the overall amount of sensible heat injected into the reservoir is increased either through an increase in the steam injection rate, quality of the injected steam, or a combination of both of these. To obtain a fifteen percent rate of return based on the economic conditions outlined above would require a minimum price of \$18.11/bbl using an injection rate of 2000 barrels per day of steam (CWE) with a surface produced quality of ninety percent. As can be easily seen the rate and quality of steam injected has a significant influence on both the expected recovery and anticipated price range of oil necessary for the required rate of return. These oil prices are for Alaska North Slope crude delivered to the Valdez terminal prior to shipment to the West coast. The West coast market price would be slightly higher (\$1-2/bbl) than the Valdez terminal price. Based on present predictions of future oil prices of \$17-21.00/bbl, results from the steamflood model would indicate that an injection rate

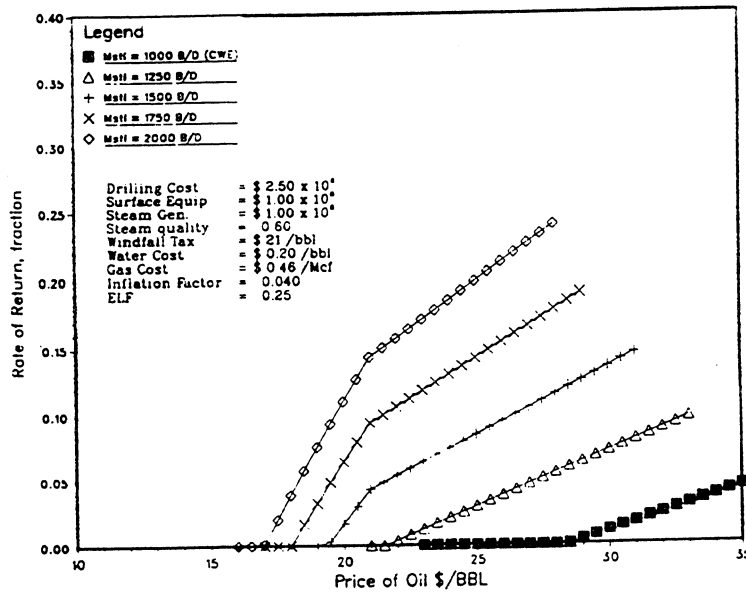


Figure 35: Preliminary Results of Price of Oil vs. Rate of Return with Steam Quality = 0.60

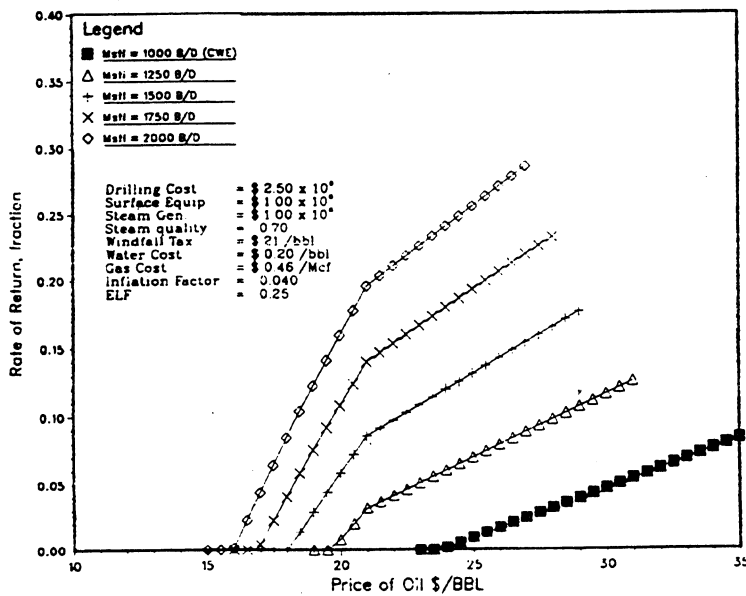


Figure 36: Preliminary Results of Price of Oil vs. Rate of Return with Steam Quality = 0.70

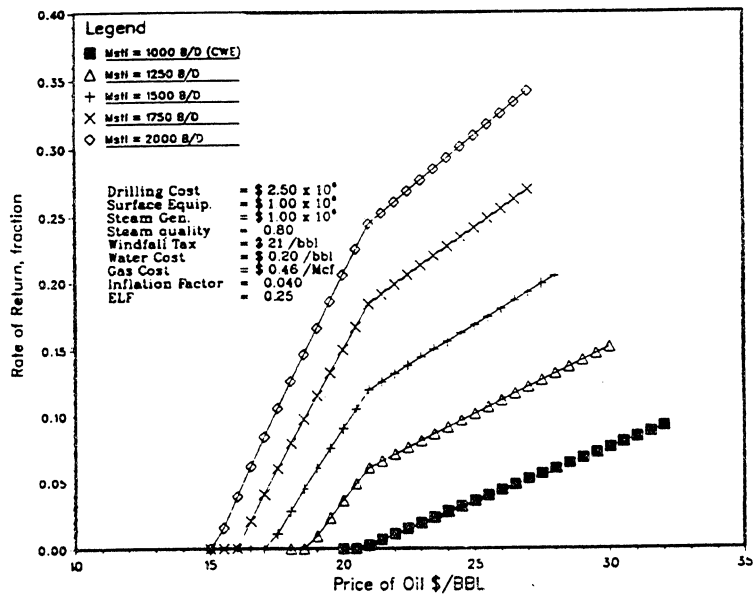


Figure 37: Preliminary Results of Price of Oil vs. Rate of Return with Steam Quality = 0.80

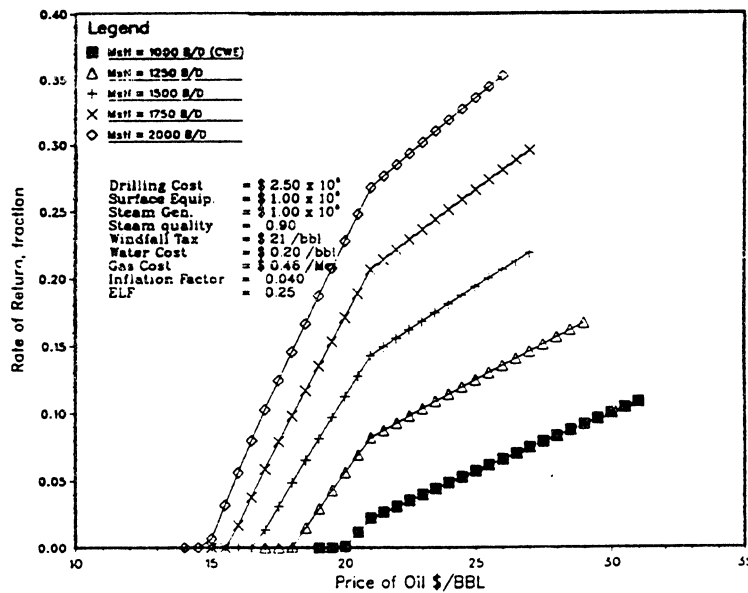


Figure 38: Preliminary Results of Price of Oil vs. Rate of Return with Steam Quality = 0.90

of 2000 barrels per day is required for steamflooding in the West Sak to be economically feasible.

D2.2 Sensitivity of Windfall Profits, Tax and ELF

The results obtained from the following sensitivity analysis are based on the same economic cost criteria mentioned previously which assumes an average drilling and well completion cost for a 7-spot pattern, expansion of the surface production facilities already in place in the Kuparuk field, and steam generator costs based on a 1981 report by Lewin and Associates that has been adjusted for future worth based on an average four percent annual inflation. Recently, an act was passed by the legislature that would repeal the Windfall Excess Profits Tax which has not affected the oil companies since the oil price collapse which occurred in late 1985 early 1986.

Another factor that has become a major topic in the political arena recently is the statutory economic limit factor (ELF) which controls the severance tax oil companies must pay the state of Alaska. As a well productivity declines, the ELF factor is designed to compensate the rate at which severance taxes are to be paid to account for the decline. One measurement of well productivity is the production rate, and results from ARCO's hot water project and from the steamflood model indicate that under the current structure of the economic limit factor the West Sak reservoir would not be subject to ELF. However, there is movement within the Alaska legislature to attempt to change the current structure of ELF which could potentially affect the West Sak reservoir. The results in Table 4 are derived from Figures 39 through 45 and illustrates the effect that the Windfall Profits Tax and various values of ELF might have on the rate of return for a given oil price range using the same values for the

Table 4: Results From Sensitivity Analysis of Windfall Profits Tax and Possible Values of ELF

RATE of RETURN	1000 BBL/DAY	1250 BBL/DAY	1500 BBL/DAY	1750 BBL/DAY	2000 BBL/DAY
Windfall Profits Tax = repealed, ELF = 0.25 - (\$/BBL)					
15%	28.52	24.51	21.85	20.00	18.59
20%	31.50	26.64	23.59	21.50	19.86
Windfall Profits Tax = \$ 21/BBL, ELF = 0 - (\$/BBL)					
15%	35.88	29.30	21.54	19.45	18.09
20%	41.57	31.88	25.30	20.88	19.31
Windfall Profits Tax - repealed, ELF = 0 - (\$/BBL)					
15%	27.68	23.81	21.24	19.45	18.09
20%	30.50	25.86	22.92	20.88	19.31
Windfall Profits Tax - repealed, ELF = 0.10 - (\$/BBL)					
15%	28.00	24.09	21.48	19.67	18.29
20%	30.65	26.16	23.18	21.11	19.53
Windfall Profits Tax - repealed, ELF = 0.20 - (\$/BBL)					
15%	28.35	24.37	21.73	19.89	18.50
20%	31.00	26.50	23.45	21.36	19.75
Windfall Profits Tax - repealed, ELF = 0.30 - (\$/BBL)					
15%	28.69	24.66	22.00	20.12	18.71
20%	31.42	26.80	23.73	21.61	20.00
Windfall Profits Tax - repealed, ELF = 0.50 - (\$/BBL)					
15%	29.43	25.28	22.52	20.61	19.15
20%	32.22	27.50	24.32	22.13	20.46

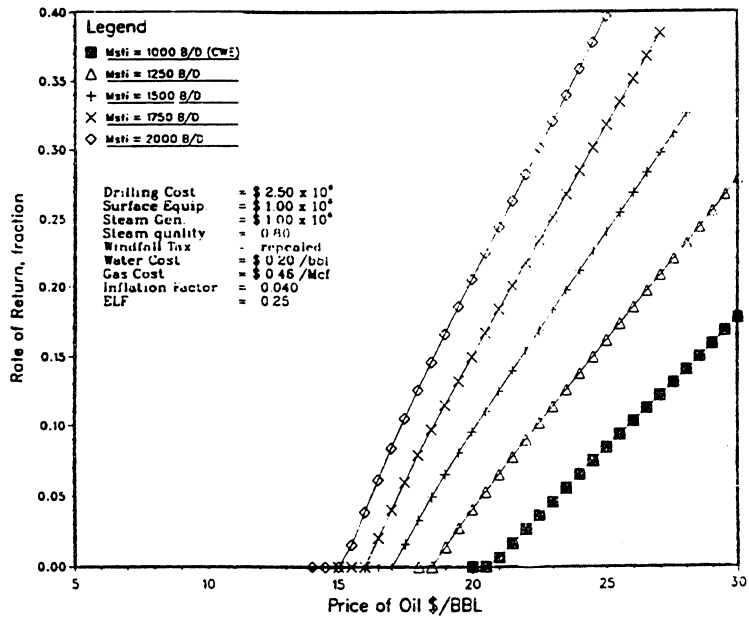


Figure 39: Sensitivity Analysis with Windfall Tax Repealed, ELF = 0.25

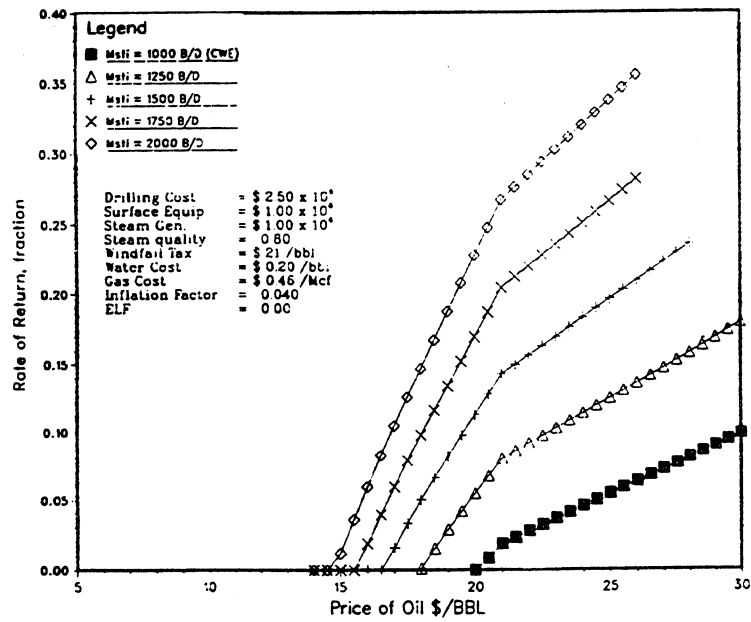


Figure 40: Sensitivity Analysis with Windfall Tax and Elf = 0

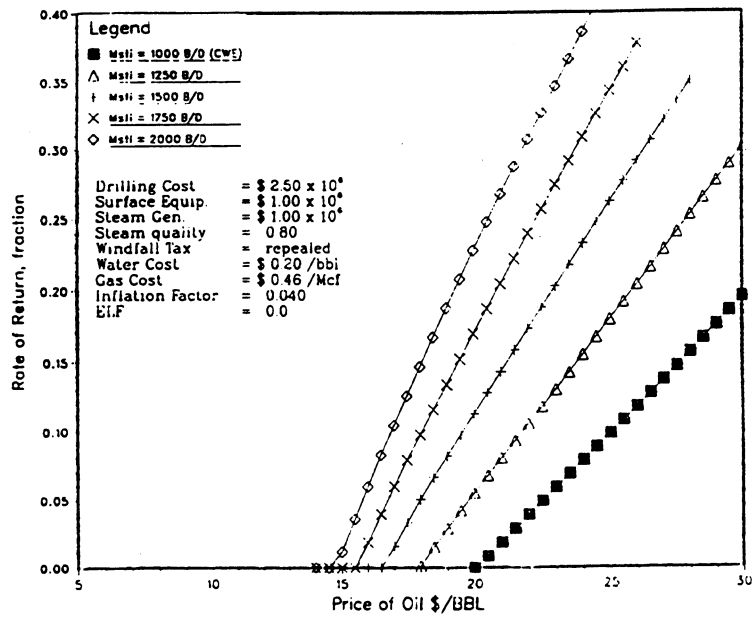


Figure 41: Sensitivity Analysis with Windfall Tax Repealed, ELF = 0.0

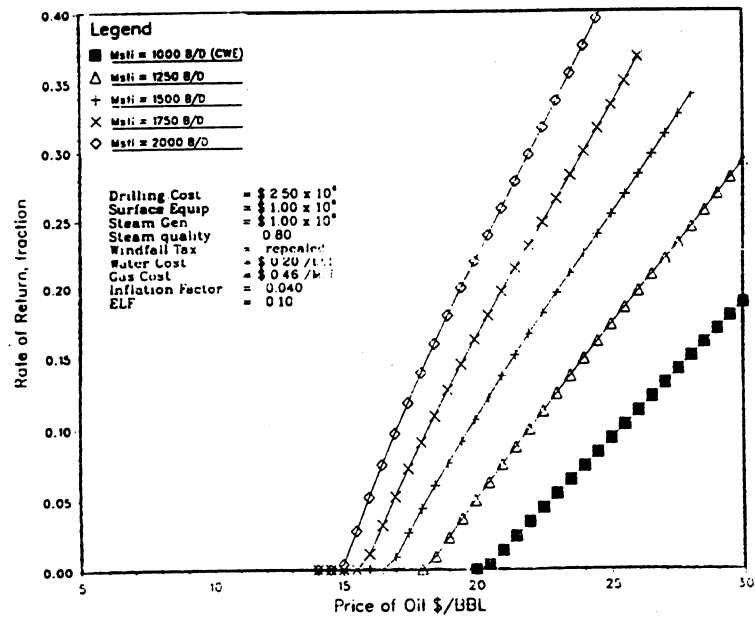


Figure 42: Sensitivity Analysis with Windfall Tax Repealed, ELF = 0.10

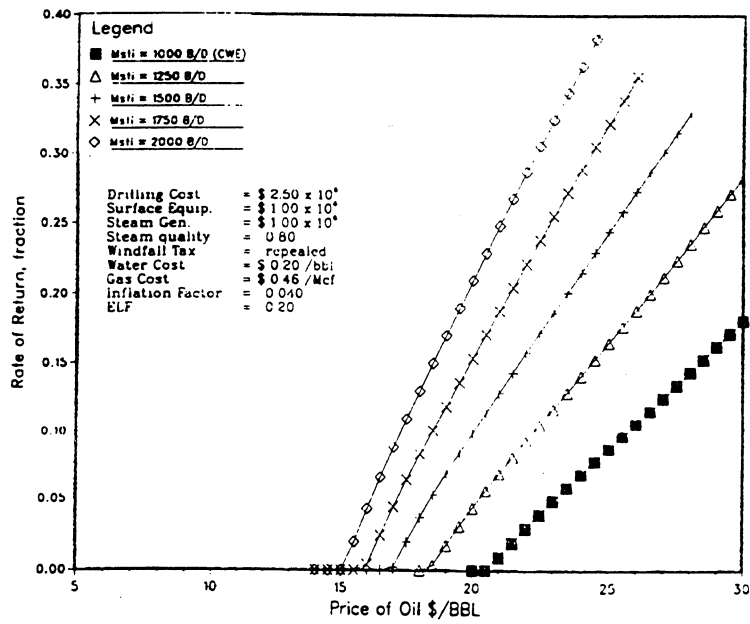


Figure 43: Sensitivity Analysis with Windfall Tax Repealed, ELF = 0.20

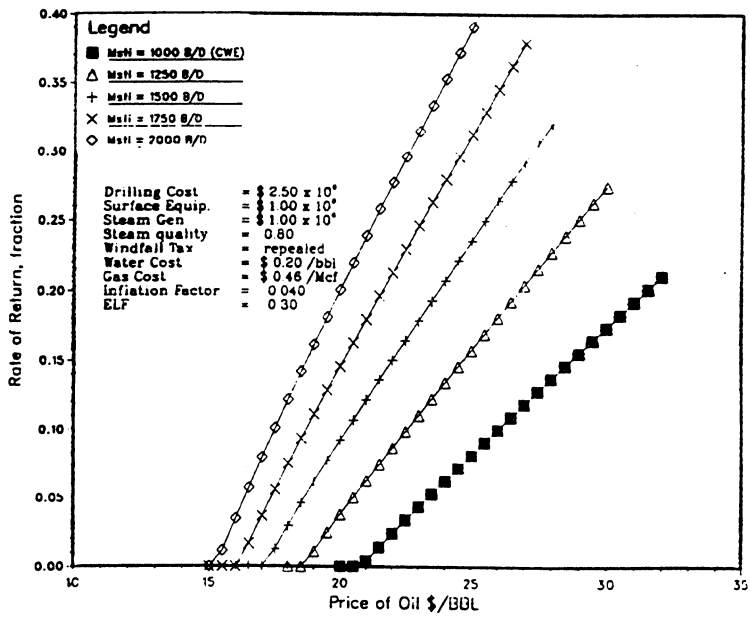


Figure 44: Sensitivity Analysis with Windfall Tax Repealed, ELF = 0.30

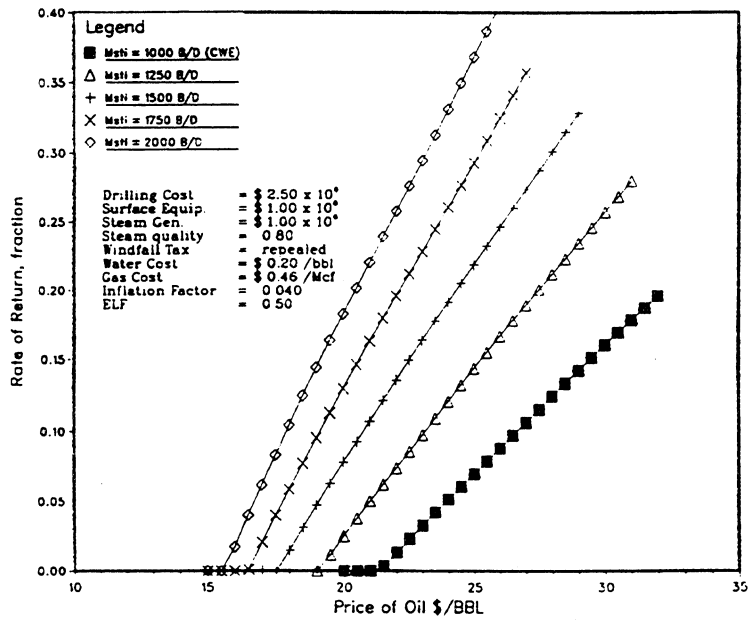


Figure 45: Sensitivity Analysis with Windfall Tax Repealed, ELF = 0.50

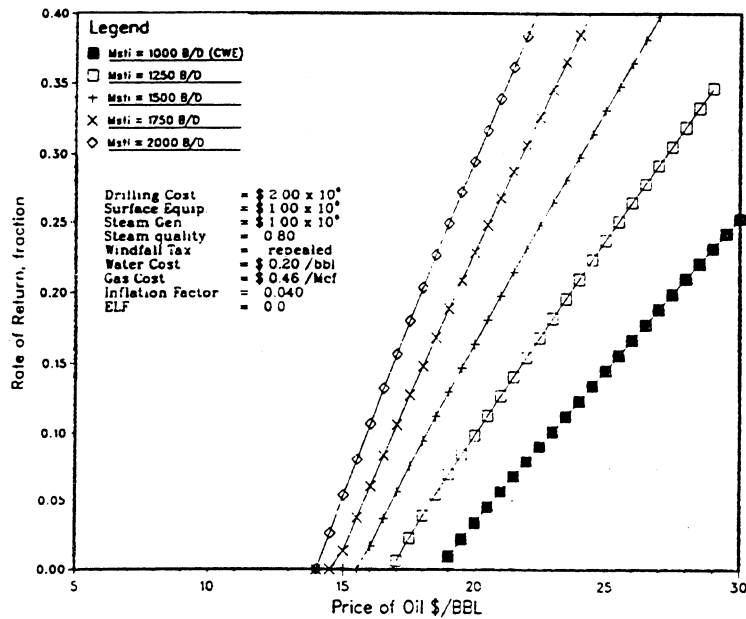


Figure 46: Sensitivity Analysis with Drilling and Well Completion Cost = \$2,000,000

various economic variables as in the preliminary study. From this analysis it was found that a 0.10 increase in the ELF factor results in an increase in the price of oil of approximately \$0.20/bbl for an assumed required 20% rate of return.

D2.3 Sensitivity of Drilling and Well Completion Costs

A major expenditure in the development of a steamflood project in the West Sak would occur in the drilling and well completion costs. Previous literature has shown that the cost of injection wells are approximately sixty five percent of a production well in a steamflood project. In this study a seven spot pattern is analyzed which has an injection to production well ratio of two to one (2:1). Using the drilling cost of \$242/foot in the Kuparuk region and a depth of 3000 feet, an average drilling and well completion cost for the West Sak 9 region would amount to \$1,700,000. However, the West Sak is composed of an unconsolidated sandstone and this presents unique completion problems which increases the costs considerably. According to ARCO Alaska, a typical well completion cost in West Sak averages approximately \$750,000 which is also the approximate cost for drilling a well. Taking this into consideration, an estimated drilling and well completion cost for a seven-spot pattern would be approximately \$2,500,000. Depth of the West Sak Reservoir varies from 2000 feet to 4500 feet, so 3000 feet would appear to be an approximate average reservoir depth. The sensitivity of the drilling and well completion costs was examined using a range of \$1,000,000 assuming an average cost of \$2,500,000. Drilling and well completion costs were examined in increments of \$200,000 from a low of \$2,000,000 to a high of \$3,000,000.

In determining the sensitivity of drilling and well completion costs it was assumed that the Windfall Profits Tax was repealed and the statutory economic limit factor was not applicable to the West Sak reservoir. Surface facilities and steam generator costs remained constant at \$1,000,000 each. Steam quality was assumed to be eight percent at the surface, and inflation remained at four percent for the time period examined. A series of plots (Figures 46 - 51) were made for each incremental cost to evaluate the varied effects of drilling and well completion costs. Table 5 presents a brief summary of the results derived from the plots of the sensitivity analysis of drilling and well completion costs. Examining the plots and the data presented in Table 5 it is clearly seen that increasing the injection rate to increase productivity significantly reduces the effect of incremental costs in drilling and well completions. Results from the sensitivity analysis indicate that for each \$200,000 increment in the drilling and well completion costs, the price of oil required for a 20% minimum rate of return increases from approximately \$1.10/bbl for an injection rate of 1000 barrels per day to approximately \$0.57/bbl for an injection rate of 2000 barrels per day. For a required 15% rate of return there would be an increase in the price of oil from approximately \$0.98/bbl for an injection rate of 1000 barrels per day to approximately \$0.50/bbl for an injection rate of 2000 barrels per day.

D2.4 Sensitivity of Surface Equipment and Steam Generator Costs

The total investments involved in an enhanced oil recovery project are composed of tangible and intangible investments. When the breakdown of the total investment costs are not known it is commonly assumed that intangible compose about 40% of the total investment and

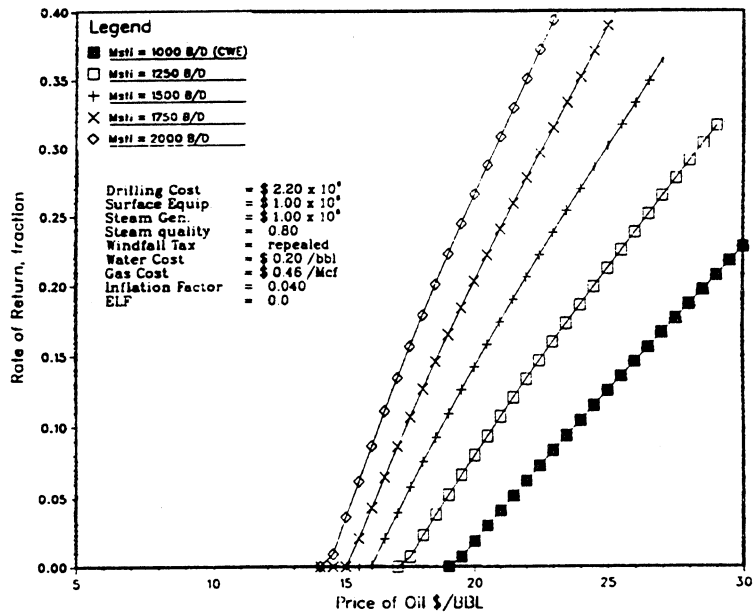


Figure 47: Sensitivity Analysis with Drilling and Well Completion Cost = \$2,200,000

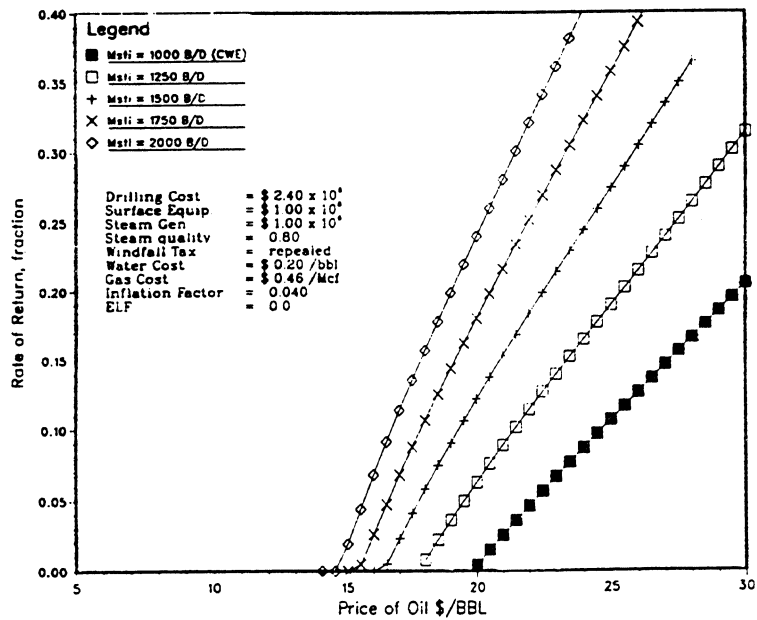


Figure 48: Sensitivity Analysis with Drilling and Well Completion Cost = \$2,400,000

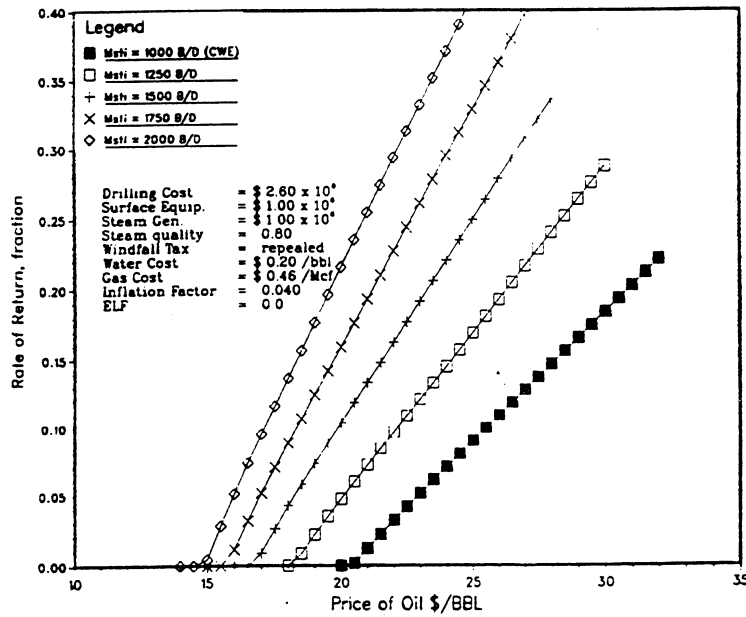


Figure 49: Sensitivity Analysis with Drilling and Well Completion Cost = \$2,600,000

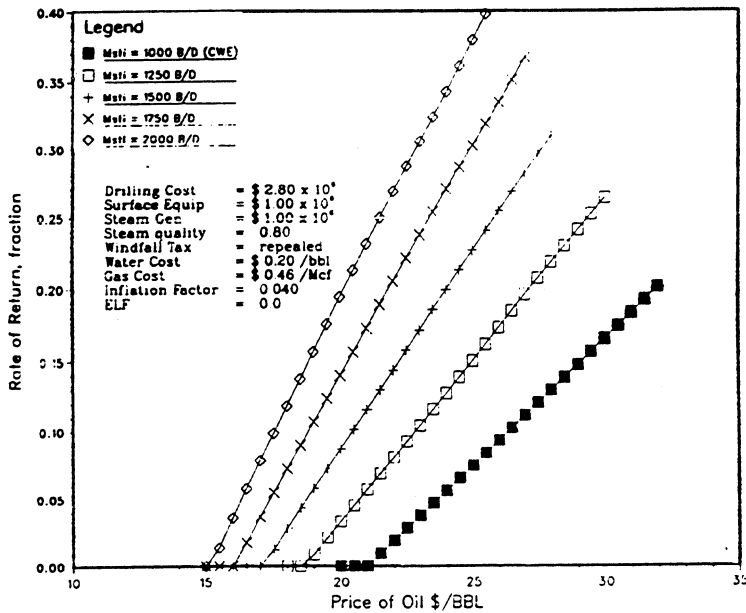


Figure 50: Sensitivity Analysis with Drilling and Well Completion Cost = \$2,800,000

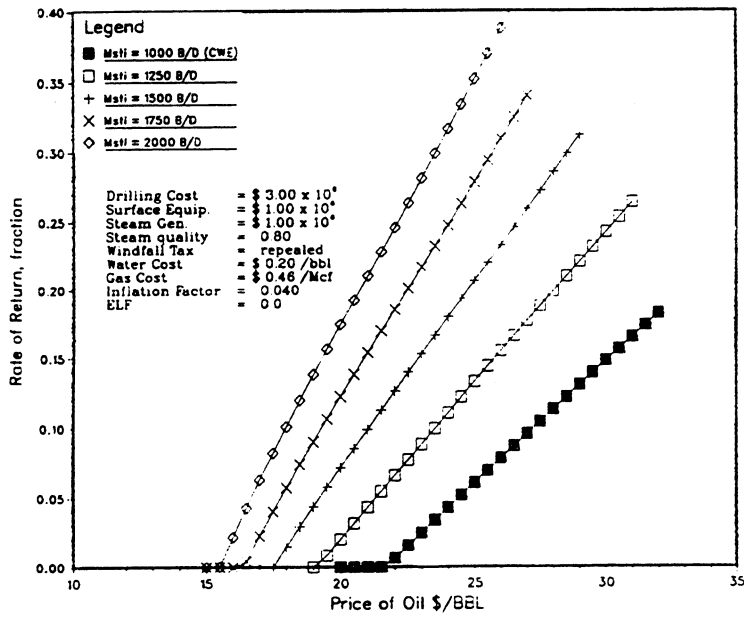


Figure 51: Sensitivity Analysis with Drilling and Well Completion Cost = \$3,000,000

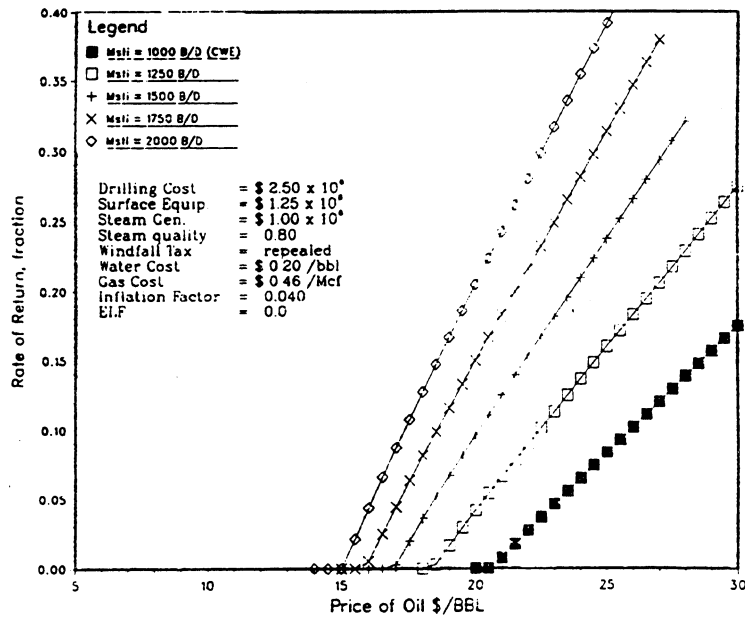


Figure 52: Sensitivity Analysis with Surface Equipment and Facilities Cost = \$1,250,000

Table 5: Results From Sensitivity Analysis of Drilling and Well Completion Costs

RATE of RETURN	1000 BBL/DAY	1250 BBL/DAY	1500 BBL/DAY	1750 BBL/DAY	2000 BBL/DAY
Drilling and Well Completion Costs = \$ 2,000,000 - (\$/BBL)					
15%	25.23	21.84	19.60	18.05	16.87
20%	27.54	23.65	21.07	19.29	17.93
Drilling and Well Completion Costs = \$ 2,200,000 - (\$/BBL)					
15%	26.21	22.63	20.25	18.61	17.35
20%	28.64	24.53	21.81	19.92	18.50
Drilling and Well Completion Costs = \$ 2,400,000 - (\$/BBL)					
15%	27.19	23.42	20.91	19.17	17.84
20%	29.74	25.42	22.85	20.56	19.04
Drilling and Well Completion Costs = \$ 2,600,000 - (\$/BBL)					
15%	28.16	24.20	21.57	19.73	18.33
20%	30.83	26.30	23.29	21.20	19.59
Drilling and Well Completion Costs = \$ 2,800,000 - (\$/BBL)					
15%	29.14	25.00	22.23	20.30	18.83
20%	31.93	27.18	24.03	21.84	20.15
Drilling and Well Completion Costs = \$ 3,000,000 - (\$/BBL)					
15%	30.12	25.78	22.89	20.87	19.32
20%	32.98	28.12	24.77	22.50	20.72

tangibles the remaining 60% (Ramage, Castanier, and Ramey, 1987). Drilling and well completion costs are generally considered intangible investments while surface and production facilities are tangible. Since the West Sak is located in the Kuparuk field it is assumed that many of the surface facilities already in place can be also used to handle production from West Sak with minimal expansion required. Assuming an average drilling cost of \$2,500,000 and using this figure as 40% of the total investment costs, the maximum surface facilities cost including the steam generator would be \$3,750,000.

Sensitivity of the expenditures for the surface facilities was determined using a cost range from \$1,000,000 to \$2,750,000 to represent various stages in either the availability or non-availability of the present surface facilities in existence at Kuparuk. An incremental cost of \$250,000 was used to study the sensitivity of the surface equipment costs. The initial cost used for the steam generator is \$1,000,000 and is based upon a present value adjusted price taken from a previous study by Lewin and Associates (1981). Also, since the steam generator and surface facilities required are considered the tangible costs for depreciation purposes in a steamflood project, a sensitivity analysis of the steam generator cost would produced the same results as for the surface facilities. To evaluate the sensitivity of the surface facilities cost, a series of plots of price of oil versus rate of return, similar to Figures 52 - 54, were made. The plots for the other incremental costs are similar in profile and would lie between the curves shown in Figures 52 and 53 which illustrate the extreme costs of \$1,250,000 and \$2,750,000 used for the surface equipment and facilities cost. Results obtained from the following sensitivity study of the surface facilities and steam generator costs which are summarized in

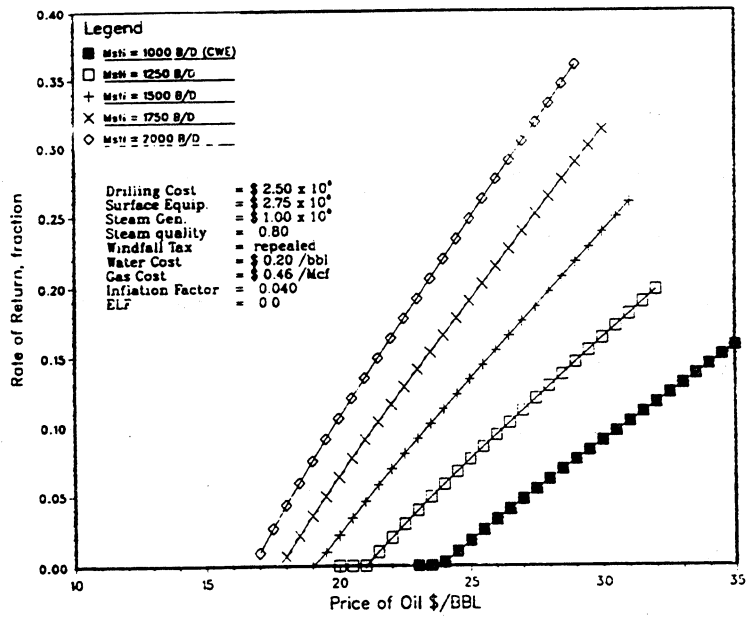


Figure 53: Sensitivity Analysis with Surface Equipment and Facilities Cost = \$2,750,000

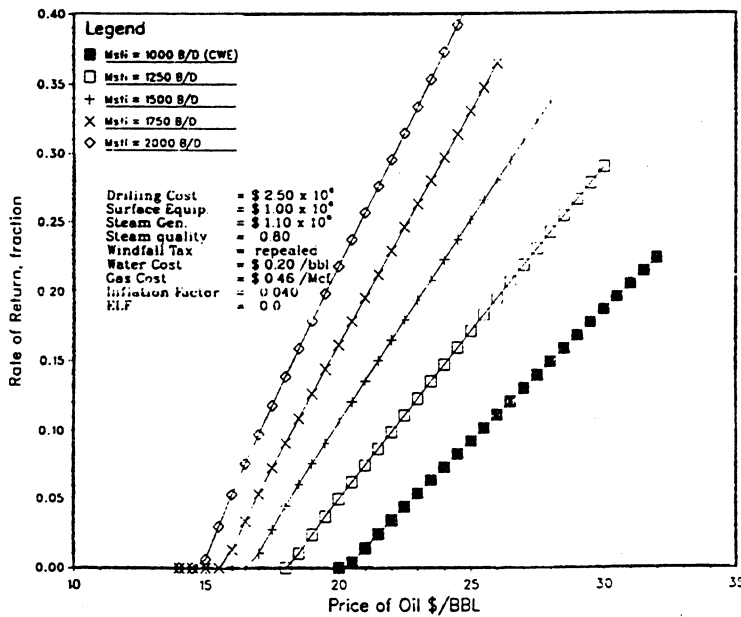


Figure 54: Sensitivity Analysis with Steam Generator Cost = \$1,100,000

Table 6 are based upon the same economic parameters used previously with the exception being that drilling and well completion costs are fixed at \$2,500,000, and surface equipment and steam generator costs are allowed to vary. Evaluating the results obtained from the sensitivity analysis of the surface equipment indicated that for each \$250,000 increment in cost to obtain a required 20% rate of return would increase the price of oil at a steam injection of 1000 barrels per day (BPD) approximately \$1.10/bbl, for 1250 BPD an increase of approximately \$0.90/bbl, for 1500 BPD an increase of approximately \$0.75/bbl, for 1750 BPD an increase of approximately \$0.65/bbl and for 2000 BPD an increase of approximately \$0.57/bbl.

D2.5 Sensitivity of Water and Fuel Costs

In addition to the investment costs involved in steamflooding, equally important are the operating costs necessary to conduct a steamflooding operation. Among the most important operating costs to be considered is the cost of the water necessary for the steam, and the fuel cost for operating the steam generator. The water required for steam generation has been relatively free of contaminants to prevent corrosion within all the steam injection lines. In a report by Lewin & Associates (1981) an average cost for produced treated water in California was \$0.025/bbl. For the North Slope, however, the costs would be expected to be much higher due to the environment and remoteness of fresh water supplies. For this study a base price for treated water of \$0.20/bbl was used; a sensitivity analysis of the cost of treated water was conducted using increments of \$0.10/bbl. Natural gas was chosen as the fuel for use by the steam generator because it is readily available on the North Slope and at present is relatively inexpensive. Sensitivity of natural

Table 6: Results From Sensitivity Analysis of Surface Equipment and Steam Generator Costs

RATE of RETURN	1000 BBL/DAY	1250 BBL/DAY	1500 BBL/DAY	1750 BBL/DAY	2000 BBL/DAY
Surface Equipment = \$ 1,250,000 - (\$/BBL)					
15%	28.63	24.59	21.89	20.01	18.58
20%	31.40	26.75	23.67	21.52	19.88
Surface Equipment = \$ 1,500,000 - (\$/BBL)					
15%	29.60	25.36	22.54	20.57	19.07
20%	32.50	27.65	24.42	22.17	20.45
Surface Equipment = \$ 1,750,000 - (\$/BBL)					
15%	30.67	26.13	23.09	21.13	19.57
20%	33.54	28.54	25.17	22.82	21.02
Surface Equipment = \$ 2,000,000 - (\$/BBL)					
15%	31.53	26.91	23.84	21.70	20.06
20%	34.73	29.43	25.92	23.50	21.59
Surface Equipment = \$ 2,250,000 - (\$/BBL)					
15%	32.50	27.69	24.50	22.26	20.55
20%	35.81	30.33	26.67	24.12	22.16
Surface Equipment = \$ 2,500,000 - (\$/BBL)					
15%	33.45	28.46	25.14	22.82	21.05
20%	36.92	31.22	27.41	24.77	22.73
Surface Equipment = \$ 2,750,000 - (\$/BBL)					
15%	34.41	29.24	25.79	23.38	21.54
20%	37.98	32.12	28.17	25.41	23.30
Steam Generator = \$ 1,100,000 - (\$/BBL)					
15%	28.06	24.12	21.50	19.67	18.28
20%	30.73	26.21	23.22	21.14	19.54
Steam Generator = \$ 1,200,000 - (\$/BBL)					
15%	28.45	24.43	21.76	19.90	18.48
20%	31.18	26.57	23.52	21.40	19.77

gas was analyzed using the current market average price of \$0.46/Mcf, and from a price of \$1.00/Mcf incrementing in steps \$0.50/Mcf and \$1.00/Mcf to evaluate the sensitivity of the cost for generating steam on the rate of return.

As in the previous analyses, plots similar to Figures 55 - 58 of the incremental cost for both the treated water and natural gas were made to evaluate this sensitivity analysis. Figures 55 and 56 illustrate the extremes in the treated water cost used, while Figures 57 and 58 illustrate the incremental cost in North Slope natural gas. Results from the sensitivity analysis for the water and gas costs are presented in Table 7. Economic data are the same as used in the previous sensitivity analysis with the exception of surface equipment and facilities cost which was \$1,500,000. This cost figure was used simply to represent an average cost in the required surface equipment and facilities. Examination of the results obtained from the sensitivity analysis of the treated water cost indicated that for each \$0.10/bbl increment in the water cost an increase of approximately \$0.50/bbl in the price of oil for a 20% required rate of return was observed for each of the steam injection rates. The sensitivity analysis of the gas cost revealed that for each \$0.50/Mcf increase in the cost of gas for the steam generator resulted in an increase of approximately \$0.90/bbl at a steam injection rate of 1250 BPD produced an increase in the required price of oil of approximately \$0.93/bbl, at 1500 BPD an increase of approximately \$0.96/bbl, at 1750 BPD an increase of approximately \$0.98/bbl and with an injection rate of 2000 BPD an increase of approximately \$1.00/bbl was found.

D2.6 Sensitivity of Inflation

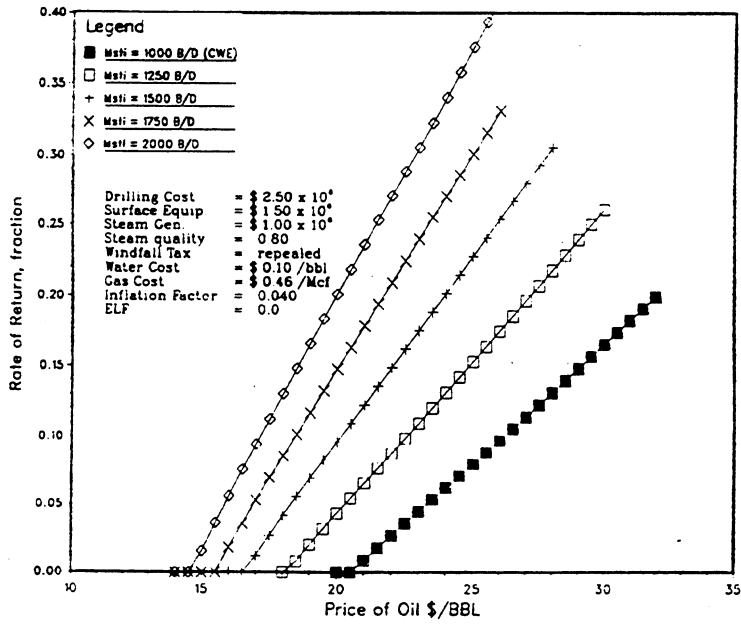


Figure 55: Sensitivity Analysis with Treated Water Cost = \$0.10/bbl

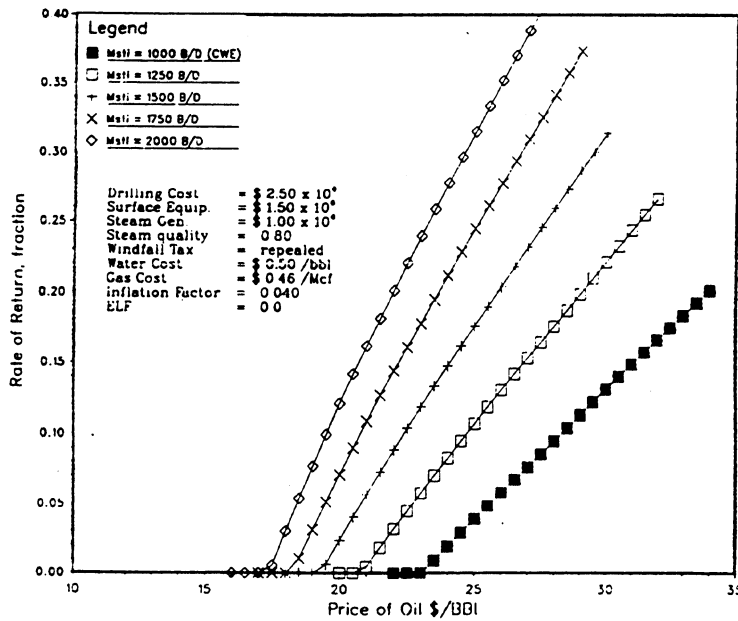


Figure 56: Sensitivity Analysis with Treated Water Cost = \$0.50/bbl

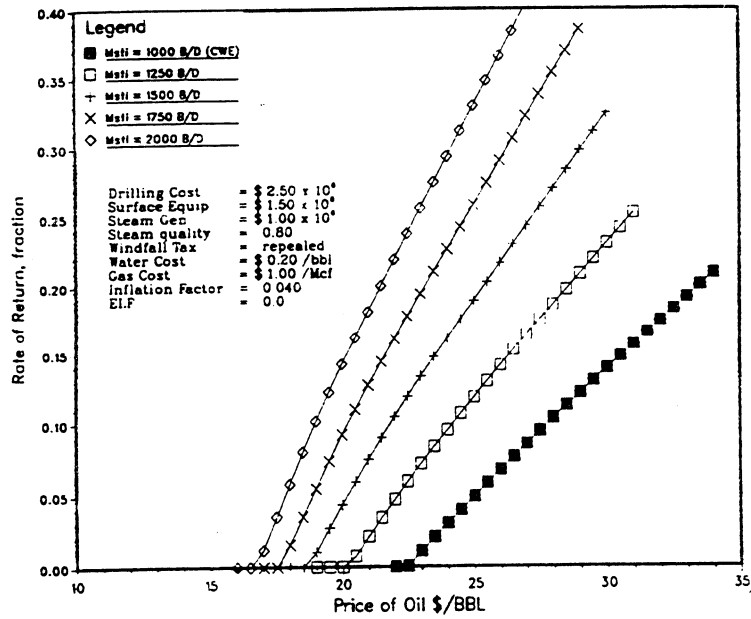


Figure 57: Sensitivity Analysis with Natural Gas Cost = \$1.00/Mcf

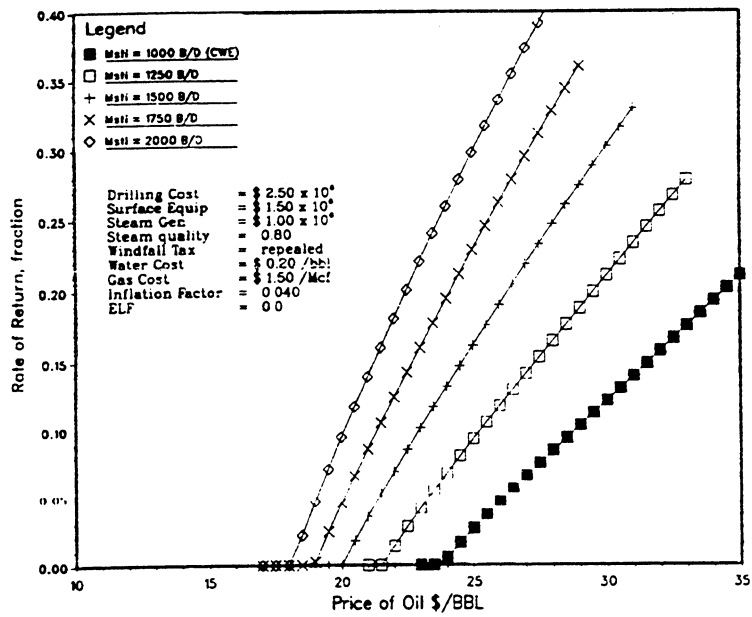


Figure 58: Sensitivity Analysis with Natural Gas Cost = \$1.50/Mcf

Table 7: Results From Sensitivity Analysis of Treated Water and Fuel Costs for Generating Steam

RESULTS FROM SENSITIVITY OF TREATED WATER COSTS

RATE of RETURN	1000 BBL/DAY	1250 BBL/DAY	1500 BBL/DAY	1750 BBL/DAY	2000 BBL/DAY
Treated water cost = \$0.10/bbl					
15%	29.11	24.86	22.04	20.07	18.55
20%	32.04	27.17	23.94	21.70	19.97
Treated water cost = \$0.30/bbl					
15%	30.09	25.86	23.04	21.10	19.61
20%	32.95	28.11	24.89	22.65	20.95
Treated water cost = \$0.40/bbl					
15%	30.59	26.35	23.56	21.63	20.15
20%	33.50	28.58	25.36	23.14	21.45
Treated water cost = \$0.40/bbl					
15%	31.08	26.85	24.08	22.17	20.70
20%	33.92	29.05	25.85	23.64	21.96
Gas cost = \$1.00/Mcf					
15%	30.63	26.40	23.60	21.68	20.20
20%	33.50	28.63	25.41	23.18	21.50
Gas cost = \$1.50/Mcf					
15%	31.58	27.37	24.61	22.72	21.26
20%	34.39	29.54	26.34	24.16	22.50
Gas cost = \$2.00/Mcf					
15%	32.53	28.37	25.64	23.77	22.33
20%	35.28	30.50	27.31	25.14	23.50
Gas cost = \$3.00/Mcf					
15%	34.50	30.40	27.74	26.00	24.53
20%	37.00	32.36	29.24	27.12	25.55

During the mid to late 1980's inflation has been steady at approximately four percent per year (Logsdon et al., 1988). To determine the possible effect that increases in the inflation rate would have on the required price of oil for a desired rate of return a sensitivity analysis of inflation was conducted. The analysis used the same base economic data for determining the sensitivity of the gas and water cost except that for this analysis gas is fixed at \$0.46/Mcf, water cost is \$0.20/bbl and the inflation factor was allowed to vary. Using inflation factor increments of 0.005 and 0.01, a series of plots similar to Figure 59 were made to determine the sensitivity effects of inflation on the required price of oil for a desired rate of return. Evaluating the results from this analysis presented in Table 8, indicated that a lower injection rates are more influenced by the effects of inflation than the higher injection rates. To obtain a 20% rate of return for a 0.5% increase in the inflation rate, increased the price of oil approximately \$0.34/bbl for an injection rate of 1000 BPD, at a 1250 BPD injection rate the required oil price increased \$0.26/bbl, at a 1500 BPD injection rate an increase of \$0.22/bbl, at a 1750 BPD injection rate an increase of \$0.18/bbl and at a 2000 BPD injection rate an increase of \$0.16/bbl was found.

D2.7 Sensitivity of Residual Oil Saturation

As mentioned previously one of the most important parameters dictating the success or failure of a steamflood is the value of the residual oil saturation (S_{or}) that can be obtained. To determine the potential effect that residual oil saturations can have on the economic and technical feasibility aspects of a steamflood, a sensitivity analysis was conducted for different values of S_{or} with the results illustrated in Figures 60 - 65. During this study an S_{or} value corresponding to twelve percent

Table 8: Results From Sensitivity Analysis of Inflation

RATE of RETURN	1000 BBL/DAY	1250 BBL/DAY	1500 BBL/DAY	1750 BBL/DAY	2000 BBL/DAY
Inflation factor = 0.045					
15%	29.92	25.61	22.75	20.75	19.22
20%	32.83	27.91	24.63	22.36	20.61
Inflation factor = 0.05					
15%	30.24	25.86	22.95	20.92	19.38
20%	33.19	28.17	24.85	22.55	20.78
Inflation factor = 0.055					
15%	30.56	26.12	23.16	21.10	19.53
20%	33.51	28.44	25.07	22.73	20.94
Inflation factor = 0.06					
15%	30.89	26.37	23.37	21.28	19.68
20%	33.85	28.70	25.29	22.92	21.10
Inflation factor = 0.07					
15%	31.53	26.87	23.78	21.63	19.98
20%	34.53	29.23	25.72	23.89	21.42

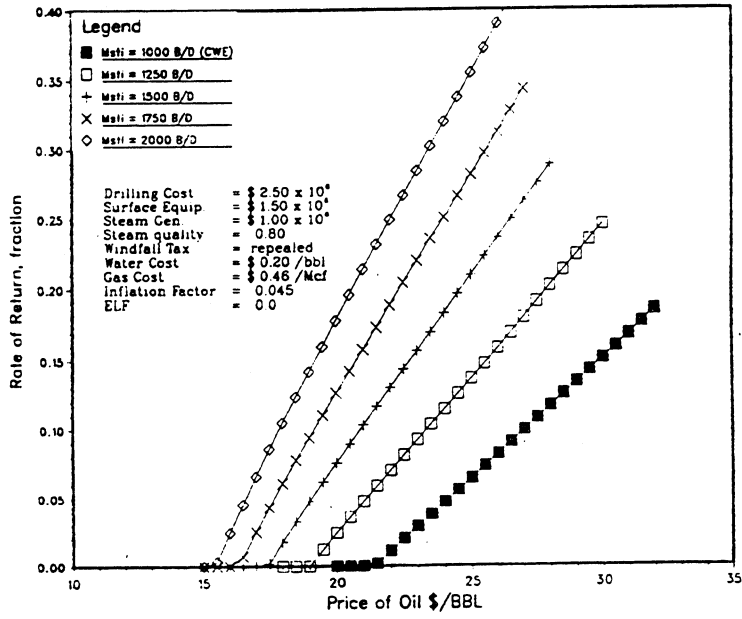


Figure 59: Sensitivity Analysis with Inflation Factor = 0.045

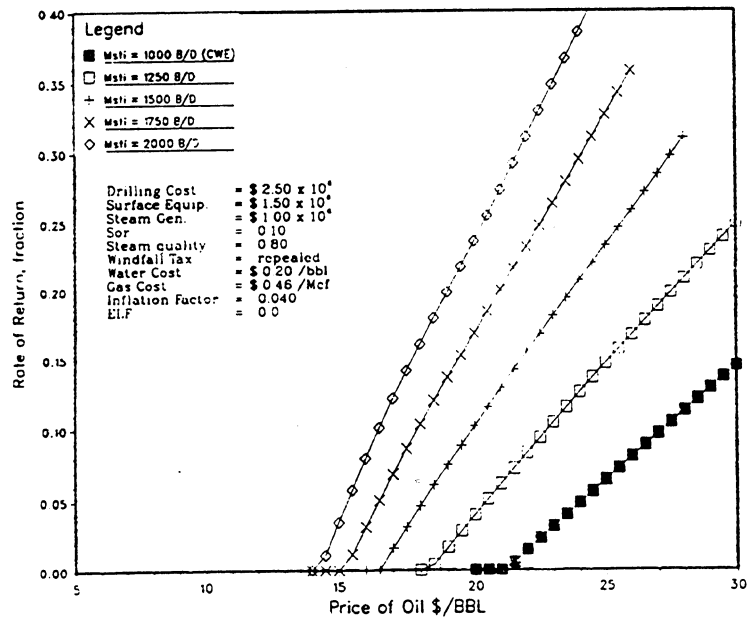


Figure 60: Sensitivity Analysis with $S_{or} = 0.10$

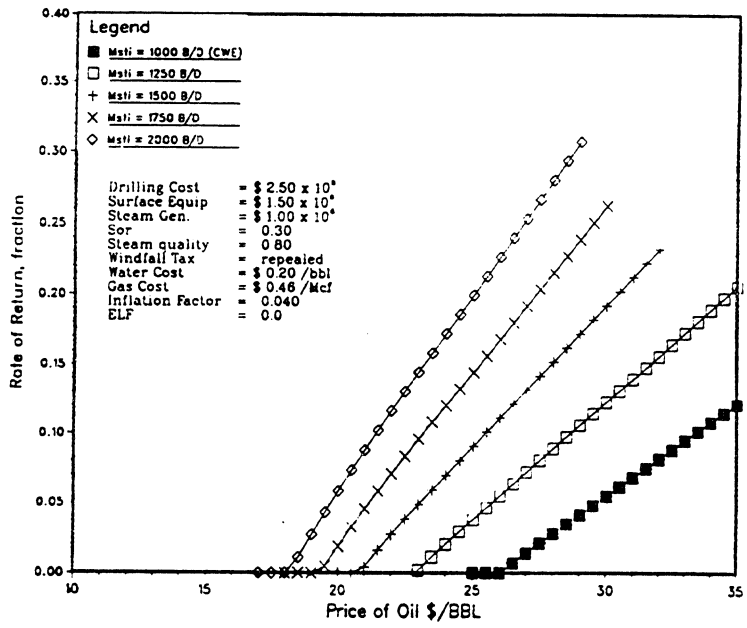


Figure 61: Sensitivity Analysis with $S_{or} = 0.30$

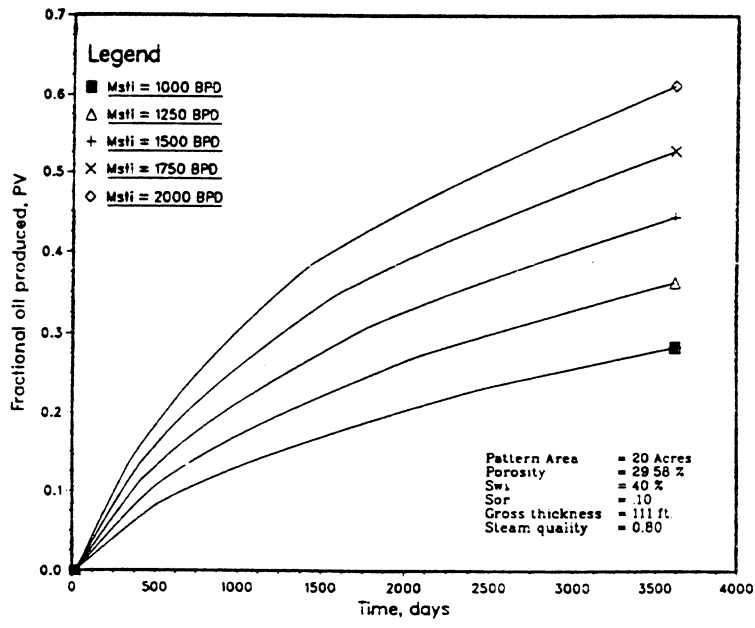


Figure 62: Sensitivity Analysis of Cumulative Fractional Recovery with $S_{or} = 0.10$

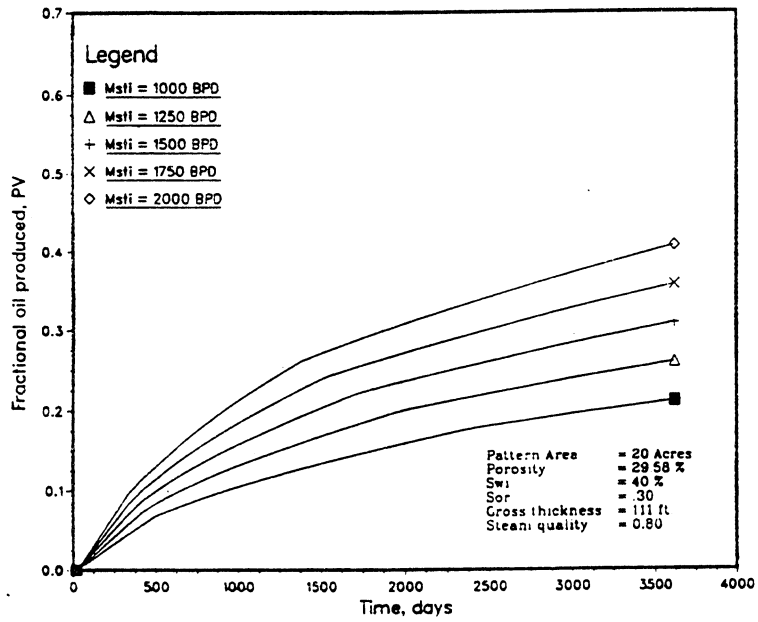


Figure 63: Sensitivity Analysis of Cumulative Fractional Recovery with $S_{OR} = 0.30$

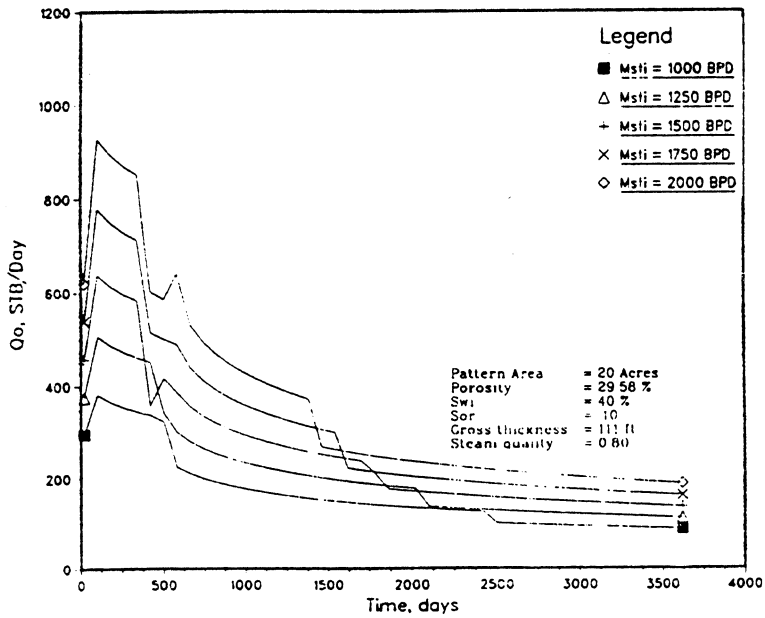


Figure 64: Sensitivity Analysis of Oil Production Rate with $S_{OR} = 0.10$

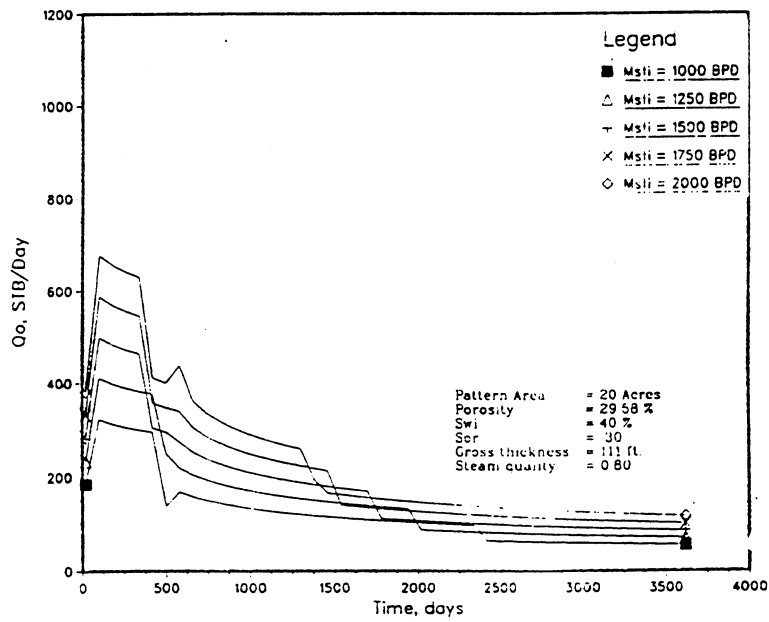


Figure 65: Sensitivity Analysis of Oil Production Rate with $S_{or} = 0.30$

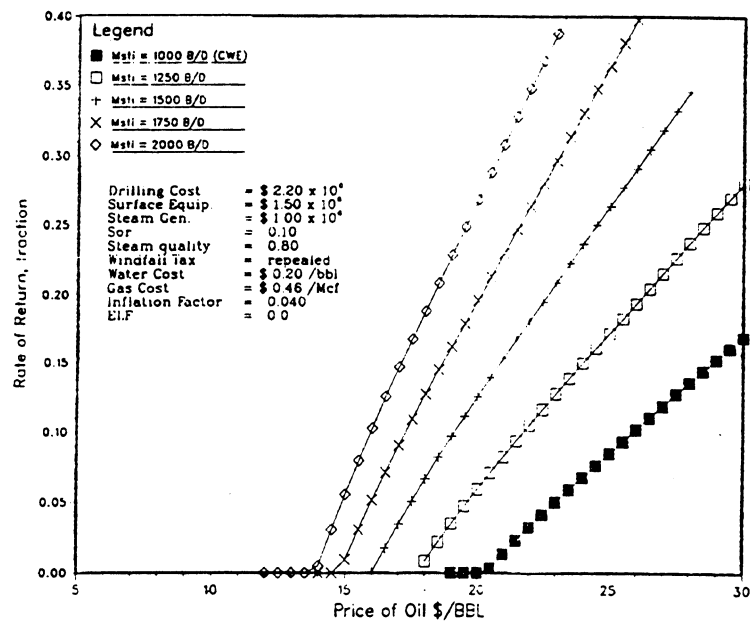


Figure 66: Best Case Scenario for Determining Economic Potential of West Sak

pore volume was used as an average value. For the sensitivity study an optimistic value of six percent pore volume and a pessimistic value of eighteen percent pore volumes was used as the extreme values of residual oil saturation to be analyzed. One would expect that for low values of S_{or} the predicted oil recovery should be greater than for high values of S_{or} and examining Figures 62 and 63 which illustrates the fractional recovery at various injection rates, the recovery with $S_{or} = 0.10$ is considerably greater than the recovery with $S_{or} = 0.30$. A comparison of Figures 64 and 65 illustrates that the estimated oil production rate is also noticeably greater for the lower S_{or} value. Results from plots (Figures 60 and 61) of oil price versus rate of return are presented in Table 9 and a can be seen the value of S_{or} that can be achieved during steamflooding has significant influence on the required oil price for economic feasibility. At an injection rate of 2000 BPD for a 20% rate of return with all other variables equal, the required oil price varies from \$19.05/bbl ($S_{or} = 0.10$) to \$25.00/bbl ($S_{or} = 0.30$) which is a variance of nearly \$6.00/bbl.

D2.8 Average Best and Worst Case Scenarios for West Sak

Based on the sensitivity analysis performed, a best case scenario for steamflooding in the West Sak would most likely be dependent on lowering the drilling and well completion costs and obtaining a low residual oil saturation value. A worst case scenario would be considered when none of the surface equipment and facilities present at West Sak can be used, and a high value for the residual oil saturation is obtained. Other economic variables such as water and gas costs, and the inflation factor remain the same as used in the base case. An average best and worst case scenario and the expected price range of oil for a required rate of return is outlined in Table 10. The data used to compile the results

Table 9: Results From Sensitivity Analysis of Residual Oil Saturation Values

VALUES.

RATE of RETURN	1000 BBL/DAY	1250 BBL/DAY	1500 BBL/DAY	1750 BBL/DAY	2000 BBL/DAY
Residual oil saturation (S_{OR}) = 0.10 (6% pore volume)					
15%	30.38	25.19	21.83	19.44	17.74
20%	33.54	27.61	23.75	21.01	19.05
Residual oil saturation (S_{OR}) = 0.30 (18% pore volume)					
15%	37.20	31.64	27.91	25.24	23.20
20%	40.96	34.66	30.40	27.35	25.00

Table 10: Results From Best and Worst Case Scenarios For Steamflooding in West Sak

Best Average Case:

Drilling & Well Completion =	\$ 2,200,000
Surface Equipment =	\$ 1,500,000
Steam Generator =	\$ 1,000,000
ELF =	0
Windfall Tax =	Repealed
Gas =	\$ 0.46/Mcf
Water Cost =	\$ 0.20/bbl
Inflation =	0.04
S_{OR} =	0.10

RATE of RETURN	1000 BBL/DAY	1250 BBL/DAY	1500 BBL/DAY	1750 BBL/DAY	2000 BBL/DAY
15%	28.37	24.00	20.88	18.65	17.08
20%	31.85	26.29	22.67	20.12	18.29

Worst Average Case:

Drilling & Well Completion =	\$ 2,500,000
Surface Equipment =	\$ 2,750,000
Steam Generator =	\$ 1,000,000
ELF =	0
Windfall Tax =	Repealed
Gas =	\$ 0.46/Mcf
Water Cost =	\$ 0.20/bbl
Inflation =	0.04
S_{OR} =	0.30

RATE of RETURN	1000 BBL/DAY	1250 BBL/DAY	1500 BBL/DAY	1750 BBL/DAY	2000 BBL/DAY
15%	43.49	36.78	32.29	28.95	26.46
20%	48.19	40.48	35.13	31.62	28.78

shown in Table 10 were derived from Figures 66 and 67. From the economic variables considered for an average best cause scenario the model predicted an oil price of approximately \$18.29/bbl assuming a required 20% rate of return. For the worst case scenario considered the model predicted an oil price of \$28.78/bbl based on a required 20% rate of return.

D2.9 Summary of Sensitivity Analysis

A sensitivity analysis of the injected steam quality showed a significant impact on the cumulative oil recovered. In retrospect, the results for an injection rate of 2000 barrels per day the fractional pore volumes of oil recovered with a steam quality of 0.60 is approximately 43.82% of original oil in place while a steam quality of 0.90 recovered 56.20% of the original oil in place for the same time period. The incremental recovery gained for an increase in the steam quality decreases when the steam quality is greater than 0.80. A steam quality of 0.80 is used in this study for sensitivity analysis of the economic variables because this is about the maximum steam quality that has been used in previous steamfloods for similar reservoir conditions.

The sensitivity analysis of the residual oil saturation values possible indicated that this variable has a significant impact on the oil recovered and as a result economic conditions necessary for feasibility. For an S_{or} value of 0.10 the possible recovery is 61.26% while an S_{or} value of 0.30 produces about 40.72% of the oil in place with an injection rate of 2000 barrels per day. This of course can be very important in determining when or if a steamflood in the West Sak reservoir is economically feasible for the conditions considered.

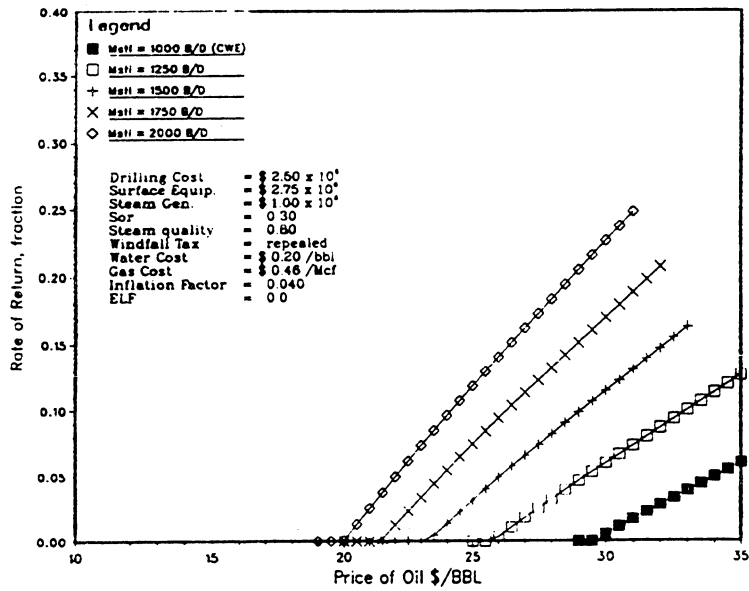


Figure 67: Worst Case Scenario for Determining Economic Potential of West Sak

Sensitivity analyses of the economic variables used in this study show that the higher injection (1750, 2000 barrels per day) rates are influenced less than the smaller injection (1000-1500 barrels per day) rates to changes in the capital, investments, operating costs, or inflation. Repealing the Windfall Tax benefits the economics of the steamflood project when the required price of oil for obtaining the required rate of return is greater than the Windfall Tax limit of \$2100/bbl. If the ELF factor were applicable to the West Sak, a 0.10 increment in the value of ELF could result in an approximate increase of \$0.20/bbl in the price of oil for a 20% required rate of return. Changes in the cost of water required for steam generation reflects much less of an influence on the rate of return than does a change in the cost of fuel required by the steam generator. The effect of inflation has shown that for an injection rate of 2000 BPD, a 0.5% increase in the inflation rate could potentially raise the required price of oil \$0.16/bbl.

E. CONCLUSIONS

Based on the results obtained from the sensitivity analysis of the various economic and reservoir parameters examined a minimum oil price range required for economic feasibility of a steamflood operation would be \$18 to \$25 per barrel. This oil price range is based on a seven spot pattern with an injection rate of 2000 BPD (CWE) of steam and specific economic conditions to obtain a required 20% rate of return. As was expected the higher injection rate produces a greater return for the same investment costs. Therefore, it is to the benefit of the operator to operate at the highest injection rate possible. The economic parameters which exhibit the greatest influence on the oil price for the required rate of return are the drilling and well completion costs and the surface facilities costs.

The wellhead price of gas on the North Slope is not expected to have much influence on the required price of oil unless major gas sales were to occur which would dramatically increase the price for natural gas. Currently, North Slope wellhead gas prices range from \$0.25/Mcf to \$3.43/Mcf, with an average price of \$0.46/Mcf. Results from the sensitivity analysis indicated that for a \$0.50/Mcf increase in the price of gas could increase the minimum required oil price by approximately one dollar per barrel for a required 20% rate of return.

The primary key to developing and operating a successful steamflood at an \$18 per barrel price of oil will require reducing the well completion costs and maximizing the use of the surface production equipment and facilities already present in the Kuparuk field. With the current over supply of crude oil on the market today and an unstable market price, steamflooding in the West Sak will probably not be economical until a stable \$18 to \$20 per barrel price of oil is established. Steamflooding the entire West Sak reservoir probably will not be technically feasible due to the heterogeneity of the reservoir sands. Also, areas of the West Sak reservoir are known to contain clays which are not amenable to steamflooding because of the swelling of the clays that would occur as steam in the reservoir condensed.

F. REFERENCES

1. Abou-Kassem, J.H., and Farouq Ali, S.M.: *"Appraisal of Steamflood Models,"* SPE 13947, 1985 California Regional Meeting.
2. Aeschliman, D.P., Meldau, R.F., and Noble, N.J.: *"Thermal Efficiency of a Steam Injection Test Well with Insulated Tubing,"* SPE 11735, 1983 California Regional Meeting.
3. Aydelotte, Robert S. and Pope, Gary A.: *"A Simplified Predictive Model for Steamdrive Performance,"* Journal of Petroleum Technology, May 1983, pp. 991-1002.

4. Aydelotte, Robert S. and Pope, Gary A.: *"Development and Verification of Simplified Prediction Models for Enhanced Oil Recovery Application: Steamflood Predictive Model,"* Scientific Software-Intercomp, October 1984.
5. Boberg, T.C. and Lantz, R.B.: *"Calculation of the Production Rate of a Thermally Stimulated Well,"* Journal of Petroleum Technology, Dec. 1966, pp. 1613-1623.
6. Chu, Chieh: *"State-of-the-Art Review of Steamflood Field Projects,"* SPE 11733, 1983 California Regional Meeting.
7. Coats, Keith H.: *"A Highly Implicit Steamflood Model,"* Society of Petroleum Engineers Journal, Oct. 1978, pp. 369-383.
8. Coats, Keith H.: *"In-Situ Combustion Model,"* Society of Petroleum Engineers Journal, Dec. 1980, pp. 533-554.
9. Donohue, David A.T.: *"An Economic Appraisal of Steam Flooding in a Pennsylvania Field,"* Journal of Petroleum Technology, Nov. 1967, pp. 1437-1443.
10. Farouq Ali, S.M.: *"Steam Injection Theories - A Unified Approach,"* SPE 10746, 1982 California Regional Meeting.
11. Farouq Ali, S.M. and Meldau, R.F.: *"Current Steamflood Technology,"* Journal of Petroleum Technology, Oct. 1979, pp. 1332-1341.
12. Gomaa, Essat E.: *"Correlations for Predicting Oil Recovery by Steamflood,"* Journal of Petroleum Technology, Feb. 1980, pp. 325-332.
13. Herrera, J.O., Birdwell, B.F., and Hanzlik, E.J.: *"Wellbore Heat Losses in Deep Steam Injection Wells S1-B Zone Cat Canyon Field,"* SPE 7117, 1978 California Regional Meeting.
14. Higgins, R.V. and Leighton, A.J.: *"A Computer Method to Calculate Two-Phase Flow in Any Irregularly Bounded Porous Medium,"* Transactions of AIME, June 1962, Vol. 225, p. 682.

15. Jones, Jeff: *"Steam Drive Model for Hand-Held Programmable Calculators,"* Journal of Petroleum Technology, Sept. 1981, pp. 1583-1598.
16. Kamath, V.A., Goldbole, S.P., and Baena, C.J.: *"Effect of Hydrates During Thermal Recovery of Heavy Oils on the North Slope, Alaska,"* SPE 14224, 60th Annual Technical Conference and Exhibition SPE Las Vegas, NV, Sept. 22-25, 1985.
17. Krueger, D.A.: *"Stability of Crude Oil Displacements,"* Final Report, Contract 46-8784, Sandia Labs, Albuquerque, Sept. 1980.
18. Lewin and Associates, Inc.: *"Economics of Enhanced Oil Recovery - Final Report,"* DOE Report DOE/BETC/2628-2, May 1981.
19. Lewin and Associates, Inc.: *"Current and Future Economics of Enhanced Oil Recovery,"* A report submitted to U.S. Department of Energy, Washington, D.C., 1984.
20. Logsdon, Dr. Charles: *"Alaska Oil Production in Perspective,"* Alaska Economic Trends., Oct. 1987, pp. 1-10.
21. Logsdon, Dr. Charles, Marks, Roger, Hansen, Eric, and Moore, J. William, Petroleum Production Revenue Forecast-Quarterly Report, Sept. 1987, Spring 1988.
22. Lucke, Robert and Toder, Eric: *"Assessing the U.S. Federal Tax Burden on Oil and Gas Extraction,"* The Energy Journal, 1987 Vol. 8, No. 4, pp. 51-64.
23. Mandl, G. and Volek, C.W.: *"Heat and Mass Transport in Steam-Drive Processes,"* Transactions of AIME 1969 Vol. 246, pp. 59-79.
24. Marks, Roger and Moore, J. William: *"A Model to Assess Economic Feasibility and Optimum Production Volume for North Slope Fields,"* Journal of Petroleum Technology, Aug. 1987, pp. 943-954.
25. Marx, J.W. and Langenheim, R.H.: *"Reservoir Heating by Hot Fluid Injection,"* Transactions of AIME 1959 Vol. 216, pp. 312-315.

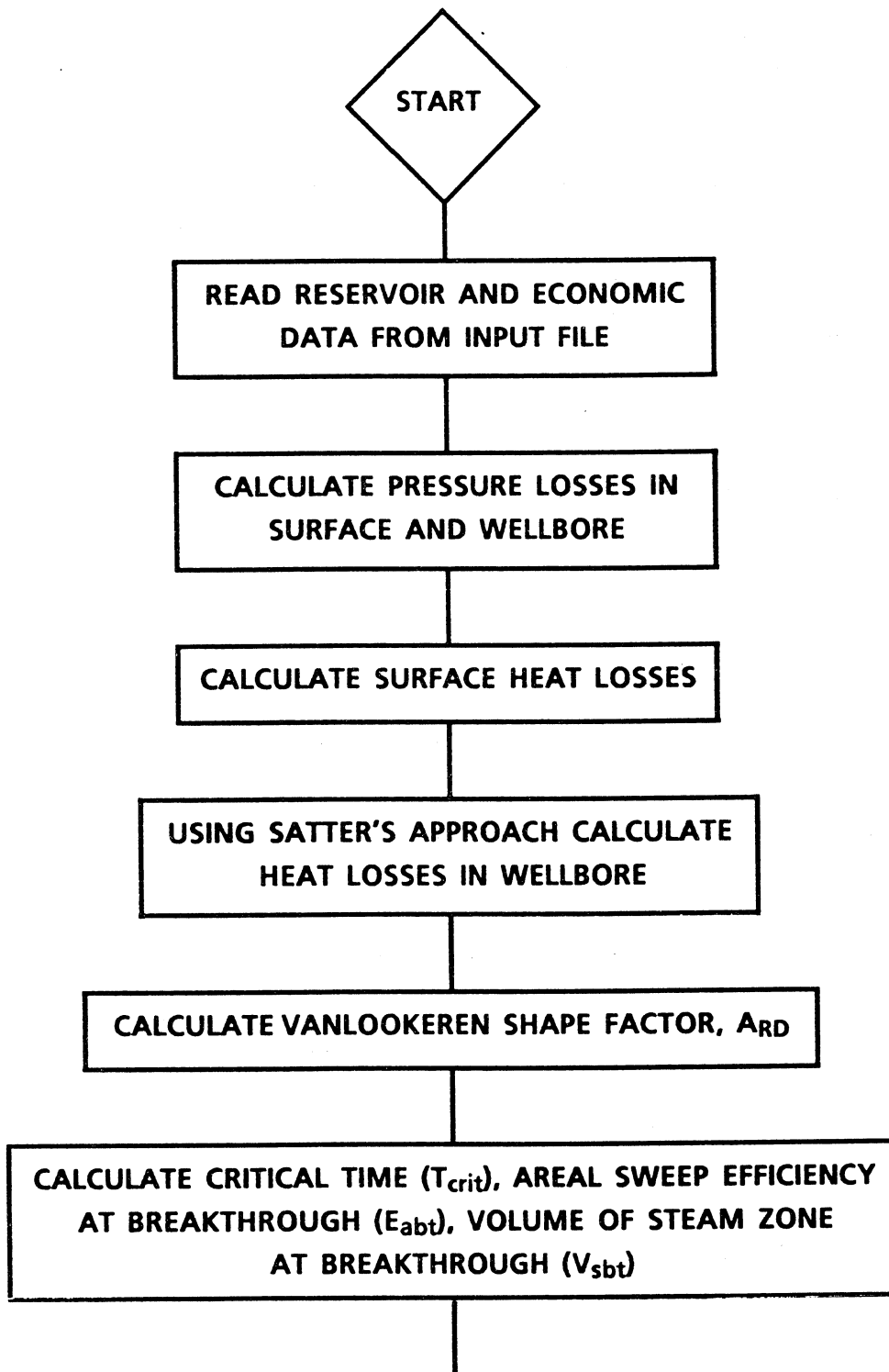
26. Matthews, C.S.: *"Steamflooding,"* Journal of Petroleum Technology, Mar. 1983, pp. 465-470.
27. Miller, M.A. and Leung, W.K.: *"A Simple Gravity Override Model of Steamdrive,"* SPE 14241, 60th Annual Technical Conference and Exhibition SPE Las Vegas, NV, Sept. 22-25, 1985.
28. Myhill, N.A. and Stegemeier, G.L.: *"Steam Drive Correlation and Prediction,"* Journal of Petroleum Technology, Feb. 1978, pp. 173-182.
29. Neuman, C.H.: *"A Gravity Override Model of Steamdrive,"* Journal of Petroleum Technology, Jan. 1985, pp. 163-169.
30. Newnan, Donald G.: Engineering Economic Analysis, Engineering Press, Inc. 1988.
31. Panda, Manmath Nanda: *"Reservoir Description and a Feasibility Study of Enhanced Oil Recovery Applications to West Sak Field,"* M.S. Thesis, University of Alaska Fairbanks, Dec. 1988.
32. Prats, Michael: Thermal Recovery - Monograph Vol. 7 American Institute of Mining, Metallurgical, and Petroleum Engineers Inc. 1982.
33. Ramage, W.E., Castanier, and L.M., Ramey, H.J. Jr.: *"Economic Evaluation of Thermal Recovery Projects,"* SPE 16852 62nd Annual Technical Conference and Exhibition of SPE Dallas, TX, Sept. 27-30, 1987.
34. Ramey, H.J. Jr.: *"Discussion of Reservoir Heating by Hot Fluid Injection,"* Transactions of AIME, 1959 Vol. 216, pp. 364-365.
35. Rhee, Shie W. and Doscher, Todd M.: *"A Method for Predicting Oil Recovery by Steamflooding Including the Effects of Distillation and Gravity Override,"* Society of Petroleum Engineers Journal, Aug. 1980, pp. 249-266.
36. Satter, Abdus: *"Heat Losses During Flow of Steam Down a Wellbore,"* Journal of Petroleum Technology, Dec. 1968, pp. 55-61.

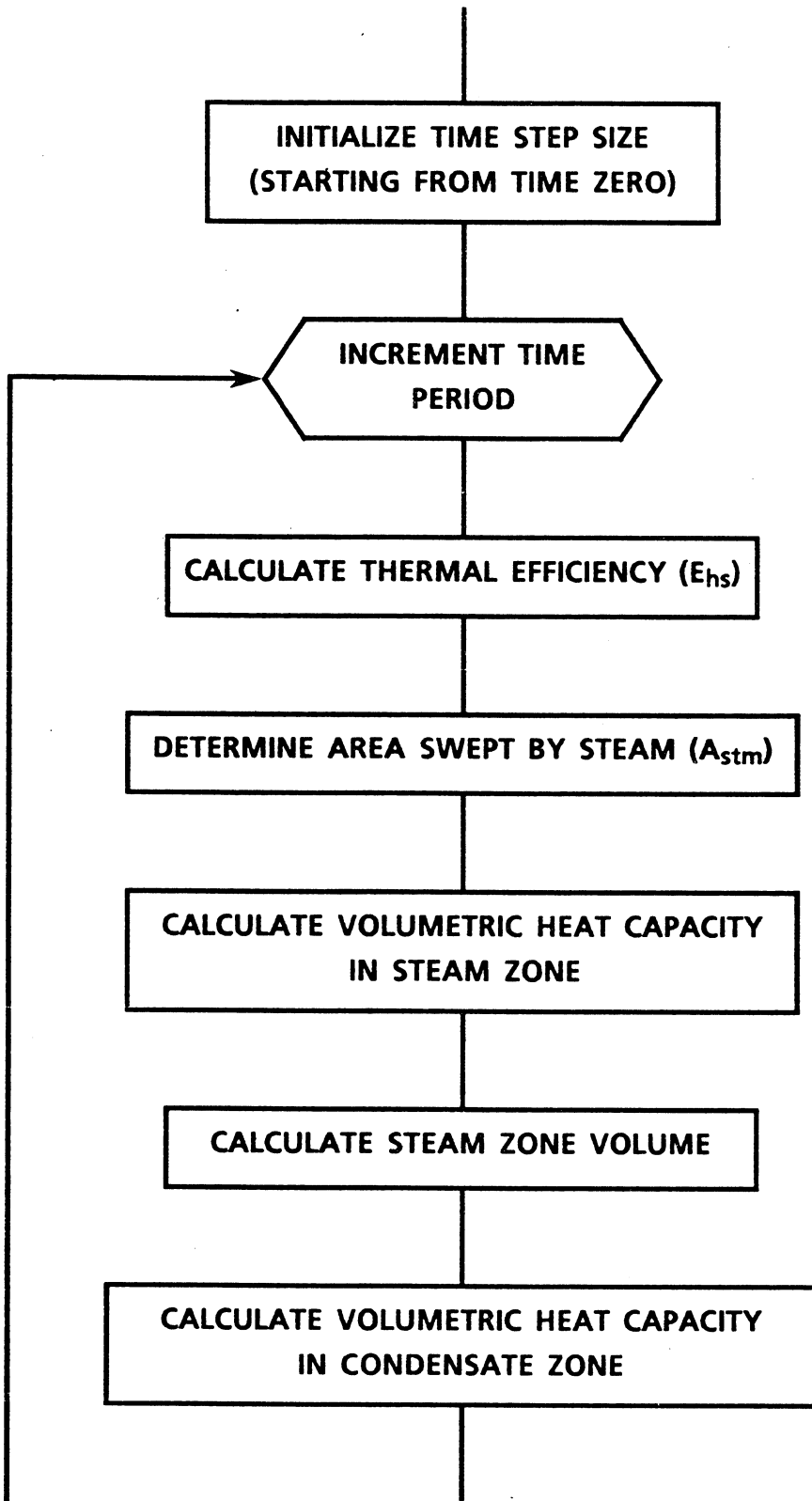
37. Satter, A. and Parrish, D.R.: "A Two-Dimensional Analysis of Reservoir Heating by Steam Injection," Society of Petroleum Engineers Journal, June 1971, pp. 185-197.
38. Shutler, N.D.: "Numerical Three-Phase Simulation of the Linear Steamflood Process," Society of Petroleum Engineers Journal, June 1969, pp. 232-246.
39. Shutler, N.D.: "Numerical Three-Phase Model of the Two-Dimensional Steamflood Process," Society of Petroleum Engineers Journal, Dec. 1970, pp. 405-417.
40. Spillette, A.G.: "Heat Transfer During Hot Fluid Injection Into an Oil Reservoir," Journal of Canadian Petroleum Technology, Oct. - Dec. 1965, p. 213.
41. Spillette, A.G. and Nielsen, R.L.: "Two-Dimensional Method for Predicting Hot Waterflood Recovery Behavior," Journal of Petroleum Technology, June 1968, pp. 627-638.
42. Standing, M.B.: Volumetric and Phase Behavior of Oil Field Hydrocarbon Systems, Dallas: Society of Petroleum Engineers of AIME, 1981.
43. van Lookeren, J.: "Calculation Methods for Linear and Radial Steam Flow in Oil Reservoirs," Journal of Petroleum Technology, June 1985, pp 427-439.
44. Vogel, J.V.: "Simplified Heat Calculations for Steamfloods," Journal of Petroleum Technology, July 1984, pp. 1127-1136.
45. Weinstein, H.G., Wheeler, J.A., and Woods, E.G.: "Numerical Model for Thermal Processes," Society of Petroleum Engineers Journal, Feb. 1977, pp. 65-78.
46. Williams, Bob: "ARCO Maps Plans for West Sak Thermal Project," Oil and Gas Journal, Nov. 7, 1983, p. 78.
47. Williams, R.L., Ramey, H.J. Jr., Brown, S.C., and Sanyal, S.K.: "An Engineering Economic Model for Thermal Recovery Methods," SPE 8906 50th Annual California Regional Meeting, Los Angeles, CA, April 9-11, 1980.

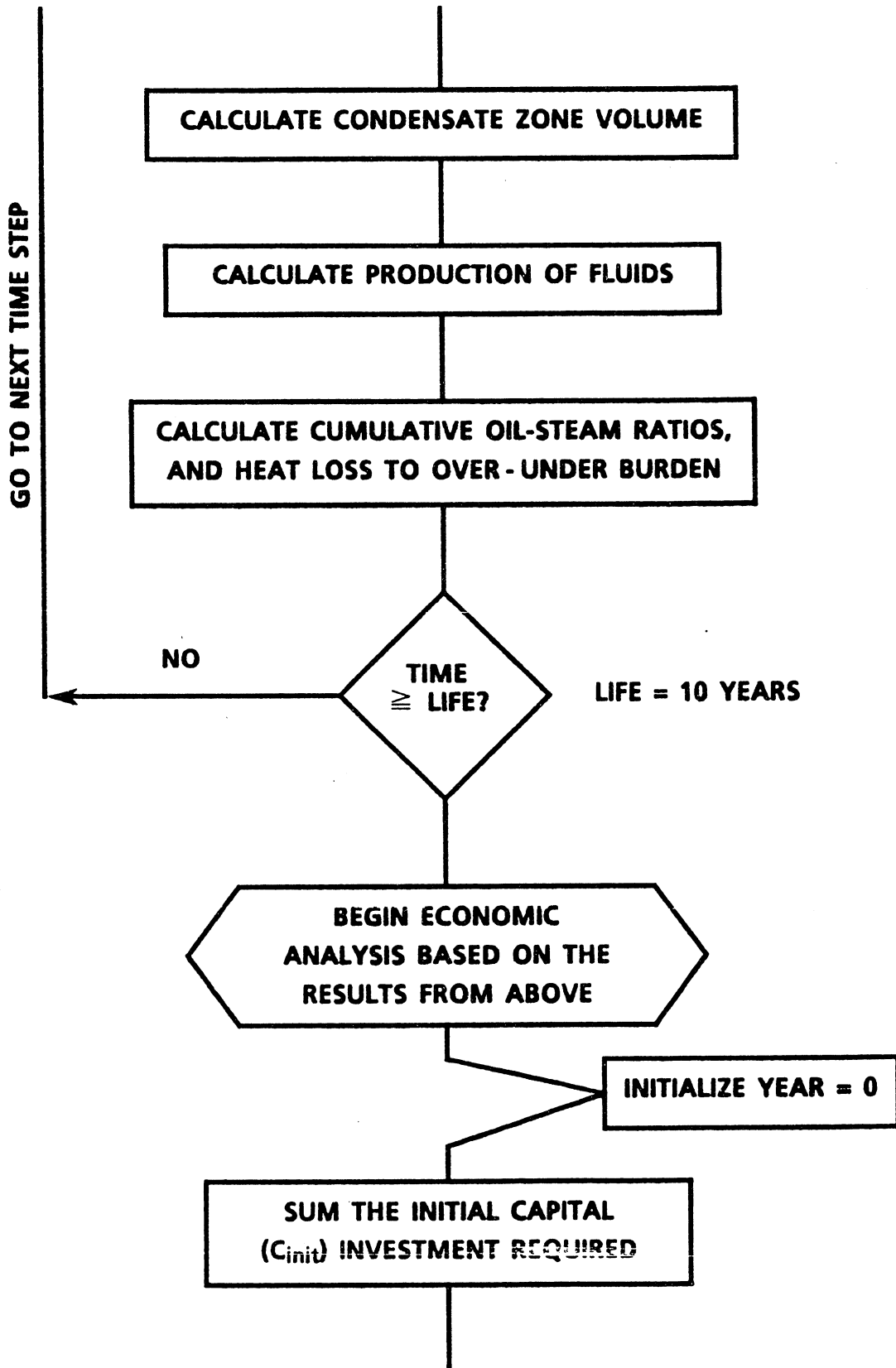
48. Willman, B.T., Valleroy, V.V., Rumberg, G.W., Cornelius, A.J., and Powers, L.W.:
"Laboratory Studies of Oil Recovery by Steam Injection," Journal of Petroleum
Technology, July 1961, pp. 681-690.

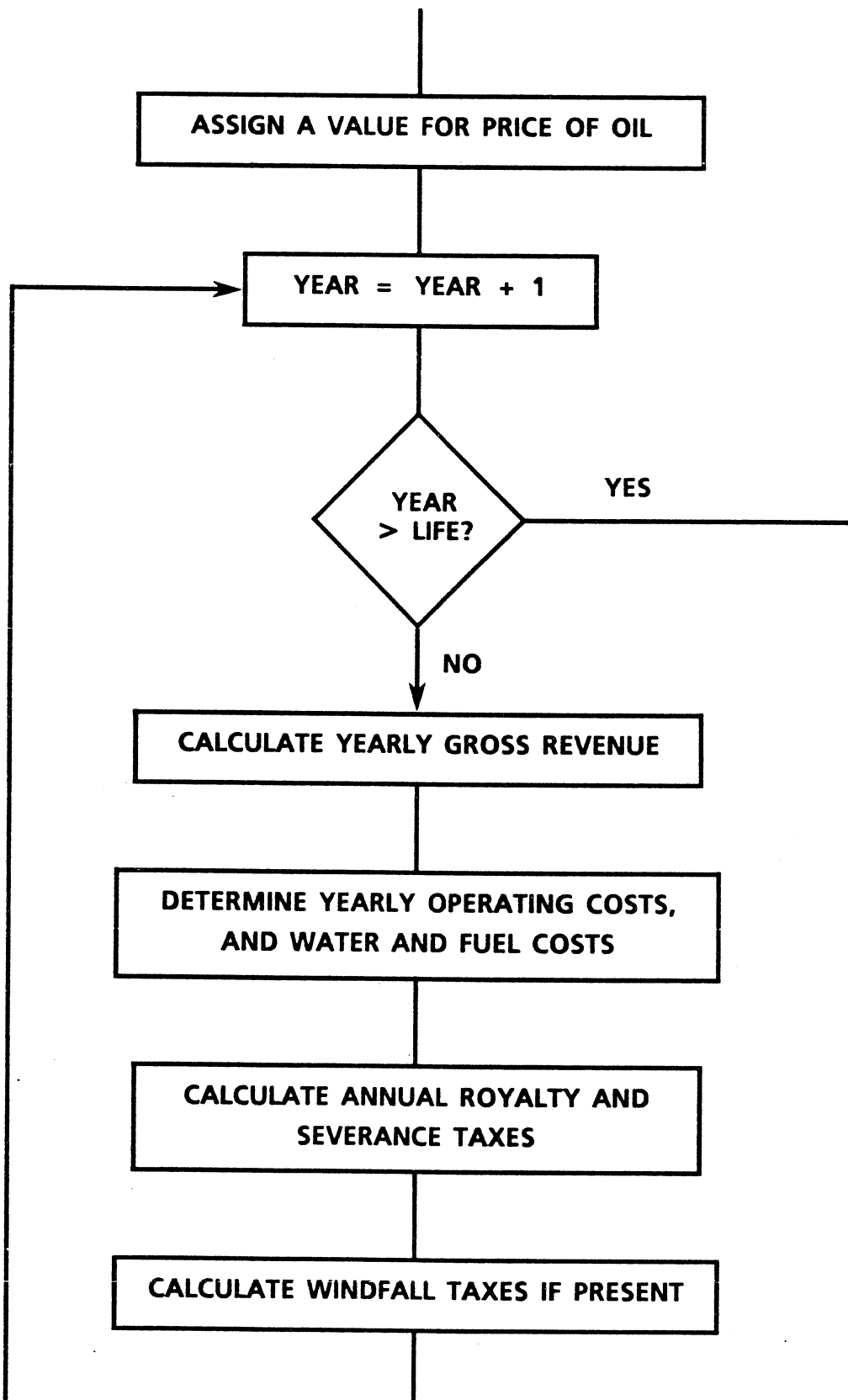
G. APPENDIX

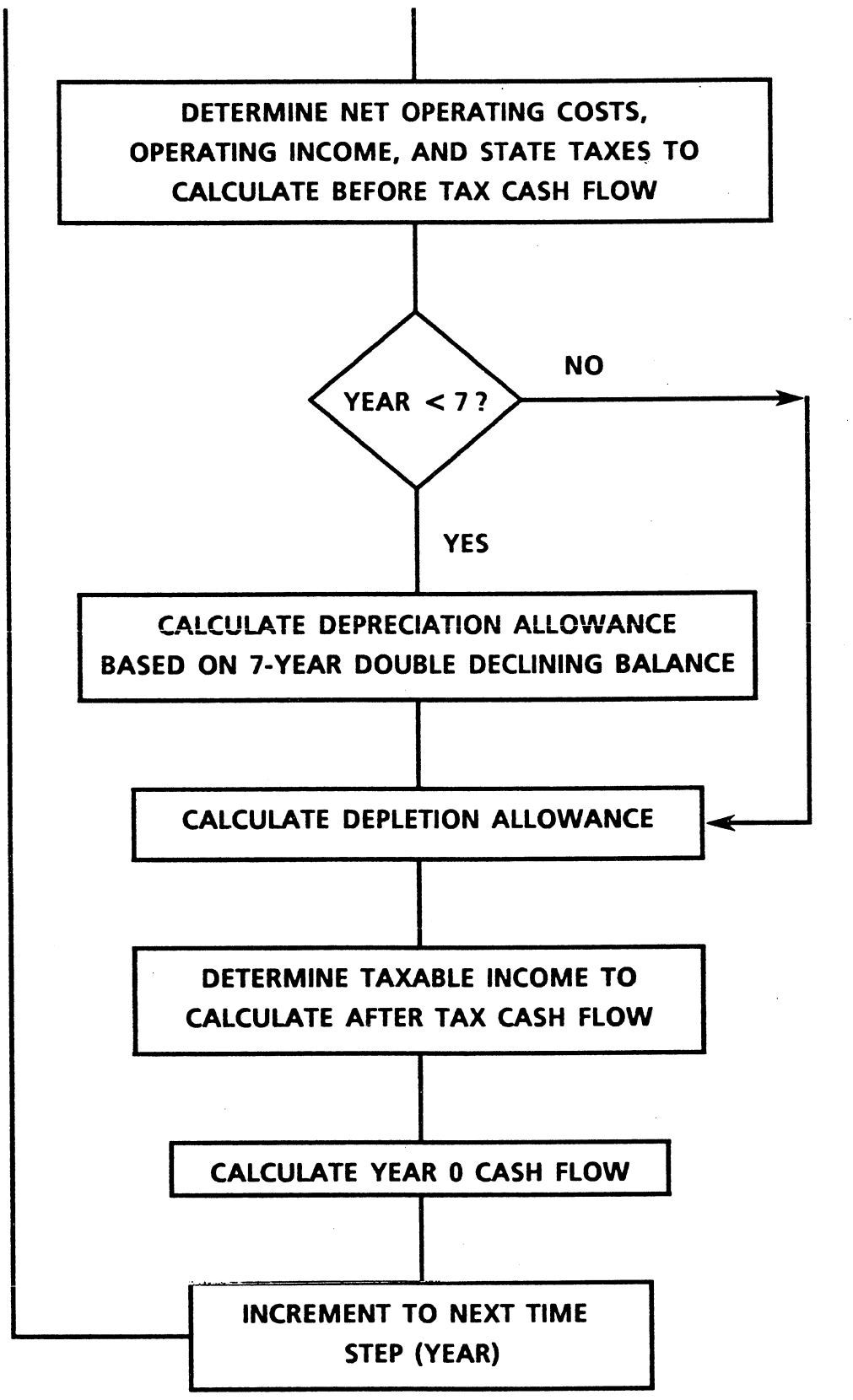
FLOWCHART OF MODEL

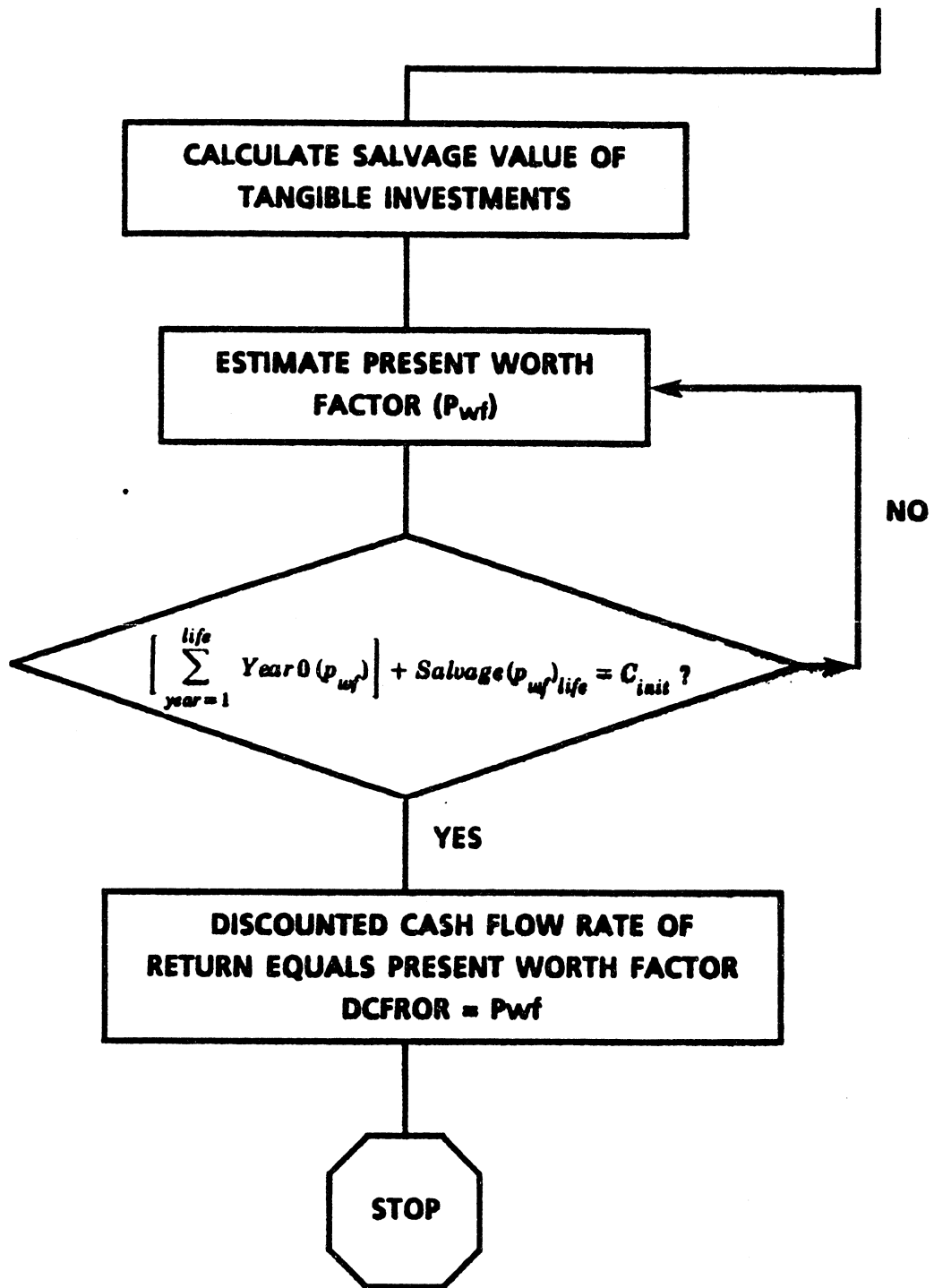












CHAPTER FIVE
STEAM-SOLVENT DISPLACEMENT STUDIES

A. ABSTRACT

High pressure one-dimensional laboratory displacement studies were undertaken to evaluate the effects of carbon dioxide addition to steam on the recovery of West Sak crude oil. To concentrate the study on how carbon dioxide affects recovery the volumetric flow rate for each run was held constant. As a base case only steam was injected in the first run and in subsequent runs the CO₂/steam ratio was varied. Furthermore, effect of solvents such as nitrogen and methane with steam was investigated as a means for improving oil recovery from West Sak sands.

The results indicate that the addition of CO₂ to steam increases ultimate recovery, increases rate of recovery and decreases the heat input required. The results also indicate there is an optimum CO₂/steam concentration. A 1:1 molar ratio increases recovery by 5.5% and a 1:3 molar ratio increases recovery by 12.8%. Holding the CO₂/steam molar ratio constant at 1:3 and decreasing the injection temperature to its dew point temperature resulted in no significant change in recovery. The results also indicate that 1:3 nitrogen/steam molar ratio increases recovery by 2.8% and 1:4 nitrogen/steam molar ratio increases recovery by 8% as compared with conventional steam displacement. A 1:3 methane/steam molar ratio increases recovery by 13.4%. Holding the methane/steam or water molar ratio constant at 1:3 and decreasing the injection temperature below its dewpoint temperature resulted in significant change in recovery.

B. INTRODUCTION

The state of Alaska contains 25 to 40 billion barrels of heavy oil of which 15 to 25 billion barrels lie in the West Sak reservoir, making it one of the largest oil fields (super giant potential (ARCO, 1983)) in North America. The West Sak reservoir is

located on the North Slope of Alaska approximately 250 miles north of the Arctic circle. More specifically, it lies west of Prudhoe Bay Unit in the Kuparuk River Unit. Due to the close proximity of the permafrost zone the average reservoir temperature ranges from 45° to 100°F making the oil quite viscous.

Alaska, also, contains large reserves of natural gas; Prudhoe Bay has approximately 29 trillion SCF of gas in place (Sharma et al., 1988) of which 12.5% is carbon dioxide. Because of the large reserves of heavy oil, natural gas for generating steam and carbon dioxide it was decided to study what effects the addition of carbon dioxide to steam has on recovery of West Sak crude oil. The literature indicates that the addition of carbon dioxide to steam improves ultimate recovery and recovery rate. If recovery of West Sak crude oil can be increased by even 2% then the incremental production can be as high as 200 to 250 million barrels.

The pioneering experimental study on steamflooding was performed by Willman et al (1961). The experiments were conducted in a linear displacement cell and were designed to determine the steam drive recovery mechanisms. They concluded that the principle steam flooding recovery mechanisms are:

1. Viscosity reduction
2. Thermal expansion
3. Solvent extraction
4. Steam distillation
5. Gas drive.

There are three principle and distinct zones in the steamflooding process: the saturated steam zone, hot water zone and the cold oil zone. In the saturated steam region oil displacement is enhanced by all five of the recovery mechanisms. In the condensation zone oil displacement is enhanced by solvent extraction, viscosity reduction and thermal extraction. In the hot water zone oil displacement is

enhanced by viscosity reduction and thermal expansion. Lo and Mungan (1973) showed that oil displacement is also enhanced by the increasing relative permeability to oil with increased temperature.

Carbon dioxide flooding displaces oil from the porous media by either miscible or immiscible drive mechanisms. Although the pressure and amount of carbon dioxide required for miscible displacement of heavy oils is too high it can be recovered by immiscible displacement. The mechanisms of immiscible carbon-dioxide flooding are:

1. Oil swelling
2. Viscosity reduction
3. Solution gas drive
4. Trapped gas effect.

Oil swelling and viscosity reduction are due to the high solubility of carbon dioxide in crude oil and both mechanisms increase the recovery efficiency. Some oil is also recovered by the trapped gas effect, which occurs because the injection of carbon dioxide creates a free gas phase which displaces a part of the residual oil.

In this experimental study, these two promising enhanced oil recovery processes, steam and immiscible carbon dioxide flooding were combined. The purposes of the study was to evaluate the feasibility of adding carbon dioxide to steam on recovery of West Sak crude oil.

C. STEAM-SOLVENT DISPLACEMENT APPARATUS

A schematic of the experimental apparatus is shown in Figure 1. Two constametric pumps were used in these experiments to supply a constant flow rate of water and CO₂ when needed. One was used to supply water for the steam generator and the other was used for injecting CO₂ into the waterline before the steam generator. One positive displacement pump was used to fill the transfer cells with CO₂ before injection.

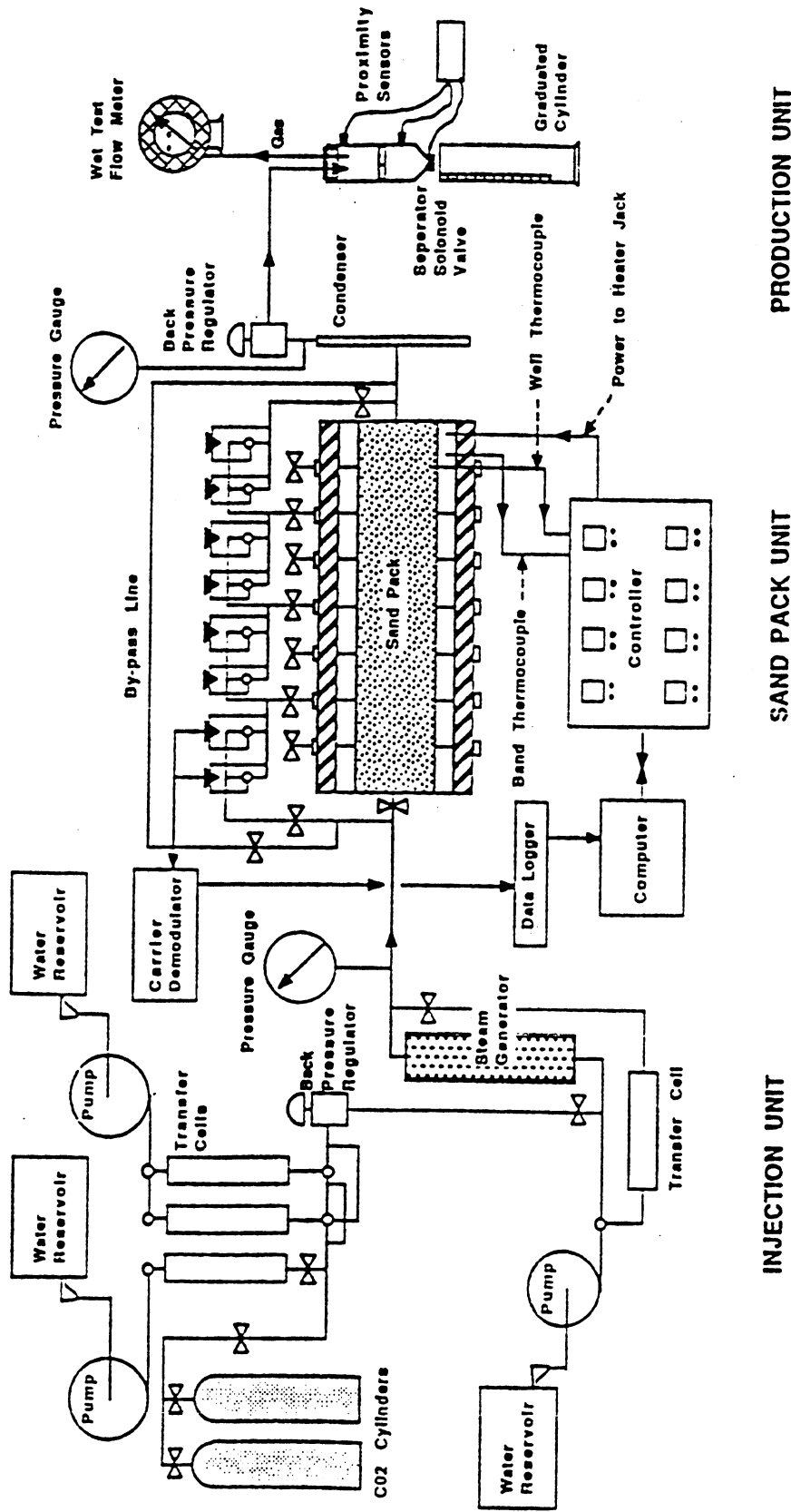


Figure 1: Schematic of the Steam/Solvent Flood Apparatus

The steam generator was 8.5 inches long, 2.25 inches outside diameter and 1.0 inch inside diameter, made of 316 stainless steel. Heat was supplied by two 6.25 amp 240 volt band heater and controlled by a control unit which measures the temperature at the thermocouple and supplies power to the band heaters depending on the set point temperature. One transfer cell was used to displace oil into the sand pack by pumping water on one side of the piston and pushing oil out on the other end. The other cells were used to inject CO₂ into the water stream.

The steam tube was four feet long and has an inside diameter of two inches and is constructed of 316 stainless steel. End caps are screwed into each end and sealed with silver plated C-ring seals. There are eight thermocouples at six inch intervals with the first at the inlet, and seven differential pressure transducers at six inch intervals. Eight 6.25 amp 240 volt band heaters with thermocouples surround the steam tube which heat the sand pack according to the controller set point. One inch of Manvel Cerawool insulation is wrapped around the band heaters and protected by a stainless steel shell. The stream tube is rated for 5000 psi and 800°F. The control unit receives the thermocouple signals and supplies power to the band heaters.

The oil, water and gas separator used, consists of a glass cylinder which is fitted with a rubber stopper in the top and a solenoid valve at the bottom. The production line from the sand pack is run through the rubber stopper allowing the effluent to flow into the separator. A second line is run through the stopper allowing the gas to flow out through a wet test flow meter. Two proximity sensors are positioned along the side of the separator to sense a metallic float which is placed in the separator to float in the fluid. When the float rises to the top sensor, the solenoid valve will open allowing the fluid to drain into graduated cylinders. When the float reaches the bottom sensor the solenoid valve will close allowing the separator to begin filling

again. The sensors can be adjusted to accommodate any volume between 40 and 500 cc.

A data logger coupled with a personal computer receives analog data from the differential pressure transducers and the steam flow line thermocouples and converts it to digital data for the personal computer. A computer program was written which can access both the computer board (which receives the thermocouple signal and was an analog to digital converter) and the data logger hardware, simultaneously recording the temperature at the thermocouples and the differential pressure at preselected time intervals.

D. STEAM DISTILLATION APPARATUS

The injection and the production units of the flooding apparatus were used along with a 500 cc distillation cell and a trap to prevent the entrainment of crude to conduct the distillation experiments. The distillation cell and the trap were positioned in a mechanical convection oven for temperature control.

E. DENSITY MEASUREMENT APPARATUS

The change in the density of crude oil and the produced samples from a steamflood run was measured by an apparatus shown in Figure 2. CO₂ and oil were brought in contact in a 10 cc stainless steel cylinder. The density of CO₂ saturated oil sample was measured with Paar - Mettler digital density meter. The system pressure was controlled by a Ruska mercury positive displacement pump. The cylinder was placed in an oil bath for temperature control. The oil from the bath was circulated around the density meter tube to keep it at the same temperature as the sample cylinder. The temperatures in the bath and in the line were monitored by two thermocouples.

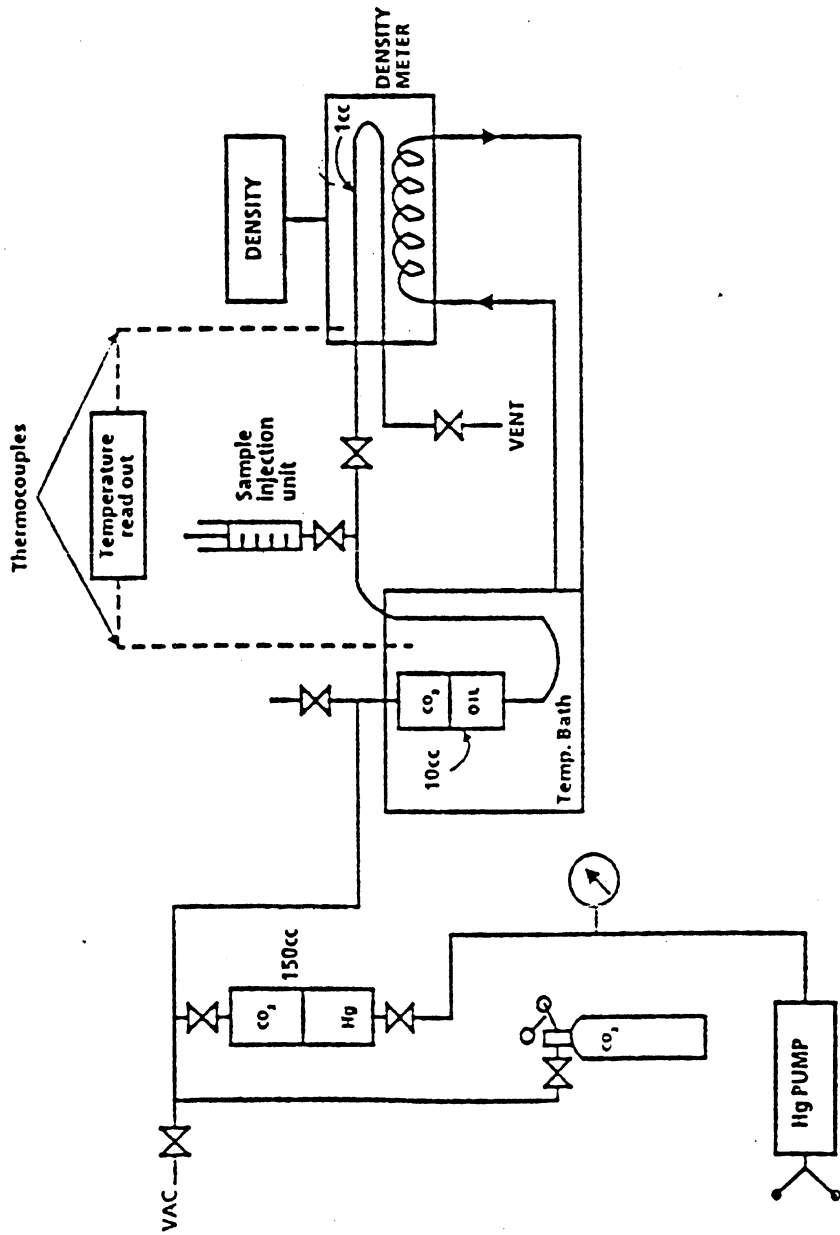


Figure 2: Schematic of the Density Measurement Apparatus

F. EXPERIMENTAL PROCEDURES

The sand used for the sand pack was Oklahoma number one fluid loss control sand supplied by Halliburton, Inc. The crude oil used in all runs was from the West Sak reservoir and was supplied by one of the North Slope operators. Table 1 shows a summary of the crude oil properties and the reservoir condition at the sampling depth. Since the gas composition from West Sak was 98% methane, it was decided to resaturate the dead oil sample with 99% pure commercial methane. Table 2 shows the compositions of dead oil and resaturated oil.

The steam tube was packed with sand and saturated with water. The West Sak dead oil sample was resaturated with methane at reservoir pressure and temperature and was injected into the sand pack while the back pressure was set to the bubble point pressure. Water or different ratios of water and liquid CO₂ were injected with constant rate into the steam generator. The produced vapor from the outlet of the generator was injected into the sand pack and the data acquisition system was activated to record pressures and temperatures along the steam tube at specified periods of time. The produced liquid samples were collected and set aside for separation and analysis.

The steam tube was packed with sand and saturated with water. The West Sak dead oil sample was resaturated with methane at reservoir pressure and temperature and was injected into the sand pack while the back pressure was set to the bubble point pressure. Water or different ratios of water and liquid CO₂ were injected with constant rate into the steam generator. The produced vapor from the outlet of the generator was injected into the sand pack and the data acquisition system was activated to record pressures and temperatures along the steam tube at specified periods of time. The produced liquid samples were collected and set aside for separation and analysis.

TABLE 1
West Sak Crude Oil Properties

Sampling depth	4603 ft.
Reservoir temp.	80°F
Bubble point (B.P.)	1690 psi
Oil gravity	19.2°API
Oil density @ B.P.	.9022 g/cc
Solution GOR @ B.P.	210 scf/stb
Viscosity @ B.P. and 80°F	35.4 cp
Oil FVF	1.069 bbl/STB
Gas composition	98% methane

TABLE 2
Compositions (Mol%) of Recombined and
Dead West Sak Crude

Component	Recombined West Sak Crude	Dead Oil
N ₂	0.03	-
CO ₂	0.02	-
C ₁	38.33	-
C ₂	0.86	-
C ₃	0.36	-
C ₄	0.18	-
C ₅	0.06	-
C ₆	0.20	-
C ₇	0.02	1.27
C ₈	0.01	1.05
C ₉	0.82	1.35
C ₁₀	1.50	1.47
C ₁₁	1.72	1.94
C ₁₂	0.35	1.97
C ₁₃	0.50	2.49
C ₁₄	0.80	2.67
C ₁₅	0.94	2.30
C ₁₆	0.80	2.35
C ₁₇	0.57	2.80
C ₁₈	1.80	2.55
C ₁₉	2.47	2.44
C ₂₀	2.84	1.90
C ₂₁ +	38.82	70.04
Mol. wt of + Fraction	455	

In order to be able to compare the results from different runs (steam or different ratios of steam and CO₂), the gas volumetric flow rate at the injection side was held constant.

Using a phase behavior package with the Chao-Sader equation of state, flow rates into the generator were calculated to deliver the desired vapor flow rate.

A total of ten flooding experiments were conducted. In the first two runs steam only was injected at 660°F. The sand pack was completely saturated with oil and connate water in the first case (run 1), but an additional free gas phase was present in the second case. The rest of the experiments were CO₂/steam runs with different molar ratios of CO₂ to water. The vapor flow rate for all these experiments was kept constant and equal to vapor flow rate of run 1. The calculated vapor flow rate for run 1 was 144.3 cc/min of steam at 660°F and 1690 psi back pressure (equivalent to 8 cc/min of water at 60°F and atmospheric pressure).

Table 3 shows experimental variables. The CO₂/steam runs were conducted with 1:1, 1:3, and 1:4 molar ratios of CO₂ to water. Except for the run with 1:1 molar ratio which was conducted only at 660°F, the rest of these experiments were conducted at both 660°F and a temperature close to but higher than the saturation temperature of the mixture.

Three distillation experiments were conducted: one with steam alone at 660°F (Run Distillation 1); one with 1:3 molar ratio of CO₂ to water at 660°F (Run Distillation 2); and the last with 1:3 molar ratio at 570°F (Run Distillation 3). In all distillation experiments the volume of crude sample used was 200 cc and the experiments were conducted with vapor flow rate equal to steam flow rate (i.e. about 43 cc/min or 2.5 cc/min of water at 60°F and atmospheric pressure). A back pressure of 1690 psi was always imposed on the system.

TABLE 3
Flooding Experimental Variables

Run #	Injection Temperature °F	Back Pressure	Solvent/Water Molar Ratio	Vapor Vol. Flow Rate	S _{oi}	S _{gi} %
CO₂						
1	660	1690	0:1	144.3	89.1	0
2	660	1690	0:1	144.3	77.5	11.2
3	660	1690	1:1	144.3	88	0
4	660	1690	1:3	144.3	89.1	0
5	660	1690	1:4	144.3	90.8	0
6	570	1690	1:3	144.3	88.1	0
7	572	1690	1:4	144.3	89.9	0
NITROGEN						
8	590	1690	1:4	144.3	85.3	0
9	580	1690	1:3	144.3	90.4	0
METHANE						
10	550	1690	1:3	144.3	83.8	0
11	570	1690	1:3	144.3	88.5	0

The density of gas free or CO₂ saturated oil samples of the produced oil from steam run 1, were measured at 100°, 150°, and 212°F. The oil samples were saturated with CO₂ at 1650 psig.

G. RESULTS AND DISCUSSION

G1. Steam Injection Only Runs

In experimental run 1 steam only was injected at 8 cc/min. water equivalent and 660°F. This experiment was conducted as a standard for comparison for all other experimental runs. The cumulative recovery for this run after six pore volumes of injection was 77.2%.

In run 2 steam only was injected in the presence of an initial gas phase saturation to investigate the effect of a free gas phase on recovery. The initial gas saturation for the run was 11.2% and steam was injected at 8 cc/min. water equivalent. Cumulative recovery after six pore volumes of injection for the run was 53.1%, significantly less than the case when no gas phase was present. Figures 3 and 4 compare the cumulative recovery and water oil ratio versus pore volumes injected for these two runs. The increase in cumulative water oil ratio in run 2 shows the bypassing of oil by steam and reduction of recovery efficiency in the presence of a free gas phase.

G2. Carbon Dioxide - Steam, Nitrogen-Steam, Methane-Steam, Injection Runs

By maintaining the volumetric flow rate constant for the steam base case and the CO₂/steam experiments, the effect of CO₂ addition could be studied. Pore volume injected in all the CO₂/steam runs was calculated by finding the equivalent pore volumes of water injected to give the same volume of steam at 660°F and 1650 psi as the volume of mixture vapor injected. For run 3, CO₂ was injected with the steam at a 1:1 molar ratio. This resulted in an increase in recovery of 4.3% over the conventional steam flood after six pore volumes of

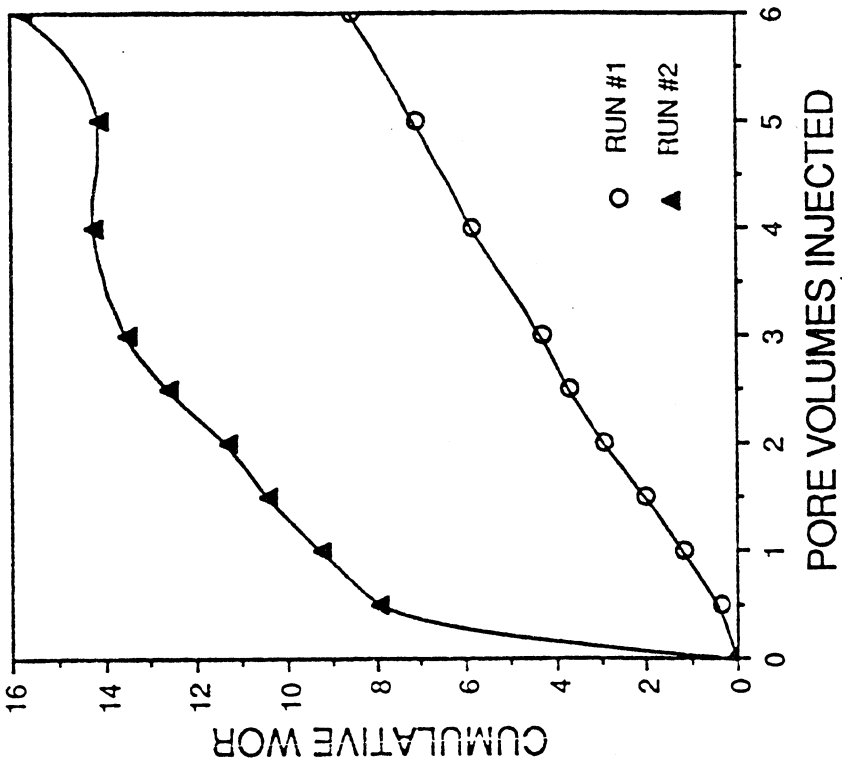


Figure 3: Cumulative Recovery vs. Pore Volumes Injected (Equivalent Water)

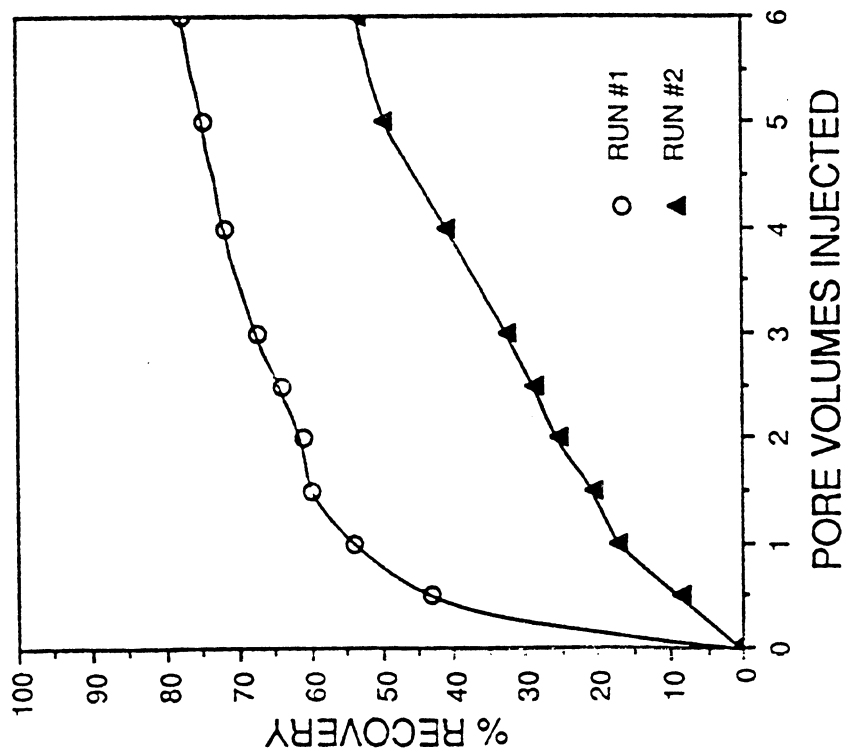


Figure 4: Cumulative Water/Oil Ratio vs. Pore Volumes Injected

injection. For run 4 the CO₂/steam molar ratio was reduced to 1:3. This resulted in an increase in recovery of 12.8% over a conventional steam flood. For run 5 CO₂/steam molar ratio was further reduced to 1:4. The cumulative recovery after six pore volumes for this run was 92%. This shows an increase of 14.8% over steam flood. Cumulative recoveries and water oil ratios versus pore volume injected for run 3, 4, and 5 are compared with those of run 1 in Figures 5 and 6 respectively. These results indicate that there is an optimum CO₂ steam ratio for maximizing recovery. This could be due to two reasons: (1) there is a finite amount of CO₂ that can dissolve in the crude oil and (2) after the crude oil has become saturated with CO₂ the addition of more CO₂ has relatively little beneficial effects and is associated with lower heat injection and thus decreased viscosity reduction.

G2.1 Reduction of Steam Injection Temperature

In run 6 the CO₂/steam molar ratio was held at 1:3 but the steam injection temperature was reduced to the dew point temperature. The recovery for this run after six pore volumes was almost the same as run 4. This is due to the fact that most of the heat is latent heat of vaporization and that superheating the steam has little effect on recovery. The enthalpy of the saturated vapor at 570°F is 1182.8 BTU/lb and superheating the steam to 660°F increases the enthalpy of the vapor to only 1276.5 BTU/lb. Of the total heat injected 575.2 BTU/lb is sensible heat, 607.6 BTU/lb is latent heat and 93.7 BTU/lb is the heat injected due to superheating the steam by 90°F. It is obvious from these numbers that the most effective way of inputting heat into the sand pack is by injecting steam because most of the heat is latent heat and relatively little is gained by superheating the steam.

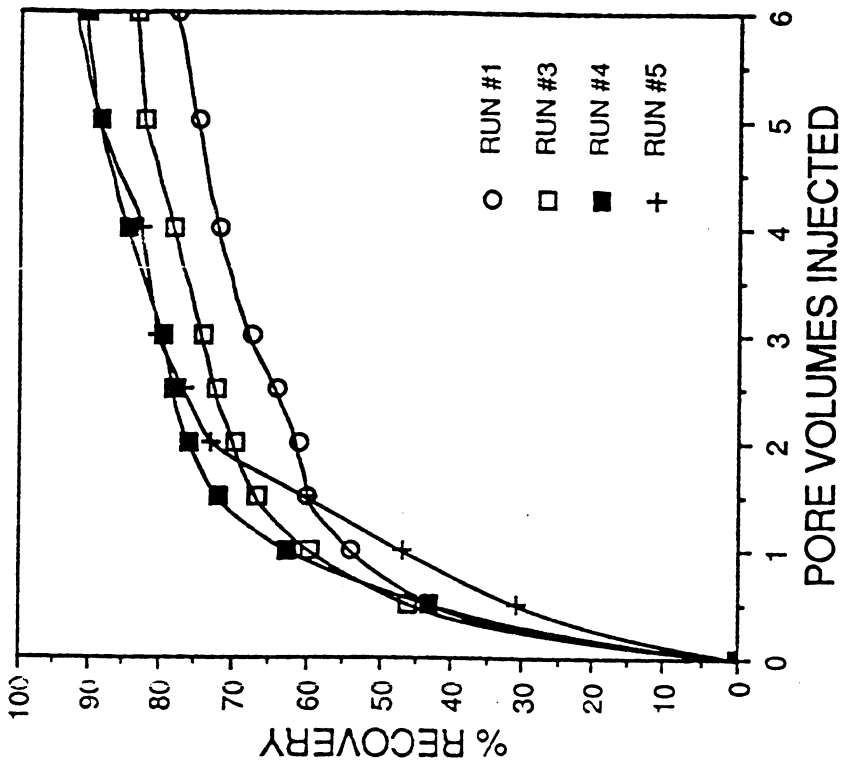


Figure 5: Cumulative Recovery vs. Pore Volumes Injected for Steam and High-Temperature CO₂/Steam Runs (Runs 1, 3, 4 and 5)

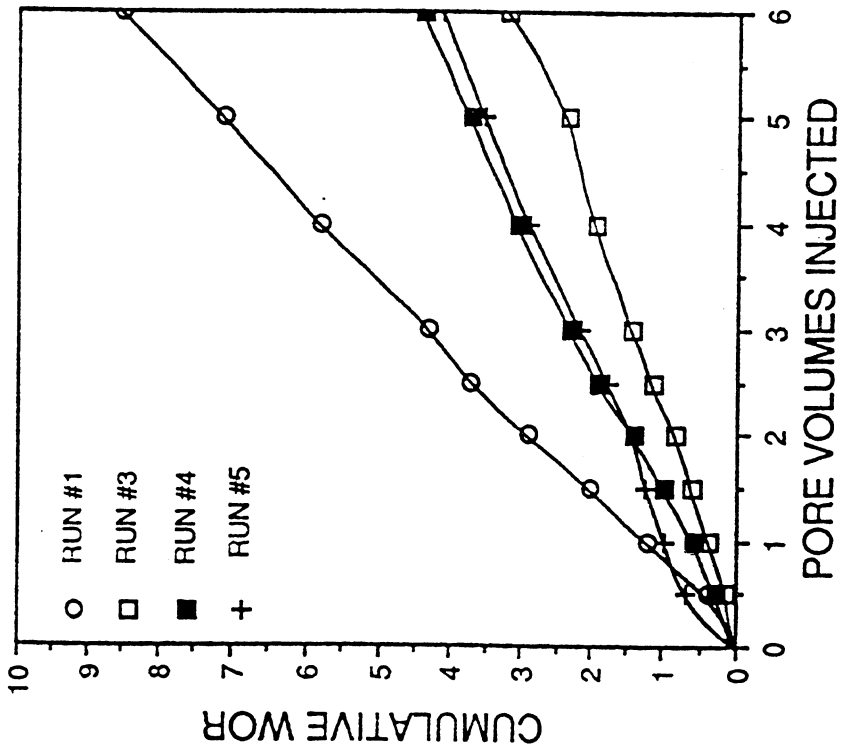


Figure 6: Cumulative Water/Oil Ratio vs. Pore Volumes

The further reduction of molar ratio at this temperature to 1:4 (run 7) caused the recovery after six pore volumes to decrease to 80.2%. Figures 7 and 8 show the comparison between cumulative recovery and water oil ratio curves for runs 4, 5, 6, and 7. These figures show that the best combination of heat and CO₂ among these experiments is run 6.

The flooding experiments show that simultaneous injection of CO₂ with steam will definitely increase the ultimate recovery over steam, and that there is an optimum ratio of CO₂ to steam which should result in the highest recovery. The second objective of this study was to investigate the effects of CO₂ addition on steamflood mechanisms and their impact on this increase in recovery.

G2.2 Effect of CO₂ on Steam Distillation

The results from three distillation experiments are shown in Figure 9. Yield as percentage of initial oil in cell (200 cc) is plotted against cumulative volume of water condensed as a fraction of initial volume of oil. These experiments show that at V_w/V_{oi} of 1.5, the yield for the 1:3 molar ratio mixture at 660°F (Distillation Run 2) is about 15% higher than the case for steam alone at 660°F (Distillation Run 1). The dissolved CO₂ in oil tends to replace some of the intermediates in the oil and as a result sends more hydrocarbon intermediates into the vapor phase than in the case of steam alone. The yield for 1:3 molar ratio at a temperature of 570°F (Distillation Run 3) and V_w/V_{oi} of 1.5 is only about 3.7% lower than steam alone at 660°F. This shows that by adding CO₂ and reducing temperature one can still gain almost the same amount of movement of hydrocarbons to the vapor phase.

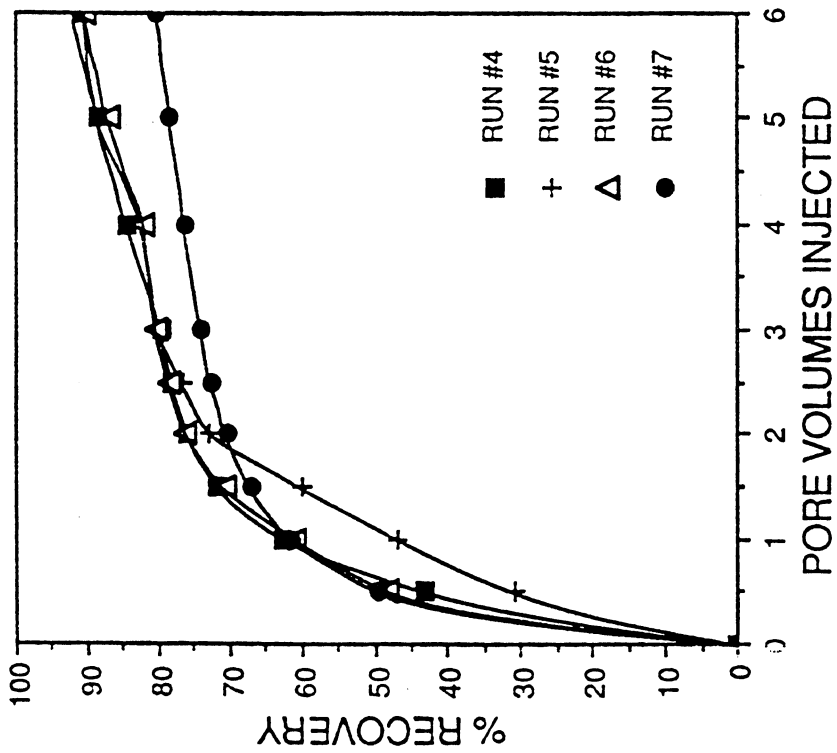


Figure 7: Cumulative Recovery vs. Pore Volumes Injected for High-Temperature and Low Temperature CO₂/Steam Runs (Runs 4, 5, 6 and 7)

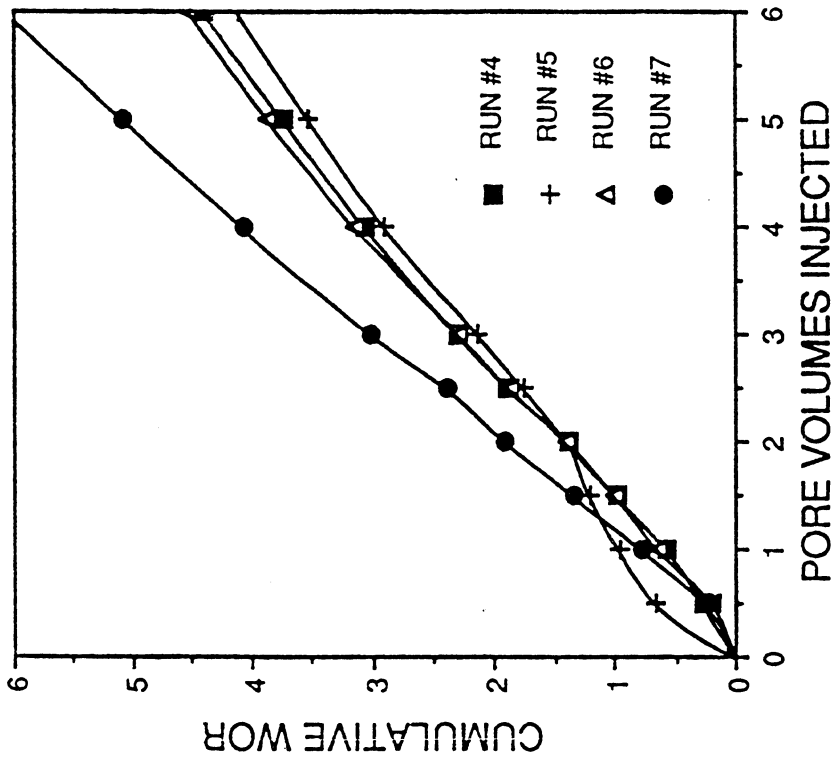


Figure 8: Cumulative Water/Oil Ratio vs. Pore Volumes Injected

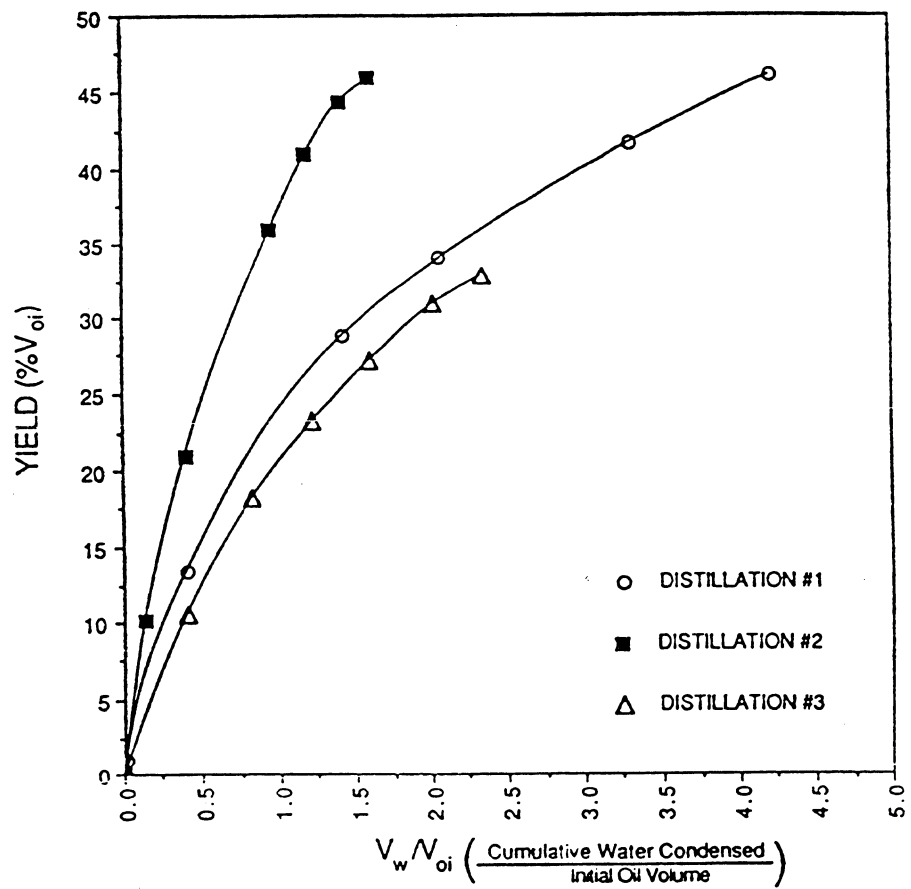


Figure9: Distillation Experiments for Steam and High-and-Low-Temperature 1:3 Molar Ratio of CO_2 /Steam

G2.3 Compositional Analysis of Produced Oil

The produced oil samples from runs 1, 5, and 7 were analyzed for comparison. The detailed analysis of samples of oil taken from batches of produced fluid after demulsification and separation from gas and water for runs 1, 5 and 7 are shown in Tables 4, 5 and 6 respectively. Also a comparison of percentage of C_7 - C_{17} and C_{18} - C_{21} for these runs are shown in Figures 10 and 11 respectively.

A close examination of Figure 10 shows that for run 1 (steam alone), the percentage of C_7 - C_{17} increases with pore volume injected and then levels off with small changes for samples between 2 to 5 pore volumes of injection. This indicates that solvent bank with higher percentage of intermediates (C_7 - C_{17}) is being produced. The final sample batch at 6 pore volumes of injection shows a drop in the C_7 - C_{17} percentage indicating the production of heavier components after the solvent bank. The sample analysis for run 5 (1:4 molar ratio of CO_2 /steam at 660°F) shows a cyclic gradual decrease in percentage of C_7 - C_{17} . This behavior could be explained by the fact that the presence of CO_2 at higher temperature will cause more gradual distillation of intermediates while at the same time the heavier components will be saturated with CO_2 . The swelling effects and viscosity reduction associated with CO_2 results in production of heavier components along with intermediates. This also explains the increase in recovery for run 5. Samples from run 7 (1:4 molar ratio of CO_2 /steam at 570°F) show that the percentage of C_7 - C_{17} increased up to 2.5 pore volumes and then decreased sharply. The reduction in viscosity of heavier portion of the oil will not be as much as the higher temperature run 5. This might be the reason for a faster production of condensates for run 7.

TABLE 4
 Analysis of the Produced Oil Samples From
 Run #1 (Steam 660°F)

Component %	Sampling Batch (Pore Volume Injected)								
	1/2	1	1 1/2	2	2 1/2	3	4	5	6
C ₇	0.41	0.046	0.23	0.76	0.53	0.29	0.387	0.28	0.03
C ₈	0.633	2.02	0.84	1.17	0.95	0.54	0.367	0.071	0.036
C ₉	0.81	1.94	1.52	1.31	1.52	0.96	0.64	3.7	0.048
C ₁₀	0.82	2.19	1.51	2.12	2.96	2.41	6.00	0.6	0.45
C ₁₁	1.39	3.09	3.86	2.44	3.82	3.73	3.2	3.03	1.53
C ₁₂	1.63	3.12	3.7	2.62	4.22	4.18	1.72	2.66	0.86
C ₁₃	1.47	2.91	4.30	2.20	3.81	2.71	2.87	1.74	0.89
C ₁₄	1.82	3.41	4.61	2.34	4.08	4.81	3.21	2.77	0.89
C ₁₅	1.89	3.01	4.02	1.82	3.38	4.39	2.9	3.57	1.00
C ₁₆	1.60	3.01	4.27	1.58	3.21	4.12	2.96	3.27	0.79
C ₁₇	1.73	3.20	1.23	1.56	2.66	4.45	2.77	3.72	1.14
C ₁₈	0.54	0.65	5.92	0.47	1.18	1.49	1.17	3.80	1.33
C ₁₉	1.93	3.92	0.67	1.71	3.42	4.62	3.43	5.2	0.84
C ₂₀	1.08	0.75	3.82	0.23	0.47	1.75	1.54	1.31	0.79
C ₂₁ +	82.24	66.73	59.5	77.66	63.79	59.55	66.83	64.28	89.37

TABLE 5
 Analysis of the Produced Oil Samples From
 Run #5 (1:4 Molar Ratio 660°F)

Component %	Sampling Batch (Pore Volume Injected)								
	1/2	1	1 1/2	2	2 1/2	3	4	5	6
C ₇	0.62	0.35	0.37	0.14	0.03	0.02	0.29	0.014	0.02
C ₈	0.35	0.48	0.56	0.21	0.09	-	0.15	0.016	0.04
C ₉	0.77	0.84	0.78	0.43	0.27	0.03	0.17	0.02	0.03
C ₁₀	1.27	0.35	1.52	0.64	0.56	0.29	0.3	0.12	0.14
C ₁₁	1.86	1.27	2.11	0.77	1.03	0.56	0.67	0.25	0.34
C ₁₂	2.21	1.37	2.48	0.91	1.10	0.63	0.77	0.29	0.42
C ₁₃	2.02	1.18	2.08	0.72	1.29	0.61	0.83	0.30	0.53
C ₁₄	2.06	1.16	2.17	0.67	1.17	0.49	0.99	0.31	0.50
C ₁₅	1.97	1.01	1.87	0.49	2.69	0.91	0.84	0.32	0.50
C ₁₆	2.01	1.16	0.93	0.44	1.19	0.08	1.02	0.32	0.50
C ₁₇	1.78	0.94	1.56	0.57	1.35	-	0.93	0.27	0.56
C ₁₈	1.05	0.03	0.59	0.19	0.65	-	0.46	0.16	0.36
C ₁₉	2.02	1.17	1.85	0.34	0.3	-	0.79	0.40	0.54
C ₂₀	0.66	0.36	0.56	0.14	0.74	-	0.53	0.15	0.44
C ₂₁ +	79.36	88.33	80.57	93.34	87.54	96.38	91.26	97.06	94.54

TABLE 6
 Analysis of the Produced Oil Samples From
 Run #7 (1:4 Molar Ratio 570°F)

Component %	Sampling Batch (Pore Volume Injected)								
	1/2	1	1 1/2	2	2 1/2	3	4	5	6
C ₇	1.77	1.44	1.50	1.66	1.4	0.13	0.06	0.16	0.03
C ₈	0.99	1.02	1.26	1.64	1.59	0.22	0.19	0.22	0.08
C ₉	1.42	1.316	1.82	2.57	2.02	0.51	0.61	0.8	0.1
C ₁₀	1.87	1.53	2.3	3.34	5.41	0.73	0.94	1.22	0.42
C ₁₁	2.28	1.89	2.53	4.93	7.45	0.91	0.64	1.55	0.74
C ₁₂	2.40	1.87	2.84	4.01	4.17	0.85	0.36	1.76	0.88
C ₁₃	3.13	1.98	2.77	3.86	4.17	0.9	0.46	1.48	0.7
C ₁₄	3.05	2.43	3.01	4.72	6.45	0.74	0.46	1.59	0.96
C ₁₅	2.71	2.17	2.04	3.26	4.79	0.53	0.40	1.53	0.81
C ₁₆	2.78	2.25	2.49	3.65	4.62	0.29	0.37	1.33	0.66
C ₁₇	2.97	2.13	2.53	3.34	6.02	0.21	0.24	1.46	0.69
C ₁₈	0.71	0.54	0.6	0.76	1.42	0.003	0.1	0.61	0.69
C ₁₉	3.97	2.92	3.19	3.37	4.83	-	0.17	1.64	0.27
C ₂₀	1.01	1.10	0.80	1.53	1.34	-	0.06	0.55	0.23
C ₂₁ +	68.94	75.41	70.32	57.36	44.32	93.97	94.94	84.1	92.67

TABLE 7
 Effect of CO₂ on the Density of Produced Oil Samples From (Run 1)

PV Injected	Density (gm/cm ³)					
	100°F		150°F		212°F	
	no CO ₂	with CO ₂	no CO ₂	with CO ₂	no CO ₂	with CO ₂
1	.9428	.9496	.9250	.9227	.8988	.8937
1.5	.9412	.9454	.9283	.9263	.9069	.9024
2	.9438	.9503	.9257	.9289	.9069	.9066
2.5	.9431	.9441	.9279	.9240	.9066	.9040
4	.9428	.9474	.9247	.9247	.9053	.9040

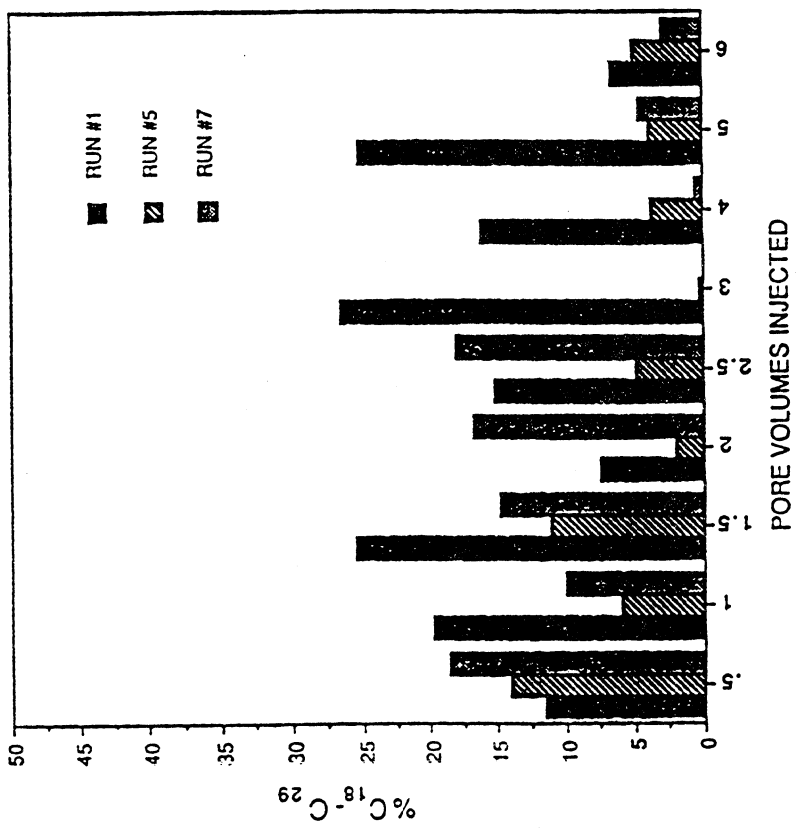


Figure 11: Percentage of $C_{18}-C_{29}$ in Produced Oil Samples

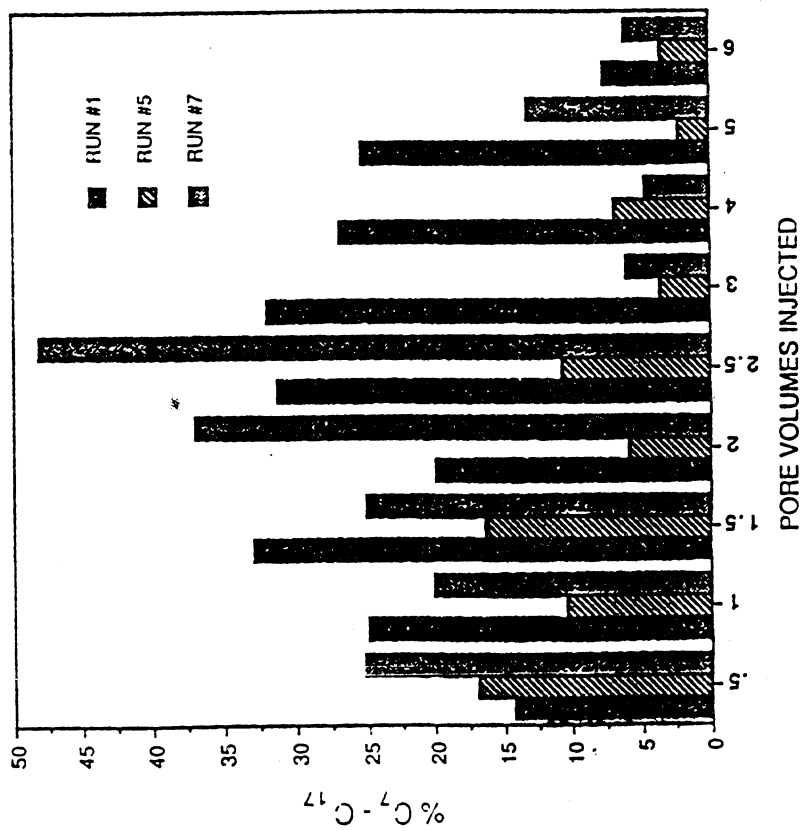


Figure 10: Percentage of C_7-C_{17} in Produced Oil Samples

Figure 11 shows the change in C_{18} - C_{29} percentage in produced oil samples for the same runs. Although the change in C_{18} - C_{29} for steam alone (run 1) does not follow any specific trend, run 5 and 7 show the same trend as C_7 - C_{17} . One interesting point is that the percentages of C_{18} - C_{29} in the samples from run 5 and 7 at 3 pore volumes of injection are almost zero.

G2.4 Effect of CO₂ on Oil Density

Experiments were conducted to determine the effect of CO₂ addition on the density of the produced oil samples from run 1. The sample sizes were generally less than 7 cc. With current equipment, we were unable to perform volumetric swelling tests, but were able to observe the change in liquid density due to CO₂ in solution. Measurements were made at 100°F, 150°F, and 212°F at 1650 psig. The results are presented in Table 7.

It should be noted that at 150°F, and 212°F, the addition of CO₂ tended to decrease the density of the oil. At 100°F, the addition of CO₂ tended to increase the oil density.

Figure 12 shows the effect of temperatures on oil density for the effluent at 1 pore volume injected for the case of CO₂ saturated oil and virgin oil. It appears that the presence of CO₂ enhances the effective thermal expansion of the liquid phase. Although small, this change is in the 'right' direction and should move towards additional recovery, above that from swelling and viscosity reduction alone.

G2.5 Nitrogen - Steam Injection Runs

By maintaining the volumetric flow rate constant for the steam base case, the effect of Nitrogen addition could be studied. Pore volume injected in both the nitrogen/steam runs was calculated by finding the

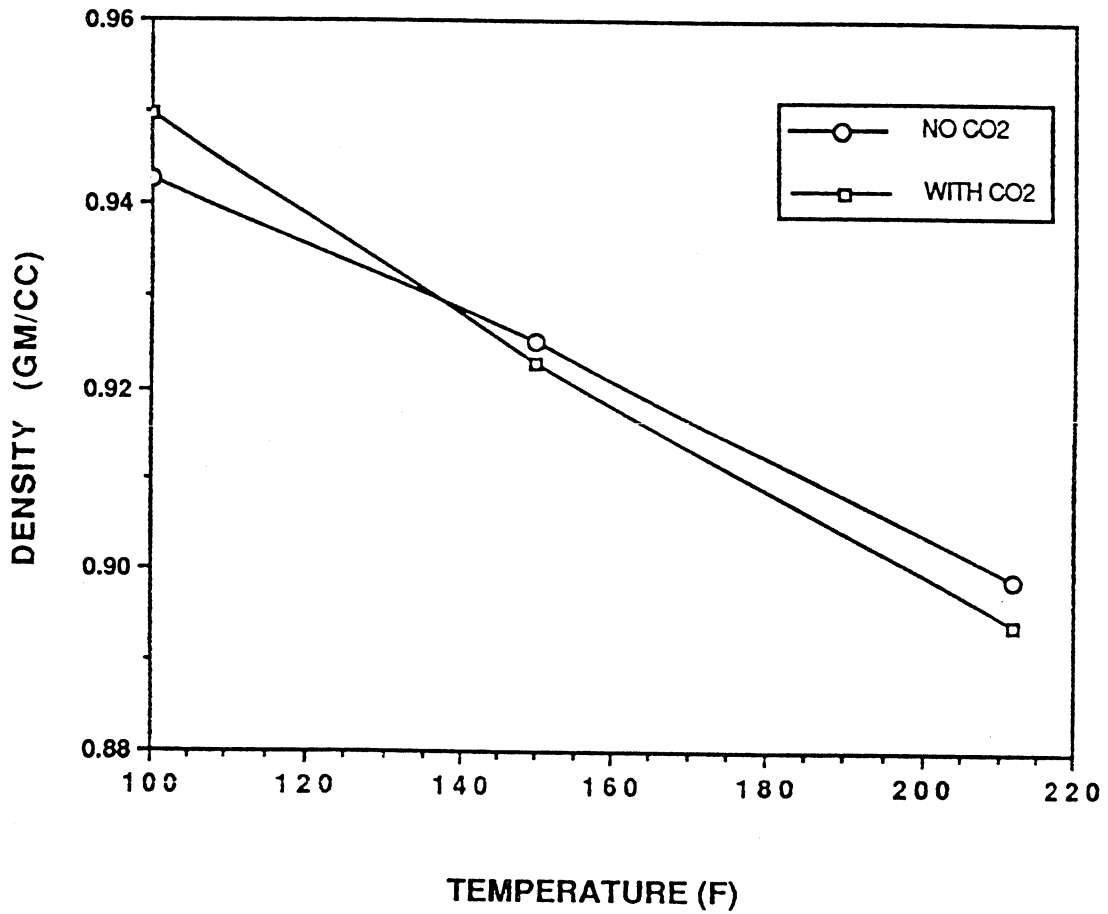


Figure 12: Effect of Temperature on Oil Density for One Pore Volume Effluent Oil Sample from Run 1

equivalent pore volumes of water injected to give the same volume of steam at 590°F and 1690 psi as the volume of mixture vapor injected. For run 8 Nitrogen was injected with the steam at 1:4 molar ratio. This resulted in an increase in recovery of 8% over the conventional steamflood after six pore volumes of injection. For run 9, the resulting increase was 2.8% when 1:3 molar ratio of nitrogen/steam was used. Cumulative recoveries and water oil ratio versus pore volume injected for run 8 and 9 are shown in Figures 13 and 14. Temperature and pressure profiles as a function of distance are shown in Figures 21 through 26.

G2.6 Methane - Steam Injection Runs

The effect of methane addition to steam was studied by controlling the volumetric flow rate constant for the steam base case. Pore volume injected was calculated by finding the equivalent pore volumes of water injected to give same volume of steam at 570°F and 1690 psi as the volume of mixture vapor injected. For run 10, Methane was injected with steam at 1:3 molar ratio. This resulted an increase in recovery of 13.4% over the conventional steamflood after six pore volumes of injection. Cumulative recovery and water oil ratio versus pore volume injected for run 10 are shown in Figures 15 and 16. Also temperature and pressure profiles as a function of distance are shown in Figure 25.

G2.7 Analysis of the Pressure Drop and Temperature Profiles

Analysis of the pressure drop and temperature profiles illustrates why there is an increase in recovery when CO₂ is added to steam. The temperature and pressure drop profiles for the steam base case run are shown in Figures 17 and 18. The purpose of comparing these graphs is to show how the pressure drop in the sand pack changes with the changing temperature profile and comparing that with the temperature and

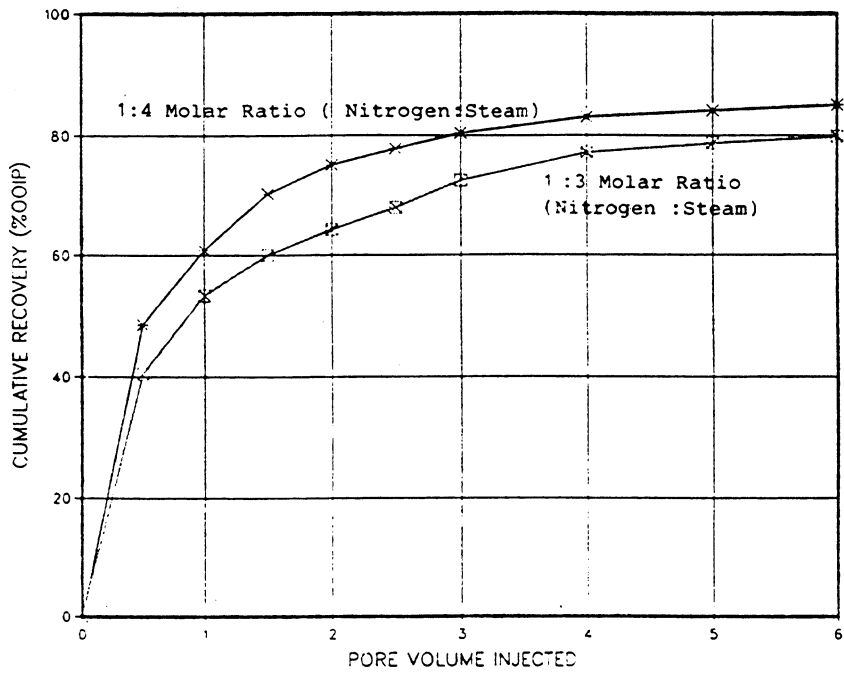


Figure 13: Cumulative Recovery vs. Pore Volumes Injected for Steam and Nitrogen Runs (Runs 8 and 9)

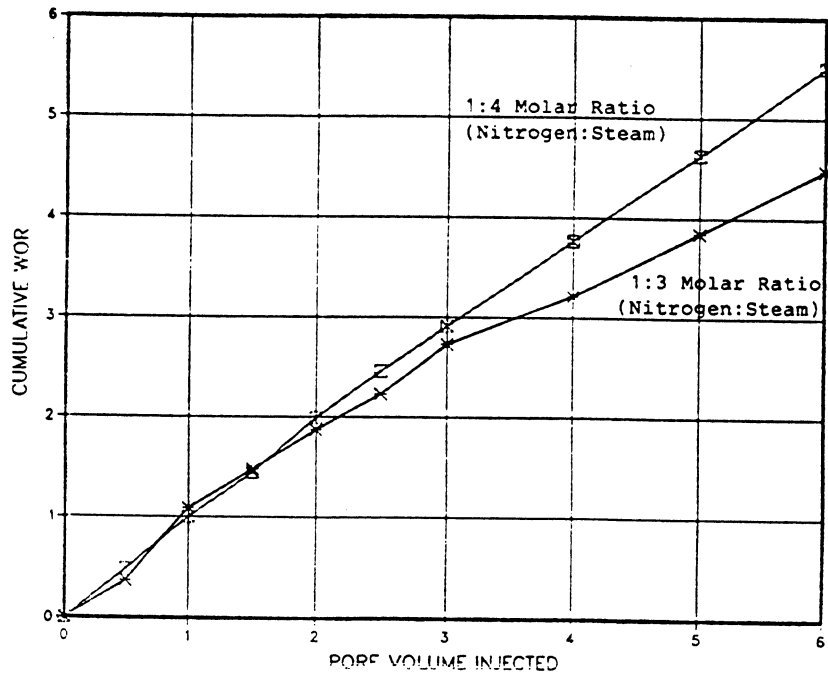


Figure 14: Cumulative Water Oil Ratio vs. Pore Volumes Injected (for Runs 8 and 9)

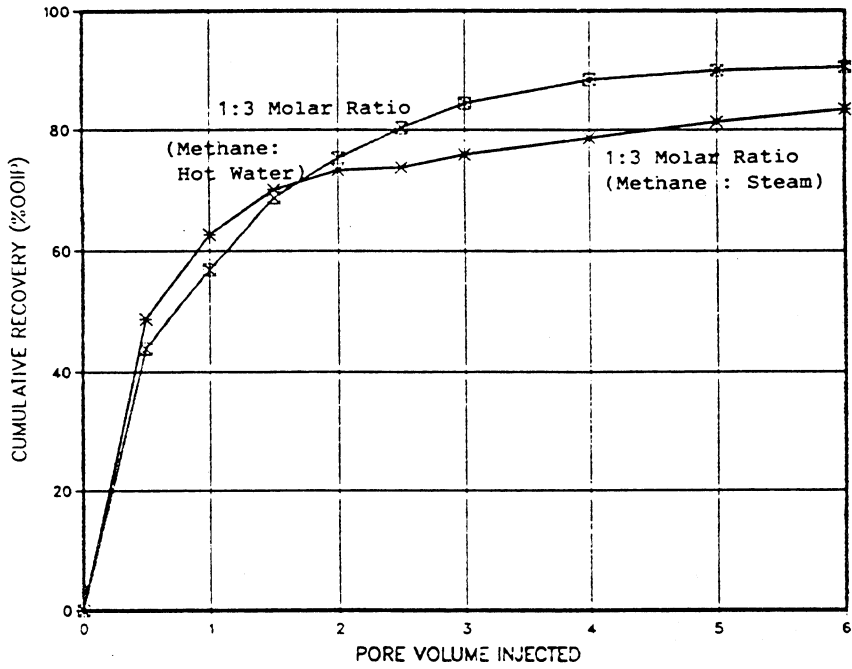


Figure 15: Cumulative Recovery vs. Pore Volumes Injected for High and Low-Temperature Methane/Steam Runs (Runs 10 and 11)

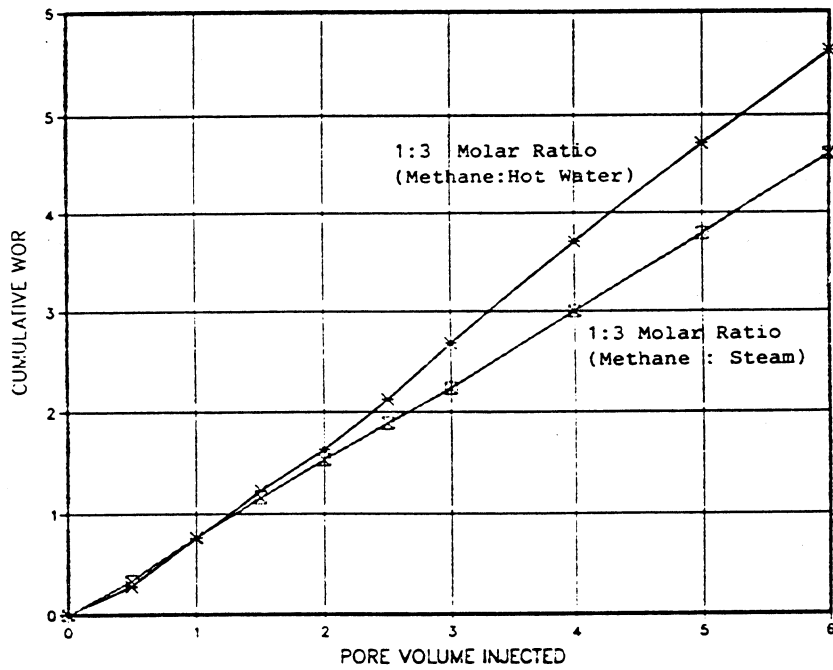


Figure 16: Cumulative Water Oil Ratio vs. Pore Volumes Injected (for Runs 10 and 11)

pressure drop profiles of a CO₂/steam run. No attempt was made to compare the experimental pressure drops observed with theoretical values. This was because the effective permeability of the sand pack and temperature-viscosity relationships of the West Sak sample were unavailable. It should also be mentioned that any pressure drop due to edge effects were considered negligible.

As can be seen from Figures 17 and 18, as pore volumes of steam are injected the temperature profile advances in the sand pack. As the sand pack is heated the corresponding pressure drop profile decreases as a result of the crude oil being heated resulting in a viscosity reduction. The pressure drop decreases uniformly until the fifth pore volume where the pressure drop became relatively constant.

As a comparison, Figures 19 and 20 show the pressure drop and temperature profiles for run 4 in which CO₂ and steam were injected in a 1:3 molar ratio. Run 4 was chosen because of the clarity of the results. Runs 3 and 5 show the same trends but due to fluctuations in the results and the experimental equipment they are not as clear. The temperature profile shows that less heat is being injected. This is illustrated by the slower and more gradual advance of the temperature profile. The corresponding pressure drop profile shows there is a pressure drop peak moving through the sand pack that is not evident in the steam base case. This is due to the effects of CO₂ displacing a slug of heavy oil not produced by a conventional steam flood. This slug of heavy oil is most probably the incremental recovery due to oil swelling and the trapped gas effects resulting from CO₂ addition. Further examination of the pressure drop profile shows that after 5 pore volumes the pressure drop suddenly dropped and became relatively constant. This corresponded

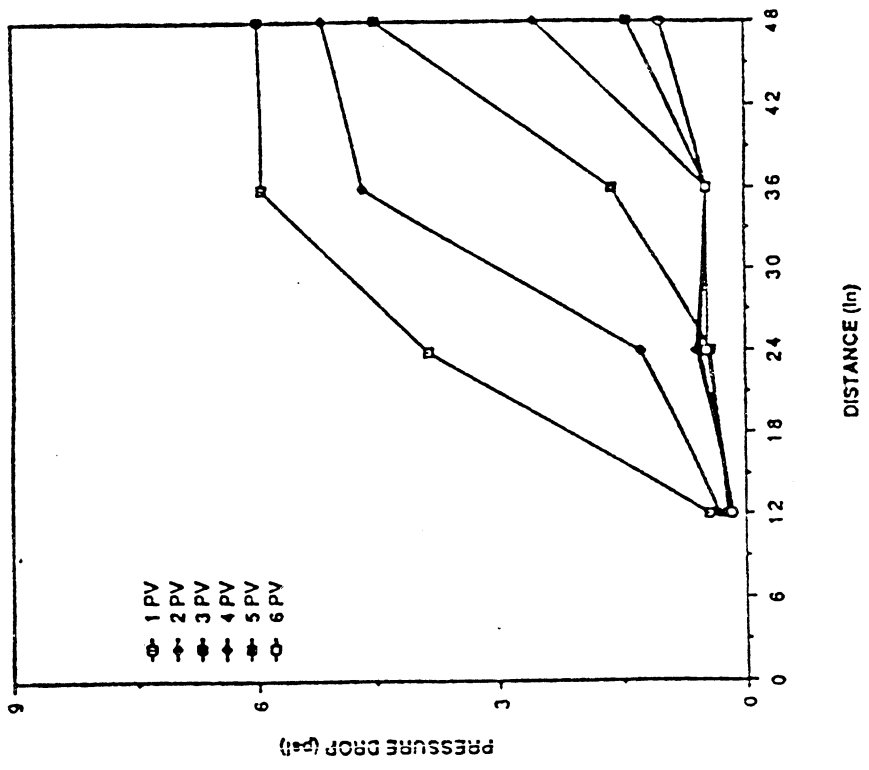


Figure 18: Pressure Drop Profile for Run 1

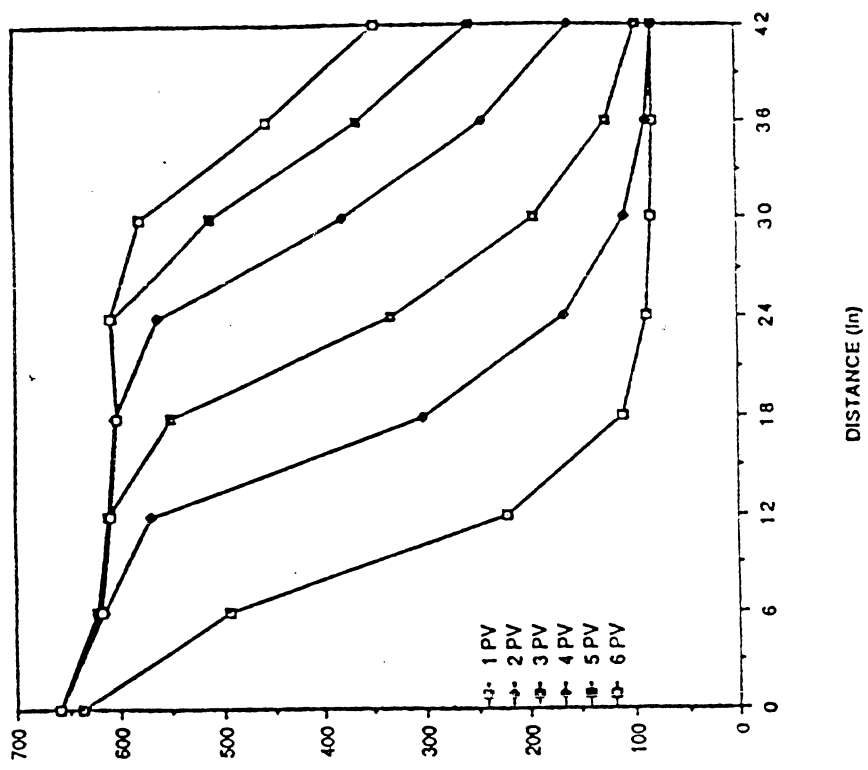


Figure 17: Temperature Profile for Run 1 (Steam Alone)

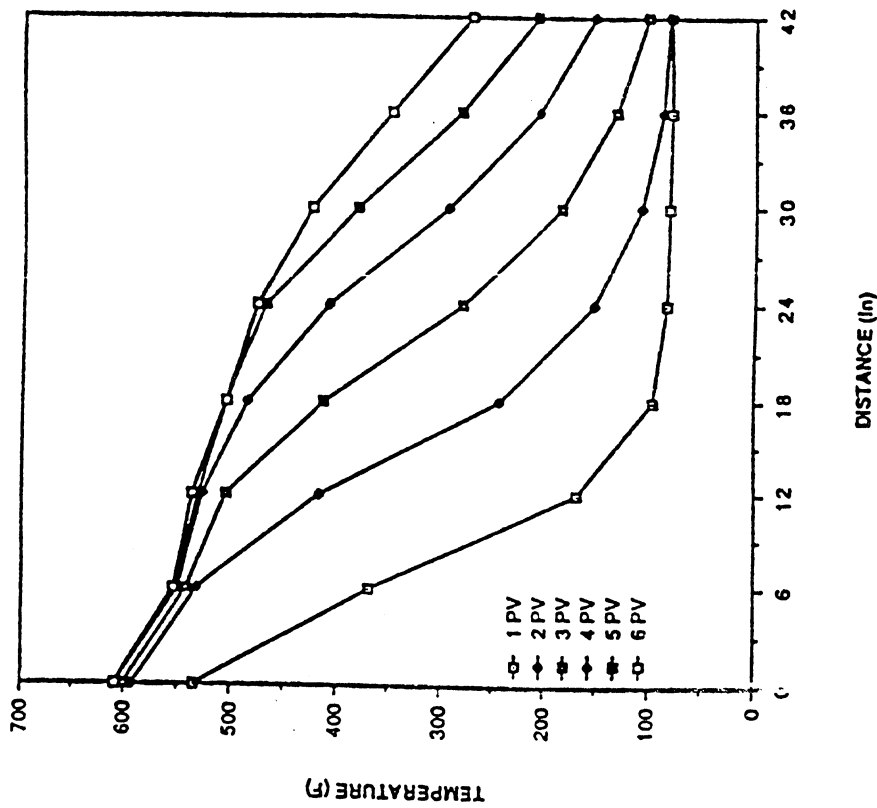


Figure 19: Temperature Profile for Run 4 (1:3 Molar Ratio of CO₂/Steam @ 660°F)

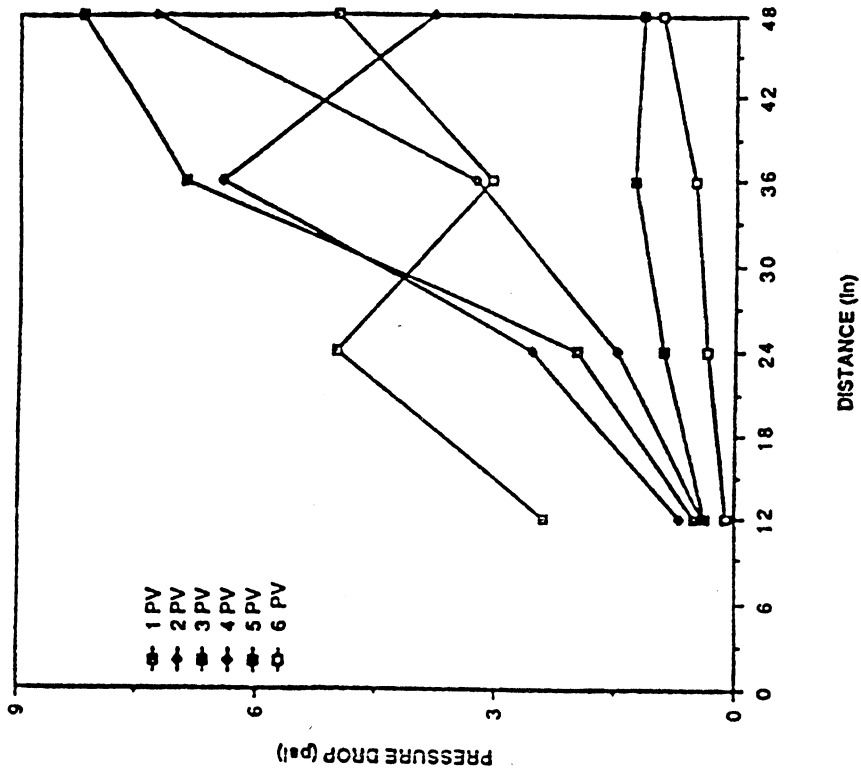


Figure 20: Pressure Drop Profile for Run 4

with an extremely viscous slug of heavy oil being produced. This viscous slug of oil was not produced in the conventional steam flood, implying further that this heavy slug of oil is the incremental oil produced by CO₂ addition to steam. Temperature and pressure profiles as a function of distance for nitrogen/steam and methane/steam run are shown in Figures 21 through 26.

H. CONCLUSIONS

The simultaneous injection of CO₂ with steam was found to be beneficial in recovering West Sak crude oil. It is believed that the primary recovery mechanisms of this process are viscosity reduction and oil swelling. Other beneficial recovery mechanisms include: solvent extraction, and enhanced steam distillation. Based on the analysis of the data from the laboratory experiments conducted in this work the following are concluded:

1. The addition of CO₂ to steam improves recovery of the West Sak crude oil sample used.
2. The addition of CO₂ to steam improves recovery rate of the West Sak crude oil sample used.
3. The results indicate there is an optimum CO₂/steam molar ratio for the highest recovery.
4. The addition of CO₂ to steam at the same temperature will increase the yield for the same amount of water distilled.
5. At higher temperatures (>150°F) the addition of CO₂ causes significant swelling in the oil phase. This should enhance oil recovery.
6. The addition of CO₂ to steam reduces the steam injection temperature required.

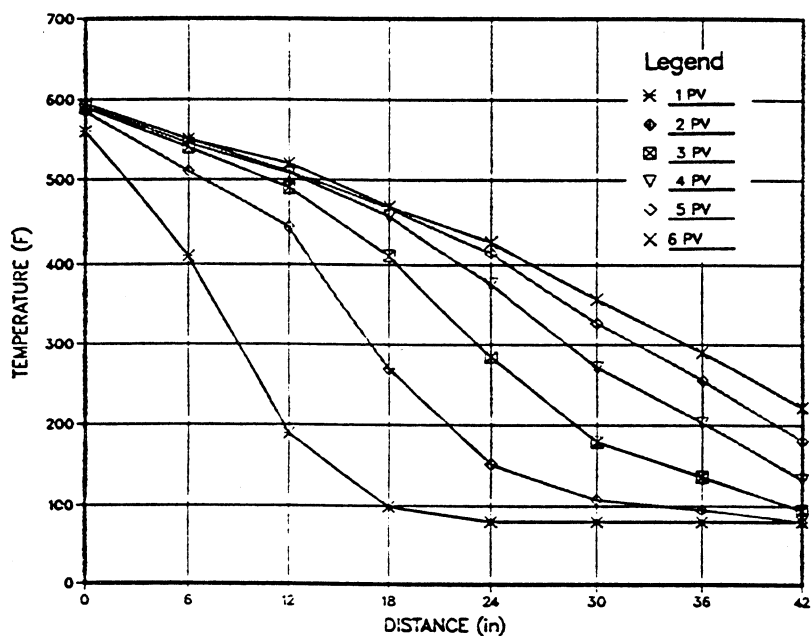


Figure 21: Temperature Profile for Run 8 (1:4 Molar Ratio of Nitrogen/Steam)

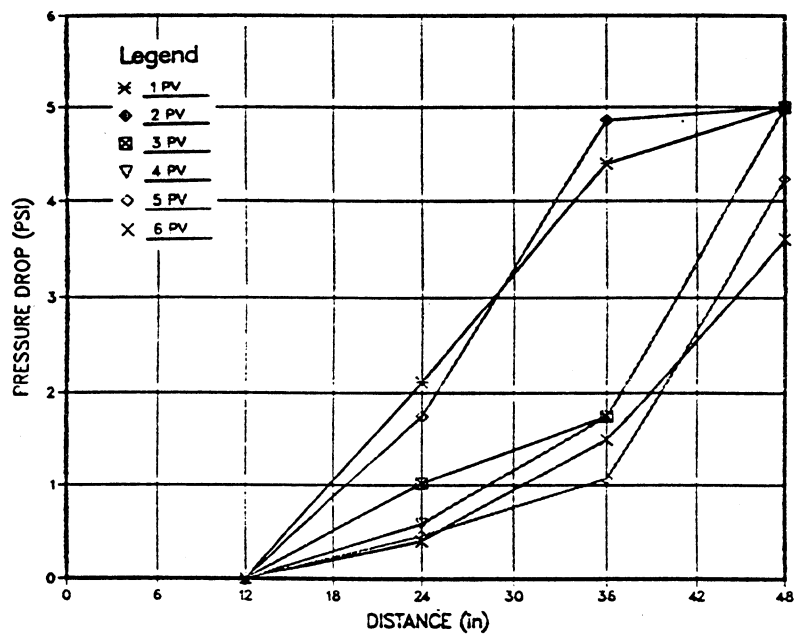


Figure 22: Pressure Drop Profile for Run 8

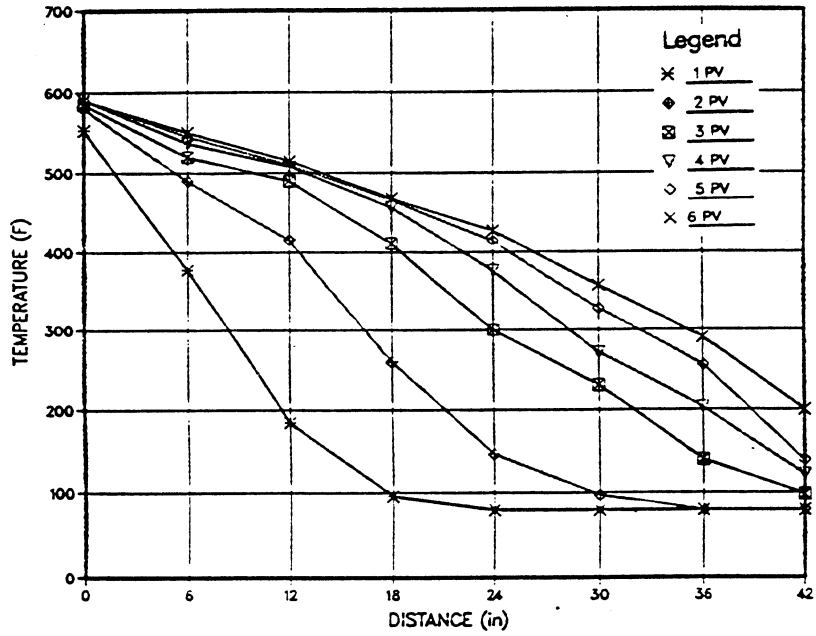


Figure 23: Temperature Profile for Run 9 (1:3 Molar Ratio of Nitrogen/Steam)

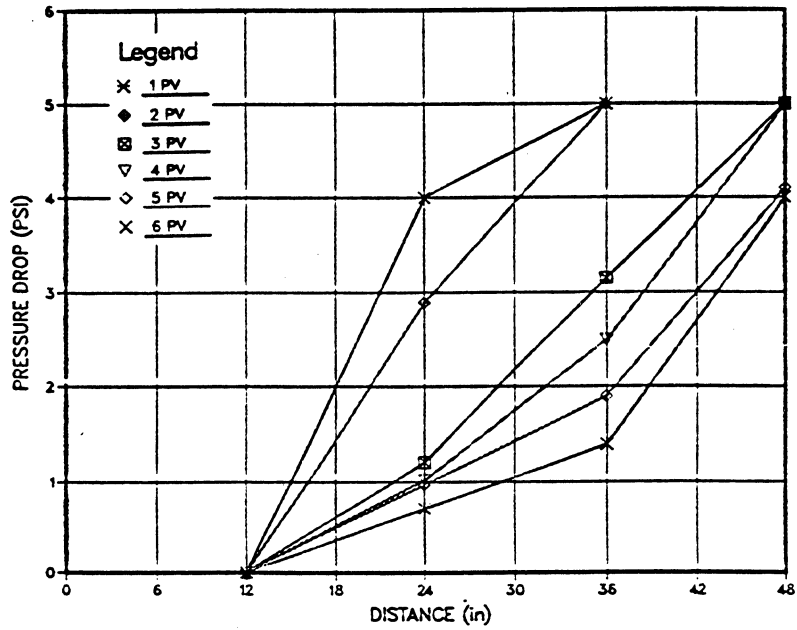


Figure 24: Pressure Drop Profile for Run 9

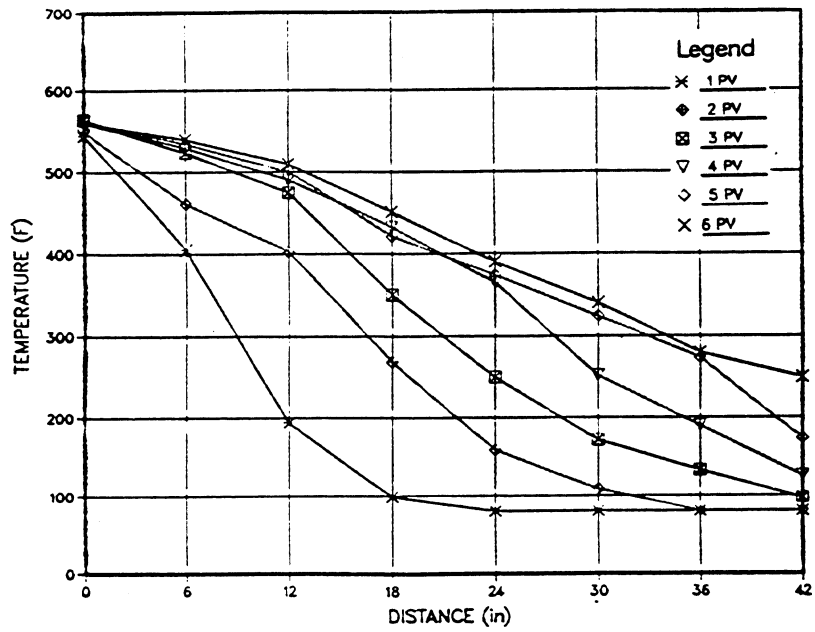


Figure 25: Temperature Profile for Run 10 (1:3 Molar Ratio of Methane/Water)

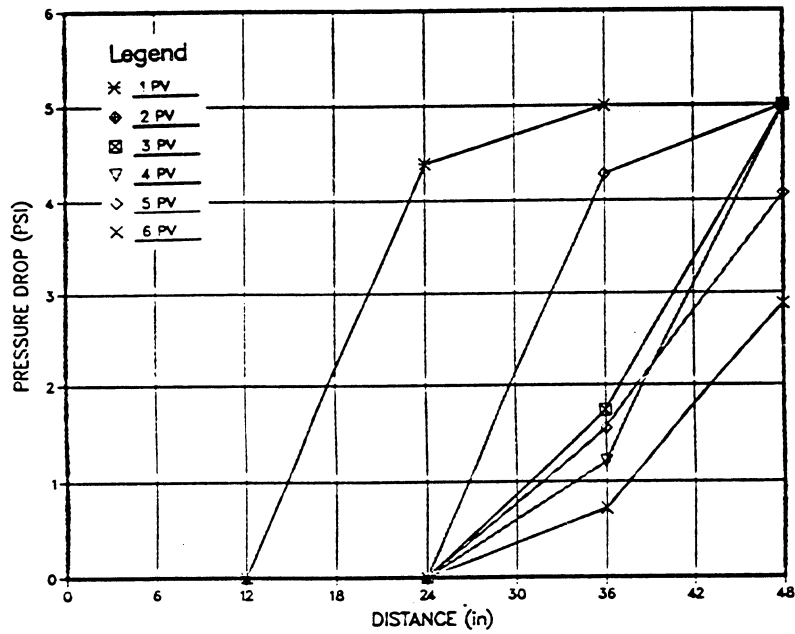


Figure 26: Pressure Drop Profile for Run 11

7. The presence of a free gas phase reduces the ultimate recovery of a conventional steam-flood.
8. The addition of Nitrogen to steam improves recovery of West Sak crude oil sample used.
9. The addition of Methane to steam also improved the recovery of West Sak crude oil sample used.

I. REFERENCES

1. ARCO, "ARCO Maps for West Sak Thermal Project," Oil and Gas Journal, Nov. 7, 1983, p. 78.
2. Hornbrook, M.W., "Effect of Carbon Dioxide Addition to Steam on Recovery of West Sak Crude Oil," M.S. Thesis, University of Alaska Fairbanks (1988).
3. Hornbrook, M.W. et al., "Effect of CO₂ Addition to Steam on Recovery of West Sak Crude Oil," SPE Paper 18753, presented at the Western Regional Meeting of SPE (April 5-7, 1989).
4. Lo, H.Y. and Mungan, N., "Effect of Temperature on Water-Oil Relative Permeabilities in Oil-Wet and Water-Wet Systems," Annual Fall Meeting of the Society of Petroleum Engineers, SPE Paper 4505 (Oct., 1973).
5. Sharma, G.D. et al., "The Potential of Natural Gas in the Alaskan Arctic," SPE Paper 17456, presented at the Western Regional Meeting of SPE (March 25-27, 1988).
6. Willman, B.T. et al., "Laboratory Studies of Oil Recovery by Steam Injection," J. Pet. Tech. (July, 1961) pp. 681-698.

CHAPTER SIX

DEVELOPMENT OF ONE DIMENSIONAL (LINEAR) HEAT TRANSFER MODEL FOR STEAM-SOLVENT INJECTION STUDY

A. Introduction

In earlier section, laboratory study of steam-solvent injection for recovery of West Sak crude is presented. Since the recovery efficiency of the steam-solvent process is a function of phase behavior, it is desirable to conduct these laboratory displacement experiments at the same temperatures and pressures existing in the reservoir. To accomplish the outlined goal, a one-dimensional heat transfer model was developed to describe the temperature distribution and heat frontal movement in the linear reservoir and in laboratory displacement experiments.

The thermal rock and fluid properties applicable to the West Sak reservoir were gathered and used as input data to the mathematical model to predict the temperature profiles that can be imposed on the laboratory sand pack. Thus, the heat transfer model allows us to maintain approximately the same temperature distribution in the West Sak reservoir and in the laboratory sand pack.

In this report we present the development and validation of the heat transfer model. A summary of the thermal rock and fluid properties of the West Sak reservoir is also presented.

B. Heat Transfer Model Development

The analytical model considers the constant injection of steam into a finite multi-layered cylindrical system (shown in Figure 1). The modified form of the Marx and Langenheim model can be applied (see Wang and Brigham, 1986).

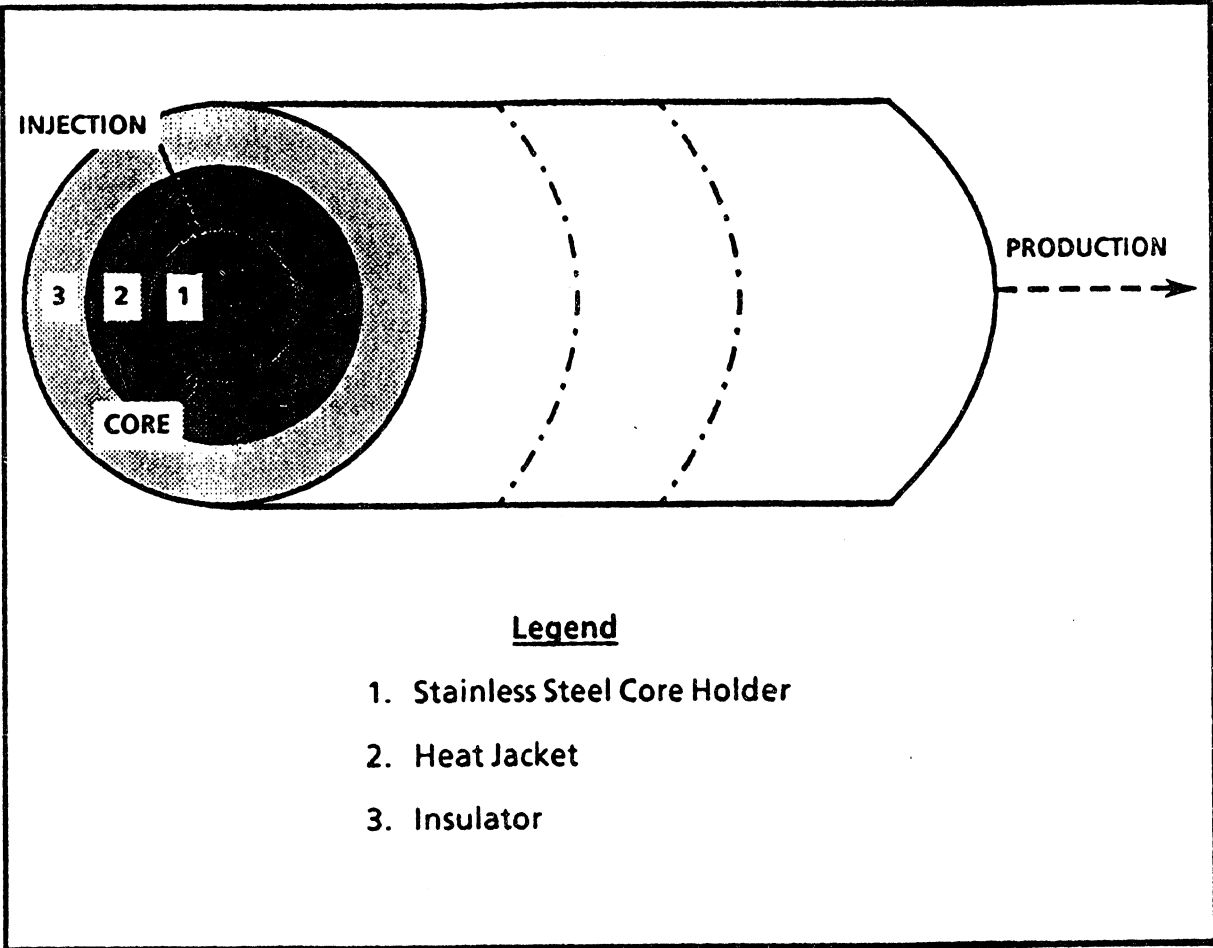


FIGURE 1: MODEL CONFIGURATION

$$\begin{aligned}
H = \int_0^t \left\{ -K_1 \left[\frac{\partial T(t-\tau)}{\partial r} \right]_{r=r_1} \left(2\pi r_1 \frac{dx}{d\tau} \right) \right\} d\tau \\
+ (\rho C)_R \Delta T \pi r_1^2 \frac{dx}{dt}
\end{aligned}
\tag{1}$$

In a manner similar to Wang and Brigham (1986), we define the following dimensionless variables:

$$t_D = \frac{\alpha_2 t}{r_1^2} \tag{2a}$$

$$r_D = \frac{r}{r_1} \tag{2b}$$

$$T_D = \frac{T - T_\infty}{T_s - T_\infty} = \frac{T - T_\infty}{\Delta T} \tag{2c}$$

$$\lambda_D = \frac{K_1}{K_2} \tag{2d}$$

$$\sigma = \frac{(\rho C)_2}{(\rho C)_1} \tag{2e}$$

$$X_D = \frac{x}{H_D L} \tag{2f}$$

$$H_D = \frac{H}{\pi L \alpha_2 (\rho C)_R \Delta T} \tag{2g}$$

Substitution of Equations (2a) through (2g) into Equation (1) provides:

$$\begin{aligned}
 H = & \left(-K_1 H_D 2\pi L \right) \int_0^{t_D} \left[\Delta T \left(\frac{\partial T_D}{\partial r_D} \right)_{r_{D=1}} \frac{dX_D}{dt_D} \right] dt_D \\
 & + H_D L \pi \Delta T \alpha_2 (\rho C)_R \frac{dX_D}{dt_D}
 \end{aligned}
 \tag{3}$$

Dividing both sides of Equation (3) by $\pi L \alpha_2 (\rho C)_R \Delta T H_D$, we get:

$$-2\lambda_{D\sigma} \int_0^{t_D} \left[\left(\frac{\partial T_D}{\partial r} \right)_{r_{D=1}} \frac{dx_D}{dt_D} \right] dt_D + \frac{dx_D}{dt_D} = 1
 \tag{4}$$

whereby

$$\lambda_{D\sigma} = \left(\frac{K_1}{K_2} \right) \frac{(\rho C)_2}{(\rho C)_R} = \frac{K_1}{\alpha_2 (\rho C)_R}
 \tag{5}$$

with

$$\alpha_2 = \frac{K_2}{(\rho C)_2}
 \tag{6}$$

The Laplace transformation of Equation (4) yields the equation for calculating the location of the front:⁴

$$\bar{X}_D = \frac{1}{s^2 \left[-2\lambda_{D\sigma} \left(\frac{dT_D}{dr_D} \right)_{r_{D=1}} + 1 \right]}
 \tag{7}$$

Note that s is the Laplace space time variable. Equation (7) was inverted numerically using the Stehfest Algorithm.²

Let us discuss how to calculate the following derivative term in Equation (7):

$$\left(\frac{d\bar{T}_D}{dr_D}\right)_{r_D=1}$$

Figure 2 shows a cross-section of the Linear Core model. The conduction heat losses to the three adjacent layers shown in Figure 2 can be described as follows:

For Stainless Steel Tube:

$$\frac{\partial^2 T_1}{\partial r^2} + \frac{1}{r} \left(\frac{\partial T_1}{\partial r}\right) = \frac{1}{\alpha_1} \left(\frac{\partial T_1}{\partial t}\right) \quad \dots\dots\dots (8)$$

For the Jacket:

$$\frac{\partial^2 T_2}{\partial r^2} + \frac{1}{r} \left(\frac{\partial T_2}{\partial r}\right) = \frac{1}{\alpha_2} \left(\frac{\partial T_2}{\partial t}\right) \quad \dots\dots\dots (9)$$

For the Insulator:

$$\frac{\partial^2 T_3}{\partial r^2} + \frac{1}{r} \left(\frac{\partial T_3}{\partial r}\right) = \frac{1}{\alpha_3} \left(\frac{\partial T_3}{\partial t}\right) \quad \dots\dots\dots (10)$$

Boundary Conditions

At the inner boundary of the stainless steel tube, $r = r_1$:

$$h_{f1}[T_s - T_1] = -K_1 \left(\frac{\partial T_1}{\partial r}\right) \quad \dots\dots\dots (11)$$

At $r = r_2$, i.e., the boundary between the steel tube and the heat jacket.

$$T_1 = T_2 \quad \dots\dots\dots (12)$$

$$-K_1 \left(\frac{\partial T_1}{\partial r}\right) = -K_2 \left(\frac{\partial T_2}{\partial r}\right) \quad \dots\dots\dots (13)$$

At the boundary between the jacket and the insulator, $r = r_3$:

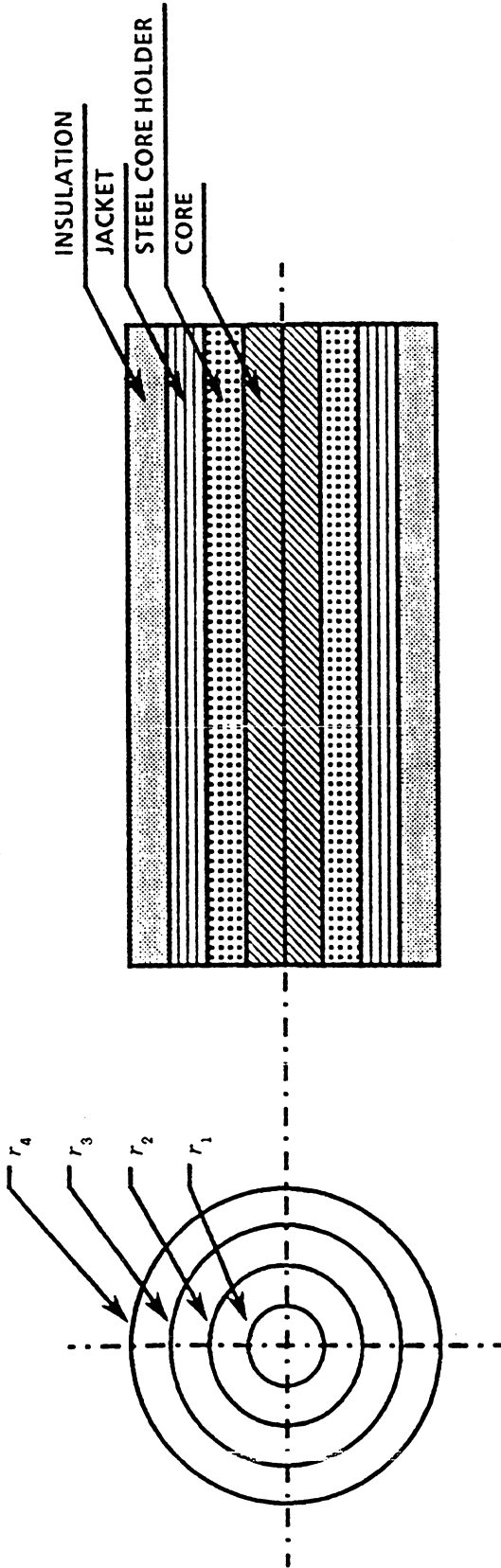


FIGURE 2: CROSS-SECTION OF THE CORE FLOOD MODEL

$$T_2 = T_3 \quad \dots\dots\dots (14)$$

$$-K_2 \left(\frac{\partial T_2}{\partial r} \right) = -K_3 \left(\frac{\partial T_3}{\partial r} \right) \quad \dots\dots\dots (15)$$

At the outer boundary of the insulation, $r = r_4$:

$$-K_3 \left(\frac{\partial T_3}{\partial r} \right) = h_{f3} (T_3 - T_\infty) \quad \dots\dots\dots (16)$$

Initial Condition

$$T_1(r,0) = T_2(r,0) = T_3(r,0) = T_\infty \quad \dots\dots\dots (17)$$

In Equations (8) through (17) we have defined the following:

- T_1 = temperature in the stainless steel tube
- T_2 = temperature in the jacket
- T_3 = temperature in the insulation
- T_s = temperature in the steam zone (core)
- T_∞ = ambient temperature
- α_1 = thermal diffusivity of the stainless steel tube
- α_2 = thermal diffusivity of the jacket
- α_3 = thermal diffusivity of the insulation
- K_1 = thermal conductivity of the stainless steel tube
- K_2 = thermal conductivity of the heat jacket
- K_3 = thermal conductivity of the insulation
- h_{f1} = heat transfer coefficient at the inner boundary (r_1) (i.e. between steam in the core and stainless steel tube)

h_{f3} = heat transfer coefficient at the outer boundary (r_4) (i.e. between the insulation and air)

To transform the above equations, we can define the following dimensionless variables:

$$t_D = \frac{\alpha_3 t}{r_1^2} \dots\dots\dots (18a)$$

$$r_D = \frac{r}{r_1} \dots\dots\dots (18b)$$

$$B_{i1} = \frac{h_{f1} r_1}{K_1} \dots\dots\dots (18c)$$

$$B_{i3} = \frac{h_{f3} r_1}{K_3} \dots\dots\dots (18d)$$

$$\alpha_{1D} = \frac{\alpha_1}{\alpha_3} \dots\dots\dots (18e)$$

$$\lambda_{1D} = \frac{K_1}{K_3} \dots\dots\dots (18f)$$

$$\alpha_{2D} = \frac{\alpha_2}{\alpha_3} \dots\dots\dots (18g)$$

$$\lambda_{2D} = \frac{K_2}{K_3} \dots\dots (18h)$$

$$\sigma_1 = \frac{(\rho C)_2}{(\rho C)_R} \dots\dots (18i)$$

$$\sigma_2 = \frac{(\rho C)_3}{(\rho C)_R} \dots\dots (18j)$$

Also:

$$H_D = \frac{H}{nL\alpha_3(\rho C)_R\Delta T} \dots\dots (19a)$$

$$T_D = \frac{T - T_\infty}{T_s - T_\infty} \dots\dots (19b)$$

$$X_D = \frac{x}{H_{DL}} \dots\dots (19c)$$

It should be noted that:

- L = length of the sand pack (core)
- $(\rho C)_2$ = volumetric heat capacity of the heat jacket
- $(\rho C)_3$ = volumetric heat capacity of the insulation

Now the dimensionless forms of Equations (8) through (17) can be written:

Governing Equations:

$$\frac{\partial^2 T_{1D}}{\partial r_D^2} + \frac{1}{r_D} \frac{\partial T_{1D}}{\partial r_D} = \frac{1}{\alpha_{1D}} \frac{\partial T_{1D}}{\partial t_D} \dots\dots (20)$$

$$\frac{\partial^2 T_{2D}}{\partial r_D^2} + \frac{1}{r_D} \frac{\partial T_{2D}}{\partial r_D} = \frac{1}{\alpha_{2D}} \frac{\partial T_{2D}}{\partial t_D} \quad \dots\dots\dots (21)$$

$$\frac{\partial^2 T_{3D}}{\partial r_D^2} + \frac{1}{r_D} \frac{\partial T_{3D}}{\partial r_D} = \frac{1}{\alpha_{3D}} \frac{\partial T_{3D}}{\partial t_D} \quad \dots\dots\dots (22)$$

Boundary Conditions:

$$r_D = 1: \quad B_{i1}(1 - T_{1D}) = - \frac{\partial T_{1D}}{\partial r_D} \quad \dots\dots\dots (23)$$

$$r_D = r_{2D}: \quad T_{1D} = T_{2D} \quad \dots\dots\dots (24)$$

$$\lambda_{1D} \frac{\partial T_{1D}}{\partial r_D} = \lambda_{2D} \frac{\partial T_{2D}}{\partial r_D} \quad \dots\dots\dots (25)$$

$$r_D = r_{3D}: \quad T_{2D} = T_{3D} \quad \dots\dots\dots (26)$$

$$\lambda_{2D} \frac{\partial T_{2D}}{\partial r_D} = \lambda_{3D} \frac{\partial T_{3D}}{\partial r_D} \quad \dots\dots\dots (27)$$

$$r_D = r_{4D}: \quad - \frac{\partial T_{3D}}{\partial r_D} = B_{i3} T_{3D} \quad \dots\dots\dots (28)$$

Initial Condition:

$$T_{1D}(r,0) = T_{2D}(r,0) = T_{3D}(r,0) \quad \dots\dots\dots (29)$$

Solution of Analytical Model

The Laplace transformation of Equations (20), (21), (22):

$$\bar{T}''_{1D} + \frac{1}{r_D} \bar{T}'_{1D} = \frac{s}{\alpha_{1D}} \bar{T}_{1D} - \frac{T_{1D}}{\alpha_{1D}}(r_D, 0) \dots\dots\dots (30)$$

From the initial condition: $\frac{T_{1D}}{\alpha_{1D}}(r_D, 0) = 0$

$$\bar{T}''_{2D} + \frac{1}{r_D} \bar{T}'_{2D} = \frac{s}{\alpha_{2D}} \bar{T}_{2D} \dots\dots\dots (31)$$

$$\bar{T}''_{3D} + \frac{1}{r_D} \bar{T}'_{3D} = s \bar{T}_{3D} \dots\dots\dots (32)$$

Where $T'_D = dT/dr_D$ and $T''_D = d^2T_D/dr_D^2$.

Laplace transformations of the Boundary Conditions are:

At $r_D = 1$: $B_{i1}[\frac{1}{s} - \bar{T}_{1D}] = \bar{T}'_{1D} \dots\dots\dots (33)$

$r_D = r_{2D}$: $\bar{T}_{1D} = \bar{T}_{2D} \dots\dots\dots (34)$

$$\lambda_{1D} \bar{T}'_{1D} = \lambda_{2D} \bar{T}'_{2D} \dots\dots\dots (35)$$

$r_D = r_{3D}$: $\bar{T}_{2D} = \bar{T}_{3D} \dots\dots\dots (36)$

$$\lambda_{2D} \bar{T}'_{2D} = \bar{T}'_{3D} \dots\dots\dots (37)$$

$$r_D = r_{4D}: \quad - \bar{T}'_{3D} = B_{i3} \bar{T}_{3D} \dots\dots\dots (38)$$

We seek solutions of the forms of modified Bessel functions, K_0, I_0 :

$$\bar{T}_{1D} = E_1 I_0 \left(r_D \sqrt{\frac{s}{a_{1D}}} \right) + F_1 K_0 \left(r_D \sqrt{\frac{s}{a_{1D}}} \right) \dots\dots\dots (39)$$

$$\bar{T}_{2D} = E_2 I_0 \left(r_D \sqrt{\frac{s}{a_{2D}}} \right) + F_2 K_0 \left(r_D \sqrt{\frac{s}{a_{2D}}} \right) \dots\dots\dots (40)$$

and

$$\bar{T}_{3D} = E_3 I_0 \left(r_D \sqrt{s} \right) + F_3 K_0 \left(r_D \sqrt{s} \right) \dots\dots\dots (41)$$

Where E_1, E_2, E_3 and F_1, F_2, F_3 are coefficients to be evaluated from the boundary conditions.

Substitution of the derivatives of Equations (39) through (41) and algebraic rearrangement yields six equations with six unknowns: E_1, E_2, E_3 and F_1, F_2, F_3 . The six equations are:

$r_D = 1$:

$$\left[B_{i1} I_0 \left(\sqrt{\frac{s}{a_{1D}}} \right) - \sqrt{\frac{s}{a_{1D}}} I_1 \left(\sqrt{\frac{s}{a_{1D}}} \right) \right] E_1 + \left[B_{i1} K_0 \left(\sqrt{\frac{s}{a_{1D}}} \right) + \sqrt{\frac{s}{a_{1D}}} K_1 \left(\sqrt{\frac{s}{a_{1D}}} \right) \right] F_1 = \frac{B_{i1}}{s} \dots\dots\dots (42)$$

$r_D = r_{2D}$:

$$\begin{aligned} & \left[I_0 \left(r_{2D} \sqrt{\frac{s}{\alpha_{1D}}} \right) \right] E_1 + \left[K_0 \left(r_{2D} \sqrt{\frac{s}{\alpha_{1D}}} \right) \right] F_1 \\ & - \left[I_0 \left(r_{2D} \sqrt{\frac{s}{\alpha_{2D}}} \right) \right] E_2 - \left[K_0 \left(r_{2D} \sqrt{\frac{s}{\alpha_{2D}}} \right) \right] F_2 = 0 \end{aligned} \quad \dots\dots (43)$$

$$\begin{aligned} & \left[\lambda_{1D} \sqrt{\frac{s}{\alpha_{1D}}} I_1 \left(r_{2D} \sqrt{\frac{s}{\alpha_{1D}}} \right) \right] E_1 - \left[\lambda_{1D} \sqrt{\frac{s}{\alpha_{1D}}} K_1 \left(r_{2D} \sqrt{\frac{s}{\alpha_{1D}}} \right) \right] F_1 \\ & - \left[\lambda_{2D} \sqrt{\frac{s}{\alpha_{2D}}} I_1 \left(r_{2D} \sqrt{\frac{s}{\alpha_{2D}}} \right) \right] E_2 + \left[\lambda_{2D} \sqrt{\frac{s}{\alpha_{2D}}} K_1 \left(r_{2D} \sqrt{\frac{s}{\alpha_{2D}}} \right) \right] F_2 = 0 \end{aligned} \quad \dots\dots (44)$$

at $r_D = r_{3D}$:

$$\begin{aligned} & \left[I_0 \left(r_{3D} \sqrt{\frac{s}{\alpha_{2D}}} \right) \right] E_2 + \left[K_0 \left(r_{3D} \sqrt{\frac{s}{\alpha_{2D}}} \right) \right] F_2 \\ & - \left[I_0 \left(r_{3D} \sqrt{s} \right) \right] E_3 + \left[K_0 \left(r_{3D} \sqrt{s} \right) \right] F_3 = 0 \end{aligned} \quad \dots\dots (45)$$

$$\begin{aligned} & \left[\lambda_{2D} \sqrt{\frac{s}{\alpha_{2D}}} I_1 \left(r_{3D} \sqrt{\frac{s}{\alpha_{2D}}} \right) \right] E_2 - \left[\lambda_{2D} \sqrt{\frac{s}{\alpha_{2D}}} K_1 \left(r_{3D} \sqrt{\frac{s}{\alpha_{2D}}} \right) \right] F_2 \\ & - \left[\sqrt{s} I_1 \left(r_{3D} \sqrt{s} \right) \right] E_3 + \left[\sqrt{s} K_1 \left(r_{3D} \sqrt{s} \right) \right] F_3 = 0 \end{aligned} \quad \dots\dots (46)$$

at $r_D = r_{4D}$:

$$\begin{aligned} & \left[B_{i3} I_0 \left(r_{4D} \sqrt{s} \right) + \sqrt{s} I_1 \left(r_{4D} \sqrt{s} \right) \right] E_3 \\ & + \left[B_{i3} K_0 \left(r_{4D} \sqrt{s} \right) - \sqrt{s} K_1 \left(r_{4D} \sqrt{s} \right) \right] F_3 = 0 \end{aligned} \quad \dots\dots (47)$$

The I_0, I_1, K_0, K_1 are the modified Bessel functions of the first and second kind, with orders zero and unity.

A computer program was written to calculate the term $(\partial TD/\partial r_D)_{r_D=1}$ used in the calculation of the steam front location. The results obtained from the validation runs of the program are presented in the following section.

C. Model Validation

The following results were obtained for a two-layer cylindrical model. The input data shown in Table 1 is taken from the work presented by Wang and Brigham (1986). Note that these results (see Figures 3 through 5) are presented here only to illustrate the procedure used to validate the analytical model.

D. West Sak Rock and Fluid Properties

The following regression equations were obtained by performing least squares fit to the PVT data measured as part of Task II of this project.

PVT Data

The PVT data are measured at $T = 80^\circ\text{F}$ and the pressure range $100 \leq P \leq 1705$ psia

1. **Oil Viscosity**

$$\mu_o (C_p) = -30.420971 + 0.021227p + 171.039105 \exp(-p/1000) \dots\dots\dots (48)$$

2. **Oil Formation Volume Factor**

$$B_o (\text{RB/STB}) = 1.011406 + 3.42824 \times 10^{-5}p \dots\dots\dots (49)$$

3. **Solution Gas Oil Ratio**

$$R_s (\text{SCF/STB}) = 5.706252 + 0.122082p \dots\dots\dots (50)$$

4. **Gas Formation Volume Factor**

$$B_g (\text{ft}^3/\text{SCF}) = 3.301176 \times 10^{-3} - 2.7039 \times 10^{-6}p + 12.721199/P \dots\dots\dots (51)$$

5. **Oil Density**

**TABLE 1: DIMENSIONLESS PARAMETERS
FOR PROGRAM VALIDATION
(After Ref. 2)**

Inner Diameter,	r_{2D}	=	1.05
Outer Diameter	r_{3D}	=	2.78
Inner Boundary Biot Modulus,	B_{i1}	=	1000
Outer Boundary Biot Modulus,	B_{i2}	=	15
Diffusivity Ratio,	α_D	=	7.3
Conductivity Ratio,	λ_D	=	290.0
Volumetric Heat Capacity Ratio,	σ	=	0.06

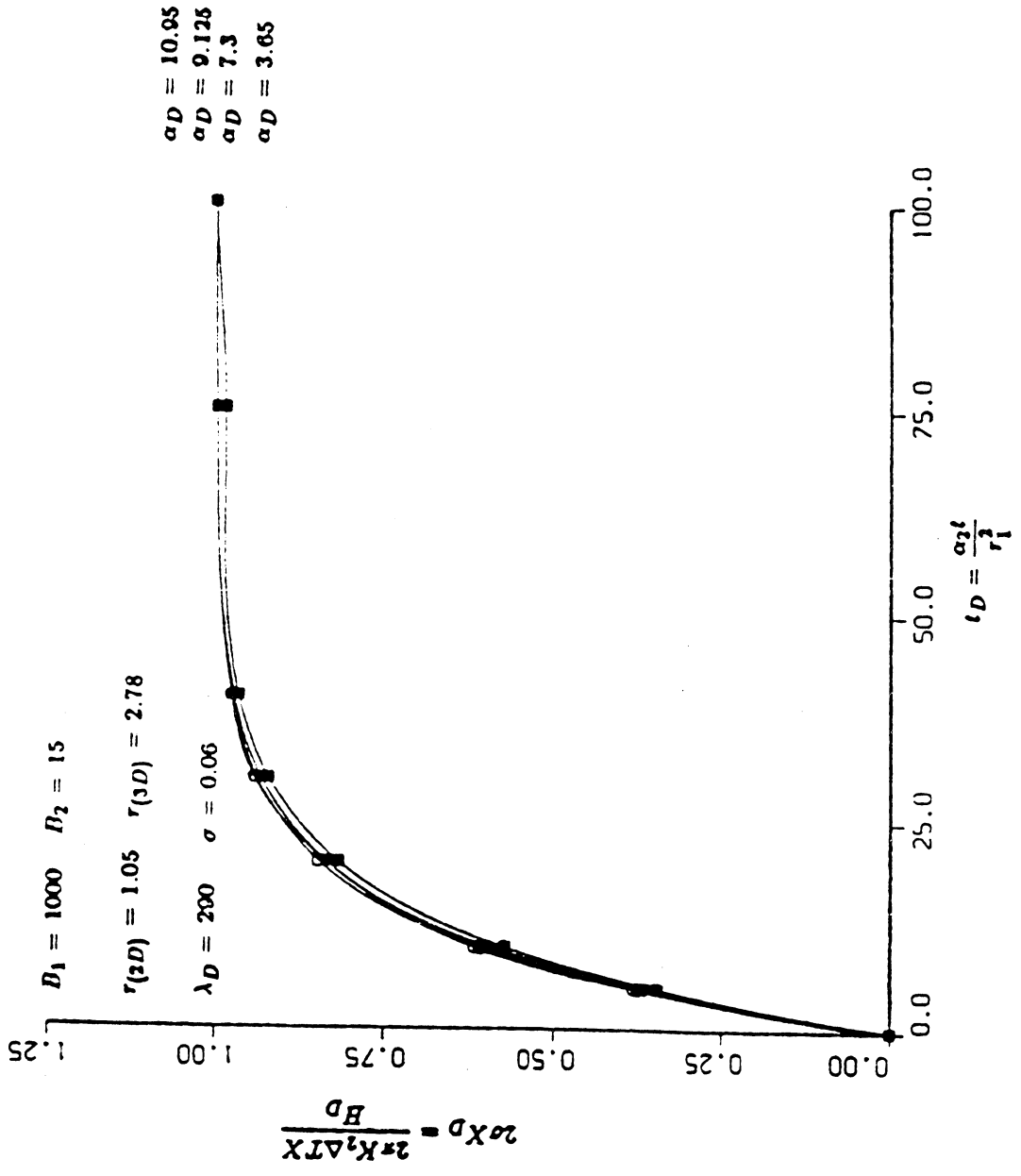


FIGURE 3

EFFECT OF DIFFUSIVITY RATIO ON HEAT FRONTAL MOVEMENT

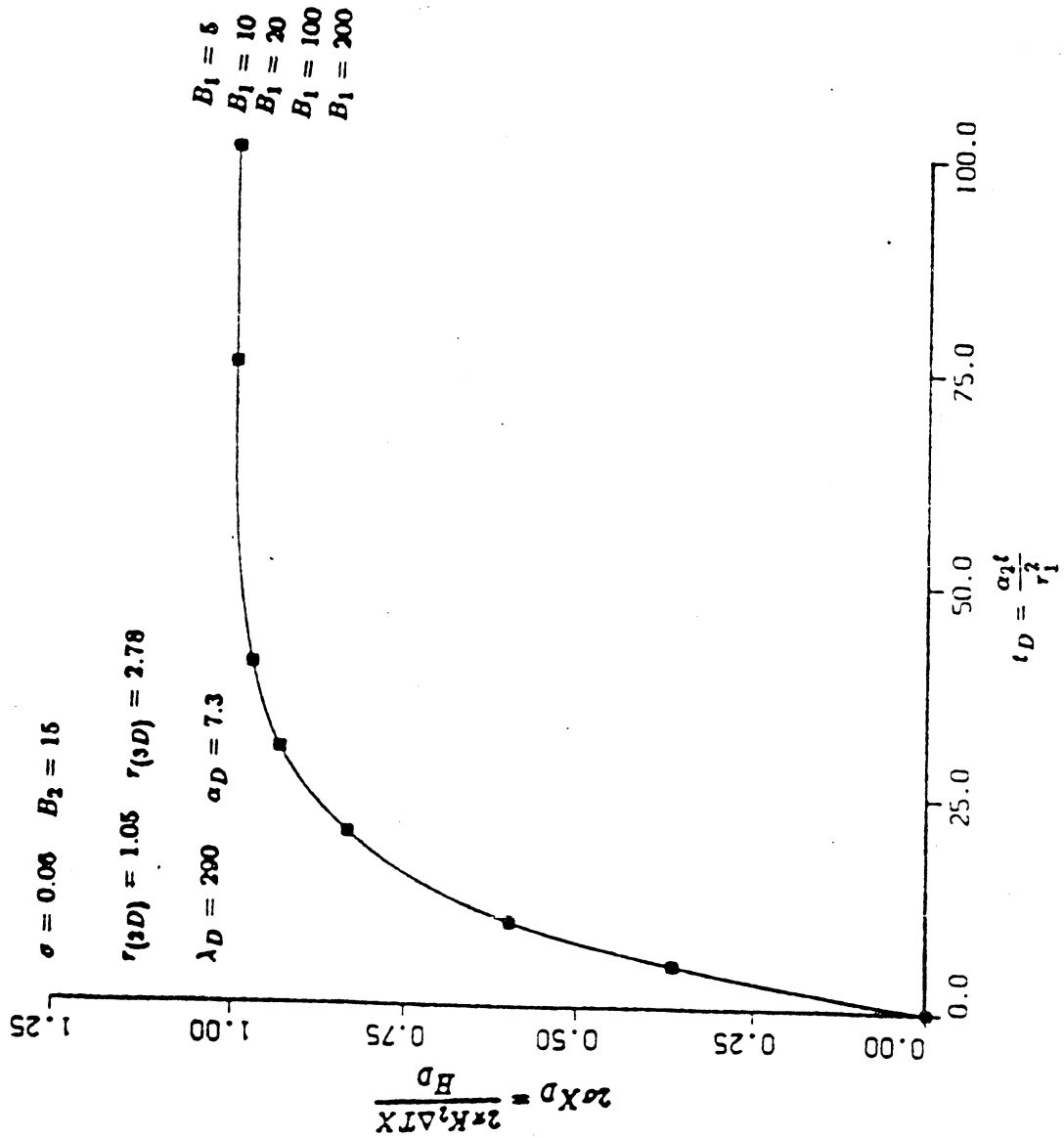


FIGURE 4
 VARYING THE INNER LAYER BIOT NUMBER

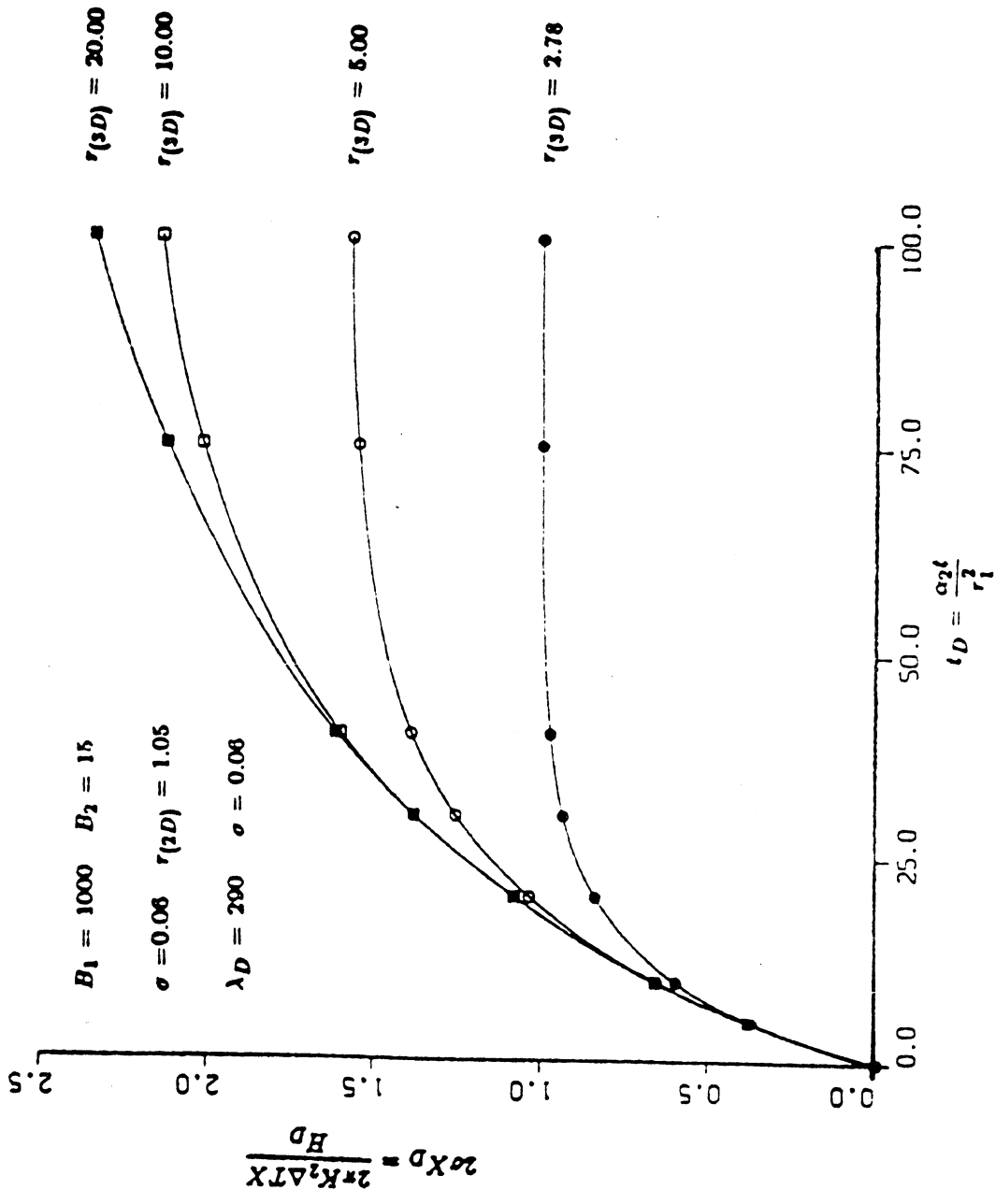


FIGURE 5
 VARYING THE OUTER LAYER THICKNESS

$$\rho_o \text{ (gm/cc)} = 0.92794 - 1.53849 \times 10^{-5}p \quad \dots\dots\dots (52)$$

Other Properties

1. **Rock Thermal Conductivity**

Table 2 summarizes the values of rock thermal conductivities at various temperatures, porosities and water saturations. These values were calculated using Somerton's correlation (Prats, 1982)

$$K_h \text{ (BTU/hr-ft-}^\circ\text{F)} = 0.735 - 1.30\phi + Sw^{0.5} \quad \dots\dots\dots (53)$$

2. **Water Saturation Pressure and Temperature**

$$T_s \text{ (}^\circ\text{F)} = 115.1p_s^{0.225} \quad \dots\dots\dots (54)$$

3. **Saturated Water Viscosity**

In the temperature range, $212 < T < 600^\circ\text{F}$, Miller (1983) presented the following correlation for calculating saturated water viscosity

$$\ln [\ln (208.9\mu_w (C_p))] = 1.3926 + 0.3084 (\ln T) - 0.05714 (\ln T)^2$$

(see Miller, 1983)

E. Summary

A one dimensional (linear) heat transfer model was developed in this work. The model can be used to calculate the temperature distribution and heat frontal movement in a linear laboratory displacement experiment. The equations were derived based upon a modified form of the Marx and Langenheim model. The solution to the partial differential equations was obtained using the method of Laplace transformation. The Stehfest algorithm was used to invert the Laplace transform solutions.

The model was validated using a two-layer cylindrical system and the data provided by Wang and Brigham (1986). A set of regression equations were also provided in this work for calculating the thermal rock and fluid properties of the

TABLE 2: ROCK THERMAL CONDUCTIVITY DATA

ϕ	S_w	Thermal Conductivity K_r BTU/hr-ft-°F						
		$T = 125^\circ\text{F}$	$T = 200^\circ\text{F}$	$T = 300^\circ\text{F}$	$T = 400^\circ\text{F}$	$T = 500^\circ\text{F}$	$T = 600^\circ\text{F}$	$T = 700^\circ\text{F}$
0.30	0.25	0.845	0.843	0.837	0.828	0.816	0.801	0.783
0.30	0.30	0.893	0.886	0.869	0.844	0.809	0.765	0.711
0.30	0.35	0.937	0.925	0.899	0.858	0.802	0.731	0.646
0.32	0.25	0.819	0.819	0.819	0.820	0.520	0.821	0.821
0.32	0.30	0.867	0.862	0.852	0.835	0.813	0.784	0.750
0.32	0.35	0.911	0.902	0.882	0.850	0.806	0.751	0.684
0.35	0.25	0.780	0.784	0.793	0.807	0.826	0.850	0.880
0.35	0.30	0.828	0.827	0.825	0.823	0.819	0.814	0.808
0.35	0.35	0.872	0.867	0.855	0.837	0.812	0.781	0.743

West Sak reservoir. These parameters served as input data to the heat transfer model to predict the temperature distribution and heat frontal positions for steam-solvent injection experiments.

F. Nomenclature

A	=	cross-sectional area, m^2
B_{i1}	=	Biot number at the inner boundary
B_{i3}	=	Biot number at the outer boundary
C, C_p	=	specific heat at constant pressure, $J/kg \text{ } ^\circ K$
h_f	=	heat transfer coefficient, $W/m^2 \text{ } ^\circ K$
$h_{\beta 1}$	=	heat transfer coefficient at inner boundary, $W/m^2 \text{ } ^\circ K$
$h_{\beta 3}$	=	heat transfer coefficient at outer boundary, $W/m^2 \text{ } ^\circ K$
H	=	total heat injection rate, J/s
H_D	=	dimensionless total heat injection rate
H_D	=	dimensionless heat injection rate in Laplace space
I_0, I_1	=	modified Bessel function of the first kind
K	=	thermal conductivity, $W/m \text{ } ^\circ K$
K_1	=	thermal conductivity of inner layer, $W/m \text{ } ^\circ K$
K_2	=	thermal conductivity of second layer, $W/m \text{ } ^\circ K$
K_3	=	thermal conductivity of third layer, $W/m \text{ } ^\circ K$
K_0, K_1	=	modified Bessel functions of the second kind
L	=	length of the core, m
m	=	mass injection rate of steam, kg/s
r	=	radial distance, m
r_D	=	dimensionless radius
r_1	=	radial distance at the inner boundary between core and stainless steel tube, m

r_2	=	radial distance at the interface between stainless steel tube and heat jacket, m
r_3	=	radial distance at the interface between heat jacket and insulation, m
r_4	=	radial distance at the outer boundary of insulation, m
s	=	Laplace space variable
t	=	elapsed time, s
t_D	=	dimensionless time
T	=	temperature, $^{\circ}K$
T_D	=	dimensionless temperature
T_i	=	injection temperature, $^{\circ}K$
T_r	=	reservoir temperature, $^{\circ}K$
T_s	=	saturation temperature, $^{\circ}K$
T_1	=	temperature in the inner insulation, $^{\circ}K$
T_2	=	temperature in the second insulation, $^{\circ}K$
T_3	=	temperature in the third insulation, $^{\circ}K$
T_{1D}	=	dimensionless temperature in inner insulation
T_{2D}	=	dimensionless temperature in the second insulation
T_{3D}	=	dimensionless temperature in the third insulation
T_{∞}	=	ambient temperature, $^{\circ}K$
T_D	=	dimensionless temperature in Laplace space
x	=	longitudinal distance, m
X_s	=	steam frontal position, m
X_D	=	dimensionless distance
X_D	=	dimensionless distance in Laplace space
α	=	thermal diffusivity, m^2/s
α_D	=	thermal diffusivity ratio
α_1	=	thermal diffusivity of the inner insulation, m^2/s

α_2 = thermal diffusivity of the second insulation, m^2/s

λ_D = conductivity ratio

σ = volumetric heat capacity ratio

ρ = density, kg/m^3

τ = elapsed time, s

μ = viscosity, $Pa.s$

ϕ = porosity, fraction

Subscript

D = dimensionless

o = oil

R = Reservoir

s = steam, steam front

t = total

w = water

1 = layer 1

2 = layer 2

3 = layer 3

∞ = ambient

G. References

1. Marx, J.W. and Langenheim, R.H.: "Reservoir Heating by Hot Fluid Injection", Trans., AIME (1959) Vol. 216, 312-315.
2. Wang, Fred P., and Brigham, W.E.: "A Study of Heat Transfer During Steam Injection and Effect of Surfactants on Steam Mobility Reduction", Stanford University Petroleum Research Institute, SUPRI Technical Report, 1986.
3. Wang, Fred: "Personal Communications", 1987.

4. Stehfest, H.: "*Algorithm 368, Numerical Inversion of Laplace Transforms*", D-5, Communications of the ACM, (Jan. 1970), Vol. 13, No. 1, 49.
5. Prats, M.: Thermal Recovery, SPE Monograph Vol. 7. Society of Petroleum Engineers, Dallas, 1982.
6. Miller, M.A.: "*Effect of Temperature on Oil-Water Relative Permeabilities of Unconsolidated and Consolidated Sands*", Ph.D Thesis, Stanford University, Stanford, CA (1983).
7. Boberg, T.C.: Thermal Methods of Oil Recovery. An Exxon Monograph, John Wiley & Son, Inc., New York, (1988).

